Dissertations, Master's Theses and Master's Reports

2019

NEAR-INFRARED FLUORESCENT PROBES FOR SENSITIVE DETERMINATION OF LYSOSOMAL & MITOCHONDRIAL pH IN LIVE CELLS

Wafa Mazi

Michigan Technological University, wamazi@mtu.edu

NEAR-INFRARED FLUORESCENT PROBES FOR SENSITIVE DETERMINATION
OF LYSOSOMAL & MITOCHONDRIAL pH IN LIVE CELLS

By

Wafa Abdurazaq Mazi

A DISSERTATION

Submitted in partial fulfillment of the requirements for the degree of

DOCTOR OF PHILOSOPHY

In Chemistry

MICHIGAN TECHNOLOGICAL UNIVERSITY

2019

This dissertation has been approved in partial fulfillment of the requirements for the Degree of DOCTOR OF PHILOSOPHY in Chemistry.

Department of Chemistry

Dissertation Advisor: *Dr. Haiying Liu*

Committee Member: *Dr. Tarun K. Dam*

Committee Member: *Dr. Loredana Valenzano*

Committee Member: *Dr. Qinghui Chen*

Department Chair: *Dr. John Jaszczak*

Table of Contents

Preface

This dissertation is submitted for the degree of Doctoral of Philosophy at the Michigan Technological University. The research described herein was conducted under the supervision of Professor Haiying Liu in the Department of Chemistry, Michigan Technological University. The author of this dissertation wrote the contents of chapter 1 and 5, and the author of this dissertation organized the contents of the other two chapters based on the published or submitted papers. These published/submitted papers and my research contributions to these papers are described below:

Chapter two of this dissertation was reproduced in its entirety with kind permission from ACS sensor publications. This article was published in *ACS Sens.*, 2016, 1 (2), pp 158–165. This was a Multi-author paper; the author of this dissertation was responsible for collecting the optical measurement. Dr. Jingtuo Zhang was responsible for the synthesis, characterization of all reported compounds, and also for the written description of the synthesis of the reported compounds. Dr. Mu Yang collected cell imaging data. Dr. Loredana Valenzano did the computation methodology. Dr. Haiying Liu was the corresponding author. He conducted data analysis and revised the manuscript.

Chapter three is the manuscript under review for the "*Methods*".

This was a Multi-author paper; the author of this dissertation was responsible for the synthesis, characterization of reported compounds A and C, collecting data for part of optical properties and the written description of the synthesis and the optical measurements of the reported compounds. The reported compound B was synthesized and characterized by Dr. Yibin Zhang. Dr. Mingxi Fang collected the fluorescence and absorption data. Rashmi Adhikari collected the collected cell imaging. Dr. Rudy L. Luck was responsible for theoretical calculation. Dr. Haiying Liu was the corresponding author. He conducted data analysis and revised the manuscript.

Chapter four is a manuscript under preparation for publication

This was a Multi-author paper; the author of this dissertation was responsible for collecting data of optical properties and the written description of the optical measurements of the reported compound. The reported compound A was synthesized and characterized by Dr. Yibin Zhang. Shuai Xia collected cell imaging. Dr. Rudy L. Luck was responsible for theoretical calculation. Dr. Haiying Liu was the corresponding author. He conducted data analysis and revised the manuscript.

Dedication

I dedicate this dissertation to the souls of my parents, Abdulrazaq and Azizah, who were waiting for this moment. May Allah grants their souls with mercy and forgiveness.

<div align="right">

With all of my love,

Dr. Wafa Abdulrazaq Mazi

</div>

Acknowledgments

The journey of earning a Ph.D. degree is a precious life experience that not only developed my scientific knowledge and skills but also burnished my personality. During my Ph.D. study journey, there were many people who stood by me and supported me, some of them have left and others are still encouraging and bolstering me. Without their prayers, help, and support I would not be able to achieve this Ph.D. degree.

First, I would like to express my sincere thanks to my advisor, Dr. Haiying Liu, for his guidance, support, and patience during my graduate study. Dr. Liu was always there with his prudent advice and guidance that helped me overcome the problems I encountered in both my course-work and research projects. This dissertation would not be possible without his diligent and enthusiastic guidance and suggestions. I would like to thank him for the priceless advice, time, and effort spent that cultivated me to be a productive and better scientist.

I would like also to acknowledge my committee members Dr. Tarun K. Dam, Dr. Loredana Valenzano, and Dr. Qinghui Chen, for their precious time, great support and excellent suggestions on my Ph.D. dissertation and oral defense. I am also grateful to our former department chair Dr. Sara A. Green and Dr. Cary F. Chabalowski, current department chair Dr. John Jaszczak for their help and support.

List of abbreviations

1. BODIPY   4,4-difluoro-4bora-3a, 4a-diaza-s-indacene

2. e.A   Electron-withdrawing groups

3. e.D   Electron-donating groups

4. Cy3   Trimethine cyanine

5. Cy5   Pentamethine cyanine

6. Cy7   Heptamethine cyanine

7. NIR   Near-infrared

8. PET   Photoinduced electron transfer

9. ICT   Intramolecular charge transfer

10. HOMO   Highest occupied a molecular orbital

11. LUMO   Lowest unoccupied molecular orbital

Abstract

Varied intracellular pH levels are critical for various physiological processes such as enzymatic activity, cell proliferation and apoptosis, ion transport, and muscle contraction. Cellular compartments, like lysosomes, must retain an acidic environment (pH ~ 4.5) to activate hydrolytic enzymes necessary for the breakdown of large biomolecules. Another cellular organelle, the mitochondria, provides the cell with energy and must retain an alkalis environment (pH ~ 8.0) for proper function. Substantial lysosomal and mitochondrial pH deviation is associated with cellular dysfunction and disease. Therefore, the precise detection of lysosomal and mitochondrial pH is essential to provide a better understanding of cellular physiological and pathological processes. Due to their superior features, such as cheap and simple operation, high spatial and temporal resolution, and noninvasive fluorescence imaging, fluorescent probes are the ideal methodology to visualize and monitor lysosomal and mitochondrial pH variation.

We have developed three morpholine-functionalized BODIPY-based fluorescent probes that can be used to monitor lysosomal pH. The fluorescent probes are highly fluorescent under basic conditions, but when exposed to an acidic environment the fluorescence is quenched via an electron donor photoinduced energy transfer. Moreover, we have developed and synthesized a series of sterically hindered fluorescent probes based on spirolactam ring modifications. These modifications were developed by introducing 2-aminophenylboronic acid pinacol ester to

rhodamine B, a near-infrared rhodamine dye, and a near-infrared hemicyanine dye. The probes display high fluorescence under acidic conditions, but exhibit weak fluorescence under basic conditions due to the significant steric hindrance in the spirolactam ring. Since the probes were functional in an acidic environment, they were successfully applied for the sensing of lysosomal pH variations in living cells.

We have also developed a NIR fluorescent probe to determine mitochondrial pH variations by incorporating an oxazolidine switch onto a near-infrared hemicyanine. The probe has the ability to rapidly switch from an oxazolidine moiety to a hemicyanine group when the pH level decreases from 10.0 to 5.0. This response to pH changes is reversible and has been successfully used to determine pH levels in mitochondria.

1 Introduction

1.1 Fluorescence spectroscopy

Chemical probes play essential roles in the investigation of biochemical processes, diagnosis of diseases, and the detection of hazardous compounds. In the last two decades, fluorescence spectroscopy, fluorescence imaging, and fluorescence indicators have become key tools in various disciplines of modern science and medicine. Some of these disciplines include molecular biology, clinical diagnostics, biochemistry, analytical and environmental chemistry, material science, and biotechnology. The implementation of chemical probes in scientific fields is due to the high sensitivity and simplicity of the operations of fluorescence[1].

1.1.1 Basic definitions of fluorescence spectroscopy

Fluorescence is a type of luminescence that emits photons from the singlet-excited state to the ground electronic state after absorbing light. In fluorescence, the spin multiplicity of the electron in the electronic excited state retains its diamagnetic properties to the electron in the ground state. Therefore, the lifetime of the excited state is relatively short ($< 10^{-5}$ S).

Phosphorescence, another type of luminescence, emits light as the electron returns to the ground state from the triplet-excited state. Phosphorescence mainly differs from fluorescence in the spin multiplicity of the electron in the triplet-excited state, which is paramagnetic to the electron in the ground state. Thus, a change in electron spin is required as the electrons return to the ground state resulting in a longer lifetime (milliseconds to seconds)[2-4].

1.1.2 The history of fluorescence spectroscopy

In 1565 Nicolás Monardes, a Spanish physician and botanist, was the first to report the phenomenon of fluorescence. Monrades described a bluish glimmer of water infused from the wood of a small Mexican tree. The wood was later named *Lignum Nephriticum* by botanist Charles de L'Écluse and was used in Europe as medicine for treating kidney ailment[2, 5-6]

In 1845, Sir John Frederick William Herschel exposed a solution of quinine sulfate to sunlight and observed the emission of blue light. In 1852 Sir George Gabriel Stokes, who had major contributions in the history of photoluminescence, named the phenomena of light emission as "fluorescence". He also discovered "Stokes Shift", which states that the wavelengths of emitted light are always longer than the wavelengths of absorbed light[2, 6-10].

Professor Alexander Jablonski, the father of fluorescence spectroscopy, illustrated and described various molecular processes that can occur in the excited state between the absorption and emission of light through a diagram, namely the Jablonski Diagram (Figure 1.1) [4]. All of these contributions aided in the development of the most essential part of fluorescence sensing technology: the fluorophore.
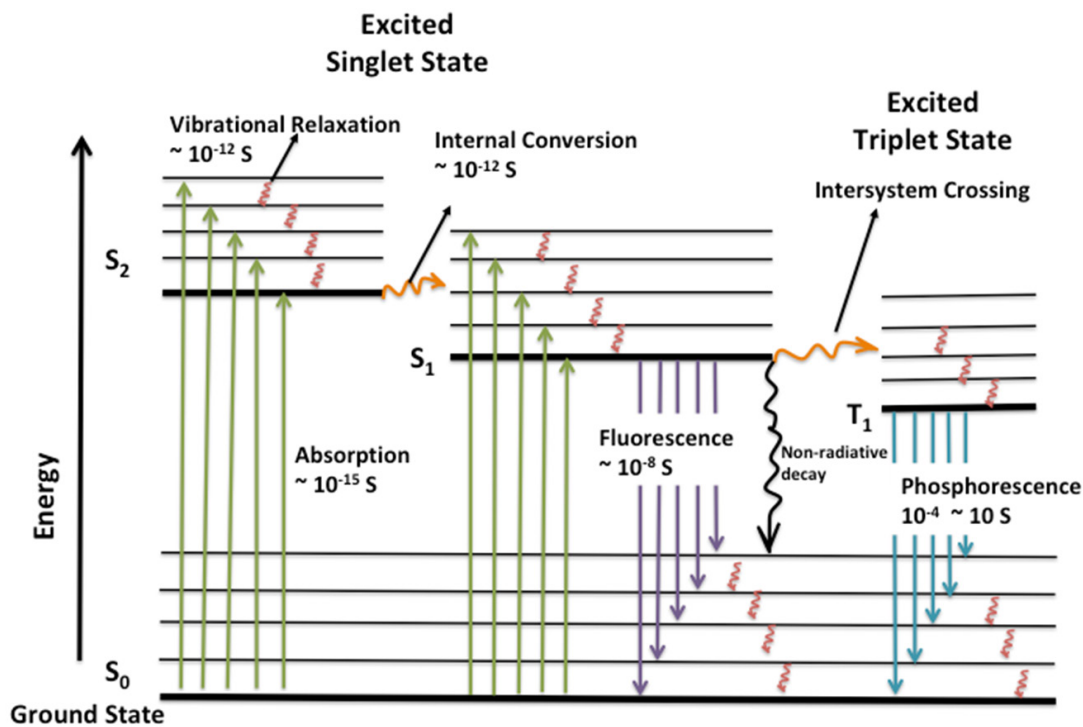
Figure 1.1. The Jablonski diagram in which an electron is promoted to an excited state by the absorption of light, and emits radiation as it returns to the ground state.

1.2 Organic fluorophores for fluorescent sensing and labeling

1.2.1 Background

A fluorophore, also known as a fluorochrome or fluorescent probe, is the most essential component of fluorescence sensing technology. It is a molecule that absorbs a photon at a specific wavelength and re-emits the photon at a different wavelength[11-12]. Fluorophores are typically aromatic, planar or cyclic molecules with multiple π- bonds that are capable of converting chemical process, such as binding, reactions, and/or conformational changes, to detectable fluorescence signals. Fluorophores are divided into two main categories: intrinsic and extrinsic. Intrinsic biochemical fluorophores are those that can be found

naturally such as aromatic amino acids, NADH, flavins, derivatives of pyridoxyl, and chlorophyll. Extrinsic chemical fluorophores are moieties that are attached either by covalent or non-covalent linkages to the sample. This attachment provides fluorescence to non-fluorescent samples or changes the spectral properties of the sample. Extrinsic fluorophores include fluorescein, rhodamine, dansyl, DNA probes, and numerous other substances[13]. Since there is a limitation of diversely applicable intrinsic fluorophores, the need to develop and design extrinsic fluorophores for specific applications or targeted analytes is growing dramatically.

1.2.2 The structure of fluorescent probes

Generally, the structure of a synthetic fluorescent probe consists of a fluorophore, a linker or spacer, and a recognition site that is also called a chelator, receptor, ligand, or binding site (Figure 1.2). The fluorophore is a signaling subunit that transforms the recognition events between the analyte and the binding site into a visible fluorescent or electrochemical readout. The linker or spacer is the moiety that links the fluorophore and the binding site. The length of the linker or spacer is highly dependent on the fluorescence modulation[14-16].
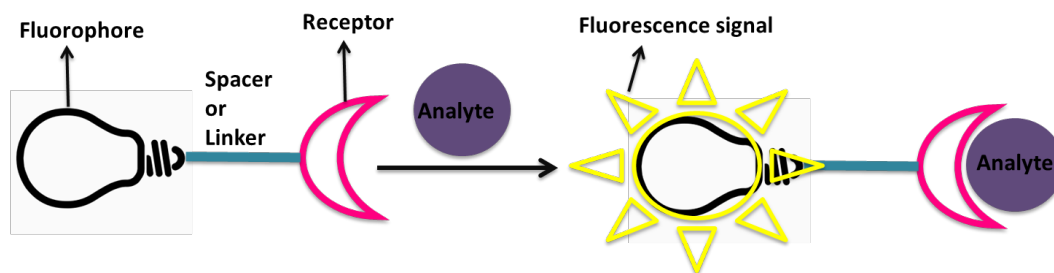
Figure 1.2. A schematic illustration of a typical fluorescent probe.

1.2.3 Parameters for fluorescent probes

There are several parameters that describe the characteristics of fluorescent probes. Those include absorption maxima (λ_{abs}), emission maxima (λ_{em}), Stokes shift, quantum yield (Φ), molar extinction coefficient ($\mathcal{E}$), brightness, and lifetime (τ). The definition for each term is described below.

Absorption and emission maxima are the maximum absorption and emission wavelength of the fluorescent probe respectively.

Stokes shift: is the difference between the maximum absorption (λ_{abs}) and maximum emission (λ_{em}) of the chromophores (Figure 1.3). Fluorescent probes that possess a large Stokes shift are preferable than those with a small Stokes shift. This is because the probes that contain a small Stokes shift are prone to self-quenching via energy transfer[9].
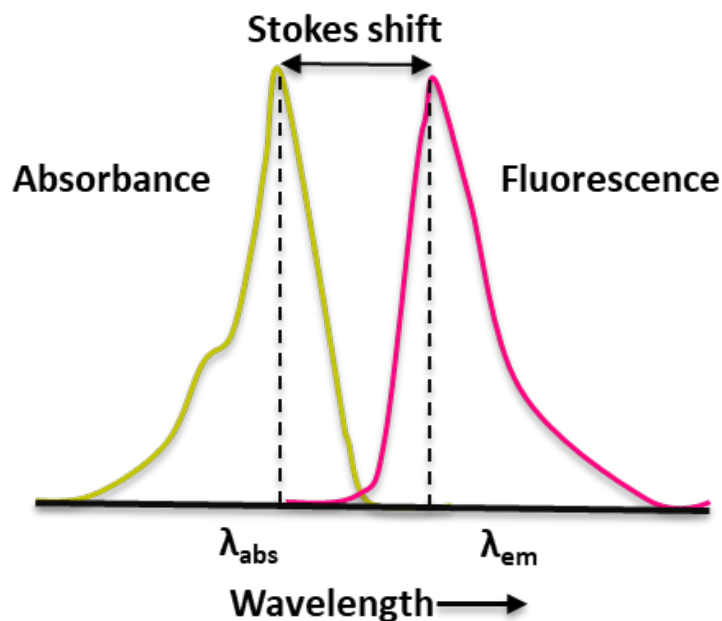
Figure 1.3. An illustration of Stokes shift.

The fluorescence quantum yield (Φ): is a measure for the efficiency of the fluorescent probe. It is determined by the ratio between the number of fluorescence photons emitted and the number of photons absorbed.

$$\phi_f = \frac{Number\ of\ photons\ emitted}{Number\ of\ photons\ absorbed} \qquad \textbf{Eq. 1.2.3.1}$$

The molar extinction coefficient (Ɛ): is a measurement of the light absorbing capacity of the fluorescent probe. Fluorescent probes with high molar extinction coefficients are considered efficient absorbers.

Brightness: the brightness of the fluorophore is an important criterion for fluorescent imaging applications. It is proportional to the product of the extinction coefficient and quantum yield.

6

$$Brightness \propto n\phi\mathcal{E} \qquad\qquad \text{Eq. 1.2.3.2}$$

The lifetime (τ): is the average time a molecule spends in its excited state before it returns to the ground state through the emission of a photon.

1.3 Fluorescence mechanisms and modulation

The changes in fluorescence intensity and/or emission wavelength for fluorescent probes result from the interaction between the recognition site and the target analyte. There are many photophysical processes that can be involved when recognition of the analyte by the binding site occurs. These processes include quenching via collision, photoinduced electron transfer, energy transfer, etc. Therefore, it is very important to carefully design a fluorophore with a controlling fluorescence mechanism, e.g. a fluorescent switch on/off the property. This mechanism can respond to the presence of a certain analyte by changes in the analyte concentration and/or pH. The frontier molecular orbitals theory is utilized to explain these mechanisms. In the following section, the most commonly used mechanisms in the designing of fluorescent sensors will be briefly discussed.

1.3.1 Photoinduced electron transfer (PET)

The PET mechanism is a process in which an electron is transferred between a fluorophore and a receptor. Many fluorescent probes based on the PET mechanism have been reported [17-18]. PET-based probes consist of a fluorophore that is linked to a chelator through a spacer. The chelator acts as a receptor, binding site, or recognition site. The spacer is a short aliphatic chain that causes an interruption in the π-electron system of the fluorescent probe

and the chelator. Activation of this mechanism is dependent on the presence and/or concentration of an analyte. When the analyte is absent, the electron is freely transferred between the fluorophore and chelator, causing the fluorescence to be quenched. However, in the presence of an analyte, the transfer of the electron from the fluorophore to the chelator is prohibited, causing the fluorescence of the sample to recover.

PET can be divided into two types: reductive PET and oxidized PET. In reductive PET, also known as A-PET, the fluorophore is reduced and serves as the electron acceptor. Since the chelator is an electron-rich moiety, e.g. amine groups, it acts as the electron donor. In these sensors, the absence of an analyte will cause the highest occupied molecular orbital (HOMO) of the electron acceptor (fluorophore) to be lower than the HOMO of the electron donor (chelator). Photo-excitation of the fluorophore results in the promotion of an electron from the HOMO to its lowest unoccupied molecular orbital (LUMO). Subsequently, an electron on the HOMO of the chelator is transferred to the HOMO of the fluorophore resulting in the quenching of fluorescence (Figure 1.4). Therefore, the electron of the fluorophore is reduced, and the chelator is oxidized. When the analyte is bound to the chelator, the electron density of the chelator is significantly reduced. This reduction lowers its HOMO and prohibits the electron transfer to the fluorophore. This results in the electron on the LUMO of the fluorophore to be transferred to its HOMO, causing the fluorescence to be enhanced or switched "on"[1, 19].
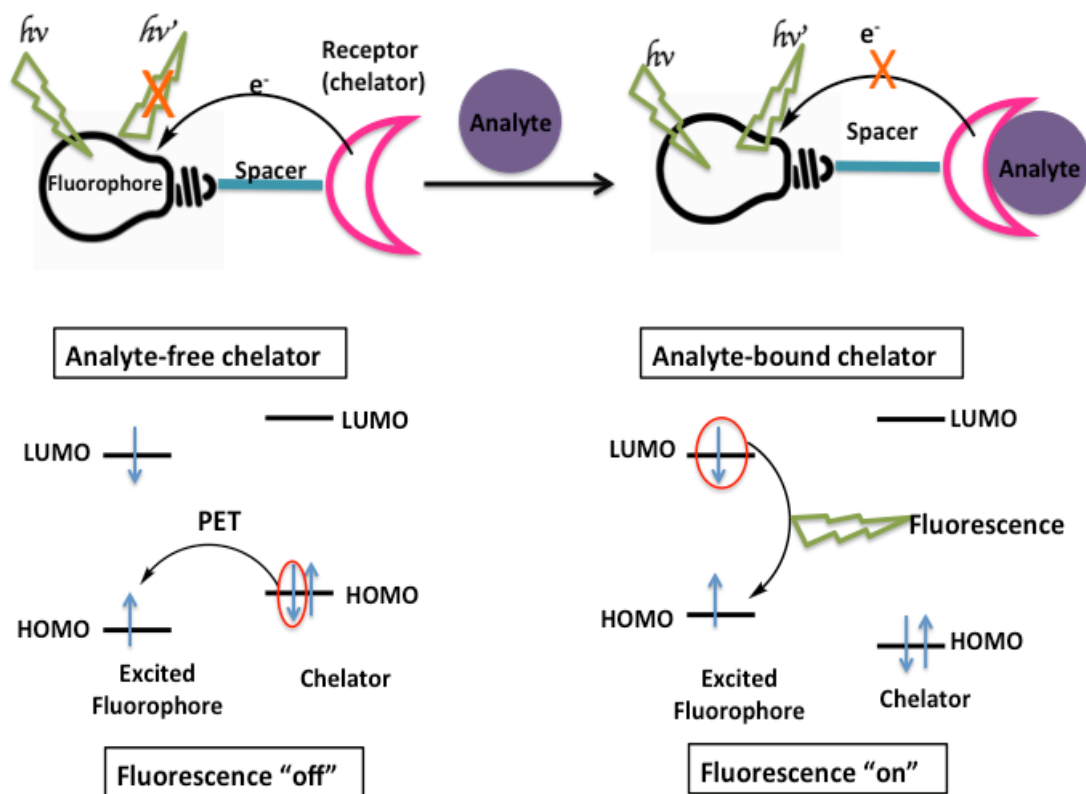
Figure 1.4 A schematic illustration of the reductive-PET mechanism based fluorescent probes.

In oxidative PET, also called D-PET, the fluorophore serves as the electron donor and the chelator is the electron acceptor. In the absence of an analyte, the LUMO of the fluorophore is higher than that of the chelator. Consequently, the electron is transferred from the LUMO of the fluorophore to the chelator, resulting in the quenching of fluorescence. Once the analyte is bound to the chelator, the LUMO of the chelator is high enough to recover the fluorescence[1] (Figure 1.5). Only a few fluorescent sensors based on oxidative-PET have been reported [20-22].
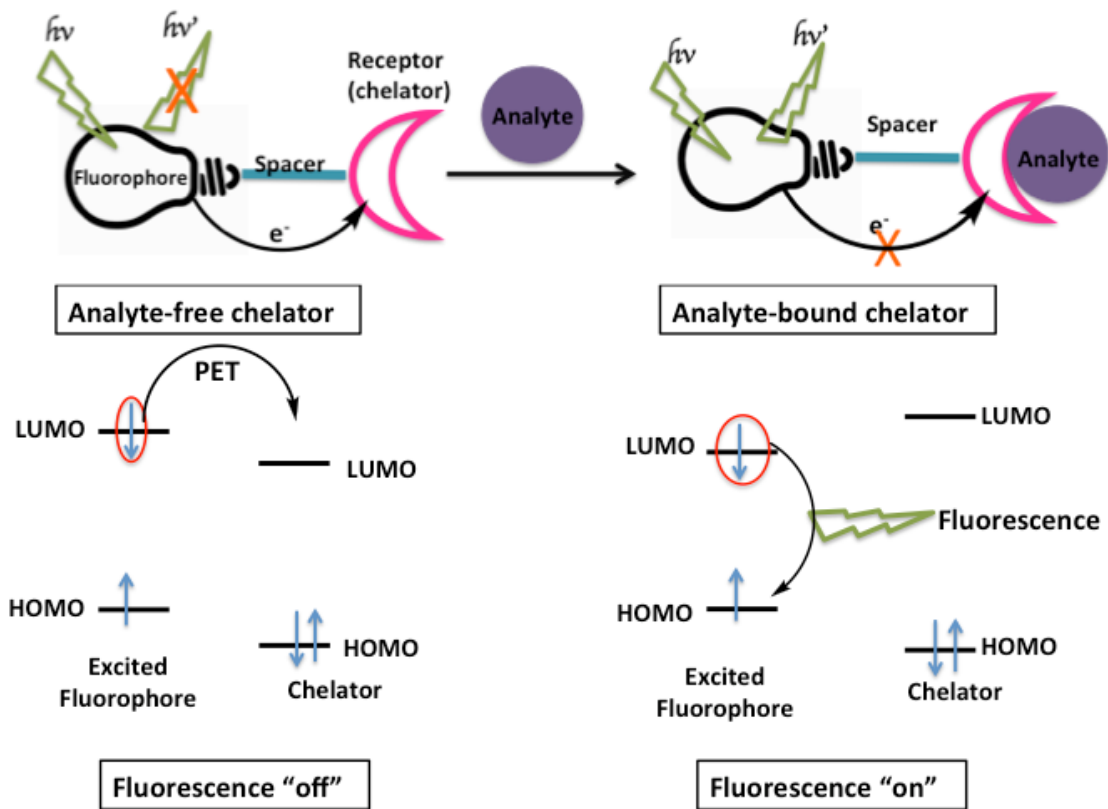
Figure 1.5 Schematic illustration of the oxidized-PET mechanism based fluorescent probes.

1.3.2 Intramolecular charge transfer (ICT)

Sensors that contain ICT properties are designed to have electron-donating groups (e.D) π-conjugated to electron-withdrawing groups (e.A) in the fluorophore "e.D-π-e.A"[23] (Figure 1.6). Upon photo-excitation, the ICT between the donor and acceptor moieties is activated, which results in a considerable increase in the dipole moment[1, 24]. The binding of the target analyte, either to the donor or acceptor moiety, will disrupt the ICT in the system. Thus, the e.D/e.A group is either enhanced or suppressed. The interaction of the target analyte with the e.D moiety will reduce the electron-donating ability of the donor. The suppression

of this ability will cause a blue shift in the absorption, accompanied with a decrease of the extinction coefficient and emission. In addition, the energy gap between the HOMO and LUMO of the fluorophore will be increased (Figure 1.6). Conversely, the binding of the analyte with the e.A. will enhance the electron-withdrawing character of the acceptor, resulting in a red shift in emission and absorption with an increase in the extinction coefficient. This will further result in a decrease in the energy gap between the HOMO and LUMO of the fluorescent probe[25-26] (Figure 1.6).
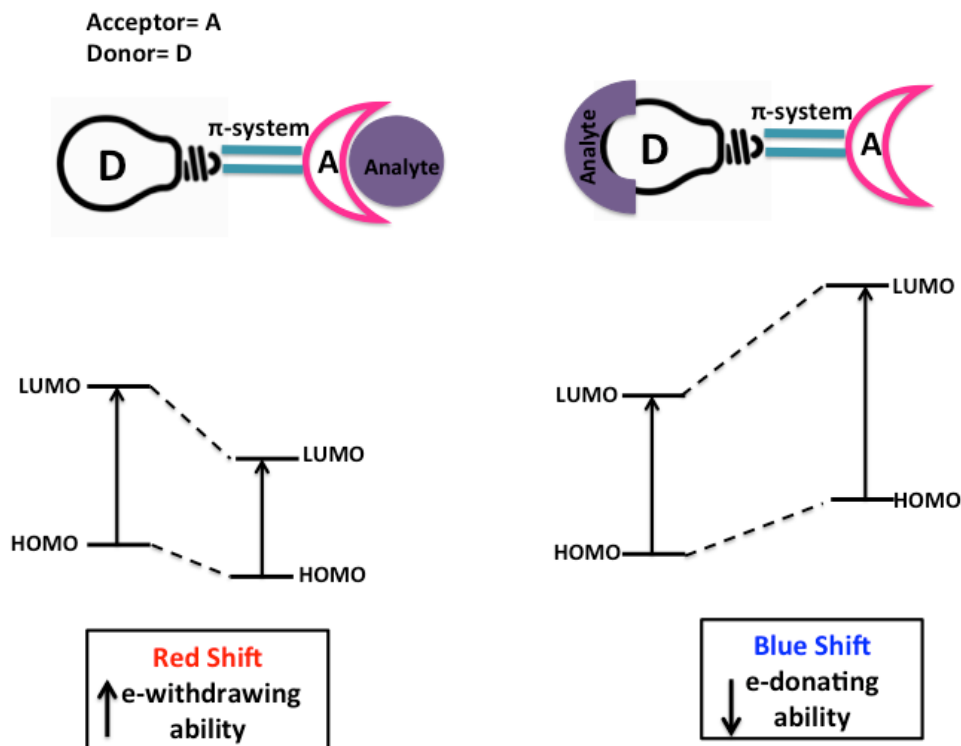
Figure 1.6 Schematic illustration of ICT mechanism based fluorescent probes.

The main distinction between PET and ICT fluorescent probes is the difference in fluorescence response after the analyte interacts with the receptor. The PET sensors will

either quench or enhance the fluorescence signal without any spectral shifts in the presence or absence of the analyte. This phenomenon gives rise to the terms 'on-off' and 'off-on'. Conversely, fluorescent probes based on the ICT mechanism display clear fluorescence and absorption band shifts upon analyte recognition. This property allows for the detection of any change at two different wavelengths, which is a ratiometric measurement. Due to the ratiometric measurement property of ICT-based fluorescent probes, many fluorescent sensors have been reported[27-31].

1.3.3 Altering π-conjugation systems

The most common and direct method to alter the spectroscopic properties of fluorophores is to change its π-conjugation system. Ideally, the recognition events of the target analyte will result in enhancing, disturbing, or reducing the π-conjugation of the sensors. When a chemical reaction, e.g. oxidation, reduction or nucleophilic attack reactions, occurs between the probe and the analyte a reduction and/or alteration of the π-conjugation is observed. These chemical reactions either enhance the conjugation of the functional groups or disturb the conjugation by forming sp^3-hybridized carbons. Consequently, this will result in significant shifts in absorption and emission accompanied with changes in fluorescence intensity. Reductions of the π-conjugations have been widely applied to design and develop many fluorescent probes with dual-channel and/or ratiometric response features[32].

The enhancement of π-conjugations in fluorophore indicators can be achieved through the spirocyclization of the fluorophore. Xanthene derivatives, such as Rhodamines and Fluorescein, are classical examples of probes with spirocyclization properties. When the

spirolactam ring is closed, these probes are colorless and lack fluorescence. However, the recognition of the analyte activates the carbonyl group, which causes the spiro-ring to open and re-aromatize (Scheme 1.1). The π-conjugation is then rebuilt, resulting in the switching on of the fluorescence[33]. Spirocyclic fluorescent probes have been reported for a variety of analytes, including heavy metal ions [34-37], thiols[38-39], and pH changes[39].
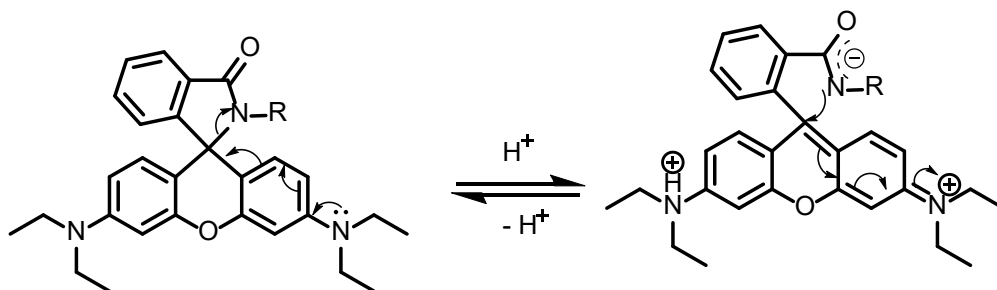
Scheme 1.1: The mechanism of spirolactam ring opening and closing in Rhodamine B.

1.4 Required criteria for the efficacy of fluorescent probes

The efficiency of fluorescence sensing is mainly dependent on the fluorescent probes. Therefore, there are several criteria that should be taken into consideration when designing and synthesizing fluorescent probes, such as appropriate optical and chemical properties for certain applications.

1.4.1 Basic criteria

1) **Selectivity and sensitivity**: The recognition site on the probe must be able to selectively bind with a target analyte without interference from competing molecules. This will result in efficient measurement and sufficient fluorescent

signal. Therefore, the selectivity and sensitivity are the essential concern when designing fluorescent probes[1, 14].

2) **Stability:** The photo-stability and chemo-stability of fluorescent probes must remain stable when exposed to harmful stimuli such as chemo-bleaching and photo-bleaching. Damage from these stimuli are irreversible and will result in permanent loss of fluorescent signal. Therefore, robust fluorescent probes are more desirable over unstable probes[40].

3) **The brightness of fluorescence:** Fluorescent probes that possess a high quantum yield and a large extinction coefficient at the excitation wavelength would have a high level of brightness (Eq.1.2.3.2). Therefore, fluorescent probes that provide bright fluorescence are desired[40].

4) **Turn-on fluorescence response:** is the detected fluorescent signal that is generated through triggered chemical reactions by the target analyte. It is a much more favored design than turn-off fluorescence because the turn-on fluorescence enhances the signal-to-noise ratio (S/N).

1.4.2 Desired criteria of fluorescent probes for biological systems

The criteria discussed above are the basic requirements for regular analytical samples. Synthetic fluorescent probes for living organisms have additional requirements due to the complicated and sensitive nature of biological systems.

1) **Good aqueous solubility and biocompatibility:** Fluorescent probes that possess high hydrophobic moieties tend to aggregate and accumulate within the membrane of the cell causing a quench in the fluorescent signal. Therefore, fluorescent probes

for biological applications must be highly soluble in the cellular environment to allow permeability through the cell[14, 41].

2) **Near-Infrared (NIR) wavelength absorption and emission:** The NIR wavelength, also known as the "biological window"[42], ranges between 650 nm-900 nm. Fluorescent probes that absorb or emit light in this wavelength minimize sample photodamage and cellular autofluorescence from endogenous biomolecules [43]. NIR fluorescent probes have the ability to reduce Raman and Rayleigh light scattering. Also, the fluorescence background of biological samples in the NIR region is very low, which results in a high signal-to-noise ratio. Additionally, it has the ability to deeply penetrate biological samples (1-2 cm), which facilitates *in vivo* detection. For all these merits, NIR fluorescent indicators are the perfect choice for *in vivo* imaging application[1, 44].

3) **Ratiometric fluorescence response:** is the measurement of fluorescence at two different excitation and/or emission wavelengths (dual-channel) simultaneously. This is especially important because it provides a high signal-to-noise ratio (S/N). Moreover, ratiometric fluorescence response is beneficial for intracellular measurements as it could eliminate any effects that are not related to the analyte of interest, e.g uneven cell thickness, unequal dye loading or distribution, dye leakage, photobleaching, etc[1].

To date, fluorescent sensors that satisfy all of the aforementioned standards have yet to be reported. Fluorescent probes that partially fulfill the standard requirements will be reviewed in the following section (**1.5.1**.)

1.5 Fluorescent probes for living cells

The understanding of biological and biochemical processes is highly dependent on the ability to visualize and quantify these processes in the cellular context. Among many radioactive technologies, such as bioluminescence, electromagnetism, and electrochemistry, fluorescence microscopy has been the ideal choice for visualizing the biological events in a living system. Fluorescence microscopy has superior merits including great spatial and temporal sampling resolution, real-time monitoring, non-invasiveness, high sensitivity and selectivity, and good membrane permeability[45]. Near-infrared fluorescent probes are essential because they help prevent the autofluorescence in tissues that may occur at shorter wavelengths. They are also beneficial because they are relatively small in size, easily modifiable, tunable, and they can penetrate biological tissues. After the reporting of fluorescent Ca^{2+} indicators in the 1980s [10], many biosensors for maintaining biological conditions, such as metal ions[18, 46], hydrogen peroxide[45], hypochlorous acid, reactive oxygen[17] and nitrogen species, thiol, and intracellular pH have been reported and applied in biological research.

1.5.1 The role of intracellular pH in biological systems

Intracellular pH is a key parameter that regulates many biological processes such as cell proliferation, growth, apoptosis, vesicle trafficking, enzymatic activity, protein degradation, and cellular metabolism. Each subcellular compartment of eukaryotic cells, specifically the mitochondria and lysosome, possess a pH value in normal conditions. For

example, the pH of the mitochondria and lysosomal environment have a pH of 8.0 and 4.5-5.0 respectively [47-48].

1.5.1.1 The importance of lysosomal pH

In eukaryotic cells, lysosomes form by budding off from the membrane of the trans-Golgi network and contain more than 50 degradative enzymes that have critical roles in cellular metabolism. The acidic environment (pH 4.5–5.5) of the lysosome activates its numerous hydrolytic enzymes to facilitate the degradation of old cell parts, microorganisms, and macromolecules. The deviation from the normal lysosomal pH causes defects in lysosomal function, which leads to lysosomal storage diseases[49], cancer, and Alzheimer's disease[50-51]. Therefore, it is important to monitor the pH fluctuations of lysosomes in living cells to understand its pathological and physiological processes.

1.5.2 Reported molecular-based pH fluorescent probes

Molecular-based pH probes that could help with the monitoring of lysosomal pH have been widely studied and reported. Some of the more influential probes have been highlighted in the following section.

1.5.2.1 BODIPY-based fluorescent pH probes

BODIPY dyes (4,4-difluoro-4bora-3a,4a-diaza-s-indacene) were fully recognized as fluorophore sensors for biological labels in the 1990s. Figure **1.7** represents the core structure of BODIPY [1]. The excellent features of BODIPY-based fluorescent probes make them the most popular probes used for pH sensing among many highly fluorescent dyes.

These features include relatively high molar absorption coefficients and quantum yield, robustness, and stability against light and chemicals, narrow absorption and emission bandwidth with high peak intensities, good solubility, resistance toward self-aggregation in solutions, and high functionality at all positions. Therefore, developing NIR BODIPY derivatives by increasing the π-conjugated systems is achievable and feasible.
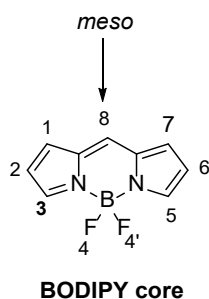
Figure 1.7. The molecular structure of the BODIPY core.

In 2015, Zhang *et. al* developed and reported three NIR BODIPY-based fluorescent probes (Figure 1.8: Probes **1.1-1.3**) for the sensitive detection of lysosomal pH. These probes respond to the lysosomal pH via the ICT and PET mechanism. Under basic conditions, the probes exhibit weak fluorescence due to the ICT from piperazine moieties to the BODIPY core. Alternatively, the lower nitrogen atoms of the piperazine substituents at positions 3,5 of the BODIPY core lead to further quenching in the fluorescence via PET at a pH of 9.98. However, as the pH decreases from 9.98 to 2.20 the probes display strong fluorescence due to the protonation of the nitrogen atoms on the piperazine moieties. Thus, both the ICT and PET processes are suppressed[52].

At pH 8.0, the fluorescence signals of aza-BODIPY fluorescent probe **1.4** (Figure 1.8) are quenched by the electron lone pair on the nitrogen and oxygen atoms of the phenol moieties due to the PET and ICT process. However, the fluorescence signals of the probe are restored when the pH decreases to 4.0. This is because the PET and/or ICT process is suppressed as the tertiary amines at positions 1 and 7 and the oxygen of the phenol moieties at 3,5 positions of the BODIPY core are protonated in the acidic pH[53].

Weak Fluorescence

Strong Fluorescence

$+ \overset{.}{H}$

$- \overset{+}{H}$

Probe 1.1

$R_1 = R_2 = (CH_2CH_2O)_3CH_3$
$R_3 = CH_3$

Probe 1.2

$R_1 = R_2 = R_3 = (CH_2CH_2O)_3CH_3$

Probe 1.3

$R_1 = R_2 = CH_2CH(CH_2O(CH_2CH_2O)_3CH_3)_3$
$R_3 = (CH_2CH_2O)_3CH_3$
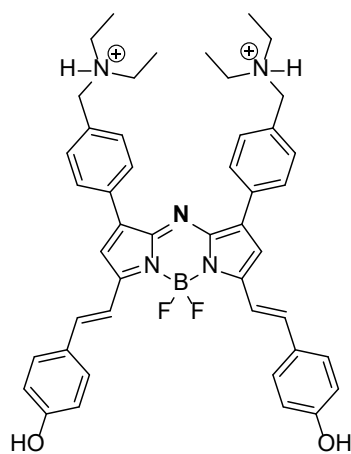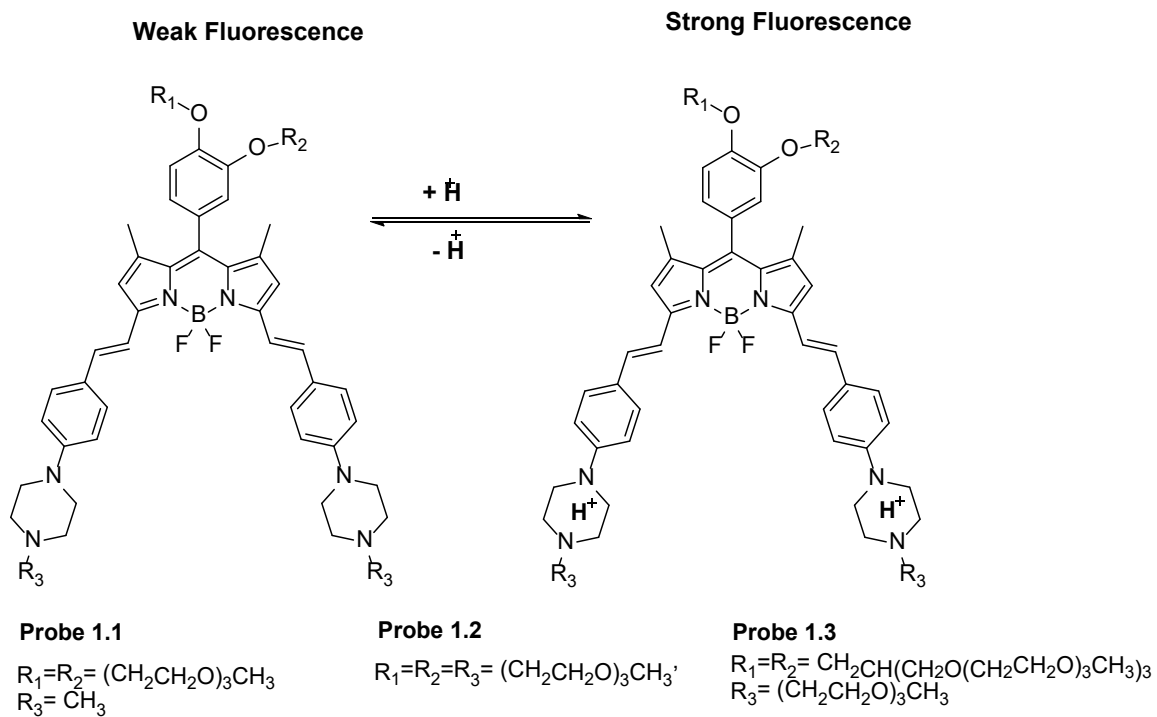
Probe 1.4

Figure 1.8. PET and/or ICT–based BODIPY fluorescent probes for pH detection[52-53].

1.5.2.2 *Cyanine-based fluorescent pH probes*

Cyanine-based sensors are considered the main source of organic long-wavelength fluorophores. These dyes absorb and emit light in the NIR region (600-900 nm) and display a high degree of photostability, low cytotoxicity, good water solubility, efficient quantum yield, and high molar extinction coefficient[11, 54-55]. These features have remarkably increased the usage of cyanine-based fluorescent probes in monitoring and investigating intracellular pH changes. The general molecular structure of cyanine dyes have two nitrogen heterocyclic rings separated by a conjugated chain of odd carbon atoms (Figure 1.9a) [16, 18, 44, 56]. The chemical structures of the molecules specifically the number of carbon atoms in the conjugated chain determines the name of the cyanine. For example, three, five and seven carbon atoms in the conjugated chain denote trimethine cyanine (Cy3), pentamethine cyanine (Cy5) and heptamethine cyanine (Cy7), respectively (Figure1.9b)[57]. Additionally, the optical properties of cyanine dyes are primarily dependent on the number of methane groups in the poly chain. Each extension of the probe by one (CH=CH) moiety leads to a 100 nm shift of the maximum absorption and emission[11, 58]. The dyes with (R=H) are known as norcyanine and they are sensitive to different pHs (Figure 1.9a). This is caused by the protonation of the amine group with the fluorophore core. Cyanine-based fluorescent sensors responsive to pH changes can be divided into two types. The first type features a non-N-alkylated indolium structure (Figure 1.10). The second type is based on the PET mechanism (Figure 1.11)[16, 54]. The following subsections will briefly discuss the two types with some recent examples of each.
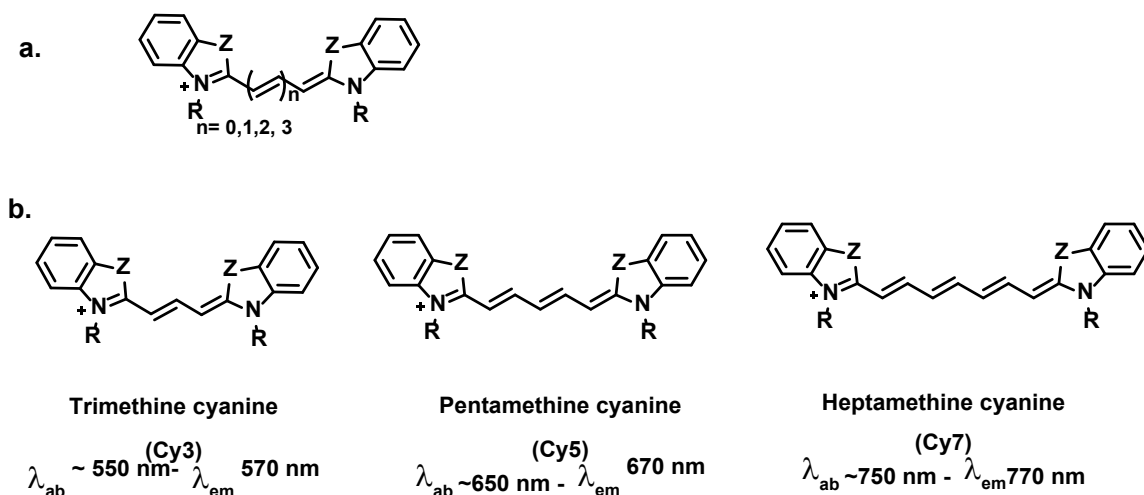
Figure 1.9. a). The general molecular structure of cyanine dyes, b). The structure of common cyanine dyes[57].

1.5.2.2.1 pH-Sensitive non-N-alkylated cyanines

The resonance effect between the two nitrogen atoms of the heterocyclic aromatic rings determines the optical properties of cyanine dyes (Figure 1.10). These dyes are non-fluorescent when the indole nitrogen is deprotonated. However, the protonation results in strong fluorescence.

Cooper and co-workers reported Cy5 based pH probes (Figure 1.10: **1.5-1.8)** are non-fluorescent under a high pH value and are highly fluorescent under acidic condition ($\lambda_{max\ abs}$ = 645 nm; $\lambda_{max\ em}$ = 665nm)[16, 44, 54]. The Cy5 fluorescent probes (**1.6-1.8)** display a similar response in high proton concentration due to protonation and deprotonation of the nitrogen atom. The Achilefu research group reported the non-N-alkylate Cy7 based pH indicator (**1.9**; Figure 1.10). This pH-sensitive probe fluoresces under acidic conditions around 800 nm due to the protonation of the indole nitrogen[16, 44, 54, 59-60].

1.5.2.2.2 pH-Sensitive cyanine probes based on PET mechanism

These probes consist of a cyanine fluorophore and a nitrogen-containing modulator. The fluorescence is switched on or off by suppressing or permitting the PET process via protonation/deprotonation of the modulator[18]. The cyanine-based probe in **1.10** was reported by the Tang research group for pH sensing with the PET mechanism (Figure 1.11)[61]. This probe displays emission fluorescence at 615 nm under acidic conditions due to the protonation of nitrogen on the aniline moiety. However, under basic conditions, the fluorescence of the probe is quenched by the PET process[61]. Similarly, the protonation of the aniline nitrogen in probe **1.11** suppresses the PET mechanism resulting in fluorescence of the dye at 750 nm accompanied with a color change from green to blue [62].

Nagano *et al*. reported cyanine sensors with diamino functional groups based on the PET mechanism (**1.12**-**1.15**, Figure 1.11). These probes can be employed as ratiometric pH probes since they display a 46-83 nm red shift in their maximum absorption at a lower pH[63].
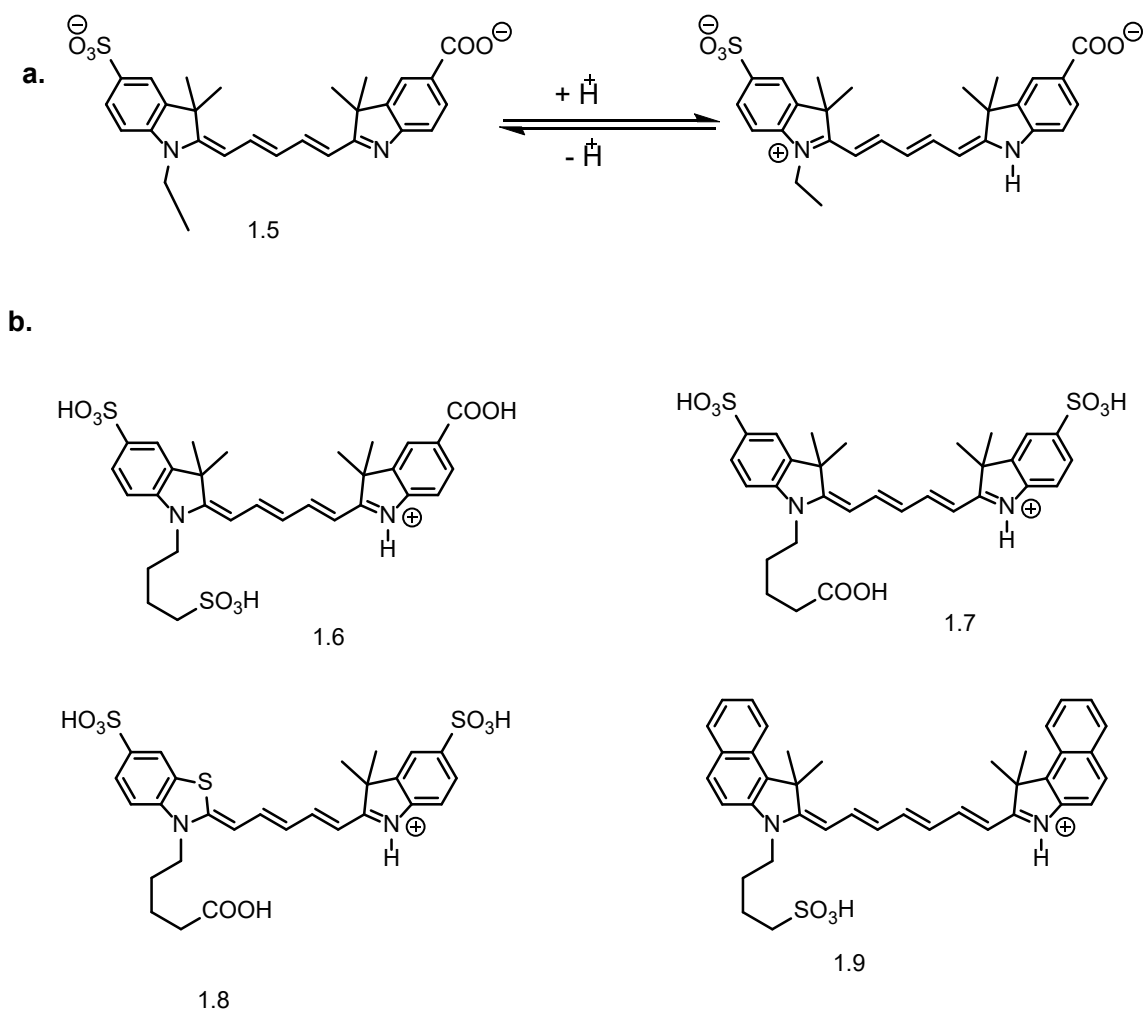
Figure 1.10. **a).** The mechanism of protonation/ deprotonation of pH-sensitive non-N-alkylated cyanine-based fluorescent probes; **b).** Reported cyanine-based fluorescent probes based on pH-sensitive non-N-alkylated[16, 44, 54, 59-60].
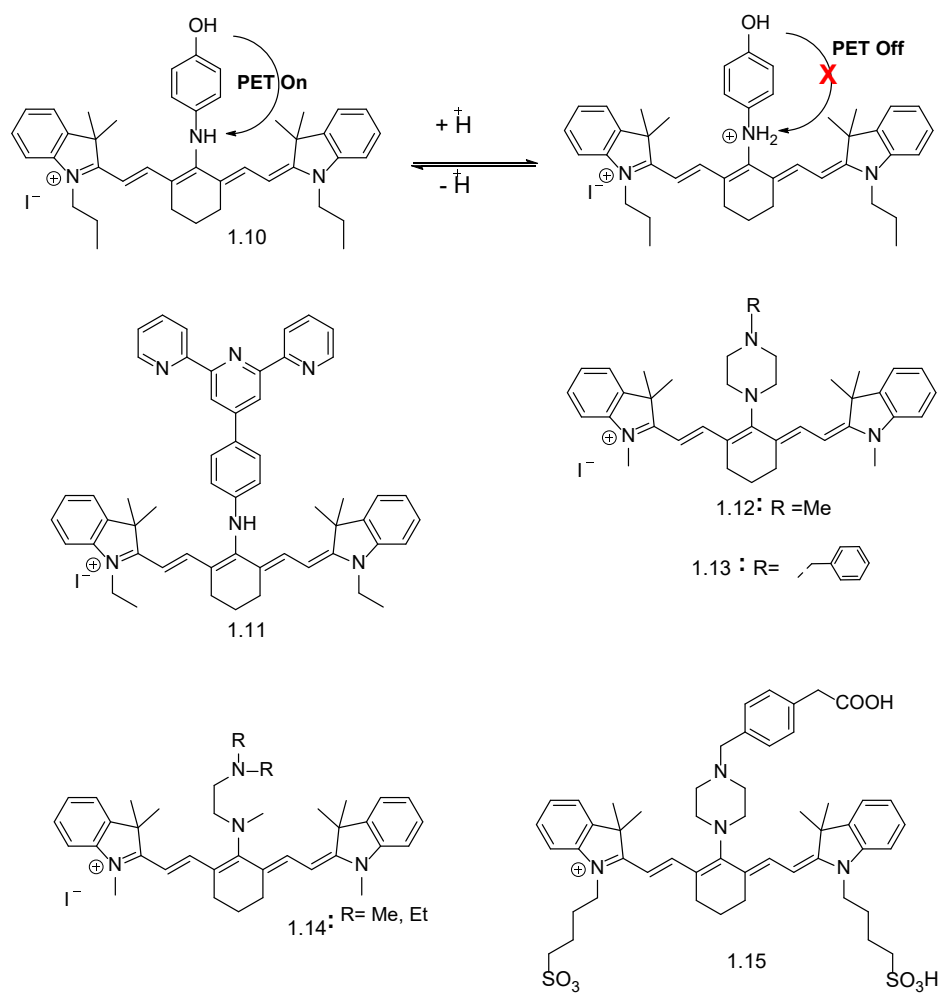
Figure 1.11. The mechanism of PET pH- sensitive and some reported cyanine-based fluorescent probes[61-63].

1.5.2.3 Hemicyanine-based fluorescent pH probes

Hemicyanines are members of the cyanine family. The general structure of hemicyanine consists of a positively charged nitrogenic heterocycle conjugated to a terminal moiety. This terminal group can be a hydroxyl, alkoxy, amino group, coumarin, or xanthene derivative. The hemicyanine structure is featured as a donor−π−acceptor (e.D−π− e.A)

system, in which the nitrogen atom acts as the electron acceptor and the terminal group (-OH, -OCH$_3$, or -NH$_2$) acts as the electron donor[16].

The photophysical properties of fluorescent chemo-sensors can be improved and modified by hybridizing the hemicyanine scaffolds with other dyes. For example, in 2012 the Lin research group reported a unique, hybrid hemicyanine-rhodamine dye that contained a spirolactam on/off switching mechanism. By accompanying the rhodamine dye with the hemicyanine group, the NIR absorption and emission wavelength were enhanced[64] (Figure 1.12).
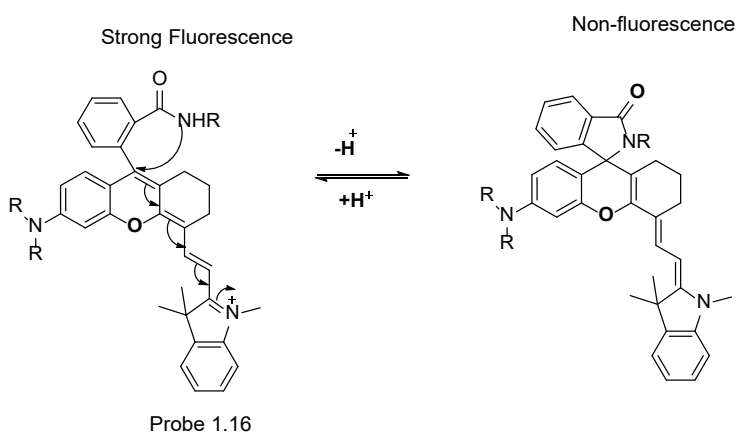
Figure 1.12. A representation of the Rhodamine-hemicyanine hybrid for pH sensing with spirolactam on/off switching mechanism[64].

After the unique design of rhodamine-hemicyanine hybrid probes for pH detection by the Lin group, many fluorophore sensors were reported. Vegesna *et. al.* reported four pH probes (**1.17- 1.20**) for the detection of lysosomal pH inside living cells. The probes were non-fluorescent when the pH was greater than 7.4. However, remarkable fluorescence enhancement (71-fold) was observed upon gradual decrease from pH 7.48 to 4.2. The π-

conjugation of the probes were enhanced when the nitrogen atom was protonated and induced the opening of the spirolactam ring[65].

Probe 1.17   Probe 1.18   Probe 1.19   Probe 1.20
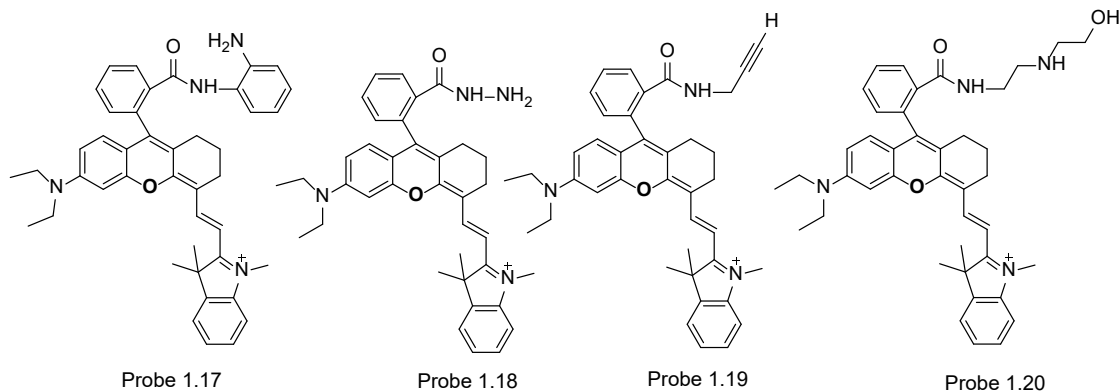
Figure 1.13. The ring opening form of near-infra red fluorescent probes in responding to acidic pH[65].

1.5.2.4 Rhodamine-based fluorescent pH probes

Rhodamine dyes (Rho) belong to a family of xanthene dyes and are among the oldest synthetic dyes used for the dying of fabrics. The general structure of xanthene and rhodamine are shown in Figure 1.14. Rhodamine-based fluorescent probes and their derivatives are widely used in cell biology. This is due to their excellent photophysical properties such as good photostability, high extinction coefficients, high quantum yield, and long absorption and emission wavelengths. Additionally, Rho dyes have a very unique merit when undergoing structural changes between their spirocyclic (non-fluorescent) and ring-opening (fluorescent) forms in response to pH changes[48, 66]. This makes them ideal for fluorescent on/off switches for pH sensing. The general mechanism of spirolactam ring opening and closing is illustrated in scheme 1.1 in section 1.4.3.

27
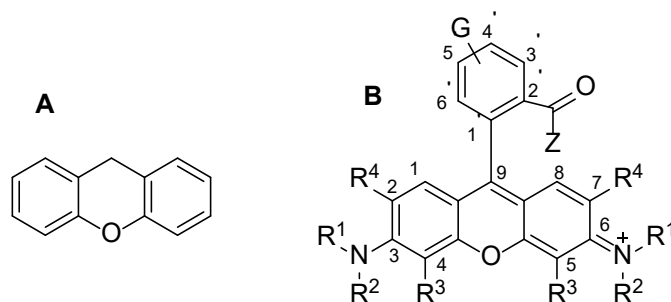
Figure 1.14. The molecular structure of xanthene (A) and rhodamine dyes (B)[66].

Some commercially available rhodamine dyes are rhodamine 6G (Rho 6G), rhodamine B (Rho B), and rhodamine 101 (Rho 101) (Figure 1.15). Rho B and Rho 101 are among the most commonly used and can exist in one of three forms, cationic, dipolar ionic (zwitterionic), and lactone, according to the pH or polarity of the solvents[66] (Figure 1.16). For example, in an acidic environment, the carboxyl group of Rho B is protonated resulting in the cationic form. However, in basic solution Rho B is converted to the dipolar form due to the dissociation process.
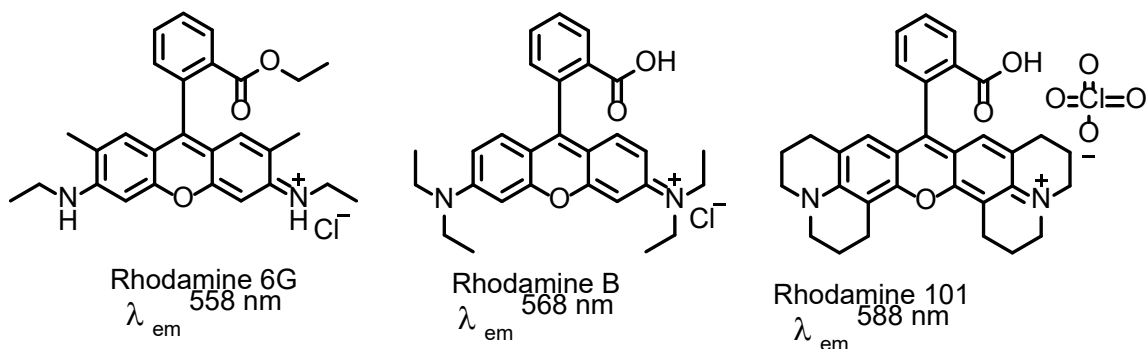
Figure 1.15. The molecular structures of the classical rhodamine dyes; rhodamine 6G, rhodamine B, and rhodamine 101[66].
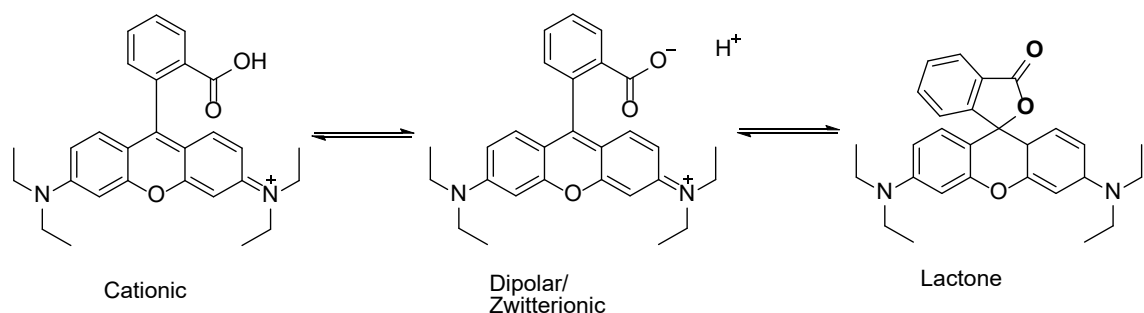
Figure 1.16. The molecular structure of three forms of Rho B in equilibrium[66].

The fluorescence switching of Rho dyes make them widely applicable for lysosomal pH detection. For example, Lv *et al.* synthesized the RCE indicator fluorescent probe, which is Rho B-based and specific for lysosomal pH (Figure 1.17: **Probe 1.21**). The fluorescence signal of the probe enhances in an acidic environment 150-fold. The enhancement in the fluorescence intensity occurs at 584 nm as the pH decreases from 7.51 to 3.53 [39]. Another fluorescent probe that is specific to lysosomal pH is the Lyso-hNR probe (Figure 1.17: **Probe 1.22**). This probe was synthesized and reported by the Niu research group. In an acidic environment the Lyso-hNR displayed NIR fluorescence at 650 nm. The high concentration of H^+ in the acidic solution caused a 280-fold fluorescence enhancement from pH 7.0 to 4.0[67]. Zhang and co-workers reported a ratiometric lysosomal pH fluorescent probe based on naphthalimide-rhodamine (RNL) (Figure 1.17: **Probe 1.23**). However, when the pH decreases from 7.2 to 4.20, the high concentration of protons results in the protonation of the piperazine nitrogen. Consequently, this leads to the opening of the spirolactam ring and an emission band at 529 nm resulting from the naphthalimide moiety is observed. Meanwhile, a new peak at 580 nm corresponding to the rhodamine moiety appears. The rhodamine moiety in its ring opening form is an effective energy acceptor.

Thus, fluorescence resonance energy transfer (FRET) from the donor (naphthalimide) to the acceptor (rhodamine) occurs (**Probe 1.23**, Figure 1.17)[48]. Similarly, Rho B-based fluorescent probe RML, (**Probe 1.24**) for lysosomal pH was non-fluorescent at pH 7.40 due to its closed-ring form. The fluorescence signals enhance 80-fold as the pH decreases from 7.40 to 4.0, leading to protonation of the nitrogen on the morpholine moiety. This significant enhancement in the fluorescent intensities is induced by protonation causing the spirocyclic ring opening[68].
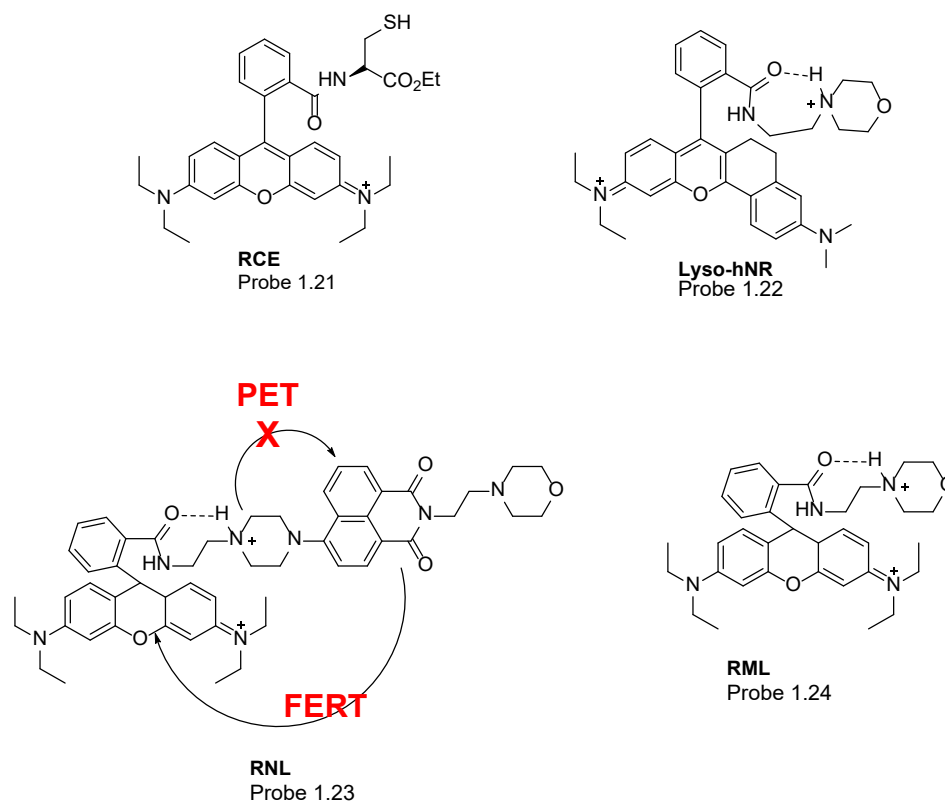
Figure 1.17. An example of some of the reported rhodamine-based fluorescent probes for lysosome pH[39, 48, 67-68].

1.6 Limitations and drawbacks of reported pH fluorescent probes

Developing fluorescent probes for biosensing applications still requires improvement. This is because the reported fluorophores are partially fulfilling the desired criteria of the ideal chromophores for biological imaging (Section **1.3.2**). For example, most of the reported BODIPY-based probes possess emissions < 700 nm that is still close to the visible region. Likewise, rhodamine-based fluorophores have short wavelength emissions (< 600 nm). This limitation dramatically restricts their applications for sensing and monitoring in biological systems. This is attributed to the strength of absorption and autofluorescence in biomolecules and organelles in the UV-Vis region. Moreover, light scattering and strong absorption in the UV-Vis region limit the penetration of the probes into living tissues. Another limitation of current UV-Vis fluorescent probes is the high autofluorescence that arises from the absorption of biomolecules in this region. This factor can lead to a low signal to noise ratio (S/N) due to high background noise, consequently reducing the ability to clearly visualize and recognize the fluorescence emission[1, 69].

Poor water solubility is another drawback in reported fluorescent probes. This problem usually arises from the large π-conjugation systems and the presence of aromatic rings. For instance, BODIPY dyes possess a hydrophobic core that brings a significant limitation of BODIPY-based pH sensors for living cell applications. Similarly, traditional cyanine dyes are less hydrophobic than BODIPY-based sensors, but they suffer from pale solubility in an aqueous environment. Fluorescent probes with hydrophobic characteristics are

susceptible to undesired self-aggregation in aqueous solution, which quenches the fluorescence signal.

Additionally, several drawbacks of reported cyanine probes limit their application for imaging. Some of these drawbacks include poor photostability, low quantum yield, and narrow Stokes shift[55, 70]. Besides the merit advantages of hemicyanine dyes like spirolactam structures, which allow for the switching process and NIR excitation and emission wavelength, hemicyanine dyes suffer from poor solubility in aqueous solution, self-aggregation, and fluorescence quenching in an aqueous environment.

For Rho-based fluorescent probes, the limited modification sites on their core structure minimize their usage in bioimaging applications. However, NIR Rho-based pH sensors have shown to be successful and applicable.

1.7 Research objective and aim

The focus of this dissertation is to overcome the current limitation and challenges discussed in Section **1.6** and better apply BODIPY, rhodamine and hemicyanine dyes to fluorescence sensing. We plan to alleviate this knowledge gap by modifying and developing highly sensitive and selective BODIPY-based and spirolactam ring-based fluorescent probes based on traditional rhodamine and hemicyanine dyes for lysosomal pH detection. To accomplish this goal, we plan to concentrate on two aspects: i) enhancing the water-solubility of BODIPY dyes and ii) developing NIR fluorescent pH probes to monitor lysosomal and mitochondrial pH.

In chapter 2, three BODIPY–based fluorescent probes (**A-C**) bearing morpholine residues at positions 4,4′ and 2,6 of the BODIPY core to selectively target lysosomes. To enhance their hydrophilicity and solubility in polar solvents, we will introduce *ortho* or *meta* substituent groups of tri(ethylene glycol)methyl ether on the *meso*-phenyl rings and at positions 1,7 of the BODIPY dyes.

To further extended lysosomal pH monitoring, we plan to develop three fluorescent probes (**A-C**) with higher pKa values (chapter 3). These fluorescent probes will contain closed spirolactam ring configurations with high pKa values for lysosomal pH detection in living cells. We plan to introduce 2-aminophenylboronic acid pinacol ester to traditional rhodamine B, its near-infrared derivative, and near-infrared hemicyanine dyes, respectively, to improve the sensitivity response. By doing this, we believe the probes will show fast, reversible, selective and sensitive fluorescence responses to pH changes, and will be capable of sensing lysosomal pH variations in living cells.

In addition to lysosomal pH, we will develop a near-infrared hemicyanine fluorescent probe with a switch "on/off" feature for mitochondrial pH sensing (chapter 4). To overcome the insensitivity of hemicyanine dyes lacking pH-dependent spirolactam switches, we will introduce oxazolidine to probe A to achieve the switch-ability for mitochondrial pH variations. If the modification to Probe A is successful, we plan to further study its use for detecting pH changes in the mitochondria, and monitoring cell nutrient starvation and drug treatment.

2 Unusual Fluorescent Responses of Morpholine-functionalized Fluorescent Probes to pH via Manipulation of BODIPY's HOMO and LUMO Energy Orbitals for Intracellular pH Detection[71]

Jingtuo Zhang,[a] Mu Yang,[a] Wafa Mazi,[a] Kapil Adhikari,[a] Mingxi Fang,[a] Fei Xie,[a]

Loredana Valenzano,[a]* Ashutosh Tiwari[a]*, Fen-Tair Luo[b]* and Haiying Liu[a]*

[a] Department of Chemistry, Michigan Technological University, Houghton, MI 49931

[b] Institute of Chemistry, Academia Sinica, Taipei, Taiwan 11529, Republic of China

Author contribution statement:

The author of this dissertation contributed to this paper by collecting and analyzing the spectroscopic data. Dr. Jingtuo Zhang was responsible for the synthesis, characterization of all reported compounds, and also for the written description of the synthesis of the reported compounds. Dr. Mu Yang collected cell imaging data. Dr. Loredana Valenzano did the computation methodology. Dr. Haiying Liu was the corresponding author. He was responsible for major writing and revision work of the manuscript.

2.1 Introduction

Intracellular pH (pHi) functions to regulate many cellular behaviors such as cell volume regulation, vesicle trafficking, cellular metabolism, cell membrane polarity, cellular signaling, and cell activation, growth, proliferation, apoptosis, enzyme activity, and protein degradation. The pHi inside cells may vary considerably among subcellular compartments such as the cytosol, mitochondria, endoplasmic reticulum, endosome, lysosome, and nucleus. The pHi in a typical mammalian cell can range from 4.7 in lysosome to 8.0 in mitochondria. The lysosomal acidic environment activates enzymes to facilitate the degradation of proteins during the cellular breakdown. Disruptive pHi variations in organelles can lead to dysfunction of the organelles that can result in pathophysiology in humans triggering cancer, stroke, and/or Alzheimer's disease. Therefore, it is very important to monitor pH changes inside living cells in order to investigate cellular functions that can provide insight into physiological and pathological processes. Fluorescence-based techniques such as fluorescence microscopy and flow cytometry with high-resolution and high-throughput analysis have been widely used to investigate intact subcellular pH and possess many technical and practical advantages over other methods because of their high sensitivity, operational simplicity, and unrivaled spatial and temporal resolution. Many fluorescent probes for pH have been developed. However, only a few of them have been successfully used to monitor lysosomal pH inside living cells[52, 54, 65, 72-76]. Most fluorescent probes for lysosomal pH, including the commercial ones have used morpholine residues for their selective accumulation in acidic lysosomes through protonation of the tertiary amine groups in a cellular acidic environment[77]. The fluorescence enhancement results

from the suppression of photoinduced electron transfer (PET) of the tertiary amine attached to the probe[77]. Our hypothesis was that fluorescent probes based on morpholine could display unusual responses to pH if we could effectively manipulate HOMO and LUMO energy orbitals of fluorophores so that the tertiary amines from morpholine residues were unable to serve as electron donors to quench the fluorophore fluorescence via a-PET ("a" denotes fluorophore serving as an electron acceptor) mechanism in a basic condition while the protonated morpholine moieties can function as electron acceptors to quench the fluorescence of the fluorophores via d-PET ("d" denotes excited fluorophore serving as an electron donor) mechanism. In this paper, we reported three uncommon morpholine based fluorescent probes (A, B, and C) to detect pH by introducing morpholine residues to BODIPY dyes at 4,4′-positions and 2,6-positions, respectively (Scheme 2.1). The fluorescent probes display high fluorescence in basic condition. However, they exhibit very weak fluorescence in an acidic condition. The theoretical calculation showed that the LUMO energy of morpholine is higher than those of the BODIPY dyes while its HOMO energy is lower than those of the BODIPY dyes. As a result, morpholine is unable to serve as an electron donor or an electron acceptor to quench the BODIPY fluorescence in the neutral and basic conditions via PET mechanism. However, the protonation of tertiary amines of the morpholine residues in an acidic environment effectively decreases the LUMO energy which locates between the HOMO and LUMO energies of the BODIPY dyes, resulting in fluorescence quenching of the BODIPY dyes via the d-PET mechanism. These probes also possess great photostability and selectivity at different pH values. Among them, fluorescent probe C has more advantages for live cell fluorescence imaging because it possesses long emission wavelength, large Stokes shifts and high pKa near

physiological pH and displays turn-on fluorescence responses to the increasing

intracellular pH, demonstrating the potential applications for noninvasive monitoring of

pH changes inside of living cells.
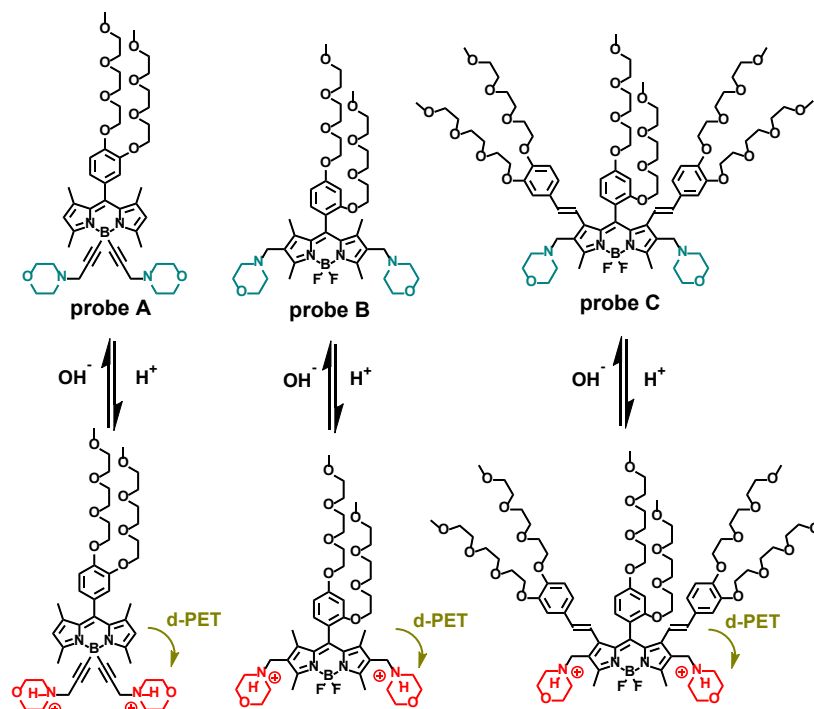
Scheme 2.1. Chemical structures of fluorescent probes **A**, **B** and **C** and their responses to

acid and base.

2.2 Experimental section

2.2.1 Instrumentation

^{1}H NMR and ^{13}C NMR spectra were collected by 400 MHz Varian Unity Inova NMR spectrophotometer instrument. ^{1}H NMR and ^{13}C NMR spectra were recorded in CDC$_{13}$ and DMSOd$_6$ solutions. Chemical shifts (δ) were given in ppm with solvent residual peaks (^{1}H: δ 7.26 for CDC$_{13}$, δ 2.50 for DMSO-d$_6$; ^{13}C: δ 77.3 for CDC$_{13}$) as internal standards. HRMS were measured with electrospray ionization (ESI) mass spectrometer. Absorption spectra were taken on a PerkinElmer Lambda 35 UV/vis spectrometer. Fluorescence spectra were recorded on a Jobin Yvon Fluoromax-4 spectrofluorometer.

Materials. Unless specifically indicated, all reagents and solvents were obtained from commercial suppliers and used without further purification. Compound 2 was prepared according to the reported literature[78].

Fluorescent Probe A. ^{1}H NMR (400 MHz, CDC$_{13}$): δ 6.99 (d, J = 8Hz, 1H), 6.85 (d, J = 2 Hz, 1H), 6.82 (dd, J = 2, 8 Hz, 1H), 6.00 (s, 2H), 4.21 (t, J = 5.2 Hz, 2H), 4.12 (t, J = 5.2 Hz, 2H), 3.91 (t, J = 5.2 Hz, 2H), 3.86 (t, J = 5.2 Hz, 2H), 3.79−3.51 (m, 24H), 3.38 (s, 3H), 3.36 (s, 3H), 3.28 (s, 4H), 2.73 (s, 6H), 2.56 (br, 8H), 1.45 (s, 6H). ^{13}C NMR (100 MHz, CDC$_{13}$): δ 155.1, 149.9, 149.5, 141.2, 130.1, 128.6, 121.5, 114.8, 114.6, 72.2, 71.2, 71.0, 70.9, 70.8, 70.0, 69.3, 69.0, 67.2, 59.3, 52.7, 48.8, 16.5, 15.0. HRMS (ESI): calculated for C$_{47}$H$_{67}$BN$_4$O$_{10}$Na [M + Na]$^+$, 881.4842; found, 881.4832.

Fluorescent Probe B. ^{1}H NMR (400 MHz, CDC$_{13}$): δ 6.95 (d, J = 8Hz, 1H), 3.59−3.55 (m, 2H), 4.13 (t, J = 4.8 Hz, 2H), 4.01 (t, J = 4.8 Hz, 2H), 3.86 (t, J = 4.8 Hz, 2H), 3.74−3.28

(m, 32H), 3.15 (s, 4H), 2.52 (s, 6H), 2.31 (br, 8H), 1.42 (s, 6H). ^{13}C NMR (100 MHz, CDCl$_3$): δ 161.2, 156.8, 155.2, 141.1, 138.7, 131.5, 130.2, 126.2, 117.2, 106.5, 100.7, 72.1, 72.0, 71.1, 71.0, 70.8, 70.7, 70.6, 70.4, 69.8, 69.2, 68.9, 67.8, 67.2, 59.2, 59.1, 53.5, 52.1, 12.9, 11.8. HRMS (ESI): calculated for C$_{43}$H$_{64}$BF$_2$N$_4$O$_{10}$ [M − H]⁻, 845.4792; found, 845.4809.

Fluorescent Probe C. ^{1}H NMR (400 MHz, CDCl$_3$): δ 7.18−7.09 (m, 3H), 6.77 (d, J = 8 Hz, 2H), 6.45 (s, 1H), 5.90 (d, J = 16 Hz, 2H), 4.14 (t, J = 5.2 Hz, 4H), 4.07 (t, J = 5.2 Hz, 4H), 3.90−3.40 (m, 72H), 3.38 (s, 3H), 3.37 (s, 6H), 3.36 (s, 3H), 3.34(s, 6H), 3.31 (s, 3H), 3.23(brs, 4H), 2.62 (s, 6H), 2.50 (s, 8H). ^{13}C NMR (100 MHz, CDCl$_3$): δ 172.5, 161.3, 157.8, 149.0, 148.9, 146.2, 142.7, 135.0, 131.3, 129.2, 124.3, 120.1, 114.4, 111.9, 106.7, 100.3, 97.5, 71.9, 71.8, 71.0, 70.8, 70.7, 70.6, 70.5, 70.4, 70.2, 69.7, 68.8, 68.6, 58.9. HRMS (ESI): calculated for C$_{85}$H$_{128}$BF$_2$N$_4$O$_{26}$ [M − H]⁻, 1669.8987; found, 1669.8971.

2.2.2 Optical measurement

Citrate-phosphate-borate buffer (20 mM) was used for pH dependency and photostability measurements of fluorescent probes. To avoid the interference caused by metal− phosphate and metal−citrate binding interactions (forming precipitates of divalent cation phosphate and forming a complex of the metal− citrate), 10 mM KHP buffer (pH 4.0) and 10 mM HEPES (pH 7.4) buffer were used for selectivity measurements of fluorescent probes A-C.

2.2.3 Computational modeling

Electronic properties of the chemical structures of the fluorescent probes were calculated using density functional theory (DFT) incorporating Hartree−Fock (HF) exchange with DFT exchange-correlation. In particular, the hybrid functional B3LYP[79-80] and all-electron basis sets 6-311G (2d, 2p)[81] as implemented in the Gaussian09 suite of programs[82] were used for full geometry optimization of the probes. HOMO and LUMO were calculated for the optimized geometries. All calculations were performed in a vacuum.

2.2.4 Live cell fluorescence imaging

Human umbilical vein endothelial cells HUVEC-C (from ATCC) were plated on 12-well culture plates at 1×10^5 cells/well and were incubated at 37 °C in 5% CO_2 incubator overnight. The next day, the medium was removed and cells were rinsed twice with 1× PBS (pH 7.4) followed by incubation with probe C for 2 h at 5, 15, or 25 μM concentration in fresh serumfree media containing 1 μM LysoSensor Green DND-189 (Life Technologies). Hoechst 33342 (Sigma-Aldrich) dye was added at 1 μg·mL^{-1}, and the cells were further incubated for 10 min. After incubation, the medium was removed, and cells were gently rinsed with 1X PBS (pH 7.4) three times. The cells were treated with nigericin (5 μg·mL^{-1}) in potassium rich PBS with pH ranging from 5.5 to 8.5 and incubated further for 15 min. Live cell images were acquired using an inverted fluorescence microscope (AMF-4306, EVOSfl, AMG) with DAPI filter for Hoechst 33342 (Sigma-Aldrich), GFP filter for LysoSensor Green, and RFP filter for fluorescent probe C. The fluorescence images were obtained at 40× magnifications. The exposure times for each filter were kept

constant. Colocalization analysis based on Pearson's coefficient was done using the JACoP plugin from ImageJ[83].

2.3 Results and discussion

2.3.1 Synthetic approach

In order to prepare morpholine functionalized BODIPY-based fluorescent probes for pH, we incorporated morpholine moieties onto the BODIPY core at 4,4′-positions and 2,6-positions while we introduced ortho- or meta-substituent group of tri(ethylene glycol)methyl ether on the meso-phenyl rings and at 1,7-positions of BODIPY dyes to enhance their hydrophilicity and solubility in polar solvents (Scheme2.2). Fluorescent probe A was prepared by replacing fluorine atoms of BOIDPY dye 1 at 4,4′-positions with 4-prop- 2-ynyl-morpholine (2) (BODIPY dye 1 was synthesized according to our reported procedure[84]. In order to incorporate morpholine moieties to 2,6-positions of BODIPY core, formyl groups were introduced to BODIPY dye 3 (which was also synthesized according to our reported procedure)[85-86] at 2,6- positions via two-step Vilsmeier−Haack reactions, affording 2, 6-diformyl BODIPY dye 4. Then a reductive amination of BODIPY dye 4 with morpholine was carried out by using sodium acetoxyborohydride to yield fluorescent probe B. To tune the BOIDPY core of fluorescence probe to a longer emission wavelength with smaller HOMO−LUMO energy gap, a Knoevenagel condensation of BODIPY dye 4 with benzaldehyde derivative (5) was conducted. The presence of formyl groups of BODIPY dye 4 at 2,6-positions initiated formation of distyryl bonds at 1,7-positions instead of 3,5-positions, yielding 2,6-diformyl-1,7-distyryl-BODIPY dye (6), which was confirmed by the clear disappearance of 1,7-dimethyl proton peak at 1.85 ppm and the preservation of

3,5-dimethyl proton peak at 2.92 ppm in ^{1}H NMR spectrum of BODIPY dye 6 (please see Figures A.3 and A.7 in the Supporting Information).
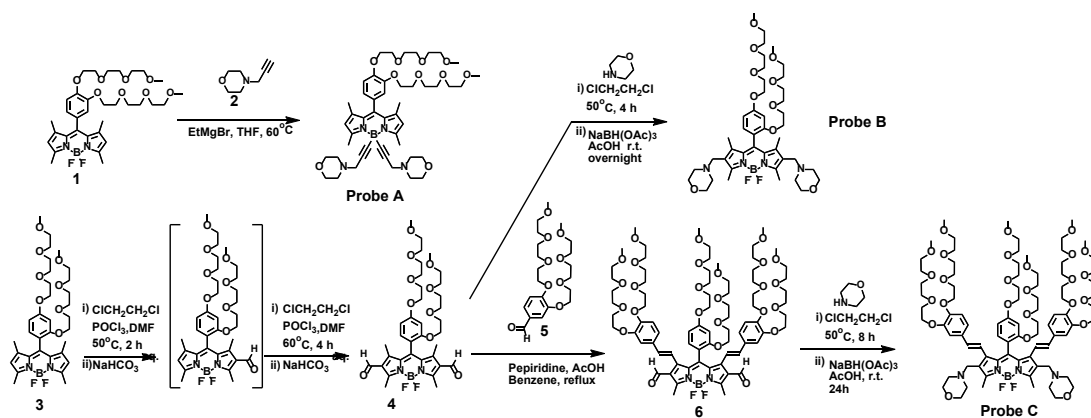
Scheme 2.2. Synthetic route to fluorescent probes **A**, **B,** and **C**.

This is because the 1,7-dimethyl groups become activated by the introduction of formyl groups at 2,6-positions to BODIPY core, which has been discussed in our previous paper[84]. 1,7-Distyryl BODIPY dye bearing morpholine groups at 2,6-positions (fluorescent probe C) was obtained by amination of BODIPY dye 6 with morpholine using sodium acetoxyborohydride in the same approach to prepare fluorescent probe B. Fluorescent probes A-C are easily dissolved in common organic solvents such as dichloromethane, ethanol, THF, DMF, and DMSO. They can also be readily dissolved in aqueous solution with the help of the small amount of polar organic solvent such as DMSO because of the hydrophilic features of tri(ethylene glycol)methyl ether residues and morpholine residues on the BODIPY cores.

2.3.2 Optical properties

Fluorescent probe A displays absorption and emission peaks of BODIPY dyes at 498 and 508 nm in ethanol, respectively. The fluorescence quantum yield of probe A in ethanol is 56%. Fluorescent probe B shows absorption and emission peaks at 515 and 529 nm with a fluorescence quantum yield of 8%, and exhibits 17 and 21 nm redshifts in absorption and emission spectra in ethanol, respectively, compared with fluorescent probe A. The redshifts in absorption and emission peaks of fluorescent probe B may be due to the enhanced electron donating effect of methylene groups with adjacent electron-donating tertiary amines from the morpholine groups at 2,6-positions to the BODIPY core compared with hydrogen atoms of fluorescent probe A at 2,6-positions, resulting in a decreased HOMO−LUMO energy gap. Compared with fluorescent probes A and B, the significant red shifts in both absorption and emission spectra were observed for fluorescent probe C with absorption and emission peaks at 565 and 652 nm in an ethanol solution, respectively, because of its significantly enhanced π-conjugation via its distyryl groups at 1,7-positions. In addition, we examined the optical properties of fluorescent

probes A-C in aqueous solution at physiological pH (with 1% DMSO as cosolvent). Fluorescent probes A and B show similar absorption and emission bands in aqueous solution with negligible shifts compared with those in ethanol while fluorescent probe C, with an enlarged Stokes shifts of 115 nm in aqueous solution which is 28 nm larger than its Stokes shift of 87 nm in ethanol, was interestingly observed with 15 nm blue shift in absorption peak and 13 nm red shift in emission peak relative to its absorption and emission peaks in ethanol (see Table A1 in the Supporting Information). The fluorescence quantum yields of the fluorescent probes A−C significantly dropped from ethanol to buffer solution

(pH 7.4) as fluorescent probes show fluorescence quantum yields of 18%, 1.3%, and 0.32% in buffer solution compared with those of 56%, 8%, and 8.6% in an ethanol solution, respectively. The low fluorescence quantum yields of the fluorescent probes in aqueous solution may result from fluorescence self-quenching due to the potential dye aggregations in aqueous solution.

2.3.3 Optical responses of fluorescent probes to pH

We investigated the pH effect of fluorescent probes A−C and their intermediates (BODIPY dyes 1, 4, and 6) in buffer solution. There were no obvious changes observed in both absorption and emission spectra of all intermediates 1, 4, and 6 in different pH conditions (see Figure A.11 in the Supporting Information). However, fluorescent probes A, B, and C exhibit very sensitive fluorescent responses to pH. They show very low fluorescence in acidic condition while most morpholine-functionalized fluorescent probes reported in the literature are highly fluorescent in acidic condition because of the prohibited a-PET effect from morpholine moiety to the fluorophore through the protonation of morpholine moiety[87]. However, change of the pH from an acidic condition of 3.0 to a basic condition of 9.5 results in significant increases of fluorescence intensity of fluorescent probes A-C with 2.4-fold, 15.7-fold and 14.3-fold enhancements, respectively (Figure 2.1). This unique pH-dependent behavior of the probes is in agreement with our hypothesis that protonated morpholine moieties can function as electron acceptors to quench the fluorescence of the BODIPY dye via d-PET mechanism while the tertiary amines from morpholine residues are unable to serve as electron donors to quench the BODIPY dye fluorescence via a-PET mechanism when the HOMO and LUMO energy orbitals of the BODIPY dye are

controlled in a certain range. Fluorescent probe A shows a significant fluorescence intensity change between pH 4.0 and pH 6.2 with a pKa of 5.0 while the significant fluorescence changes of fluorescent probes B and C shift to the window between pH 4.5 and 7.4 with the same pKa of 6.2 (Figure 2.1). The different pKa values indicate the different availability (or basicity) of the nitrogen lone-pair electrons on the morpholine moieties of the probes for protonation, where fluorescent probe A possesses the least availability due to the electron-withdrawing property of the alkyne groups adjacent to the morpholine moieties. In addition, 11 and 10 nm blue shifts in fluorescence and absorption spectra were observed for probe B, respectively, when pH decreases from 9.5 to 3.0. The blue shifts may arise from weaker electron donating effect of methylene groups with adjacent electron-withdrawing protonated tertiary amines from morpholine moieties at 2,6-positions in an acid condition. The similar blue shifts (13 and 16 nm shifts in fluorescence and absorption, respectively) of probe C were also observed due to the same weaker electron-donating effect of methylene groups at 2,6-positions in an acid condition. In addition, the absorbance of probes A−C at 470, 480, and 535 nm respectively, which were used as the excitation wavelengths for their corresponding fluorescence spectra, display negligible changes under different pH values, (Figure2.1). This further indicates that the pH responses of the probes are mainly due to d-PET effect instead of the absorbance change.
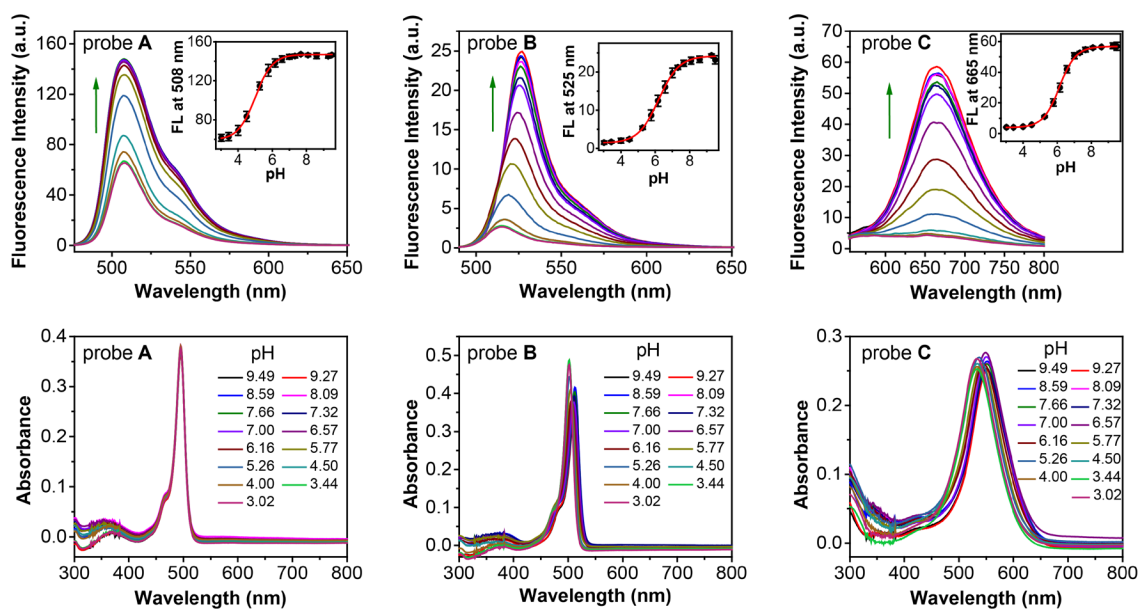
Figure 2.1. Fluorescence (upper row) and absorption spectra (lower row) of fluorescent probes A−C (5 μM) in buffer solutions with different pH conditions (1% DMSO as cosolvent). Insets in the upper row: the corresponding curves of fluorescence intensity versus pH.

2.3.4 Theoretical modeling

In order to further reveal the structural properties of the fluorescent probes, and more importantly, to verify the hypothesis that the fluorescent probes respond to pH via a modulation of d-PET effect from BODIPY core to protonated morpholine moieties in different pH conditions, we calculated the HOMOs and LUMOs of fluorescent probes A-C, N-methylmorpholine and protonated N-methylmorpholine using density functional theory (DFTB3LYP/ 6-311G(2d,2p)). The obtained results are shown in Figure 2.2. The results show that fluorescent probe B has a slightly smaller HOMO−LUMO energy gap (2.97 eV) than that of fluorescent probe A (3.07 eV), indicating a mild electron donating

effect of methylene groups with adjacent electron donating tertiary amine groups to the BODIPY core at 2,6- positions. This is in accord with the spectra redshifts observed in absorption and emission spectra of fluorescent probe B relative to those of fluorescent probe A in a basic condition (Figure 2 and Table A.1 in the Supporting Information). Fluorescent probe C possesses the smallest energy gap (2.39 eV) among three probes; an increase in the HOMO and a decrease in the LUMO arise from the enhanced π-conjugation occurring via the distryl groups on the BODIPY core at 1,7- positions. The density distributions of HOMO- and LUMO electrons on the probes show that there are no π-electrons spared onto the morpholine moieties for three probes (Figure 2.2), indicating that the morpholine moieties are isolated from π-conjugations of the BODIPY cores. We calculated the HOMO and LUMO energy of morpholine moieties before and after protonation using N-methylmorpholine as a model. As we expected, the calculated HOMO energy of morpholine moieties is lower than those of all three probes while its LUMO energy is higher than those of all three probes. This leads to a prohibited a-PET effect from morpholine moiety to the BODIPY cores. However, the protonation of the morpholine moiety in acidic condition dramatically reduces its HOMO and LUMO energies so that the LUMO energy of protonated morpholine moiety lies between the HOMO and LUMO energies of the probes. As a result, the protonated morpholine moiety is able to serve as an electron acceptor allowing for the electron transition be possible from the LUMO of the fluorescent probes A, B, or C to the LUMO of protonated morpholine moiety, resulting in the fluorescence quenching of the probes via a d-PET effect.
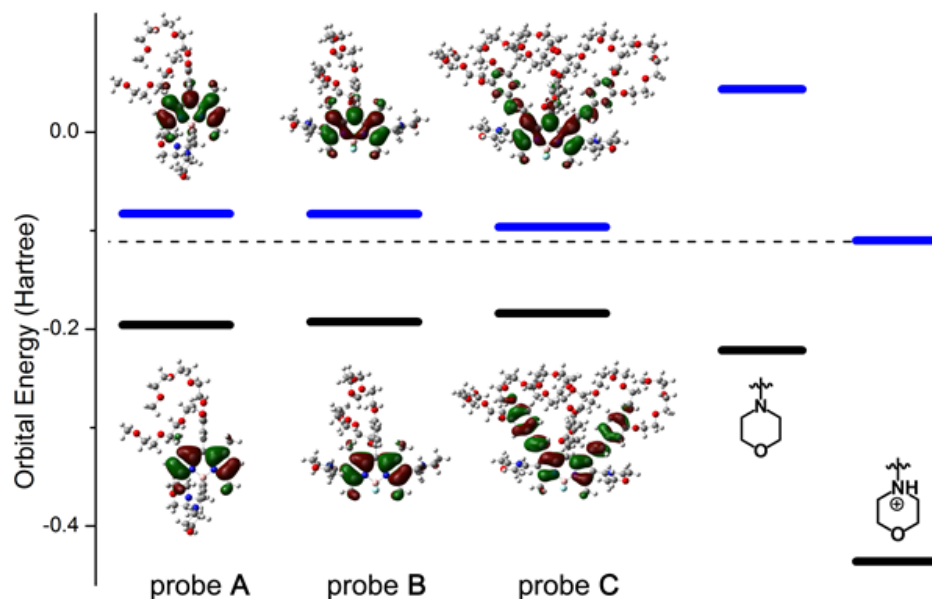
Figure 2.2. Comparisons of calculated HOMO and LUMO energies of fluorescent probes A-C, morpholine moiety (N-methylmorpholine), and protonated morpholine moiety (protonated N-methylmorpholine), as well as the electron density distributions in HOMO and LUMO of fluorescent probes A-C.

2.3.5 Selectivity and photostability

Considering the potential binding events between amines and metal ions when applying the fluorescent probes in complex environments such as physiological condition, we further investigate the selectivity of fluorescent probes to pH over other metal ions. The results showed that 5 μM fluorescent probes A−C display excellent selective responses to pH over other metal ions because there is no significant change observed in terms of fluorescence intensity of the probes in the absence and presence of different metal ions (200 μM) such as K^+, Na^+, $Mg2^+$ and $Ca2^+$, $Cu2^+$, $Zn2^+$, $Ni2^+$, $Mn2^+$, $Co2^+$, $Fe2^+$ and $Fe3^+$ in buffer solution at pH 4.0 and 7.4 (Figure 2.3: upper row). We also studied the

photostability of fluorescent probes A-C in both acidic (pH 4.0) and near neutral conditions (pH 7.4). Under 2-hour excitation (with an excitation wavelength of 470, 490, and 580 nm for fluorescent probes A-C, respectively), fluorescent probe A showed an excellent photostability with less than 1% decrease of fluorescence intensity within 2 h. Fluorescent probes B and C also showed very good photostability in pH 4.0. While in pH

7.4, the fluorescence intensity of fluorescent probe B decreased by 7.5% in the first hour and further decreased by 2% in the second hour under excitation and fluorescent probe C had a gradual decrease by 3% in fluorescence intensity within 2-hour excitation (Figure 2.3: lower row).
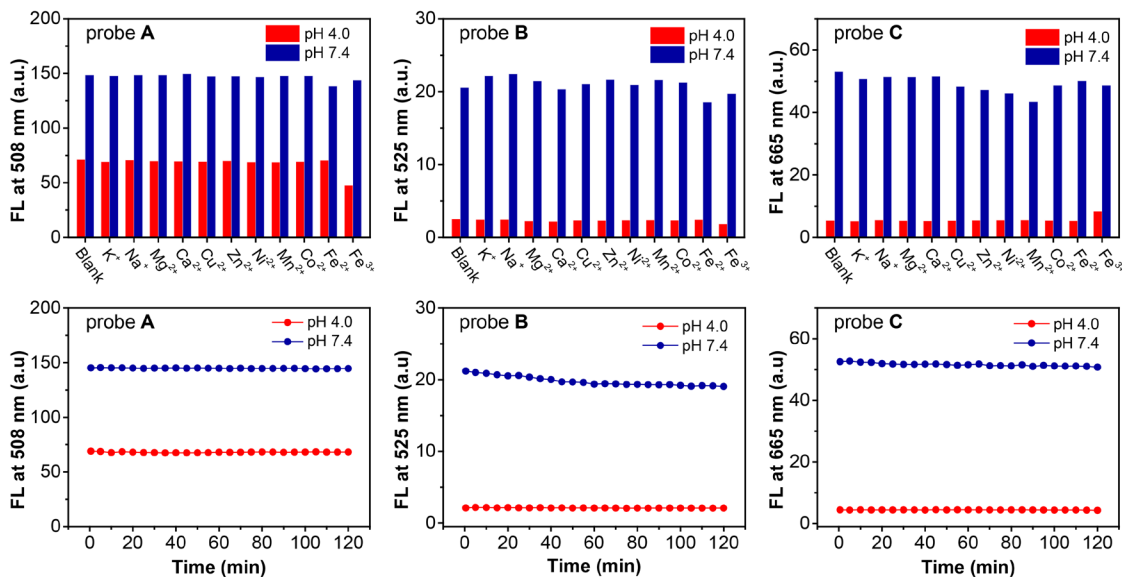
Figure 2.3. Upper row: fluorescence responses of fluorescent probes **A**, **B** and **C** (5 μM) to pH at 4.0 and 7.4 in the absence and presence of various metal ions (200 μM) in buffer solutions (with 1% DMSO as co-solvent). Lower row: fluorescence intensities changes of

fluorescent probes **A**, **B** and **C** (5 µM) as a function of time in 2 hours under excitation in buffer solutions (1% DMSO as co-solvent) at pH 4.0 and 7.4.

2.3.6 In vitro cell imaging and intracellular pH detection

In order to determine if the fluorescent probes could selectively detect intracellular pH changes in live cells, we chose the fluorescent probe C for live cell fluorescence imaging with normal endothelial (HUVEC-C) cells at different intracellular pH values. This is because fluorescent probe C has sensitive pH responses (14.3-fold enhancement from pH 3.02 to pH 9.49), pKa value near physiological pH, deep-red emission that prevents the cell photo-damage, and large Stokes shift (115 nm in buffer solution at pH 7.4) that minimizes the potential interference caused by excitation signals. It should be noted that many reported morpholine-bearing fluorescent probes show labeling of lysosomes and other acidic organelles in mammalian cells due to their accumulative effect of tertiary amines on the morpholine moieties in acidic conditions.[9] Therefore, to investigate whether our probe could respond to intracellular pH by identifying inherent acid compartments and determine concentration effect of the fluorescent probe on cell proliferation, we first incubated HUVEC-C cells with 5, 15, and 25 µM fluorescent probe C and compared with a well-known commercial lysosome probe, LysoSensor Green DND-189 that specifically labels the acidic organelles in cells. The results show that probe C exhibited very weak fluorescence signals in all three concentrations although slight fluorescence enhancements could be observed with increased probe concentrations (Figure 2.4).

| | Bright field | Hoechst | Lyso-Sensor Green | Probe **C** | Merged |

5 µM Probe C

15 µM Probe C

25 µM Probe C

100 µm
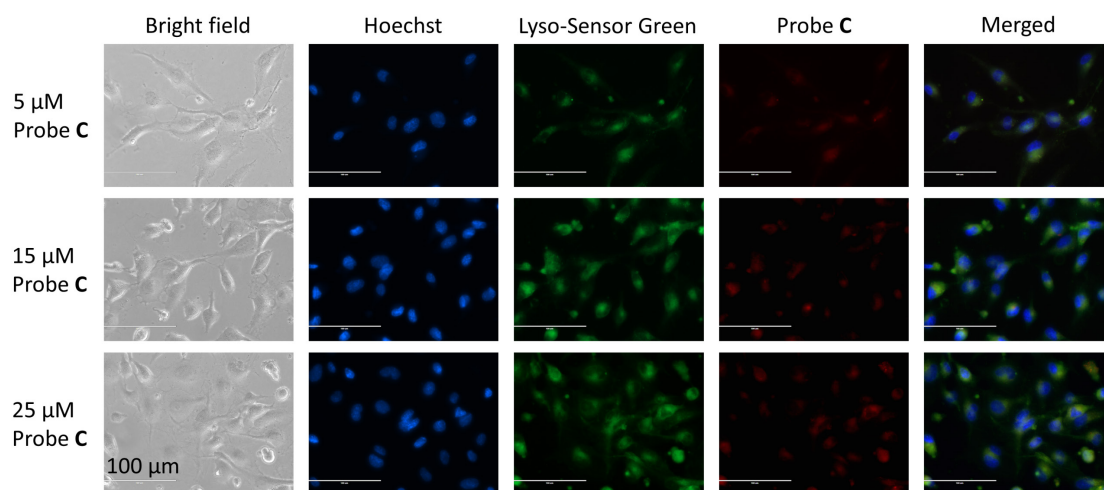
Figure 2.4. Fluorescence images of HUVEC-C cells incubated with 5, 15, or 25 µM fluorescent probe C. HUVEC-C cells were incubated with fluorescent probe C for 2 h, post serum starvation (2 h) and imaged for colocalization with 1 µM LysoSensor Green and 1 µg·mL^{-1} Hoechst 33342.stains. Images were acquired using the inverted fluorescence microscope (AMF-4306, EVOSfl, AMG) at 40× magnification; scale bars = 100 µm.

The merged fluorescence images show green-yellowish areas around the nucleus and many green-yellowish dot structures also can be observed by a careful examination (Figure 2.4). The calculated Pearson's coefficients of red (fluorescent probe C) and green (LysoSensor Green) channels are 0.92, 0.85, and 0.88 for 5, 15, and 25 µM probe C, respectively (please see Figures A.15−A.17 in the Supporting Information for cytofluorograms). The results indicate the area stained by the fluorescent probe C matches those stained by LysoSensor Green DND-189 in cells, which confirms fluorescent probe C mainly stained lysosomes or other acidic organelles in cells (Figure 2.4). Therefore, the weak fluorescence of probe C observed in the cells is able to be elucidated via a d- PET modulated fluorescence quenching by the protonated morpholine moieties under lysosomal

pH (4.5−5.5), which demonstrates feasible pH response of probe C to the inherent acidic environment in live cells. In order to examine the fluorescence responses of fluorescent probe C to different pH values inside of cells, we further incubated HUVEC-C cells with 5, 15, and 25 μM fluorescent probe C in buffer solutions (K^+ rich PBS) at pH 5.5, 6.5, 7.5, or 8.5 having nigericin (H^+/K^+ ionophore). Nigericin is a widely used ionophore for adjusting the intracellular pH (pHi) through equilibrating the intracellular and extracellular pHs. At all three concentrations, fluorescent probe C displayed very weak fluorescence at acidic pH (pH 5.5), whereas its fluorescence intensity showed gradual enhancement as intracellular pH increased from 5.5 to 8.5 (Figure 2.5). In addition, at each intracellular pH, higher probe concentration resulted in stronger fluorescence signals (Figure 2.5).
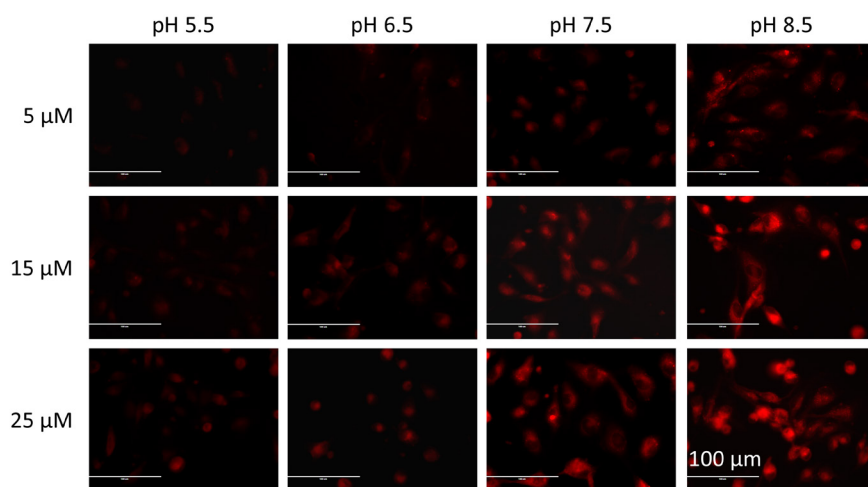
Figure 2.5. Fluorescence images of HUVEC-C cells incubated with 5, 15, or 25 μM fluorescent probe C in buffers at different pH values of 5.5, 6.5, 7.5, or 8.5 having nigericin. Images were acquired using the inverted fluorescence microscope (AMF-4306, EVOSfl, AMG) at 40× magnification; scale bars = 100 μm.

These responses of fluorescent probe C to intracellular pH are in line with its optical responses to pH changes in buffer solutions (Figure 2.1), which further proved the d-PET mechanism of fluorescent probe C at different pH values in live cells. However, the commercial lysosome probe LysoSensor Green DND-189 did not exhibit any fluorescent responses to intracellular pH changes (please see Figures A.18−A.20 in the Supporting Information). We also investigated the toxicity of fluorescent probe C to HUVEC-C cells using the MTS assay (Figure 2.6). At low concentration of 5 μM, the fluorescent probe C provided more than 80% cell viability, when the concentration increased to 15 μM, the cell viability dropped to 60−70%, indicating the low to moderate toxicity of fluorescent probe C to the cells in this concentration range. However, fluorescent probe C at higher concentrations like 25 μM and 50 μM were very toxic to the cells as less than 10% cell viability was observed, which may limit the application of the probe C with this high concentration, and the reason for this toxicity is still under investigation. However, we are still able to effectively image and visualize pH changes by using a low concentration of probe C (with less than 15 μM) with the relatively low cellular toxicity.
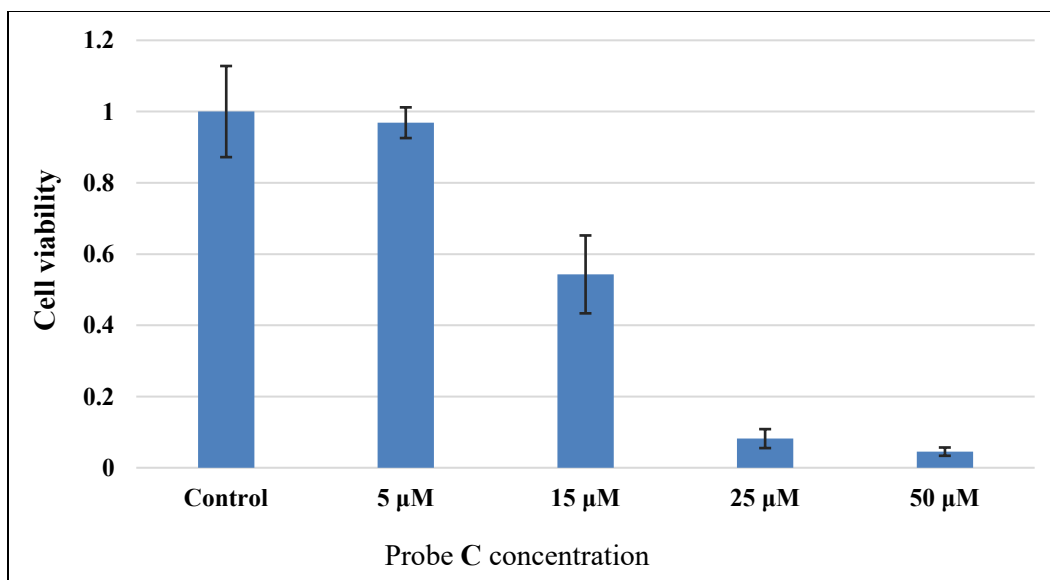
Figure 2.6. Concentration effects of fluorescent probe C on cell proliferation measured by MTS assay. HUVEC-C cells were incubated with 5, 15, 25, or 50 μM fluorescent probe C for 48 h. To this, 20 μL of MTS reagent was added per well, and absorbance at 490 nm was to determine cell viability. Error bars indicate ± SD.

2.4 Conclusion

We have successfully prepared three pH sensitive morpholine functionalized fluorescent probes A−C. These probes display unusual pH responses in aqueous solutions with high fluorescence in basic conditions while they exhibit very weak fluorescence in acidic condition due to the d-PET effect from protonated morpholine moieties to the BODIPY cores. All three probes are photostable and display selective responses to pH over common metal ions. Fluorescent probe C provided a potential noninvasive method with deep-red fluorescence and low background for monitoring intracellular pH changes inside of living cells.

3 Fluorescent Probes with High pKa Values Based on Traditional, Near-infrared Rhodamine, and Hemicyanine Fluorophores for Sensitive Detection of Lysosomal pH Variations

Wafa Mazi, Rashmi Adhikari, Yibin Zhang, Shuai Xia, Mingxi Fang, Rudy L. Luck, * Momoko Tajiri*, Ashutosh Tiwari* and Haiying Liu*

Department of Chemistry, Michigan Technological University, Houghton, MI 49931, E-mail: rluck@mtu.edu; mtajiri@mtu.edu; tiwari@mtu.edu; hyliu@mtu.edu

Author contribution statement:

The author of this dissertation was responsible for the synthesis, characterization of reported compounds A and C, collecting data for part of optical properties and the written description of the synthesis and the optical measurements of the reported compounds. The reported compound B was synthesized and characterized by Dr. Yibin Zhang. Dr. Mingxi Fang collected the fluorescence and absorption data. Rashmi Adhikari collected the collected cell imaging. Shuai Xia did the toxicity and colocalization experiment. Dr. Rudy L. Luck was responsible for the computation methodology. Dr. Haiying Liu was the corresponding author. He conducted data analysis and revised the manuscript.

3.1 Introduction

Various cellular processes including cell proliferation, cell growth, apoptosis, signal transduction, and cellular metabolism are very dependent on intracellular pH levels[54, 65, 68, 88-92]. Any pH variance from normal levels is often associated with cellular dysfunctions and serious diseases such as cancer and Alzheimer's [54, 88, 92-94]. The pH values inside cancer cells are different from those in normal cells [95]. For example, the extracellular pH (pH_{ex}) of tumor tissues is often acidic and at pH values between 6.2 to 6.9. Lysosomes function to break down biological molecules under acidic pH values from 4.0 to 6 [96-97]. Abnormal lysosomal pH can lead to lysosomal storage disorders. Therefore, accurate determinations of intracellular pH values are important in order to understand various physical, biological and pathological progressions. Many fluorescent probes have been developed for detection of intracellular pH and they normally demonstrate high sensitivity, selectivity, real-time spatial imaging, minimal damaging effects, and simplicity of operation [18, 96-101]. Traditional rhodamine dyes and their near-infrared derivatives have been used to develop fluorescent probes based on spirolactam molecular switches for pH detection in living cells because of their outstanding photophysical properties including high molar extinction coefficients, high fluorescence quantum yield, excellent photostability, and a large signal-to-background ratio [18, 100, 102-109]. These fluorescent probes are highly fluorescent under acidic conditions and are non-fluorescent under neutral and basic pH conditions. Introducing steric hindrance by attaching bulky residues to traditional rhodamine and derivatives to facilitate the acid-activated opening of the closed spirolactam rings at higher pKa values has been studied. However, most fluorescent probes with closed spirolactam molecular

switches are still non-fluorescent under basic pH conditions [104-110]. Therefore, it is important to overcome the non-fluorescent limitation of these fluorescent probes with closed spirolactam switches under basic pH conditions in order to take advantage of the outstanding photophysical properties of rhodamine and its derivatives.

In this article, we detail the design and syntheses of three fluorescent probes (**A-C**), Scheme 1, bearing closed spirolactam ring configurations with high pKa values for lysosomal pH detection in living cells by introducing a significantly sterically bulky 2-aminophenylboronic acid pinacol ester to traditional rhodamine B and its near-infrared derivative, and near-infrared hemicyanine dyes, respectively, in order to improve the spectroscopic properties of the dyes. Probes **B** and **C** based on near-infrared rhodamine and hemicyanine dyes, with pKa values of 5.45 and 6.97, display significant fluorescence peaks at 644 nm and 744 nm respectively under basic pH level of 8.8. Probe **A** similar to traditional rhodamine dyes is non-fluorescent with a pKa value of 5.81 under basic pH conditions. Probes **B** and **C** display activated fluorescent responses to both acidic and basic intracellular pH ranges and are capable of monitoring acidic pH variations in lysosomes.
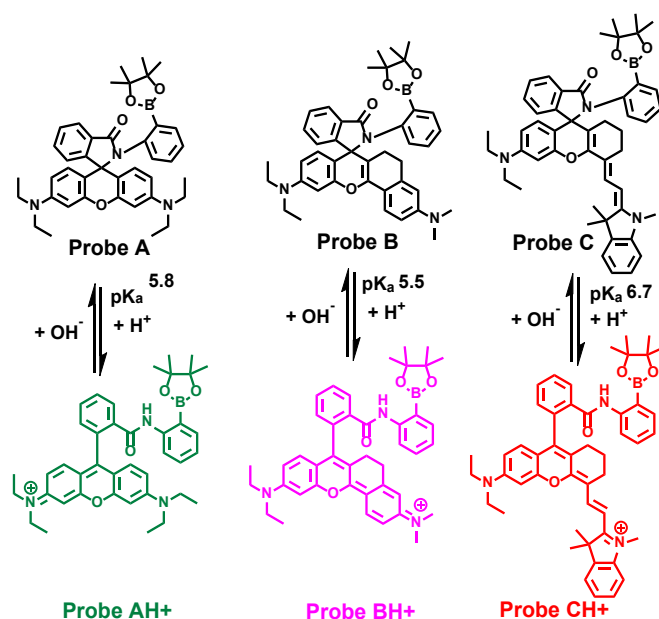
Scheme 3.1. Chemical structures of fluorescent probes in responses to pH changes.

3.2 Experimental section

3.2.1 Materials

Unless specifically indicated, all reagents and solvents were obtained from commercial suppliers and used without further purification.

3.2.1.1 Synthesis of fluorescent probe A

Rhodamine B (0.498 g, 1.04 mmol) was dissolved in 10 mL of dry dichloromethane, Bop reagent (0.707g, 1.6 mmol) and 0.5 mL of trimethylamine were added to the solution. After the reaction was stirred for 30 min, 2-aminophenylboronic acid pinacol ester (0.300g, 1.36 mmol) was added to the reaction mixture, the reaction mixture was stirred overnight at room temperature under a nitrogen atmosphere. The solvent was removed from the reaction mixture and the crude product purified by column chromatography using a four solvent

system hexane/ dichloromethane /ethyl acetate/MeOH 5/3/1/0.18 resulting in the product as a light pink solid with 58% yield.

^{1}HNMR (400 MHz, CDCl$_3$) δ: 7.99 (1H, d, J=6.88), 7.71 (1H, dd, J=5.92), 7.50 (3H, m), 7.09 (2H, m), 6.92 (1H, m), 6.59 (1H, d, J=8.2), 6.57 (1H, d, J=8.88), 6.42 (2H, d, J= 2.44), 6.14 (2H, dd, J= 2.52), 3.31 (8H, q, J= 7.08, 7.17), 1.44 (12H, s), 1.15 (13H, m); ^{13}C NMR (75 MHz, CDCl$_3$) δ: 167.54, 154.89, 152.15, 149.12, 131.57, 128.39, 127.98, 127.57, 126.71, 125.85, 123.59, 123.35, 116.58, 108.22, 104.42, 98.05, 80.96, 69.89, 44.46, 29.88, 26.44, 25.11, 12.78.

3.2.1.2 Synthesis of fluorescent probe B

Near-infrared rhodamine dye (4) was prepared by the condensation of 6-(dimethylamino)-3,4-dihydronaphthalen-1(2H)-one (3) with 2-(4-(diethylamino)-2-hydroxybenzoyl)benzoic acid in sulfuric acid at high temperature according to the literature [111]. Near-infrared rhodamine dye (4) (100.0 mg, 0.21 mmol) was then dissolved in 5 mL of dry dichloromethane, trimethylamine 0.5 ml and Bop (140 mg, 0.32 mmol) added and the mixture stirred for 15 min. 2-Aminophenylboronic acid pinacol ester (95.0 mg, 0.21 mmol) was dissolved in 2 ml of DCM and added to the reaction mixture and stirred at room temperature overnight under N2. The solvent was removed and crude was washed with water, extracted with DCM and dried over anhydrous sodium sulfate. The solvent was evaporated and the crude product was purified by column chromatography with dichloromethane/methanol (v/v) 50:1 and then (v/v) 20:1 producing the product as a blue solid in 20% yield.

^{1}HNMR (400 MHz, Acetonitrile-d3) δ: 10.20 (1H, s), 8.21 (1H, d, J=8.4), 8.15 (1H, m), 8.07 (1H, m), 7.79 (2H, m), 7.72 (1H, m), 7.60 (1H, m), 7.53 (1H, m), 7.33 (1H, m), 7.05 (1H, m), 6.86 (1H, d, J=2.48), 6.80 (2H, m), 6.47 (1H, d, J=2.48), 3.54 (4H, q, J= 7.24 and 7.24), 3.16 (4H, s), 2.87 (6H, s,s), 2.64 (4H, q, J= 9.12 and 8.88), 1.40 (12H, d, J= 2.92), 1.27 (6H, m); ^{13}CNMR (75 MHz, Acetonitrile-d_3) δ: 164.51, 164.27, 158.99, 156.83, 155.42, 153.49, 145.52, 144.27, 136.57, 135.37, 134.03, 133.03, 132.18, 131.27, 129.97, 129.84, 129.34, 127.04, 126.42, 123.78, 120.97, 119.33, 115.20, 114.88, 112.28, 110.75, 107.88, 96.43, 85.01, 45.79, 40.66, 37.80, 37.76, 37.12, 31.23, 30.00, 28.06,25.33, 25.29, 24.39, 12.80.

3.2.1.3 Synthesis of fluorescent probe C

Near-infrared hemicyanine dye (**8**) were prepared by the condensation of Fisher aldehyde (**7**) with 9-(2-carboxyphenyl)-6-(diethylamino)-1,2,3,4-tetrahydroxanthylium percloride (**6**) [64, 112]. Hemicyanine dye (**8**) (140 mg, 0.25 mmol) was then dissolved in dry dichloromethane (7 ml) and stirred under N_2. Trimethylamine (0.5 mL) and Bop (110 mg, 0.5 mmol) were added to the mixture. After the reaction was stirred for 15 min, 2-aminophenylboronic acid pinacol ester (114 mg, 0.52 mmol) in 2 ml of dichloromethane was added. This reaction mixture was stirred at room temperature overnight under N_2. The solvent was removed and the crude product washed with water and brine solution, extracted with dichloromethane and dried over sodium sulfate. The solvent was evaporated and the crude product was purified by column chromatography with dichloromethane /methanol (v/v) 50:1 and then (v/v) 20:1 to produce the product as a green solid with 15% yield.

^{1}HNMR (400 MHz, Acetonitrile-d_3) δ: 8.13 (1H, d, J=6 Hz), 8.04 (1H, m), 7.78 (2H, m), 7.45 (2H, m), 7.33 (3H, m), 7.11 (1H, m), 6.82 (1H, m), 6.71 (2H, m), 6.12 (2H, d, J=12Hz), 3.58 (3H, s), 3.53 (4H, m), 3.33 (1H, d, J= 6 Hz), 2.64 (2H, m), 2.37 (2H, t, J=6 Hz), 1.76 (6H, s), 1.35 (8H,s), 1.29 (2H, d, J=4.83), 1.23 (5H, m), 1.13 (2H, s); ^{13}CNMR (75 MHz, Acetonitrile-d_3) δ: 175.08, 168.32, 152.57, 136.63, 133.23, 132.25, 130.59, 130.18, 129.38, 128.90, 125.95, 124.30, 123.04, 119.70, 118.12, 116.58, 114.05, 112.68, 111.79, 96.90, 92.58, 85.49, 74.67, 50.26, 45.64, 32.20, 28.45, 27.53, 25.27, 21.33, 12.70.

3.2.2 Optical measurement

We investigated the effect of pH on the absorption spectra of the fluorescent probes. A citrate–phosphate buffer (0.1 M) was used for acidic pH and a carbonate-bicarbonate buffer (0.2 M) was used for basic pH. Ethanol 1.0% was used as a co-solvent. The photostability and selectivity measurements of the fluorescent probes were conducted under similar conditions to those employed for the investigation of the pH dependency.

3.2.3 Live cell imaging

MDA-MB231 and HUVEC-C cells were obtained from ATCC and cultured according to published protocols [113]. For imaging experiments, cells were plated in 12 well plates at the seeding density of $1x10^5$ cells/well and incubated overnight at 37 °C in a 5% CO_2 incubator. The cells were then rinsed twice with 1x PBS and subjected to serum starvation for two hours. Incubation with probe **A** (5µM/10µM), **B** (5µM) and **C** (5µM) was carried out for one hour in fresh serum free media containing 1 µM Lysosensor green DND-189 (Life Technologies) at 37 °C. Hoechst 33342, a nuclear stain (1 µg/mL) was added to the cells

and allowed to incubate for 10 minutes. After incubation, cells were rinsed thrice with potassium rich PBS prepared at different pH values of 4.5, 5.5, 6.5, 7.5 or 8.5. The cells were further incubated with nigericin (1 µg/mL) for 5 minutes in potassium rich PBS buffers at different pHs [53, 114]. Finally, the images were acquired using an inverted fluorescence microscope (AMF-4306, EVOSfl, AMG) at 60X magnification.

3.2.4 Computational details

Models suitable for calculations for probes **A**-**C** and their protonated versions were obtained as described previously[115] using Chem3d with MM2 minimization of energies[116], followed by force field (UFF) calculations in Avogadro[117]. The molecular data were refined using density functional theory (DFT) employed with the APFD functional [118] and electron basis sets initially at the 6-31*g(d) level to convergence in Gaussian 16 [119]. The final model was conducted with 6-311+g(2d,p) basis sets for all structures. Imaginary frequencies were not obtained in any of the frequency calculations. The excited states were assessed on the basis of TD-DFT optimizations[120] in a Polarizable Continuum Model (PCM) of water [121]. Results were interpreted using GaussView 6 [122] for all data and figures. The results of the calculations (including drawings of the molecular orbitals discussed) are given in detail in the Supporting Information.

3.3 Results and discussion

3.3.1 Probe design and synthesis

We chose traditional rhodamine and its near-infrared derivative, and near-infrared hemicyanine dye as fluorophore probes not only because of their excellent photophysical properties including high extinction coefficient, high fluorescence quantum yields, and excellent photostability,[93, 111, 123] but also their easy functionalization with amine derivatives to form different unique spirolactam molecular switches for different sensing and imaging applications. In order to increase pKa values of the fluorescent probes, we selected a considerably sterically bulky molecule, 2-aminophenylboronic acid pinacol ester, to modify these fluorophores. Traditional rhodamine B, Scheme 2, is commercially available while a near-infrared rhodamine dye (**4**) was prepared by the condensation reaction of 6-(dimethylamino)-3,4-dihydronaphthalen-1(2H)-one (**3**) with 2-(4-(diethylamino)-2-hydroxybenzoyl) benzoic acid (**2**) in sulfuric acid at high temperature [110]. Near-infrared hemicyanine dye (**8**) was prepared by the condensation reaction of 2-(4-(diethylamino)-2-hydroxybenzoyl) benzoic acid (**2**) with cyclohexanone (**5**) in sulfuric acid at high temperature, affording 9-(2-carboxyphenyl)-6-(diethylamino)-1,2,3,4-tetrahydroxanthylium perchlorate (**6**) upon addition of perchloric acid, and followed by further condensation of intermediate (**6**) with Fisher's aldehyde (**7**). Fluorescent probes **A**, **B** and **C** were each prepared by coupling the carboxylic acid residues of rhodamine B, near-infrared rhodamine dye (**4**) and hemicyanine dye (**8**) respectively with 2-aminophenylboronic acid pinacol ester (**1**) in the presence of benzotriazol-1-

yloxytris(dimethylamino)phosphonium hexafluorophosphate (BOP) reagent in methylene

chloride containing triethylamine, see Scheme 2. The chemical structures of the probes

were characterized by ^{1}H and ^{13}C NMR and electrospray ionization mass spectrometer

(ESI-MS).
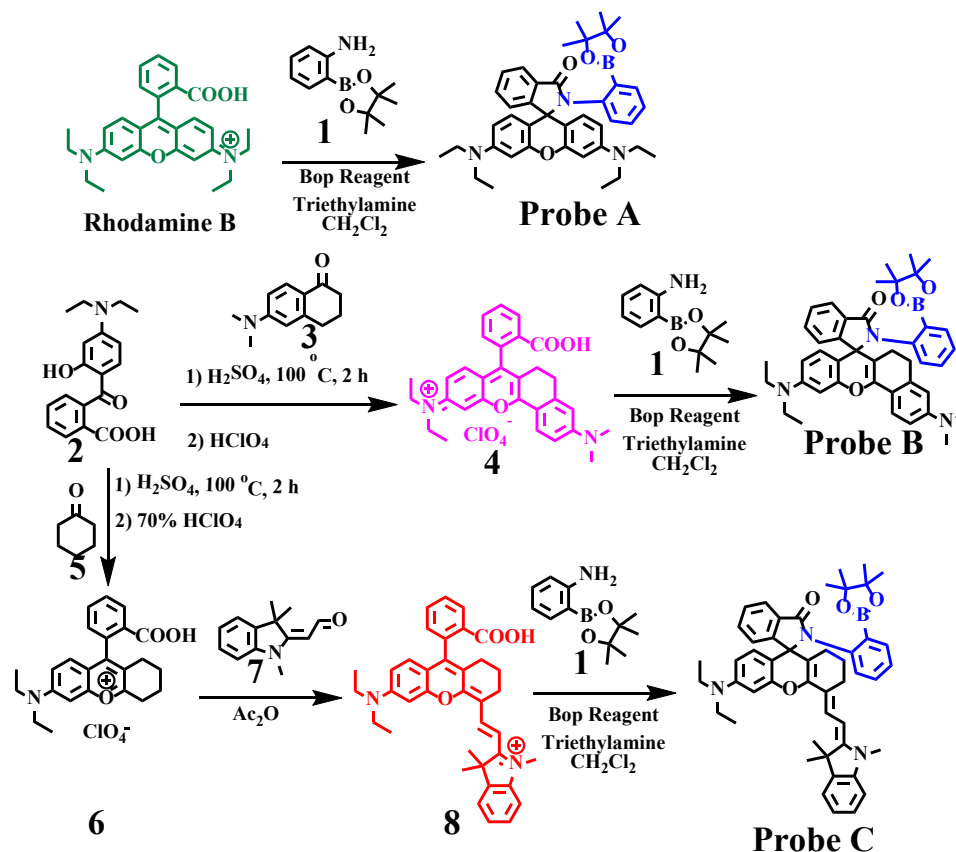
Scheme 3.2. Synthetic approach to prepare fluorescent probes **A**, **B, and C**.

3.3.2 Absorption responses of the probes to pH changes

We obtained the absorption spectra of the probes in 0.1 M citrate–phosphate (pH 2.0 to

7.0) and phosphate-phosphate buffers (pH 7.0 to 10.8) containing 1% ethanol (Figure 3.1).

Probe **A** displays no absorption above 400 nm at neutral and basic pH environments as it

retains a closed spirolactam configuration. Gradual pH decreases from 7.6 to 2.0 results in gradual absorbance increases of an absorption peak in now probe AH^+ at 567 nm (Figure 3.1). Probe **A** has a pKa value of 5.8 based on a plot obtained by titration of absorption and pH, Figure B.16. Probe **B** has moderate absorption peak at 619 nm at basic pH 8.8, indicating that partial opening of the spirolactam ring configuration occurs under basic conditions due to the interactions between the sterically bulky 2-aminophenylboronic acid pinacol ester residue and the H atoms in the dihydronaphtyl moiety. Decreases of pH from 8.8 to 2.0 lead to substantial absorbance increases in the absorption peak at 619 nm. Probe **B** was assessed to have a similar pKa value at 5.5 compared to probe **A**, Figure B.14. Probe **C** exhibits noticeable a near-infrared absorption peak at 724 nm and two short absorption peaks at 538 nm and 387 nm at a basic pH level of 10.8. Probe **C** responds to gradual pH decreases from 10.8 to 3.0 with significant absorbance increases of the near-infrared absorption peak, which is gradually blue shifted to a maximum of 10 nm upon attaining a pH of 3.0. Probe **C** has the highest pKa value of 6.31 among the three probes. The different pKa values of the probes can be ascribed to differences in the magnitude of steric hindrance between the closed spirolactam moiety, xanthene and its derivative cores and also the different nature of the conjugation obtained upon protonation.
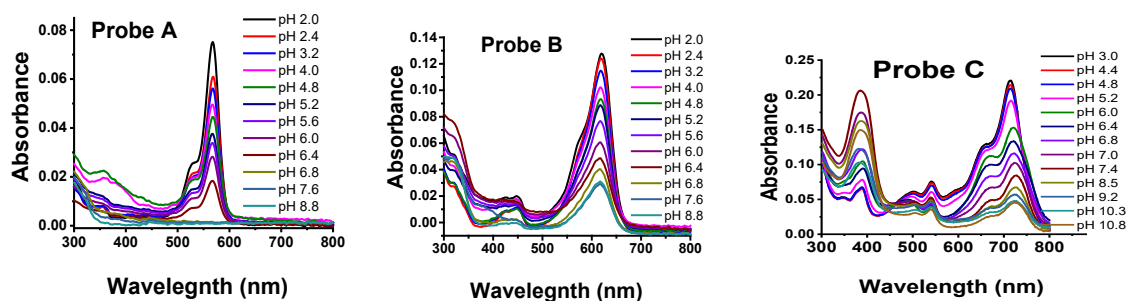
Figure 3.1. Absorption spectra of probes **A**, **B**, and **C** and their respective protonated versions in different pH buffers containing 1% ethanol. Citrate-phosphate buffers were used for pH values from 2.0 to 7.0 while phosphate buffers were employed for pH values from 7.0 to 10.8.

We also evaluated fluorescence responses of the probes to pH changes in 0.1 M citrate-phosphate or phosphate buffer solutions containing 1% ethanol (Figure 3.2). Via this method, probes **A-C** have pKa values of 5.81, 5.45 and 6.97, respectively as calculated using the Boltzmann equation, see Figs B.13-B.15. These pKa values obtained via fluorescence measurements are in good agreement with those obtained by absorption but these data had better R^2 values. Probe **A** based on traditional rhodamine B is non-fluorescent under neutral and basic pH conditions as it contains a closed spirolactam ring. Probe **A** reacts to pH decreases from 6.8 to 2.0 with significant fluorescence increases at 580 nm which is due to extended conjugation in the rhodamine moiety as a result of the opening of the spirolactam ring structure. In contrast, probes **B** and **C** show moderate fluorescence peaks at 650 nm and 740 nm at pH 8.8 and 10.8, respectively. Under basic pH conditions, a small percentage of probes **B** and **C** may exist in the protonated ring-opened spirolactam form. It may be possible for the larger steric hindrance (as described

69

above) in probe **B** to more than compensate for the slightly lower pKa value as compared

to that in probe **A**, whereas probe **C** has the steric hindrance and the highest pKa value.

Additionally, our previously reported probe containing a dihydronaphthyl moiety and an

adjacent ethylenediamine instead of the much larger aminophenylboronic acid pinacol

ester group exhibited a pKa of 5.15 and was only fluorescent under acidic conditions [124].

Decreasing the pH from 8.8 to 2.0 (in probe **B**) and from 10.8 to 3.0 (in probe **C**) further

activates ring opening of the spirolactam structures which significantly enhances

fluorophore π-conjugation, and, consequently increases the fluorescence intensity of probe

B and **C** at 650 nm and 740 nm, respectively.
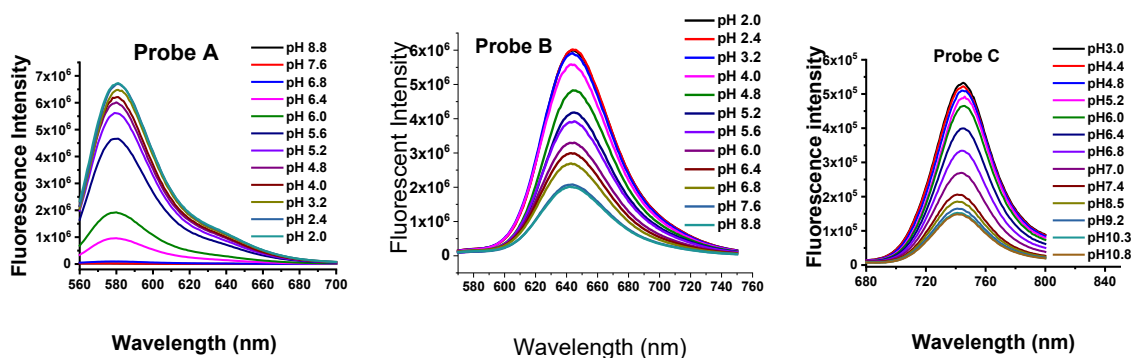
Figure 3.2. Fluorescence spectra of probes **A**, **B**, and **C** in different pH buffers containing

1% ethanol after excitation at 530 nm, 560 nm, and 660 nm, respectively. Citrate-phosphate

buffers were used for pH values from 2.0 to 7.0 while phosphate buffers were employed

for pH values from 7.0 to 10.8.

3.3.3 Calculations

In order to understand the nature of any structural changes that the probes may experience

upon protonation and to clarify the nature of the electronic transitions, theoretical

calculations were conducted in Gaussian 16[119] using the Austin-Frisch-Petersson functional with dispersion (APFD)[118]. TD-DFT optimizations[120] in a Polarizable Continuum Model (PCM) of water[121] were employed to calculate excited states. Visible evidence of the hindrance between the 2-aminophenylboronic acid pinacol ester residue and an adjacent H atom in the dihydronaphtyl moiety in probes **B** and **C** is displayed in Figure 3.
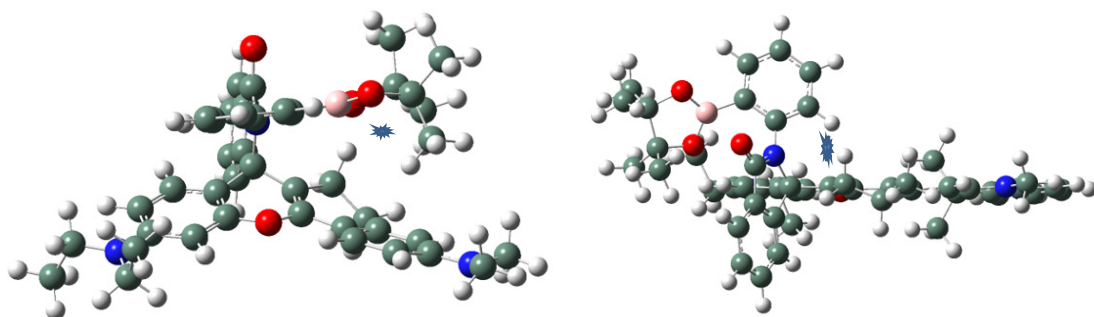
Figure 3.3. GaussView [122] drawings of probes **B** (left) and **C** (right) where the steric interactions are indicated with a ✷.

Comparing the optimized geometries of the probes **A-C** to the protonated versions **AH+-CH+**, as is presented in Figures: B.22 to B.28, Figures: B.33 to B.40 and Figures: B.45 to B.50 respectively, it is clear a more open structure was reached in the protonated probes as the N to C atom bond in the spirolactam ring breaks and the rhodamine part of the molecule become more conjugated. This can also be observed in the data listed in Table 3.1, which list a comparison of selected distances and reveals that shorter distances are obtained upon

protonation. Specifically, there is a shortening of the bond distances in going from probe **A** to probe **AH**$^+$ as there is extended and equivalent resonance structures in the rhodamine moiety as the equal distances for 4-5 and 6-7 would indicate, see Table 3.1.

However, due to the insertion of the dihydronaphtyl moiety in probes **B** and **C**, evidence of the resonance structure depicted in Table 3.1 for these molecules is present in the different distances calculated for the equivalent bond lengths, in particular between 1-2 and 1-3. Interestingly there was no difference between 4-5 and 6-7 for probe **B** but in probe **C** a difference was obtained possible signifying a more electron rich N atom at position 7.

We find transitions for probes **A** and **B** occur in the UV range as excited state 6 in Table S4 and excited state 4 in Table B.8 occur at 300 and 327 nm, respectively. The addition of acid for these probes results in ring opening, a conjugated rhodamine moiety and a shift in the transition to the visible range calculated (expt) to be at 473 nm (567 nm) and 522 nm (619 nm) for probes **AH**$^+$ and **BH**$^+$ respectively. For probe **C**, a transition at 388 nm as excited state 2 in Table B12 was calculated and involved π to π^* orbitals on the hemicyanine moiety as the MOs in Figs. B.48 and B.49 indicate.

Table 3.1. Comparison of equivalent bond distances in the probe **A-C** and their protonated versions.

Probe **AH**$^+$ Probe **BH**$_+$ Probe **CH**$^+$
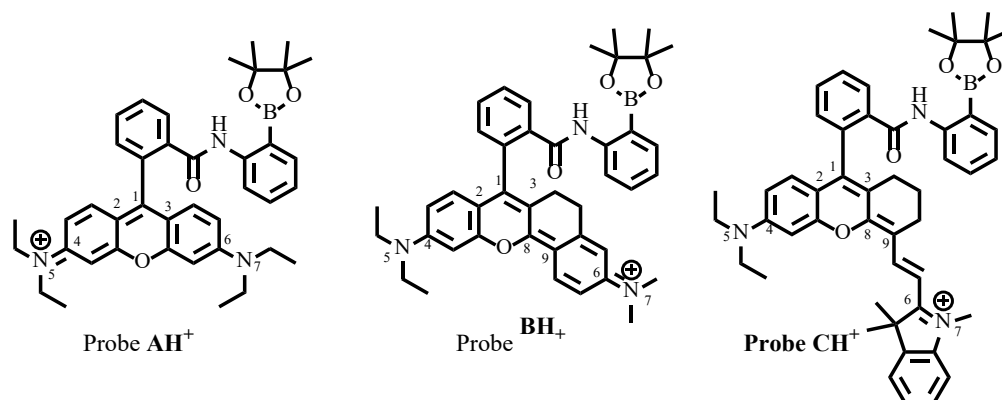
Bond distances	Probe A	Probe B	Probe C
1-2	1.503	1.498	1.498
1-3	1.507	1.505	1.507
4-5	1.366	1.366	1.367
6-7	1.365	1.375	1.376
8-9		1.455	1.454
Bond distances	**Probe AH**$^+$	**Probe BH**$^+$	**Probe CH**$^+$
1-2	1.401	1.409	1.415
1-3	1.398	1.384	1.377
4-5	1.343	1.348	1.359
6-7	1.343	1.348	1.349
8-9		1.421	1.406

The extended conjugation upon protonation to produce probe **CH**$^+$ resulted in a transition at 591 nm (724 nm) listed as excited state 1 in Table B14. The nature of the conjugation is best summarized in an inspection of the current density diagrams, which illustrates the direction of the electron flow from the HOMO to the LUMO. The illustration shows that electron density originates from the N atoms located at either end of the bottom section of the illustrations and moves towards the middle. The 2-aminophenylboronic acid pinacol ester residues are not involved with these transitions.
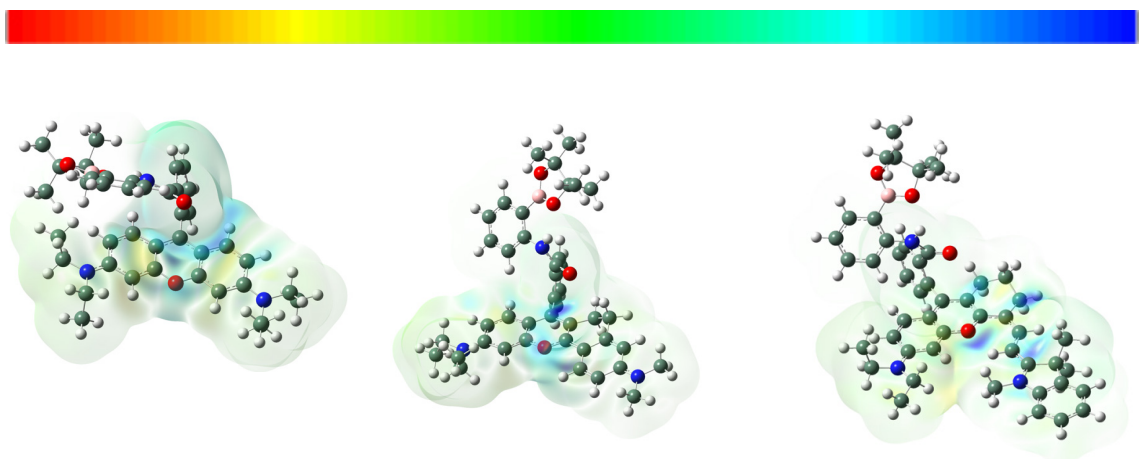
AH⁺-ES1, 473 (567) nm   BH⁺-ES1, 522 (619) nm   CH⁺-ES1, 591 (724) nm

172 → 173, 99.0%   178 → 179, 98.8%   203 → 204, 99.8%

Figure 3.4. Current density difference illustrations as iso-surfaces for probe **AH⁺** (left), **BH⁺** (middle) and **CH⁺** (right) as indicated for the excited states (ES) and the calculated and (experimental) wavelength. The composition of that specific ES together with percentage contribution is also indicated. Drawings of the molecular orbitals (MOs) are available in Supporting Information. The different density color scale ranges are $\pm7.562e^{-5}$ for **AH⁺**, $\pm4.797e^{-5}$ for **BH⁺** and $\pm6.454e^{-5}$ for **CH⁺**, see the scale at the top of the illustration with red negative and blue positive.

3.3.4   The selectivity of the probes

We investigated whether the probes react with 200 μM concentrations of various separate cations and anions in buffers at two different pH levels, namely, 2.0 and 7.4, see Fig. 3.5. There is no significant interference with probe responses to pH in the presence of cations

such as Al^{3+}, Ca^{2+}, Co^{2+}, Cr^{3+}, Cu^{2+}, Fe^{3+}, Hg^{2+}, K^+, Mg^{2+}, Mn^{2+}, Ni^{2+} and Zn^{2+} ions, or anions such as Cl^-, Br^-, SO_3^{2-}, NO_2^-, NO_3^-, S^{2-}, CO_3^{2-} and HCO_3^-. These results indicate that the probes maintain high selective fluorescence responses to pH without interference from these cations and/or anions.
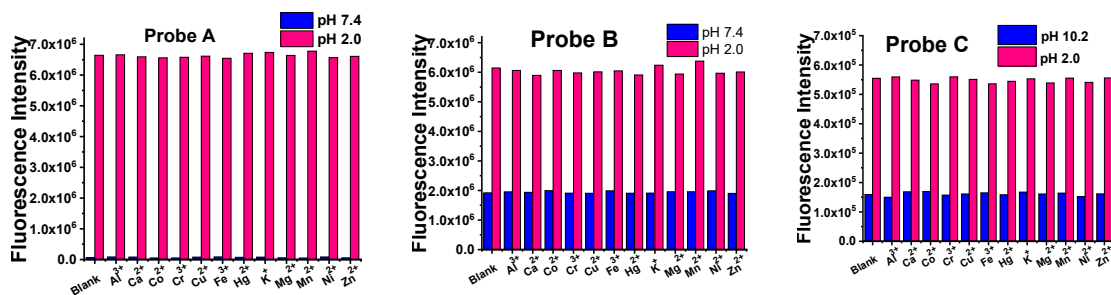
Figure 3.5. Fluorescence responses of probes **A**, **B** and **C** to pH in the absence and presence of cations and anions under excitation of 530 nm, 560 nm, and 660 nm, respectively.

3.3.5 Probe photostability and their reversible responses to pH

We investigated the photostability of fluorescent probes **A**, **B** and **C** in a pH 2.4 buffer under three-hour continual excitation at 530 nm, 560 nm, and 660 nm, respectively. Fluorescent probes **A-C** showed excellent photostability with less than 4% decrease in fluorescence intensity during the three-hour excitation (Figure 3.6). In addition, probes **A**, **B** and **C** show reversible response to pH change between 7.4 and 2.4 (Figure 3.7).
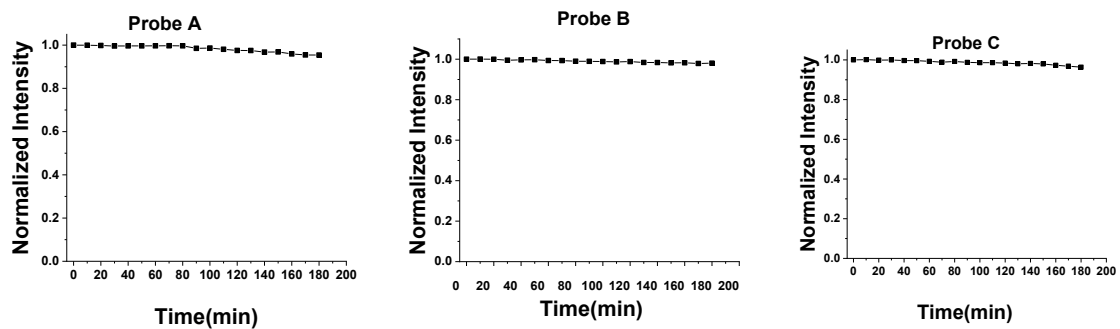
Figure 3.6. Fluorescence intensity of probes **A, B,** and **C** in a pH 2.4 buffer under three-hour continual excitation of 530 nm, 560 nm, and 660 nm.
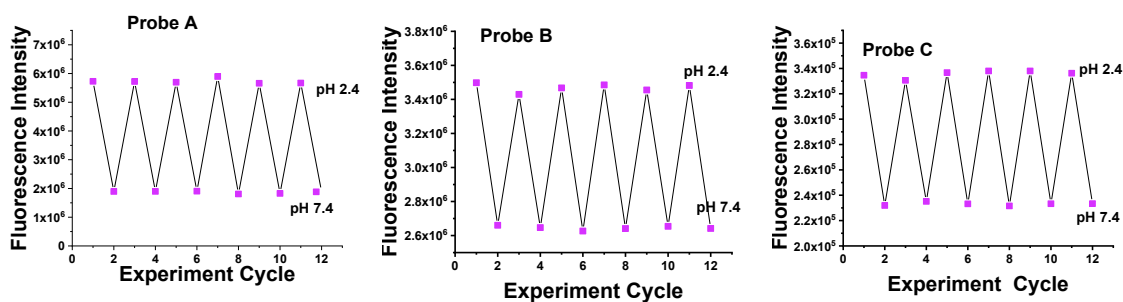
Figure 3.7. The reversible response of pH changes between pH 2.4 and 7.4 of probes **A-C** under excitation of a wavelength of 530 nm, 560 nm, and 660 nm respectively.

3.3.6 Low cytotoxicity of the probes

An MTS assay was employed to evaluate the cytotoxicity of the probes with different concentrations from 5 μM to 50 μM for the viability of HeLa cells. We observed that cell viability values with 50 μM probes are higher than 82.3% suggesting no significant cytotoxicity occurs. Therefore, the low cytotoxicity and thus excellent biocompatibility allow for cellular imaging application (Figure 3.8).

76
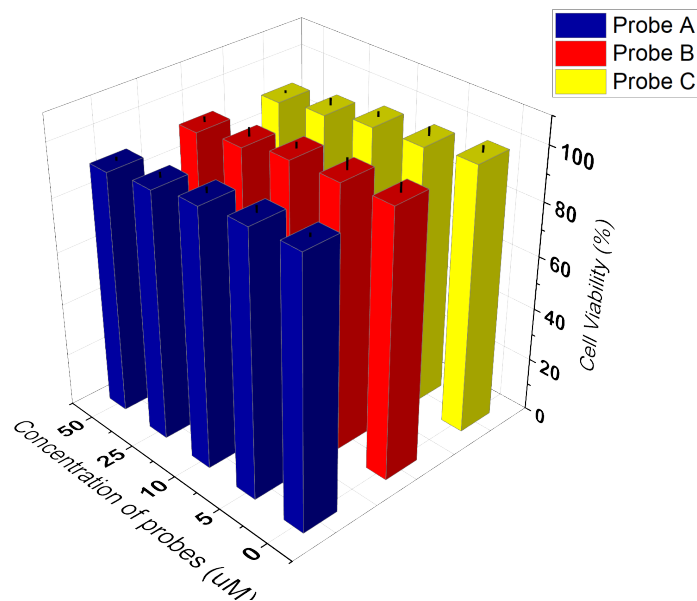
Figure 3.8. Cytotoxicity of probes **A**, **B**, and **C** obtained by MTS assay. The HeLa cells were incubated with 0, 5, 10, 25, and 50 μM of probes **A**, **B**, and **C** for 48 h. The relative cell viability was normalized to untreated cells and the cell viability has a linear relationship with the absorbance at 490 nm. The error bars indicate ± SD.

3.3.7 Live cell fluorescence imaging

We conducted cellular imaging of the probes by costaining breast cancer cell line (MDA-MB231) and human umbilical vein cells (HUVEC-C) with probes **A**, **B** and **C**, and a commercially available lysosome-targeting lysosensors Green DND-189 for co-localization analysis to determine whether the probes are located in the organelles of living cells (Figure 3.9). The high Pearson's colocalization coefficients of more than 0.92 confirmed that the probes are localized in the lysosomes of living cells.
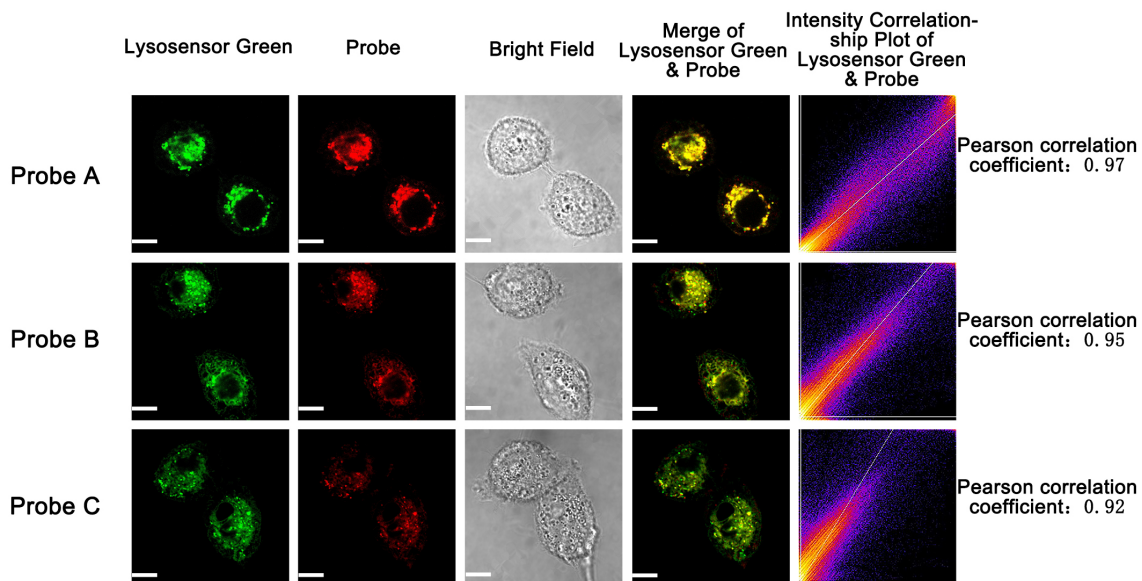
Figure 3.9. Fluorescence images of probes **A, B,** and **C** in HeLa cells were incubated with 5 µM probe **A, B,** and **C** in pH 7.4 buffer. Lysosensor Green DND-189 (1 µM) was used for co-localization. The images were acquired using confocal fluorescence microscopy at 200X magnification and the scale bar is 20 µm. The excitation of Lysosensor Green was 488 nm and the images of Lysosensor Green were collected from 500 to 550 nm. For probe **A** and **B**, the excitation wavelength was 559 nm and the images were collected from 580 to 630 nm. For probe **C**, the excitation wavelength was 635 nm and the images were collected from 720 to 770 nm

In order to quantitatively appraise fluorescence responses of the probes to intracellular pH changes, we incubated two different cell lines, breast cancer cell line (MDA-MB231) and HUVEC-C (see supplemental Figures B.56-B.61) with the probes in different pH buffers from pH 4.5, 5.5, 6.5, 7.5, to 8.5 in the presence of 1 µg/mL nigericin ionophore, which is employed to exchange K^+ ions for H^+ ions across most cellular membranes, and equilibrate intracellular pH with extracellular pH in buffer solutions[104, 107-109, 114, 125-129]. All cellular imaging for probe **A** were acquired by using an RFP light cube and for probes **B** and **C**, a CY5 light cube was used. The fluorescence intensity of probe **A** gradually becomes enhanced when the intracellular pH is lowered from 8.5 to 4.5 since pH decreases leads to the opening of closed spirolactam ring of probe **A**, and enhance the fluorescence of probe **A** with extended π-conjugation (Figures 10, B.56, B.60 and B.61). Probes **B** and **C** also respond to intracellular pH decreases from 8.5 to 4.5 with gradually fluorescence increases (Figures 11-12, B.57-B.61).
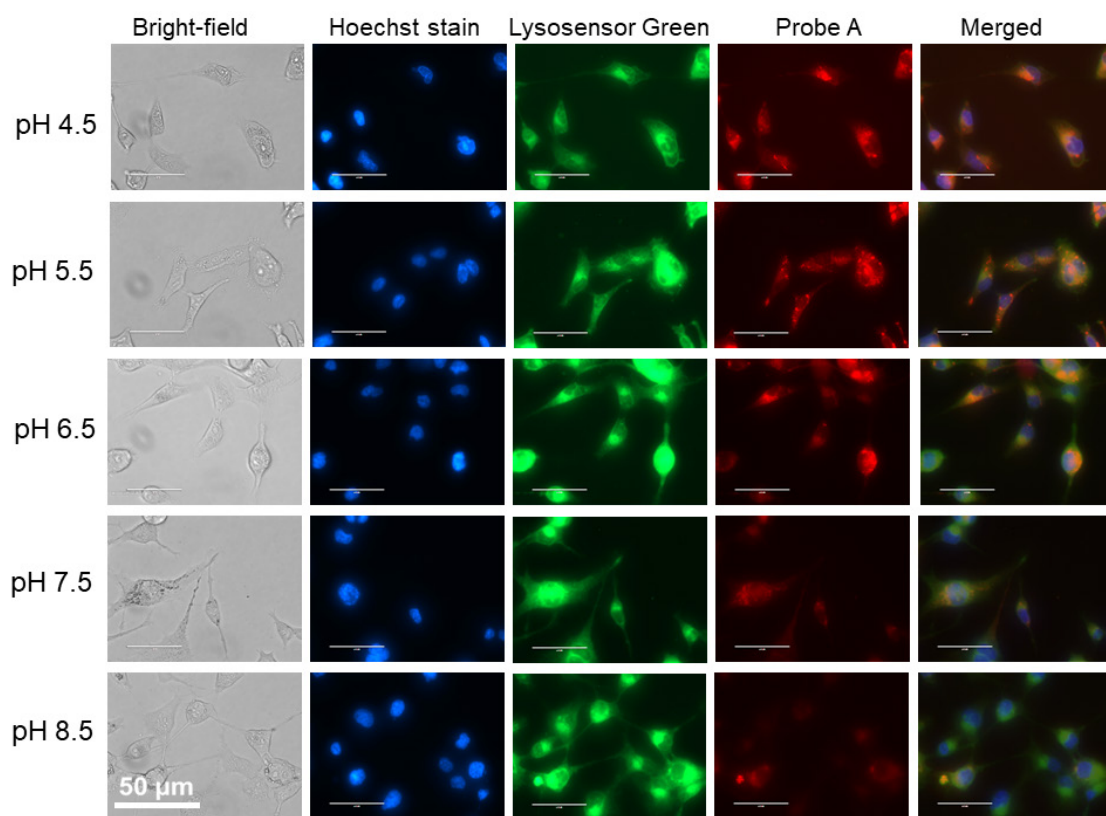
Figure 3.10. Fluorescence images of probe **A** in MDA-MB231 cells. MDA-MB231 cells were incubated with 10 µM probe **A** in buffers with different pH values ranging from pH 4.5 to 8.5 in the presence of nigericin (1 µg/mL) for 1 h before imaging. Lysosensor Green DND-189 (1 µM) and Hoechst 33342 (1 µg/mL) were used for co-localization. The images were acquired using an inverted fluorescence microscope (AMF-4306, EVOSfl, AMG) at 60X magnification.
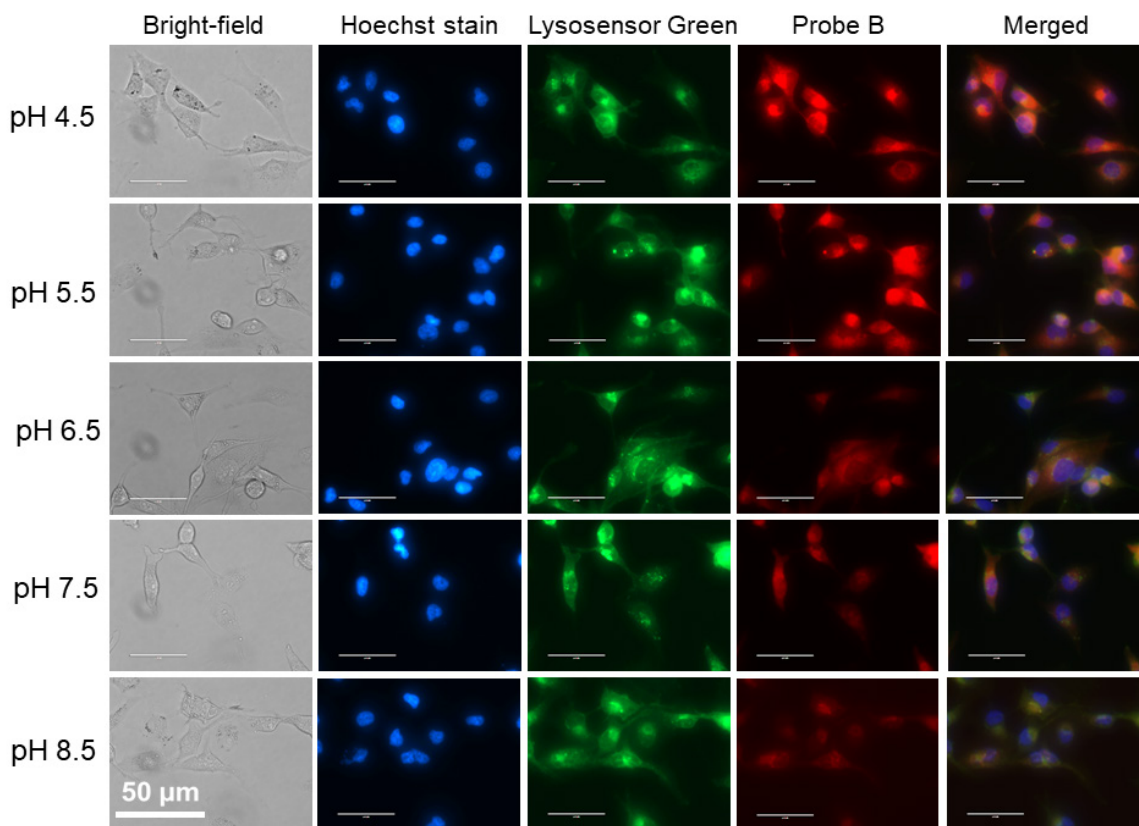
Figure 3.11. Fluorescence images of probe **B** in MDA-MB231 cells. MDA-MB231 cells were incubated with 5 µM probe **B** in buffers with different pH values ranging from pH 4.5 to 8.5 in the presence of nigericin (1 µg/mL) for 1 h before imaging. Lysosensor Green DND-189 (1 µM) and Hoechst 33342 (1 µg/mL) were used for co-localization. The images were acquired using an inverted fluorescence microscope (AMF-4306, EVOSfl, AMG) at 60X magnification.
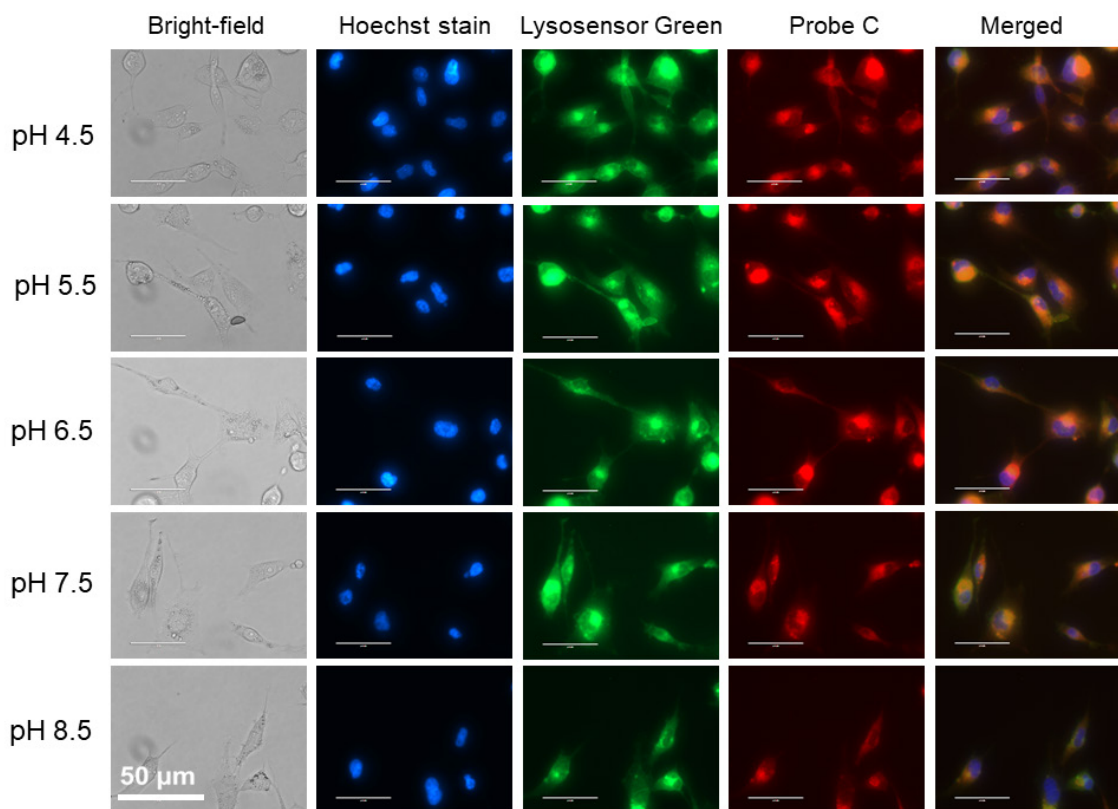
Figure 3.12. Fluorescence images of probe **C** in MDA-MB231 cells. MDA-MB231 cells were incubated with 5 μM probe **C** in buffers with different pH values ranging from pH 4.5 to 8.5 in the presence of nigericin (1 μg/mL) for 1 h before imaging. Lysosensor Green DND-189 (1 μM) and Hoechst 33342 (1 μg/mL) were used for co-localization. The images were acquired using an inverted fluorescence microscope (AMF-4306, EVOSfl, AMG) at 60X magnification.

3.4 Conclusion

Three lysosome-targeting fluorescent probes with high pKa values have been developed by coordination of the sterically bulky 2-aminophenylboronic acid pinacol ester to traditional rhodamine, a near-infrared rhodamine dyes, and a near-infrared hemicyanine dye to form closed spirolactam ring structures. The probes have low cytotoxicity, excellent reversible pH responses, and high selectivity to pH over cations and anions. They have been applied to visualize intracellular pH changes in live cells.

4 A Near-infrared Fluorescent Probe Based on an Hemicyanine Dye with an Oxazolidine Switch for Mitochondrial pH Detection

Wafa Mazi, Shuai Xia, Yibin Zhang, Yunnan Yan, Shulin Wan, Momoko Tajiri,* Rudy L. Luck* and Haiying Liu*

Department of Chemistry, Michigan Technological University, Houghton, MI 49931, E-mail: rluck@mtu.edu; mtajiri@mtu.edu; tiwari@mtu.edu; hyliu@mtu.edu

---

This chapter is a manuscript under preparation for publication.

Author contribution statement:

The author of this dissertation was responsible for collecting data for optical properties and the written description of the optical measurements of the reported compound. Dr. Yibin Zhang synthesized and characterized the reported compound A. Shuai Xia collected the cell imaging. Dr. Rudy Luck was responsible for the computation methodology. Dr. Haiying Liu was the corresponding author. He conducted data analysis and revised the manuscript.

4.1 Introduction

Mitochondria possess double-membranes composed of phospholipid bilayers and proteins, and act as the energy-supplying organelle in almost all eukaryotic cells. Mitochondria have vital roles for cells metabolism such as regulating the cellular redox state, production of reactive oxygen species (ROS), regulation of Ca^{2+} homeostasis, regulation of the cell cycle and cell growth, and cellular death and apoptosis[130-134]. Under ideal physiological conditions, mitochondrial function under a slightly alkaline microenvironmental at a pH value of ~ 8.0 compared to the other subcellular compartments of the cell.[135-136-137] These functions of the mitochondria depend on the pH level within the mitochondrial. Deviations of the normal mitochondrial pH is associated with mitochondrial dysfunction that is present with many human disorders such as neurodegenerative and neuromuscular diseases, obesity and diabetes, cancer and inherited mitochondrial disease[133, 138-139]. Therefore, an accurate and sensitive detection of mitochondrial pH will provide a better understanding of mitochondrial biology.

Small organic fluorescent probes are the essential tool for bioanalysis and real-time bioimaging technologies because of their superior features of excellent sensitivity and high spatial resolution[18, 132, 140]. Fluorescent probes with near-infrared absorption and emission wavelengths have advantages of deep tissue penetration, low biological fluorescence background, and lest photodamage impact to live cells and tissues. Near-infrared hemicyanine and rhodamine dyes bearing spirolactam switches have been developed to monitor pH changes in live cells, and their pKa values significantly depend on bulky degrees of residues in spirolactam switches[48, 64]. In order to monitor pH in mitochondria,

ideal fluorescent probes should possess mitochondria-targeting capability and high pKa values, which it is difficult to achieve by using spirolactam switches in hemicyanine and rhodamine dyes. In addition, fluorescent probes based on hemicyanine and rhodamine dyes with spirolactam switches are often used to detect pH changes in lysosomes instead of mitochondria because these neutral probes serve as weak bases and specifically accumulate in lysosomes. With this in mind, we developed a near-infrared fluorescent probe (**A**) for the detection of pH changes in mitochondria by introducing an oxazolidine switch into a hemicyanine dye to overcome pH insensitivity of the near-infrared hemicyanine dyes without spirolactam switches. Under basic conditions, the hemicyanine dye undergoes a ring-closing reaction to form an oxazolidine switch, resulting in fluorescence quenching as the free hydroxyl group engages in a nucleophilic attack onto the indolenium moiety. Acidic pH effectively converts the oxazolidine switch into a hemicyanine moiety with significant π-conjugation through proton-activated oxazolidine ring-opening, and leads to gradual fluorescence enhancement at 725 nm and absorbance increases at 713 nm upon pH decreases from 10.0 to 5.0. Probe **A** shows good photostability, good selectivity to pH, low cytotoxicity, and reversible fluorescence to pH changes with pKa value of 7.5(1). The probe has been successfully used to determine pH changes in mitochondria.
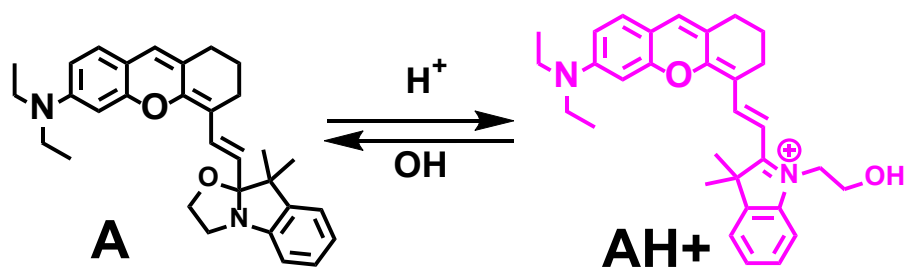
Scheme 4.1. Chemical structure of fluorescent probe with an oxazolidine switch in response to pH changes.

4.2 Experimental

4.2.1 Materials

Unless specifically indicated, all reagents and solvents were obtained from commercial suppliers and used without further purification. 6-(Diethylamino)-2,3-dihydro-1H-xanthene-4-carbaldehyde (3) (283 mg, 1 mmol) and 1-(2-hydroxyethyl)-2,3,3-trimethyl-3H-indol-1-ium salt (4) were prepared according to reported procedure.

4.2.1.1 Synthesis of fluorescent probe A

After 6-(diethylamino)-2,3-dihydro-1H-xanthene-4-carbaldehyde (3) (283 mg, 1 mmol) and 1-(2-hydroxyethyl)-2,3,3-trimethyl-3H-indol-1-ium (4) (204 mg, 1 mmol) were added to 10 mL of acetic anhydride, the mixture was stirred for 5 hours at 80 °C. The reaction mixture was concentrated in vacuo and diluted with dichloromethane, washed by water and brine, dried over anhydrous Na_2SO_4. The solution was filtered and the filtrate was concentrated. The residue was purified by using flash column chromatography through gradient elution with methanol to dichloromethane ratio from 5 % to 10 %, affording the

product as a green sold. ^{1}HNMR (400 MHz, Chloroform-d) δ 8.48 (d, J = 14.1 Hz, 1H), 7.49 (s, 1H), 7.43 – 7.34 (m, 3H), 7.23 (d, J = 1.2 Hz, 1H), 6.79 (dd, J = 9.0, 2.5 Hz, 1H), 6.49 (d, J = 2.4 Hz, 1H), 6.23 (d, J = 14.2 Hz, 1H), 4.55 (d, J = 5.2 Hz, 2H), 4.50 (d, J = 5.3 Hz, 2H), 3.53 (q, J = 7.1 Hz, 4H), 2.75 (t, J = 6.1 Hz, 2H), 2.70 (t, J = 6.0 Hz, 2H), 2.03 (s, 2H), 1.87 (d, J = 0.7 Hz, 2H), 1.74 (s, 2H), 1.32 – 1.23 (m, 6H). ^{13}CNMR (101 MHz, Chloroform-d) δ 170.68, 170.59, 163.54, 156.42, 142.33, 140.72, 130.01, 128.88, 125.59, 122.43, 117.73, 116.01, 111.21, 77.50, 60.82, 60.62, 49.74, 45.47, 44.25, 29.98, 29.10, 28.84, 24.93, 20.99, 20.92, 16.72, 12.72. MS/Z=469.4

4.2.2 Optical measurement

A citrate–phosphate buffer (0.1 M) was used for acidic pH and a carbonate-bicarbonate buffer (0.2 M) was used for basic pH and a 10% ethanol as a co-solvent was used to investigate the effect of pH on the absorption spectra of the fluorescent probe. The photostability and selectivity measurements of the fluorescent probes were conducted under similar conditions to those employed for the investigation of the pH dependency.

4.2.3 Live cell imaging

HeLa cells were seeded in 35 mm confocal glass bottom dishes (MatTek) with $1×10^5$ cells per dish and cultured for 24 h before cellular imaging was conducted. For co-localization experiment, HeLa cells were incubated with 5 µM probe **A**, 1 µM Hoechst and either 1 µM Lysotracker Red or 1 µM Rhodamine 6G for 30 min, followed by washing the cells twice with PBS buffer before cellular imaging was performed. For visualization of intracellular pH changes, HeLa cells were rinsed with PBS buffer twice before they were incubated with

nigiricin (5 µg/ml) in different pH citric buffers ranging from 5.0, 6.0, 7.0, 8.0, 9.0 to 10.0 for 30 min to equilibrate the intracellular and extracellular pH.[109, 114, 126, 128-129, 141] The cells were further incubated with 10 µM probe **A** for 30 min and followed by rinsing the cells with FBS buffer twice before imaging was carried out. The cells were imaged with a 200X objective lens for the colocalization study and with a 60X objective lens for the other imaging experiments. The fluorescence of nucleus dye Hoechst (blue channel) under 405 nm excitation was collected emission from 425 nm to 475 nm; the fluorescence (red channel) of the probe under 635 nm excitation was collected from 725 nm to 775 nm. The fluorescence of commercial Lysotracker Red and Rhodamine 6G (green channel) under the excitation of 559 nm were collected from 600 nm to 650 nm. The images were further processed with Olympus FV10-ASW 3.1 viewer and Image Pro6.

4.2.4 Theoretical calculations

Computer modelling of probes **A** and **AH**$^+$ was accomplished using procedures published previously in order to establish base geometries [124]. The molecular data were initially refined using density functional theory (DFT) employed with the B3LYP functional[142] and electron basis sets initially at the 6-31*g(d) level to convergence in Gaussian 16[119] in a Polarizable Continuum Model (PCM) of water.[121] The final models were calculated with the APFD functional[118] and 6-311+g(2d,p)[143-144] basis sets. Imaginary frequencies were not obtained in any frequency calculations. The excited states were assessed on the basis of TD-DFT optimizations[120] also in a PCM of water. Results were interpreted using GaussView 6[122] for all data and figures. The results of the calculations (including drawings

of the molecular orbitals, MOs, discussed) are given in detail in the Supporting Information.

4.3 Results and discussion

4.3.1 Probe design and synthesis

Near-infrared hemicyanine molecules possess unique advantageous photophysical properties such as high fluorescence quantum yield, excellent chemical stability and photostability with near-infrared emission at 725 nm. However, hemicyanine dyes without spirolactam switches are insensitive to pH. In order to develop near-infrared fluorescent probes (N,N-diethylamino dihydroxanthene dye) for sensitive detection of mitochondrial pH, we introduced an oxazolidine switch to a near-infrared hemicyanine through a Knoevenagel condensation of 6-(diethylamino)-2,3-dihydro-1H-xanthene-4-carbaldehyde (**3**) with 1-(2-hydroxyethyl)-2,3,3-trimethyl-3H-indol-1-ium salt (**4**) in acetic anhydride at 80° C. The oxazolidine switch activates upon immersion in mitochondrial pH producing a hemicyanine structure with π-conjugation of the fluorophore. 6-(Diethylamino)-2,3-dihydro-1H-xanthene-4-carbaldehyde (**3**) was prepared by reacting β-bromoenal (**2**) 4-(diethylamino)-2-hydroxybenzaldehyde (**1**) with Cs_2CO_3 in DMF solution at room temperature. NMR and mass spectrometer have been used to characterize the probe.
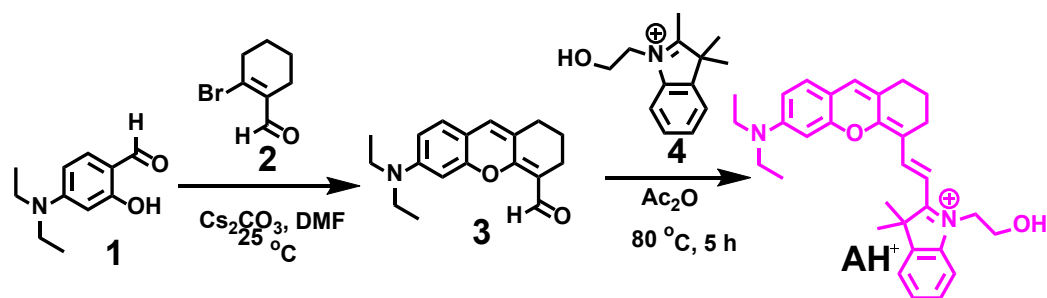
Scheme 4.2. Synthetic approach to prepare fluorescent probe **AH⁺.**

4.3.2 Optical responses of the probe to pH changes

We investigated whether the probe can respond to pH changes as verified by absorption and fluorescence spectra in two different buffer solutions, 0.1 M citrate–phosphate (pH from 5.0 to 7.0) and phosphate-phosphate buffers (pH from 7.0 to 10.0) containing 10% ethanol (Figure 4.1). Under basic pH 10.0 conditions, the dangling hydroxyl group reacts as a nucleophile with the indolenium moiety forming an oxazolidine switch through a ring-closing reaction (Scheme 4.1). As a result, probe **A** shows low absorption at 713 nm, and weak fluorescence peak at 727 nm with fluorescence quantum yield of 29 (Figures 4.1 and 4.2) at basic pH 10.0. Gradual pH decreases from 10.0 to 5.0 result in significantly gradual absorbance increases at 713 nm and gradual fluorescence enhancement at 727 nm with fluorescence quantum yield of 31 at pH 5.0 because acidic pH effectively coverts the probe oxazolidine switch to hemicyanine structure with significantly extended π-conjugation (Figures 4.1 and 4.2).

92
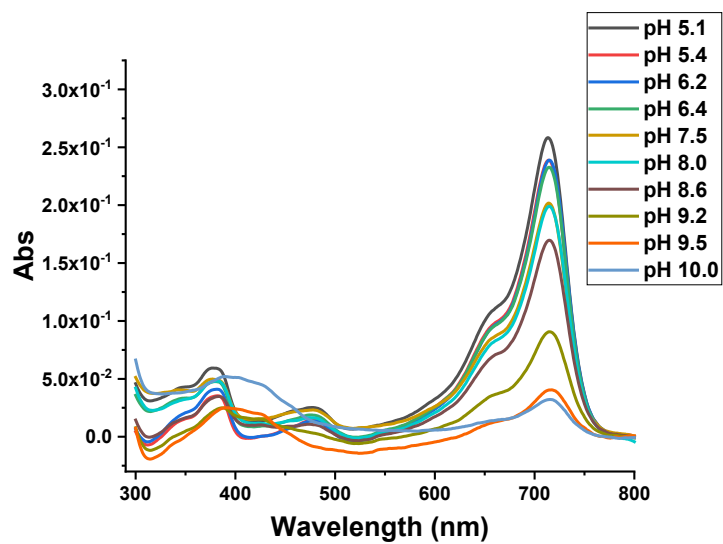
Figure 4.1. Absorption spectra of 5 μM fluorescent probe **AH⁺** in different pH buffers containing 10% ethanol. Citrate-phosphate buffers were used for pH from 5.0 to 7.0 while phosphate buffers were employed for pH from 7.0 to 10.0.
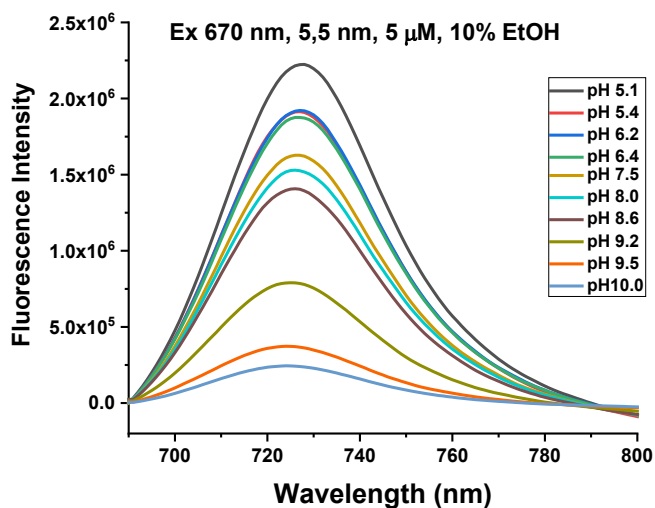
Figure 4.2. Fluorescence spectra of 5 μM fluorescent probe **AH$^+$** in different pH buffers containing 10% ethanol under excitation at 670 nm. Citrate-phosphate buffers were used for pH from 5.0 to 7.0 while phosphate buffers were employed for pH from 7.0 to 10.0.

4.3.3 Theoretical modeling

The structures of probes **A** and **AH$^+$** were assessed in order to understand the nature of the p-delocalization that occurs in basic media and to speculate as to any other conformational changes that may be occurring. We find that for probe **A** as illustrated in Figs. 3 and S5, the rhodamine plane and that comprising the oxazolidine switch are at an acute angle of approximately 72°. Excited state calculations employing the TD-DFT calculation for six excited states reveal two possible transitions at 290.68 nm (i.e., excited state 6 in Table C.2) and 417 nm (i.e., excited state 1 in Table C.2). The nature of the lower energy transition was depicted in the form of a current density plot, Figure 4.3 (left) that shows that the plane encompassing the oxazolidine ring is not involved in this transition. The

individual MOs from which the image for probe **A** in Figure 4.3 was derived are presented as Figures. C9 and C10.
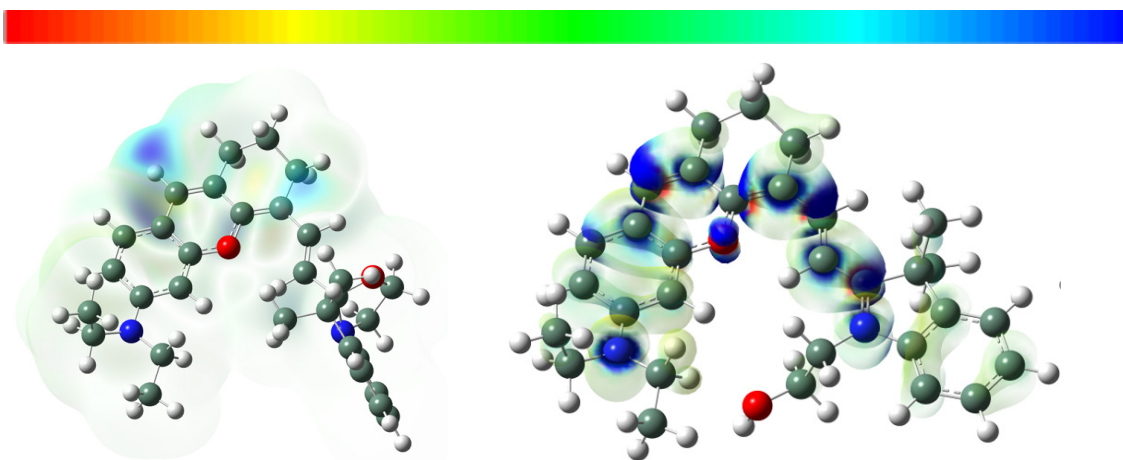
Figure 4.3. Current density illustrations as iso-surfaces of probes **A** (left) and **AH⁺** (right). Red to blue areas indicate -ve to +ve values for the different density of 1.428e-4 for **A** and 1.2023-2 for **AH⁺**.

For probe **AH⁺** as illustrated in Figure 4.3 and C11, there is a major conformation change when the oxazolidine ring switch is activated. Specifically, the planes formed by the rhodamine moiety and that for the hemicyanine are roughly coplanar (angle of 1.72º) as is evident in the overall delocalization in the current density image for probe **AH⁺** depicted in Figure. 4.3. The MOs from which this image was obtained are given as Figures. C14 and C15. The excited state calculation for six excited states revealed that two transitions as evident in Fig. S12 at 333.75 nm for excited state 4 and 593.26 nm for excited state 1 as listed in Table S4. Clearly the transition at 593.26 nm (expt. 725 nm) results from the extended p-delocalization as a consequence of activation of the oxazolidine switch.

4.3.4 Probe selectivity, photostability and pH responsive reversibility

The possible interference of other analytes was tested by recording the fluorescence spectrum of probe **A** (5 µM) in the absence and presence of high concentration (200 µM) of various essential metal ions such as Al^{3+}, Fe^{3+}, Fe^{2+}, Cr^{3+}, Ca^{2+}, Co^{2+}, Hg^{2+}, Mg^{2+}, Mn^{2+}, Ni^{2+}, Zn^{2+} K^+, and Na^+ ions, or I^-, Br^-, Cl^-, SO_3^{2-}, NO_2^-, NO_3^-, S^{2-}, CO_3^{2-} and HCO_3. The results indicate that the probes maintain high selective fluorescence responses to pH without interference from these cations and/or anions (Figure 4.4).
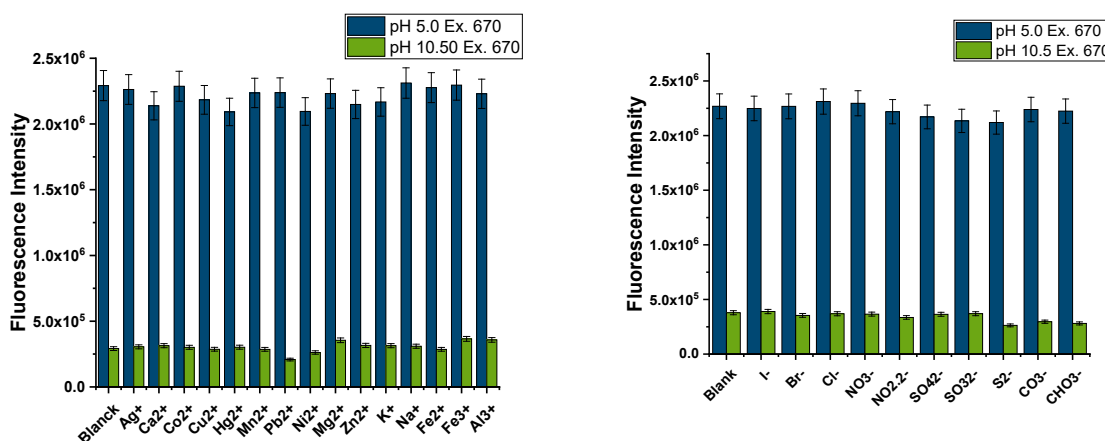
Figure 4.4. Fluorescent responses of 5 µM fluorescent probe A to pH at 5.0 and 10.5 in the absence and presence of different metal ions (200 µM), respectively.

Fluorescent probe A was excited continuously at its optimal excitation (670 nm) for 5 min intervals and fluorescence intensity was measured every 5 min. The result indicates that probe **A** displayed a moderate photostability with less than 15% decrease in fluorescence

intensity under three-hour excitation (Figure 4.5A). Fluorescent probe **A** exhibits a reversible response to pH changes between 5.0 and 10.0 (Figure 4.5B).
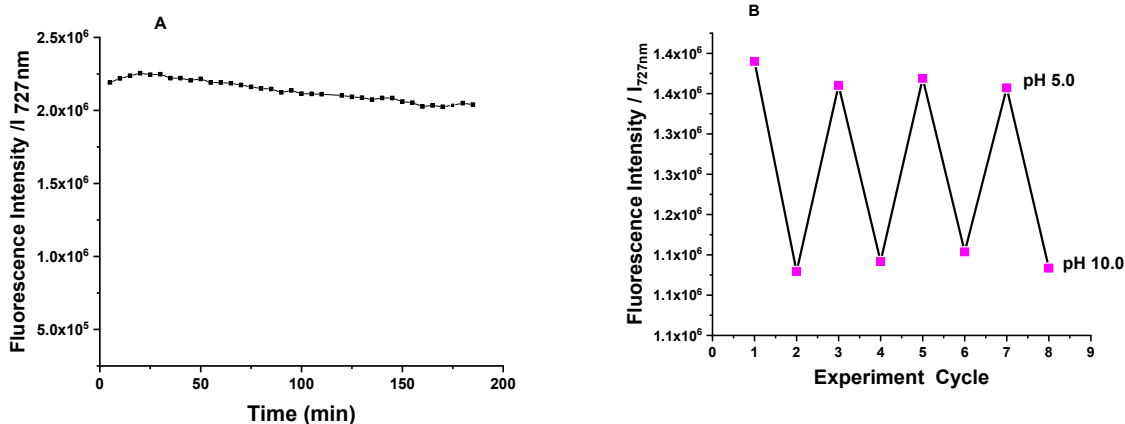
Figure 4.5. A). Photostability of 5 μM fluorescent probe A at pH 5.0 in 10% ethanol solution. Sample was exposed under respective optimal excitation wavelength (670 nm) and fluorescence intensities were measured at 5-min intervals., B**).** The reversible response of pH changes between pH 5.0 and 10.0 of **5** μM probes **A** under excitation of wavelength of 670 nm.

4.3.5 Probe cytotoxicity

We evaluated cell cytotoxicity of the probe for its biocompatibility by the MTT assay. The cytotoxicity of the probe increases slightly with the probe concentration with lower cell viability. High centration (50 μM) of the probe does not cause any considerable cytotoxicity because cell viability is still higher than 91%, indicating that the probe shows excellent biocompatibility and low toxicity (Figure 4.6).
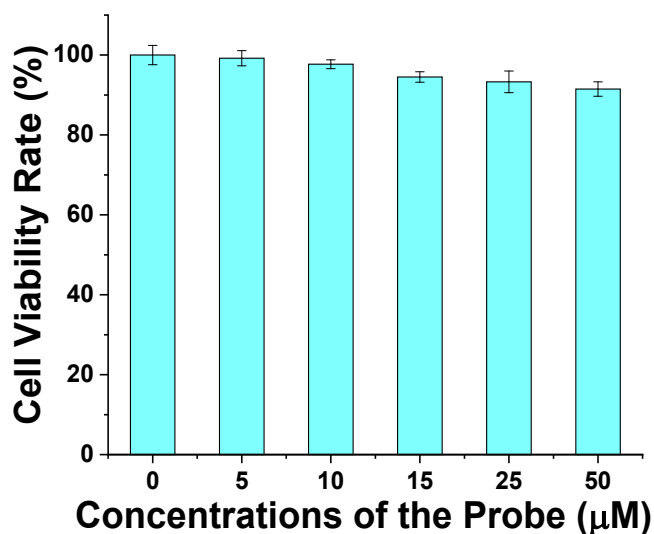
Figure 4.6. Cytotoxicity and cell proliferation effect of probe was tested by MTT assay. The HeLa cells were incubated with different concentrations of the probe for 2 hours for mitochondria staining.

4.3.6 Selective staining of mitochondria

We elevated the probe performance by testing its cell permeability. We found out that the probe displayed excellent cell permeability. Probe **A** carrying a positive charge could be used to specifically target the negatively-charged matrix of mitochondria. We next performed colocalization imaging experiments in HeLa cells to observe intracellular distribution. The lysotracker Red and rhodamine 6G were used to confirm the specificity targeting mitochondria capability of probe **A**. The probe fluorescence is impeccably overlapped with fluorescence mitochondria-targeting rhodamine 6G with Person correlation coefficient of 0.923 while the probe fluorescence shows poor Person correlation

coefficient of 0.631 with lysosome-targeting Lysotracker Red in HeLa cells. These results confirm that the probe exhibits excellent mitochondria selectivity.
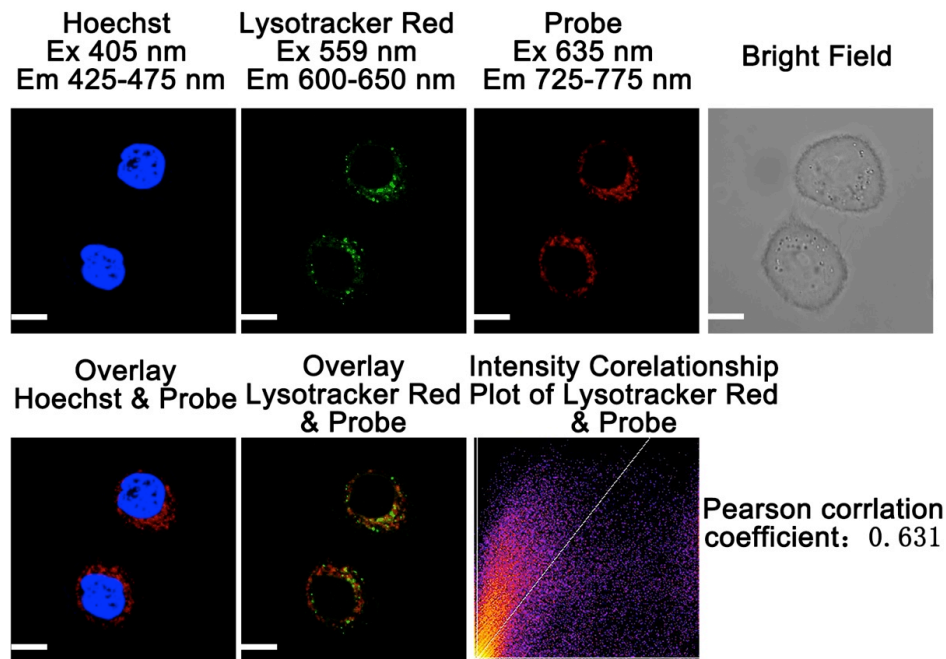
Figure 4.6. Confocal microscopic cellular images and merged images of the probe colocalized with Hoechst, and Lysotracker Red in HeLa cells. Colocalization scatterplot of the probe with Lysotracker Red. Scale bar: 20 μm.
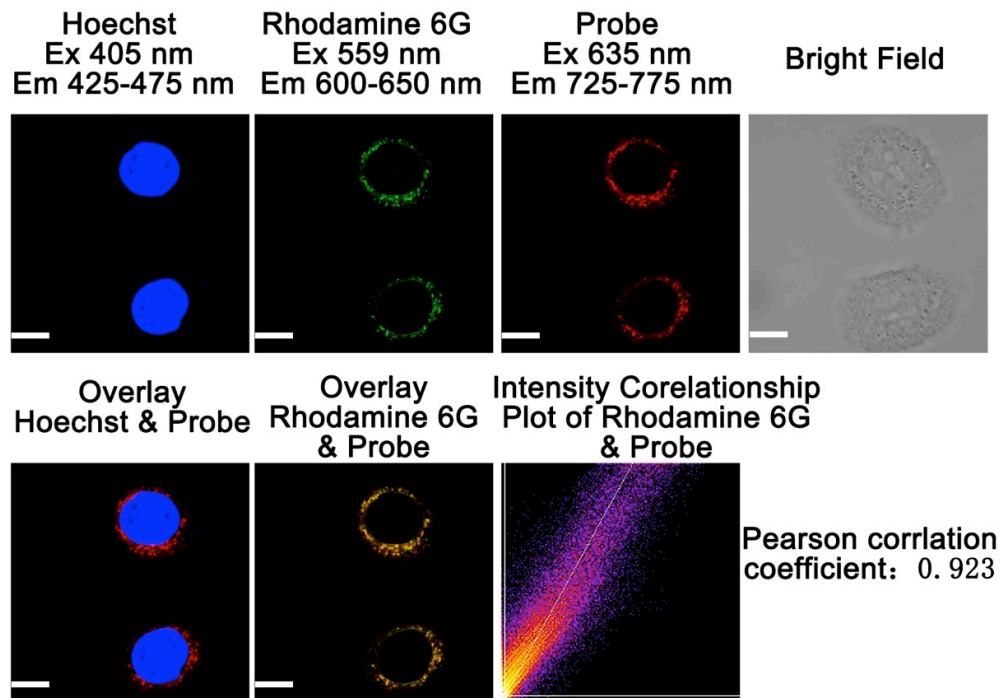
Figure 4.7. Confocal microscopic cellular images and merged images of the probe colocalized with Hoechst, and rhodamine 6G in HeLa cells. Colocalization scatterplot of the probe with rhodamine 6G. Scale bar: 20 μm.

In order to further demonstrate that the probe specifically stain mitochondria, we employed to treat HeLa cells with carbonyl cyanide 4-(trifluoromethoxy)phenylhydrazone) (FCCP), a uncoupler of oxidative phosphorylation in mitochondria after the cells were incubated with the probe. Our results show that FCCP treatment increases fluorescence intensity of the probe because FCCP can disrupt the mitochondrial H+ gradient and lead to acidification of mitochondria (Figure 4.8).
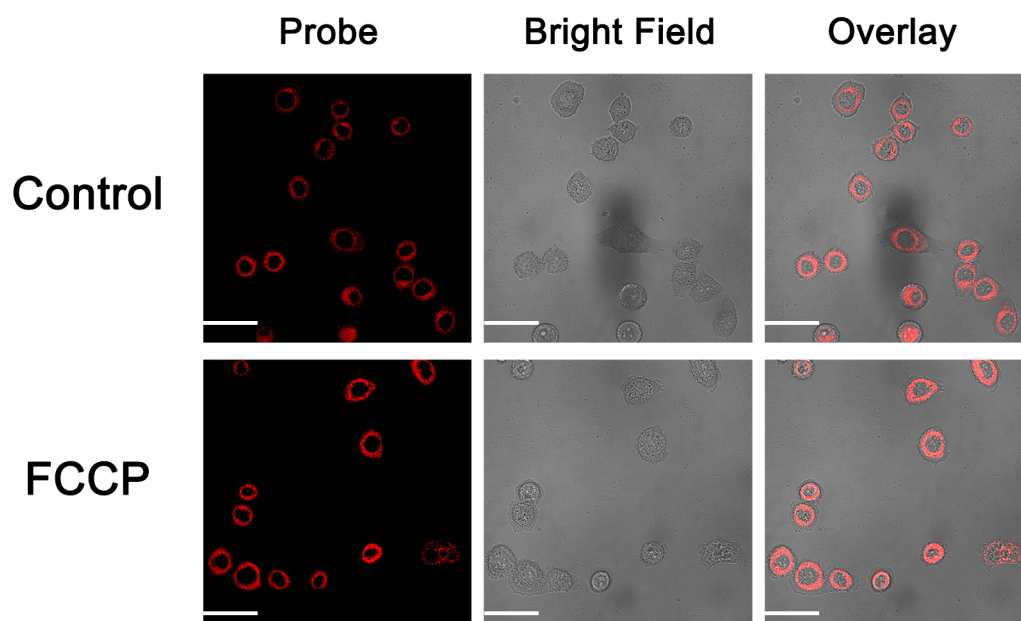
Figure 4.8. Confocal microscopic cellular images of HeLa cells with 10 µM probe **A** in absence and in the presence of 200 nM Carbonyl cyanide 4-(trifluoromethoxy)phenylhydrazone) (FCCP) treatment. Scale bar: 50 µm.

4.3.7 Visualization of mitochondrial pH changes in live cells

Since we demonstrated that the probe could selectively accumulate in mitochondria, we further studied whether the probe could be used to determine mitochondrial pH changes in live cells. We incubated HeLa cells with 10 µM probe **A** in different pH buffers containing 5 µM nigericin, which was used to adjust intracellular pH to external buffer pH. Our results show that gradual decreases of intracellular pH values from pH 10.0 to 5.0 significantly enhance cellular fluorescence of the probe, which is consistent with fluorescence responses of the probe to buffer pH changes (Figures 4.9 and 4.2) as acidic pH effectively converts

the oxazolidine switch into hemicyanine with significant π-conjugation through proton-activated oxazolidine ring-opening.
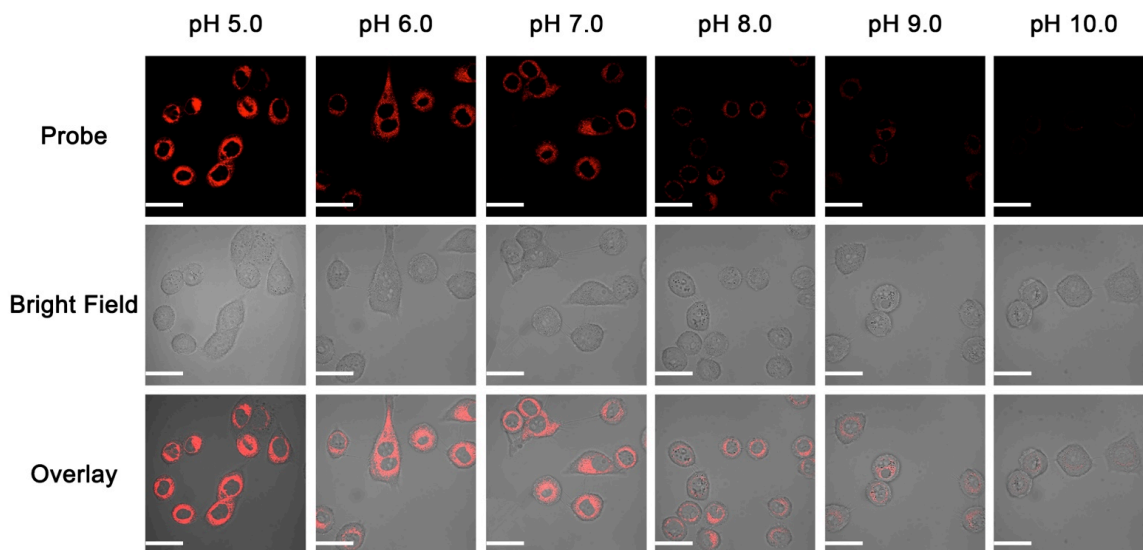
Figure 4.9. Confocal microscopic cellular images of HeLa cells with 10 µM probe **A** incubated in different pH buffers containing 5 µM nigericin. Scale bar: 50 µm.

4.4 Conclusion

We have successfully developed a near-infrared fluorescent probe by incorporating the oxazolidine switch into hemicyanine for specific targeting of mitochondria. Effective monitoring of mitochondrial pH changes in live cells is achieved through π-conjugation modulation between oxazolidine switch and hemicyanine structure upon pH changes.

5 Summary of the dissertation

In summary, the ultimate goal of this dissertation was to develop near-infrared and water-soluble fluorescent probes for the detection of pH variation in living cells. BODIPY, rhodamine and hemicyanine dyes were used as scaffold platforms to construct small organic fluorescent probes for lysosomal and mitochondrial pH detection. The fluorescence mechanisms are based on PET, ring opening and closing, and the oxazolidine switch.

In chapter two, the hydrophilicity and solubility of BODIPY in polar solvent was enhanced by introducing ortho- or meta-substituent group of tri(ethylene glycol)methyl ether on the meso-phenyl rings and positions 1,7. The morpholine moieties introduced at positions 4,4′ and 2,6 of the BODIPY dyes selectively targeted the lysosome.

3,4-bis(2-(2-(2-methoxyethoxy)ethoxy)ethoxy)benzaldehyde introduced at positions 1,7 tuned the absorption and emission wavelength of the probe to the near infrared region. The fluorescent probes were highly fluorescence in natural and basic conditions. However, the probes displayed weak fluorescence under acidic conditions due to the d-PET effect from the protonated morpholine to the BODIPY dyes. Probe **C** was successfully applied for monitoring lysosomal pH changes with low background and deep-red fluorescence.

In order to further expand the scope of lysosomal pH monitoring, we developed three sterically hindered fluorescent probes-based on the spirolactam ring switch (**A-C**) with

high pKa values (chapter three). 2-aminophenylboronic acid pinacol ester was introduced to traditional rhodamine B, **probe A**, near infrared rhodamine derivative, **probe B**, and near infrared hemicyanine dye, **probe C**, to tune the pKa and facilitate spirolactam ring opening and closing. The probes were highly fluorescent under acidic condition due to the ring open form. Under basic and neutral conditions fluorescent probe A was non-fluorescent as the spirolactam ring retained its closed form. However, probes B and C weakly fluoresced under both neutral and basic conditions, which indicated a partial opening of the ring due to the steric hindrance caused by the bulky 2-aminophenylboronic acid pinacol ester and the sp^3 hybridized carbon on the dihydronaphtyl moiety. All probes possessed excellent water solubility, high biocompatibility, excellent reversibility, and high selectivity to pH. The probes were successfully applied to detect the lysosomal pH changes in living cells.

Additionally, in chapter four we designed and synthesized a NIR fluorescent probe that possesses high biocompatibility, good photostability, selectivity, and water solubility for the effective detection of mitochondrial pH changes in living cells. The probe was prepared by combining an oxazolidine switch with a near-infrared hemicyanine dye, which allowed us to overcome the pH insensitivity of the dye. When we decreased the pH from 10.0 to 5.0, the acidic environment expanded the π-conjugation of the probe and activated the fluorescence by converting the oxazolidine switch to hemicyanine. The positive charge of the probe acted as a mitochondrial targeting moiety and effectively monitored the mitochondrial pH

6 Reference List

1. Boens, N.; Leen, V.; Dehaen, W., Fluorescent indicators based on BODIPY. *Chemical Society Reviews* **2012,** *41* (3), 1130-1172.

2. Valeur, B.; Berberan-Santos, M. N., A brief history of fluorescence and phosphorescence before the emergence of quantum theory. *Journal of Chemical Education* **2011,** *88* (6), 731-738.

3. West, D., *Principles of instrumental analysis*. Philadelphia: Sounders College: 2002.

4. Skoog, D. A.; Holler, F. J.; Crouch, S. R., *Principles of instrumental analysis*. Cengage learning: 2017.

5. Acuna, A. U.; Amat-Guerri, F.; Morcillo, P.; Liras, M.; Rodriguez, B., Structure and Formation of the Fluorescent Compound of Lignum nephriticum. *Organic letters* **2009,** *11* (14), 3020-3023.

6. Stockert, J. C.; Blazquez-Castro, A., *Fluorescence Microscopy in Life Sciences*. Bentham Science Publishers: 2017.

7. Kaufman, T. S.; Rúveda, E. A., The quest for quinine: those who won the battles and those who won the war. *Angewandte Chemie International Edition* **2005,** *44* (6), 854-885.

8. Dawson, W. R.; Windsor, M. W., Fluorescence yields of aromatic compounds. *The Journal of Physical Chemistry* **1968,** *72* (9), 3251-3260.

9. Lavis, L. D.; Raines, R. T., Bright ideas for chemical biology. *ACS chemical biology* **2008,** *3* (3), 142-155.

10. Terai, T.; Nagano, T., Small-molecule fluorophores and fluorescent probes for bioimaging. *Pflügers Archiv-European Journal of Physiology* **2013,** *465* (3), 347-359.

11. Wang, F.; Tan, W. B.; Zhang, Y.; Fan, X.; Wang, M., Luminescent nanomaterials for biological labelling. *Nanotechnology* **2005,** *17* (1), R1.

12. Johnsson, N.; Johnsson, K., Chemical tools for biomolecular imaging. *ACS chemical biology* **2007,** *2* (1), 31-38.

13. Valeur, B.; Berberan-Santos, M. N., *Molecular fluorescence: principles and applications*. John Wiley & Sons: 2012.

14. Jun, M. E.; Roy, B.; Ahn, K. H., "Turn-on" fluorescent sensing with "reactive" probes. *Chemical communications* **2011,** *47* (27), 7583-7601.

15.   Geddes, C. D.; Lakowicz, J. R., *Advanced concepts in fluorescence sensing: Part A: Small molecule sensing*. Springer Science & Business Media: 2007; Vol. 9.

16.   Sun, W.; Guo, S.; Hu, C.; Fan, J.; Peng, X., Recent development of chemosensors based on cyanine platforms. *Chemical reviews* **2016,** *116* (14), 7768-7817.

17.   Zhu, H.; Fan, J.; Wang, J.; Mu, H.; Peng, X., An "enhanced PET"-based fluorescent probe with ultrasensitivity for imaging basal and elesclomol-induced HClO in cancer cells. *Journal of the American Chemical Society* **2014,** *136* (37), 12820-12823.

18.   Yin, J.; Hu, Y.; Yoon, J., Fluorescent probes and bioimaging: alkali metals, alkaline earth metals and pH. *Chemical Society Reviews* **2015,** *44* (14), 4619-4644.

19.   He, H.; Mortellaro, M. A.; Leiner, M. J.; Young, S. T.; Fraatz, R. J.; Tusa, J. K., A fluorescent chemosensor for sodium based on photoinduced electron transfer. *Analytical chemistry* **2003,** *75* (3), 549-555.

20.   Zhang, X.; Wu, Y.; Ji, S.; Guo, H.; Song, P.; Han, K.; Wu, W.; Wu, W.; James, T. D.; Zhao, J., Effect of the electron donor/acceptor orientation on the fluorescence transduction efficiency of the d-PET effect of carbazole-based fluorescent boronic acid sensors. *The Journal of organic chemistry* **2010,** *75* (8), 2578-2588.

21.   Wu, Y.; Guo, H.; Zhang, X.; James, T. D.; Zhao, J., Chiral Donor Photoinduced-Electron-Transfer (d-PET) Boronic Acid Chemosensors for the Selective Recognition of Tartaric Acids, Disaccharides, and Ginsenosides. *Chemistry–A European Journal* **2011,** *17* (27), 7632-7644.

22.   Zhang, X.; Chi, L.; Ji, S.; Wu, Y.; Song, P.; Han, K.; Guo, H.; James, T. D.; Zhao, J., Rational design of d-PeT phenylethynylated-carbazole monoboronic acid fluorescent sensors for the selective detection of α-hydroxyl carboxylic acids and monosaccharides. *Journal of the American Chemical Society* **2009,** *131* (47), 17452-17463.

23.   Chen, R.; Zhao, G.; Yang, X.; Jiang, X.; Liu, J.; Tian, H.; Gao, Y.; Liu, X.; Han, K.; Sun, M., Photoinduced intramolecular charge-transfer state in thiophene-π-conjugated donor–acceptor molecules. *Journal of Molecular Structure* **2008,** *876* (1-3), 102-109.

24.   Lakowicz, J. R., *Topics in fluorescence spectroscopy: volume 4: probe design and chemical sensing*. Springer Science & Business Media: 1994; Vol. 4.

25.   Dias, F. B.; Pollock, S.; Hedley, G.; Pålsson, L.-O.; Monkman, A.; Perepichka, I. I.; Perepichka, I. F.; Tavasli, M.; Bryce, M. R., Intramolecular charge transfer assisted by conformational changes in the excited state of fluorene-dibenzothiophene-S, S-dioxide co-oligomers. *The Journal of Physical Chemistry B* **2006,** *110* (39), 19329-19339.

26.   Slama-Schwok, A.; Blanchard-Desce, M.; Lehn, J., Intramolecular charge transfer in donor-acceptor molecules. *Journal of Physical Chemistry* **1990,** *94* (10), 3894-3902.

27.   Xu, Z.; Xiao, Y.; Qian, X.; Cui, J.; Cui, D., Ratiometric and selective fluorescent sensor for CuII based on internal charge transfer (ICT). *Organic letters* **2005,** *7* (5), 889-892.

28.   Srikun, D.; Miller, E. W.; Domaille, D. W.; Chang, C. J., An ICT-based approach to ratiometric fluorescence imaging of hydrogen peroxide produced in living cells. *Journal of the American Chemical Society* **2008,** *130* (14), 4596-4597.

29.   Chen, X.; Wang, J.; Cui, J.; Xu, Z.; Peng, X., A ratiometric and exclusively selective CuII fluorescent probe based on internal charge transfer (ICT). *Tetrahedron* **2011,** *67* (26), 4869-4873.

30.   Ma, Y.; Chen, H.; Wang, F.; Kambam, S.; Wang, Y.; Mao, C.; Chen, X., A highly sensitive and selective ratiometric fluorescent sensor for Zn2+ ion based on ICT and FRET. *Dyes and Pigments* **2014,** *102*, 301-307.

31.   Yuan, L.; Lin, W.; Song, J.; Yang, Y., Development of an ICT-based ratiometric fluorescent hypochlorite probe suitable for living cell imaging. *Chemical Communications* **2011,** *47* (47), 12691-12693.

32.   Yi Zhang, D. Y., Guoqiang Feng, Colorimetric and near infrared fluorescent detection of cyanide by a new phenanthroimidazole–indolium conjugated probe. *RSC Advances* **2014**, 14752-14757.

33.   Kim, H. N.; Lee, M. H.; Kim, H. J.; Kim, J. S.; Yoon, J., A new trend in rhodamine-based chemosensors: application of spirolactam ring-opening to sensing ions. *Chemical Society Reviews* **2008,** *37* (8), 1465-1472.

34.   Yang, Y.-K.; Yook, K.-J.; Tae, J., A rhodamine-based fluorescent and colorimetric chemodosimeter for the rapid detection of Hg2+ ions in aqueous media. *Journal of the American Chemical Society* **2005,** *127* (48), 16760-16761.

35.   Xu, L.; Xu, Y.; Zhu, W.; Zeng, B.; Yang, C.; Wu, B.; Qian, X., Versatile trifunctional chemosensor of rhodamine derivative for Zn 2+, Cu 2+ and His/Cys in aqueous solution and living cells. *Organic & biomolecular chemistry* **2011,** *9* (24), 8284-8287.

36.   Kumar, M.; Kumar, N.; Bhalla, V.; Sharma, P. R.; Kaur, T., Highly selective fluorescence turn-on chemodosimeter based on rhodamine for nanomolar detection of copper ions. *Organic letters* **2011,** *14* (1), 406-409.

37.   Chen, X.; Pradhan, T.; Wang, F.; Kim, J. S.; Yoon, J., Fluorescent chemosensors based on spiroring-opening of xanthenes and related derivatives. *Chemical reviews* **2011,** *112* (3), 1910-1956.

38.   Tang, B.; Yin, L.; Wang, X.; Chen, Z.; Tong, L.; Xu, K., A fast-response, highly sensitive and specific organoselenium fluorescent probe for thiols and its application in bioimaging. *Chemical Communications* **2009,** (35), 5293-5295.

39.   Lv, H.-S.; Huang, S.-Y.; Zhao, B.-X.; Miao, J.-Y., A new rhodamine B-based lysosomal pH fluorescent indicator. *Analytica chimica acta* **2013,** *788*, 177-182.

40.   Wang, L.; Frei, M. S.; Salim, A.; Johnsson, K., Small-Molecule Fluorescent Probes for Live-Cell Super-Resolution Microscopy. *Journal of the American Chemical Society* **2018**.

41.   Thompson, K.; Dockery, P.; Horobin, R., Predicting and avoiding subcellular compartmentalization artifacts arising from acetoxymethyl ester calcium imaging probes. The case of fluo-3 AM and a general account of the phenomenon including a problem avoidance chart. *Biotechnic & Histochemistry* **2012,** *87* (7), 468-483.

42.   Frangioni, J. V., In vivo near-infrared fluorescence imaging. *Current opinion in chemical biology* **2003,** *7* (5), 626-634.

43.   Weissleder, R., A clearer vision for in vivo imaging. Nature Publishing Group: 2001.

44.   Kiyose, K.; Kojima, H.; Nagano, T., Functional Near-Infrared Fluorescent Probes. *Chemistry–An Asian Journal* **2008,** *3* (3), 506-515.

45.   Guo, Z.; Park, S.; Yoon, J.; Shin, I., Recent progress in the development of near-infrared fluorescent probes for bioimaging applications. *Chemical Society Reviews* **2014,** *43* (1), 16-29.

46.   Domaille, D. W.; Que, E. L.; Chang, C. J., Synthetic fluorescent sensors for studying the cell biology of metals. *Nature chemical biology* **2008,** *4* (3), 168.

47.   Pérez-Sala, D.; Collado-Escobar, D.; Mollinedo, F., Intracellular alkalinization suppresses lovastatin-induced apoptosis in HL-60 cells through the inactivation of a pH-dependent endonuclease. *Journal of Biological Chemistry* **1995,** *270* (11), 6235-6242.

48.   Zhang, X.-F.; Zhang, T.; Shen, S.-L.; Miao, J.-Y.; Zhao, B.-X., A ratiometric lysosomal pH probe based on the naphthalimide–rhodamine system. *Journal of Materials Chemistry B* **2015,** *3* (16), 3260-3266.

49.   Fukuda, T.; Ewan, L.; Bauer, M.; Mattaliano, R. J.; Zaal, K.; Ralston, E.; Plotz, P. H.; Raben, N., Dysfunction of endocytic and autophagic pathways in a lysosomal storage disease. *Annals of Neurology: Official Journal of the American Neurological Association and the Child Neurology Society* **2006,** *59* (4), 700-708.

50. Shi, X.-L.; Mao, G.-J.; Zhang, X.-B.; Liu, H.-W.; Gong, Y.-J.; Wu, Y.-X.; Zhou, L.-Y.; Zhang, J.; Tan, W., Rhodamine-based fluorescent probe for direct bio-imaging of lysosomal pH changes. *Talanta* **2014,** *130*, 356-362.

51. Zhang, X.-F.; Zhang, T.; Shen, S.-L.; Miao, J.-Y.; Zhao, B.-X., A ratiometric lysosomal pH probe based on the coumarin–rhodamine FRET system. *RSC Advances* **2015,** *5* (61), 49115-49121.

52. Zhang, J.; Yang, M.; Li, C.; Dorh, N.; Xie, F.; Luo, F.-T.; Tiwari, A.; Liu, H., Near-infrared fluorescent probes based on piperazine-functionalized BODIPY dyes for sensitive detection of lysosomal pH. *Journal of Materials Chemistry B* **2015,** *3* (10), 2173-2184.

53. Zhang, X.-X.; Wang, Z.; Yue, X.; Ma, Y.; Kiesewetter, D. O.; Chen, X., pH-Sensitive Fluorescent Dyes: Are They Really pH-Sensitive in Cells? *Molecular Pharmaceutics* **2013,** *10* (5), 1910-1917.

54. Han, J.; Burgess, K., Fluorescent indicators for intracellular pH. *Chemical reviews* **2009,** *110* (5), 2709-2728.

55. Gonçalves, M. S. T., Fluorescent labeling of biomolecules with organic probes. *Chemical reviews* **2008,** *109* (1), 190-212.

56. Shindy, H., Fundamentals in the chemistry of cyanine dyes: A review. *Dyes and Pigments* **2017,** *145*, 505-513.

57. Mujumdar, R. B.; Ernst, L. A.; Mujumdar, S. R.; Lewis, C. J.; Waggoner, A. S., Cyanine dye labeling reagents: sulfoindocyanine succinimidyl esters. *Bioconjugate chemistry* **1993,** *4* (2), 105-111.

58. Luo, S.; Zhang, E.; Su, Y.; Cheng, T.; Shi, C., A review of NIR dyes in cancer targeting and imaging. *Biomaterials* **2011,** *32* (29), 7127-7138.

59. Zhang, Z.; Achilefu, S., Design, synthesis and evaluation of near-infrared fluorescent pH indicators in a physiologically relevant range. *Chemical Communications* **2005,** (47), 5887-5889.

60. Xu, Y.; Liu, Y.; Qian, X., Novel cyanine dyes as fluorescent pH sensors: PET, ICT mechanism or resonance effect? *Journal of Photochemistry and Photobiology A: Chemistry* **2007,** *190* (1), 1-8.

61. Tang, B.; Liu, X.; Xu, K.; Huang, H.; Yang, G.; An, L., A dual near-infrared pH fluorescent probe and its application in imaging of HepG2 cells. *Chemical Communications* **2007,** (36), 3726-3728.

62.   Tang, B.; Yu, F.; Li, P.; Tong, L.; Duan, X.; Xie, T.; Wang, X., A near-infrared neutral pH fluorescent probe for monitoring minor pH changes: imaging in living HepG2 and HL-7702 cells. *Journal of the American Chemical Society* **2009,** *131* (8), 3016-3023.

63.   Myochin, T.; Kiyose, K.; Hanaoka, K.; Kojima, H.; Terai, T.; Nagano, T., Rational design of ratiometric near-infrared fluorescent pH probes with various p K a values, based on aminocyanine. *Journal of the American Chemical Society* **2011,** *133* (10), 3401-3409.

64.   Yuan, L.; Lin, W.; Yang, Y.; Chen, H., A unique class of near-infrared functional fluorescent dyes with carboxylic-acid-modulated fluorescence ON/OFF switching: rational design, synthesis, optical properties, theoretical calculations, and applications for fluorescence imaging in living animals. *Journal of the American Chemical Society* **2012,** *134* (2), 1200-1211.

65.   Vegesna, G. K.; Janjanam, J.; Bi, J.; Luo, F.-T.; Zhang, J.; Olds, C.; Tiwari, A.; Liu, H., pH-activatable near-infrared fluorescent probes for detection of lysosomal pH inside living cells. *Journal of Materials Chemistry B* **2014,** *2* (28), 4500-4508.

66.   Beija, M.; Afonso, C. A.; Martinho, J. M., Synthesis and applications of Rhodamine derivatives as fluorescent probes. *Chemical Society Reviews* **2009,** *38* (8), 2410-2433.

67.   Niu, G.; Zhang, P.; Liu, W.; Wang, M.; Zhang, H.; Wu, J.; Zhang, L.; Wang, P., Near-infrared probe based on rhodamine derivative for highly sensitive and selective lysosomal pH tracking. *Analytical chemistry* **2017,** *89* (3), 1922-1929.

68.   Shen, S.-L.; Chen, X.-P.; Zhang, X.-F.; Miao, J.-Y.; Zhao, B.-X., A rhodamine B-based lysosomal pH probe. *Journal of Materials Chemistry B* **2015,** *3* (5), 919-925.

69.   Yuan, L.; Lin, W.; Zheng, K.; Zhu, S., FRET-based small-molecule fluorescent probes: rational design and bioimaging applications. *Accounts of chemical research* **2013,** *46* (7), 1462-1473.

70.   Xiong, X.; Song, F.; Chen, G.; Sun, W.; Wang, J.; Gao, P.; Zhang, Y.; Qiao, B.; Li, W.; Sun, S., Construction of Long-Wavelength Fluorescein Analogues and Their Application as Fluorescent Probes. *Chemistry–A European Journal* **2013,** *19* (21), 6538-6545.

71.   Zhang, J.; Yang, M.; Mazi, W.; Adhikari, K.; Fang, M.; Xie, F.; Valenzano, L.; Tiwari, A.; Luo, F.-T.; Liu, H., Unusual fluorescent responses of morpholine-functionalized fluorescent probes to pH via manipulation of BODIPY's HOMO and LUMO energy orbitals for intracellular pH detection. *ACS sensors* **2015,** *1* (2), 158-165.

72.   Fan, J.; Dong, H.; Hu, M.; Wang, J.; Zhang, H.; Zhu, H.; Sun, W.; Peng, X., Fluorescence imaging lysosomal changes during cell division and apoptosis observed

using Nile Blue based near-infrared emission. *Chemical Communications* **2013,** *50* (7), 882-884.

73.	Fan, J.; Lin, C.; Li, H.; Zhan, P.; Wang, J.; Cui, S.; Hu, M.; Cheng, G.; Peng, X., A ratiometric lysosomal pH chemosensor based on fluorescence resonance energy transfer. *Dyes and Pigments* **2013,** *99* (3), 620-626.

74.	Zhang, H.; Fan, J.; Dong, H.; Zhang, S.; Xu, W.; Wang, J.; Gao, P.; Peng, X., Fluorene-derived two-photon fluorescent probes for specific and simultaneous bioimaging of endoplasmic reticulum and lysosomes: group-effect and localization. *Journal of Materials Chemistry B* **2013,** *1* (40), 5450-5455.

75.	Zhang, X.; Wang, C.; Han, Z.; Xiao, Y., A photostable near-infrared fluorescent tracker with pH-independent specificity to lysosomes for long time and multicolor imaging. *ACS applied materials & interfaces* **2014,** *6* (23), 21669-21676.

76.	Wang, L.; Xiao, Y.; Tian, W.; Deng, L., Activatable rotor for quantifying lysosomal viscosity in living cells. *Journal of the American Chemical Society* **2013,** *135* (8), 2903-2906.

77.	Galindo, F.; Burguete, M. I.; Vigara, L.; Luis, S. V.; Kabir, N.; Gavrilovic, J.; Russell, D. A., Synthetic macrocyclic peptidomimetics as tunable pH probes for the fluorescence imaging of acidic organelles in live cells. *Angewandte Chemie* **2005,** *117* (40), 6662-6666.

78.	Chauhan, D. P.; Varma, S. J.; Vijeta, A.; Banerjee, P.; Talukdar, P., A 1, 3-amino group migration route to form acrylamidines. *Chemical Communications* **2014,** *50* (3), 323-325.

79.	Becke, A. D., Density-functional thermochemistry. III. The role of exact exchange. *The Journal of chemical physics* **1993,** *98* (7), 5648-5652.

80.	Lee, C.; Yang, W.; Parr, R. G., Development of the Colle-Salvetti correlation-energy formula into a functional of the electron density. *Physical review B* **1988,** *37* (2), 785.

81.	Hehre, W.; Radom, L.; Schleyer, P., v. R.; Pople, JA Ab initio molecular orbital theory. Wiley: New York: 1986.

82.	Frisch, M.; Trucks, G.; Schlegel, H.; Scuseria, G.; Robb, M.; Cheeseman, J.; Scalmani, G.; Barone, V.; Mennucci, B.; Petersson, G., Gaussian 09. 2009, Gaussian. *Inc.: Wallingford, CT, USA* **1990,** *542*.

83.	Bolte, S.; Cordelieres, F., A guided tour into subcellular colocalization analysis in light microscopy. *Journal of microscopy* **2006,** *224* (3), 213-232.

84.   Zhu, S.; Zhang, J.; Vegesna, G. K.; Pandey, R.; Luo, F.-T.; Green, S. A.; Liu, H., One-pot efficient synthesis of dimeric, trimeric, and tetrameric BODIPY dyes for panchromatic absorption. *Chemical communications* **2011,** *47* (12), 3508-3510.

85.   Zhu, S.; Zhang, J.; Vegesna, G.; Tiwari, A.; Luo, F.-T.; Zeller, M.; Luck, R.; Li, H.; Green, S.; Liu, H., Controlled Knoevenagel reactions of methyl groups of 1, 3, 5, 7-tetramethyl BODIPY dyes for unique BODIPY dyes. *RSC Advances* **2012,** *2* (2), 404-407.

86.   Zhu, S.; Bi, J.; Vegesna, G.; Zhang, J.; Luo, F.-T.; Valenzano, L.; Liu, H., Functionalization of BODIPY dyes at 2, 6-positions through formyl groups. *RSC Advances* **2013,** *3* (14), 4793-4800.

87.   Galindo, F.; Burguete, M. I.; Vigara, L.; Luis, S. V.; Kabir, N.; Gavrilovic, J.; Russell, D. A., Synthetic macrocyclic peptidomimetics as tunable pH probes for the fluorescence imaging of acidic organelles in live cells. *Angew Chem Int Ed Engl* **2005,** *44* (40), 6504-8.

88.   Lv, H.-S.; Liu, J.; Zhao, J.; Zhao, B.-X.; Miao, J.-Y., Highly selective and sensitive pH-responsive fluorescent probe in living Hela and HUVEC cells. *Sensors and Actuators B: Chemical* **2013,** *177*, 956-963.

89.   Casey, J. R.; Grinstein, S.; Orlowski, J., Sensors and regulators of intracellular pH. *Nature reviews Molecular cell biology* **2010,** *11* (1), 50.

90.   Unusual Fluorescent Responses of Fluorescent Probes to pH via Manipulation of BODIPY's HOMO and LUMO Energy Orbitals for Intracellular pH Detection. **2016**, 158-165

91.   Burleigh, S. C.; van de Laar, T.; Stroop, C. J.; van Grunsven, W. M.; O'Donoghue, N.; Rudd, P. M.; Davey, G. P., Synergizing metabolic flux analysis and nucleotide sugar metabolism to understand the control of glycosylation of recombinant protein in CHO cells. *BMC biotechnology* **2011,** *11* (1), 95.

92.   Vingtdeux, V.; Hamdane, M.; Bégard, S.; Loyens, A.; Delacourte, A.; Beauvillain, J.-C.; Buée, L.; Marambaud, P.; Sergeant, N., Intracellular pH regulates amyloid precursor protein intracellular domain accumulation. *Neurobiology of disease* **2007,** *25* (3), 686-696.

93.   Stratton, S. G.; Taumoefolau, G. H.; Purnell, G. E.; Rasooly, M.; Czaplyski, W. L.; Harbron, E. J., Tuning the pKa of Fluorescent Rhodamine pH Probes through Substituent Effects. *Chemistry–A European Journal* **2017,** *23* (56), 14064-14072.

94.   Zhou, L.; Liu, Y.; Hu, S.; Wang, H.; Sun, H.; Zhang, X., A new ratiometric two-photon fluorescent probe for imaging of lysosomes in living cells and tissues. *Tetrahedron* **2016,** *72* (31), 4637-4642.

95.   Gerweck, L.; Seetharaman, K., Cellular pH gradient in tumor versus normal tissue: potential exploitation for the treatment of cancer. *Cancer research* **1996,** *56* (6), 1194-1198.

96.   Dong, B. L.; Song, X. Z.; Kong, X. Q.; Wang, C.; Zhang, N.; Lin, W. Y., A tumor-targeting and lysosome-specific two-photon fluorescent probe for imaging pH changes in living cells. *Journal of Materials Chemistry B* **2017,** *5* (5), 988-995.

97.   Dong, B. L.; Song, X. Z.; Wang, C.; Kong, X. Q.; Tang, Y. H.; Lin, W. Y., Dual Site-Controlled and Lysosome-Targeted Intramolecular Charge Transfer-Photoinduced Electron Transfer-Fluorescence Resonance Energy Transfer Fluorescent Probe for Monitoring pH Changes in Living Cells. *Analytical Chemistry* **2016,** *88* (7), 4085-4091.

98.   Hou, J. T.; Ren, W. X.; Li, K.; Seo, J.; Sharma, A.; Yu, X. Q.; Kim, J. S., Fluorescent bioimaging of pH: from design to applications. *Chemical Society Reviews* **2017,** *46* (8), 2076-2090.

99.   Yue, Y. K.; Huo, F. J.; Lee, S.; Yin, C. X.; Yoon, J., A review: the trend of progress about pH probes in cell application in recent years. *Analyst* **2017,** *142* (1), 30-41.

100.   Wang, R.; Yu, C. W.; Yu, F. B. A.; Chen, L. X., Molecular fluorescent probes for monitoring pH changes in living cells. *Trac-Trends in Analytical Chemistry* **2010,** *29* (9), 1004-1013.

101.   Yuan, L.; Lin, W. Y.; Cao, Z. M.; Wang, J. L.; Chen, B., Development of FRET-Based Dual-Excitation Ratiometric Fluorescent pH Probes and Their Photocaged Derivatives. *Chemistry-a European Journal* **2012,** *18* (4), 1247-1255.

102.   Yu, H.; Li, G.; Zhang, B.; Zhang, X.; Xiao, Y.; Wang, J.; Song, Y., A neutral pH probe of rhodamine derivatives inspired by effect of hydrogen bond on pKa and its organelle-targetable fluorescent imaging. *Dyes and Pigments* **2016,** *133*, 93-99.

103.   Zhang, R. Q.; Yan, F. Y.; Huang, Y. C.; Kong, D. P.; Ye, Q. H.; Xu, J. X.; Chen, L., Rhodamine-based ratiometric fluorescent probes based on excitation energy transfer mechanisms: construction and applications in ratiometric sensing. *Rsc Advances* **2016,** *6* (56), 50732-50760.

104.   Lee, D.; Swamy, K. M. K.; Hong, J.; Lee, S.; Yoon, J., A rhodamine-based fluorescent probe for the detection of lysosomal pH changes in living cells. *Sensors and Actuators B-Chemical* **2018,** *266*, 416-421.

105.   Li, H. M.; Wang, C. L.; She, M. Y.; Zhu, Y. L.; Zhang, J. D.; Yang, Z.; Liu, P.; Wang, Y. Y.; Li, J. L., Two rhodamine lactam modulated lysosome-targetable fluorescence probes for sensitively and selectively monitoring subcellular organelle pH change. *Analytica Chimica Acta* **2015,** *900*, 97-102.

106.   Shen, S. L.; Chen, X. P.; Zhang, X. F.; Miao, J. Y.; Zhao, B. X., A rhodamine B-based lysosomal pH probe. *Journal of Materials Chemistry B* **2015,** *3* (5), 919-925.

107.   Wang, J. B.; Xia, S.; Bi, J. H.; Zhang, Y. B.; Fang, M. X.; Luck, R. L.; Zeng, Y. B.; Chen, T. H.; Lee, H. M.; Liu, H. Y., Near-infrared fluorescent probes based on TBET and FRET rhodamine acceptors with different pK(a) values for sensitive ratiometric visualization of pH changes in live cells. *Journal of Materials Chemistry B* **2019,** *7* (2), 198-209.

108.   Zhang, Y. B.; Bi, J. H.; Xia, S.; Mazi, W.; Wan, S. L.; Mikesell, L.; Luck, R. L.; Liu, H. Y., A Near-Infrared Fluorescent Probe Based on a FRET Rhodamine Donor Linked to a Cyanine Acceptor for Sensitive Detection of Intracellular pH Alternations. *Molecules* **2018,** *23* (10).

109.   Zhang, Y. B.; Xia, S.; Fang, M. X.; Mazi, W.; Zeng, Y. B.; Johnston, T.; Pap, A.; Luck, R. L.; Liu, H. Y., New near-infrared rhodamine dyes with large Stokes shifts for sensitive sensing of intracellular pH changes and fluctuations. *Chemical Communications* **2018,** *54* (55), 7625-7628.

110.   Niu, G. L.; Zhang, P. P.; Liu, W. M.; Wang, M. Q.; Zhang, H. Y.; Wu, J. S.; Zhang, L. P.; Wang, P. F., Near-Infrared Probe Based on Rhodamine Derivative for Highly Sensitive and Selective Lysosomal pH Tracking. *Analytical Chemistry* **2017,** *89* (3), 1922-1929.

111.   Gong, Y.-J.; Zhang, X.-B.; Mao, G.-J.; Su, L.; Meng, H.-M.; Tan, W.; Feng, S.; Zhang, G., A unique approach toward near-infrared fluorescent probes for bioimaging with remarkably enhanced contrast. *Chemical science* **2016,** *7* (3), 2275-2285.

112.   Xie, J.-Y.; Li, C.-Y.; Li, Y.-F.; Fu, Y.-J.; Nie, S.-X.; Tan, H.-Y., A near-infrared chemosensor for determination of trivalent aluminum ions in living cells and tissues. *Dyes and Pigments* **2017,** *136*, 817-824.

113.   Zhu, S.; Zhang, J.; Janjanam, J.; Bi, J.; Vegesna, G.; Tiwari, A.; Luo, F.-T.; Wei, J.; Liu, H., Highly water-soluble, near-infrared emissive BODIPY polymeric dye bearing RGD peptide residues for cancer imaging. *Anal. Chim. Acta* **2013,** *758*, 138-144.

114.   Zhang, J. T.; Yang, M.; Mazi, W. F.; Adhikari, K.; Fang, M. X.; Xie, F.; Valenzano, L.; Tiwari, A.; Luo, F. T.; Liu, H. Y., Unusual Fluorescent Responses of Morpholine-Functionalized Fluorescent Probes to pH via Manipulation of BODIPY's HOMO and LUMO Energy Orbitals for Intracellular pH Detection. *Acs Sensors* **2016,** *1* (2), 158-165.

115.   Zhang, Y.; Bi, J.; Xia, S.; Mazi, W.; Wan, S.; Mikesell, L.; Luck, R.; Liu, H., A near-infrared fluorescent probe based on a FRET rhodamine donor linked to a cyanine acceptor for sensitive detection of intracellular pH alternations. *Molecules* **2018,** *23* (10), 2679.

116.   ChemBio3D *ChemBio3D* http://www.cambridgesoft.com/software/chembio3d, 2012.

117.   Hanwell, M. D.; Curtis, D. E.; Lonie, D. C.; Vandermeersch, T.; Zurek, E.; Hutchison, G. R., Avogadro: an advanced semantic chemical editor, visualization, and analysis platform. *J. Cheminform.* **2012,** *4*.

118.   Austin, A.; Petersson, G. A.; Frisch, M. J.; Dobek, F. J.; Scalmani, G.; Throssell, K., A Density Functional with Spherical Atom Dispersion Terms. *Journal of Chemical Theory and Computation* **2012,** *8* (12), 4989-5007.

119.   Frisch, M. J.; Trucks, G. W.; Schlegel, H. B.; Scuseria, G. E.; Robb, M. A.; Cheeseman, J. R.; Scalmani, G.; Barone, V.; Petersson, G. A.; Nakatsuji, H.; Li, X.; Caricato, M.; Marenich, A. V.; Bloino, J.; Janesko, B. G.; Gomperts, R.; Mennucci, B.; Hratchian, H. P.; Ortiz, J. V.; Izmaylov, A. F.; Sonnenberg, J. L.; Williams-Young, D.; Ding, F.; Lipparini, F.; Egidi, F.; Goings, J.; Peng, B.; Petrone, A.; Henderson, T.; Ranasinghe, D.; Zakrzewski, V. G.; Gao, J.; Rega, N.; Zheng, G.; Liang, W.; Hada, M.; Ehara, M.; Toyota, K.; Fukuda, R.; Hasegawa, J.; Ishida, M.; Nakajima, T.; Honda, Y.; Kitao, O.; Nakai, H.; Vreven, T.; Throssell, K.; Montgomery, J. A., Jr; Peralta, J. E.; Ogliaro, F.; Bearpark, M. J.; Heyd, J. J.; Brothers, E. N.; Kudin, K. N.; Staroverov, V. N.; Keith, T. A.; Kobayashi, R.; Normand, J.; Raghavachari, K.; Rendell, A. P.; Burant, J. C.; Iyengar, S. S.; Tomasi, J.; Cossi, M.; Millam, J. M.; Klene, M.; Adamo, C.; Cammi, R.; Ochterski, J. W.; Martin, R. L.; Morokuma, K.; Farkas, O.; Foresman, J. B.; Fox, D. J. *Gaussian 16, Revision A.03*, Gaussian, Inc.: Wallingford CT, 2016.

120.   Casida, M. E.; Jamorski, C.; Casida, K. C.; Salahub, D. R., Molecular excitation energies to high-lying bound states from time-dependent density-functional response theory: Characterization and correction of the time-dependent local density approximation ionization threshold. *J. Chem. Phys.* **1998,** *108* (11), 4439-4449.

121.   Cances, E.; Mennucci, B.; Tomasi, J., A new integral equation formalism for the polarizable continuum model: Theoretical background and applications to isotropic and anisotropic dielectrics. *J. Chem. Phys.* **1997,** *107* (8), 3032-3041.

122.   GaussView; 6, V.; Dennington, R.; Keith, T. A.; Millam, J. M. Semichem Inc. Shawnee Mission, KS, 2016.

123.   Hu, Z.-Q.; Li, M.; Liu, M.-D.; Zhuang, W.-M.; Li, G.-K., A highly sensitive fluorescent acidic pH probe based on rhodamine B diethyl-2-aminobutenedioate conjugate and its application in living cells. *Dyes and Pigments* **2013,** *96* (1), 71-75.

124.   Zhang, Y.; Bi, J.; Xia, S.; Mazi, W.; Wan, S.; Mikesell, L.; Luck, R. L.; Liu, H., A near-infrared fluorescent probe based on a FRET rhodamine donor linked to a cyanine acceptor for sensitive detection of intracellular pH alternations. *Molecules* **2018,** *23* (10), 2679/1-2679/15.

125.   Fang, M. X.; Adhikari, R.; Bi, J. H.; Mazi, W.; Dorh, N.; Wang, J. B.; Conner, N.; Ainsley, J.; Karabencheva-Christova, T. G.; Luo, F. T.; Tiwari, A.; Liu, H. Y., Fluorescent probes for sensitive and selective detection of pH changes in live cells in visible and near-infrared channels. *Journal of Materials Chemistry B* **2017,** *5* (48), 9579-9590.

126.   Fang, M. X.; Xia, S.; Bi, J. H.; Wigstrom, T. P.; Valenzano, L.; Wang, J. B.; Mazi, W.; Tanasova, M.; Luo, F. T.; Liu, H. Y., A cyanine-based fluorescent cassette with aggregation-induced emission for sensitive detection of pH changes in live cells. *Chem. Commun.* **2018,** *54* (9), 1133-1136.

127.   Vegesna, G. K.; Janjanam, J.; Bi, J. H.; Luo, F. T.; Zhang, J. T.; Olds, C.; Tiwari, A.; Liu, H. Y., pH-activatable near-infrared fluorescent probes for detection of lysosomal pH inside living cells. *Journal of Materials Chemistry B* **2014,** *2* (28), 4500-4508.

128.   Wang, J. B.; Xia, S.; Bi, J. H.; Fang, M. X.; Mazi, W. F.; Zhang, Y. B.; Conner, N.; Luo, F. T.; Lu, H. P.; Liu, H. Y., Ratiometric Near-Infrared Fluorescent Probes Based On Through Bond Energy Transfer and pi-Conjugation Modulation between Tetraphenylethene and Hemicyanine Moieties for Sensitive Detection of pH Changes in Live Cells. *Bioconjugate Chemistry* **2018,** *29* (4), 1406-1418.

129.   Zhang, S. W.; Chen, T. H.; Lee, H. M.; Bi, J. H.; Ghosh, A.; Fang, M. X.; Qian, Z. C.; Xie, F.; Ainsley, J.; Christov, C.; Luo, F. T.; Zhao, F.; Liu, H. Y., Luminescent Probes for Sensitive Detection of pH Changes in Live Cells through Two Near-Infrared Luminescence Channels. *Acs Sensors* **2017,** *2* (7), 924-931.

130.   Yue, Y.; Huo, F.; Lee, S.; Yin, C.; Yoon, J., A review: the trend of progress about pH probes in cell application in recent years. *Analyst* **2017,** *142* (1), 30-41.

131.   Li, P.; Xiao, H.; Cheng, Y.; Zhang, W.; Huang, F.; Zhang, W.; Wang, H.; Tang, B., A near-infrared-emitting fluorescent probe for monitoring mitochondrial pH. *Chemical Communications* **2014,** *50* (54), 7184-7187.

132.   Liu, X.; Wang, L.; Bing, T.; Zhang, N.; Shangguan, D., A Mitochondria-Targeted Ratiometric Fluorescent pH Probe. *ACS Applied Bio Materials* **2019**.

133.   Wallace, D. C., Mitochondria and cancer. *Nature Reviews Cancer* **2012,** *12* (10), 685.

134.   Hou, J.-T.; Ren, W. X.; Li, K.; Seo, J.; Sharma, A.; Yu, X.-Q.; Kim, J. S., Fluorescent bioimaging of pH: from design to applications. *Chemical Society Reviews* **2017,** *46* (8), 2076-2090.

135.   Lee, M. H.; Park, N.; Yi, C.; Han, J. H.; Hong, J. H.; Kim, K. P.; Kang, D. H.; Sessler, J. L.; Kang, C.; Kim, J. S., Mitochondria-immobilized pH-sensitive off–on

fluorescent probe. *Journal of the American Chemical Society* **2014,** *136* (40), 14136-14142.

136.   Wu, M.-Y.; Li, K.; Liu, Y.-H.; Yu, K.-K.; Xie, Y.-M.; Zhou, X.-D.; Yu, X.-Q., Mitochondria-targeted ratiometric fluorescent probe for real time monitoring of pH in living cells. *Biomaterials* **2015,** *53*, 669-678.

137.   Chen, Y.; Zhu, C.; Cen, J.; Bai, Y.; He, W.; Guo, Z., Ratiometric detection of pH fluctuation in mitochondria with a new fluorescein/cyanine hybrid sensor. *Chemical science* **2015,** *6* (5), 3187-3194.

138.   Yamada, Y.; Harashima, H., Mitochondrial drug delivery systems for macromolecule and their therapeutic application to mitochondrial diseases. *Advanced Drug Delivery Reviews* **2008,** *60* (13-14), 1439-1462.

139.   Xu, Z.; Xu, L., Fluorescent probes for the selective detection of chemical species inside mitochondria. *Chemical Communications* **2016,** *52* (6), 1094-1119.

140.   Chen, T.-H.; Zhang, S.; Jaishi, M.; Adhikari, R.; Bi, J.; Fang, M.; Xia, S.; Zhang, Y.; Luck, R. L.; Pati, R., New Near-Infrared Fluorescent Probes with Single-Photon Anti-Stokes-Shift Fluorescence for Sensitive Determination of pH Variances in Lysosomes with a Double-Checked Capability. *ACS applied bio materials* **2018,** *1* (3), 549-560.

141.   Chen, T. H.; Zhang, S. W.; Jaishi, M.; Adhikari, R.; Bi, J. H.; Fang, M. X.; Xia, S.; Luck, R. L.; Pati, R.; Lee, H. M.; Luo, F. T.; Tiwari, A.; Liu, H. Y., New Near-Infrared Fluorescent Probes with Single-Photon Anti-Stokes-Shift Fluorescence for Sensitive Determination of pH Variances in Lysosomes with a Double-Checked Capability. *ACS Applied Bio Materials* **2018,** *1* (3), 549-560.

142.   Lee, C.; Yang, W.; Parr, R. G., Development of the Colle-Salvetti correlation-energy formula into a functional of the electron density. *Physical Review B* **1988,** *37* (2), 785-789.

143.   Binning Jr., R. C.; Curtiss, L. A., Compact contracted basis sets for third-row atoms: Ga–Kr. *J. Comput. Chem.* **1990,** *11* (10), 1206-1216.

144.   Raghavachari, K.; Trucks, G. W., Highly correlated systems. Excitation energies of first row transition metals Sc–Cu. *The Journal of Chemical Physics* **1989,** *91* (2), 1062-1065.

145.   Velapoldi, R. A.; Tønnesen, H. H., Corrected emission spectra and quantum yields for a series of fluorescent compounds in the visible spectral region. *Journal of fluorescence* **2004,** *14* (4), 465-472.

146.   Kubin, R. F.; Fletcher, A. N., Fluorescence quantum yields of some rhodamine dyes. *Journal of Luminescence* **1982,** *27* (4), 455-462.

147.   Du, H.; Fuh, R. C. A.; Li, J.; Corkan, L. A.; Lindsey, J. S., PhotochemCAD‡: a computer-aided design and research tool in photochemistry. *Photochemistry and photobiology* **1998,** *68* (2), 141-142.

148.   Cielen, E.; Tahri, A.; Ver Heyen, K.; Hoornaert, G. J.; De Schryver, F. C.; Boens, N., Synthesis and spectroscopic characterisation of fluorescent indicators for Na+ and K+. *Journal of the Chemical Society, Perkin Transactions 2* **1998,** (7), 1573-1580.

149.   Yuan, Y.; Xu, S.; Cheng, X.; Cai, X.; Liu, B., Bioorthogonal Turn-On Probe Based on Aggregation-Induced Emission Characteristics for Cancer Cell Imaging and Ablation. *Angewandte Chemie International Edition* **2016,** *55* (22), 6457-6461.

150.   Whitaker, J. E.; Haugland, R. P.; Prendergast, F. G., Spectral and photophysical studies of benzo [c] xanthene dyes: dual emission pH sensors. *Analytical biochemistry* **1991,** *194* (2), 330-344.

151.   Qin, W.; Baruah, M.; Stefan, A.; Van der Auweraer, M.; Boens, N., Photophysical properties of BODIPY-derived hydroxyaryl fluorescent pH probes in solution. *ChemPhysChem* **2005,** *6* (11), 2343-2351.

152.   Yao, S.; Schafer-Hales, K. J.; Belfield, K. D., A new water-soluble near-neutral ratiometric fluorescent pH indicator. *Organic letters* **2007,** *9* (26), 5645-5648.

153.   Billo, E. J., *Excel for chemists: a comprehensive guide*. John Wiley & Sons: 2004.

154.   Cheng, C.-C.; Liu, M.-C., Novel Ca2+-specific receptors derived from 3-formyl-2-hydroxybenzoic acid. *Tetrahedron Letters* **2000,** *41* (51), 10047-10053.

A   Appendix A: Supporting information of chapter 2

A.1   Synthesis

A.1.1   Synthesis of fluorescent probe A:

To a solution of compound 2 (0.9 mmol, 113 mg) in anhydrous THF (1 mL) was added

ethylmagnesium bromide (0.9 mmol, 0.9 mL of 1.0 M solution). When the mixture was

heated at 60 °C for 2 hours and cooled down to room temperature, this freshly made

Grignard reagent was transferred to a Schlenk flask containing a solution of BODIPY dye

1 (100 mg, 0.15 mmol) in anhydrous THF (2 mL) via cannula under nitrogen protection.

The resulting mixture was stirred at 60 °C overnight until complete consumption of the

starting material which was monitored by TLC plates. When water (10 mL) was added to

the mixture, the resulting mixture was extracted with CH_2Cl_2 (25 mL). The organic layer

was washed with water (50 mL) and brine solution (50 mL), dried over anhydrous Na_2SO_4

and filtered. The filtrate was concentrated under reduced pressure and the crude product

was purified by column chromatography using CH_2Cl_2/MeOH (9:0.5, v/v) as eluent to

yield fluorescent probe A as orange oil (29 mg, 23%).

BODIPY dye 4: A mixture of DMF (10.0 mL) and $POCl_3$ (10.0 mL) was stirred in an ice

bath for ten minutes under an argon atmosphere. The mixture was warmed to room

temperature and further stirred for 35 minutes. After adding BODIPY dye 3 (600 mg, 0.93

mmol) in $ClCH_2CH_2Cl$ (70 mL) to the reaction mixture, the resulting mixture was stirred

at 50 °C for two hours. The reaction mixture was cooled down to room temperature and

then was slowly poured into saturated $NaHCO_3$ aqueous solution at 0 °C in an ice bath.

The mixture was warmed to room temperature and was further stirred for 2 hours until no more bubble was generated. The mixture was then washed with water and brine solution. The organic layers were combined, dried over anhydrous Na_2SO_4, and concentrated under reduced pressure to give crude intermediate BODIPY dye. This crude intermediate BODIPY dye was used directly for the next step reaction without any purification. The BODIPY dye 4 was prepared from the crude product in the last step by the similar procedures but was run at higher temperature of 60 °C for 4 hours instead of 50 °C for 2 hours. The crude product was purified by column chromatography using hexanes/CH_2Cl_2/acetone/EtOH (4/2/2/0.5, v/v/v/v) as eluent to yield BODIPY 4 as deep red oil (295 mg, overall yield: 45%). ^{1}H NMR (400 MHz, $CDCl_3$): δ 9.97 (s, 2H), 6.92 (d, J = 8 Hz, 1H), 6.63 – 6.60 (m, 2H), 4.13 (t, J = 4.8 Hz, 2H), 4.02 (t, J = 4.8 Hz, 2H), 3.84 (t, J = 4.8 Hz, 2H), 3.71 – 3.58 (m, 8H), 3.50 – 3.47 (m, 2H), 3.44 – 3.28 (m, 11H), 3.25 (s, 3H), 2.27 (s, 6H), 1.78 (s, 6H). ^{13}C NMR (100 MHz, CDCl3): δ 185.8, 162.0, 159.9, 156.4, 148.0, 145.2, 132.5, 129.4, 127.7, 114.9, 107.0, 100.9, 70.6, 69.6, 67.8, 59.0, 58.9, 13.4, 11.6. HRMS (ESI): calculated for $C_{35}H_{47}BF_2N_2O_{10}Na$ [M+Na]$^+$,727.3184; found, 727.3196.

A.1.2   Synthesis of fluorescent probe B

A mixed solution of BODIPY 4 (100 mg, 0.14 mmol) and morpholine (75 mg, 0.84 mmol) in 30 mL dry ClCH2CH2Cl was stirred at 50 °C for 4 hours. When NaBH(OAc)$_3$ (118 mg, 0.56 mmol) and acetic acid (1 drop) were added to the flask at room temperature, the mixture was stirred overnight at room temperature, diluted with CH_2Cl_2 and washed with water and brine solutions. The organic layer was collected, dried over Na_2SO_4 and

concentrated in reduced pressure. The crude product was purified by column chromatograph using CH_2Cl_2/MeOH, (9/0.5, v/v) as eluent to obtain fluorescent probe B as deep orange oil (72 mg, 61%).

BODIPY dye 6: When BODIPY dye 4 (88 mg, 0.125 mmol), compound 5 were dissolved in a mixture of toluene (30 mL), piperidine (0.2 mL) and acetic acid (0.2 mL), the reaction mixture was refluxed at 120 ºC for 3 hours. Any water formed during the reaction was removed azeotropically by using a Dean-Stark apparatus. After the reaction was quenched by water (5 mL) at room temperature, the mixture was concentrated under reduced pressure and re-dissolved in CH_2Cl_2 (100 mL). It was then washed sequentially with saturated NH_4Cl solution (100 mL), water (100 mL) and brine solution (100 mL), dried over anhydrous Na_2SO_4 and filtered. The filtrate was concentrated under reduced pressure and the crude product was purified by column chromatography using hexane/CH_2Cl_2/acetone/EtOH (3/3/2/0.7, v/v/v/v) as eluent to obtain BODIPY dye 6 as violet color oil (35 mg, 10.4%). ^1H NMR (400 MHz, $CDCl_3$): δ 9.88 (s, 2H), 7.10 (d, J = 8 Hz, 1H), 6.64 – 6.58 (m, 5H), 6.52 (d, J = 16 Hz, 2H), 6.43 (d, J = 2.4 Hz, 1H), 5.96 (d, J = 16 Hz, 2H), 4.14 (t, J = 4.8 Hz, 4H), 4.07 (t, J = 4.8 Hz, 4H), 3.94 – 3.40 (m, 64H), 3.38 – 3.32 (m, 18H), 3.30 (s, 3H), 2.91 (s, 6H). ^{13}C NMR (100 MHz, $CDCl_3$): δ 186.9, 161.9, 159.8, 157.5, 150.0, 148.9, 147.5, 142.0, 140.0, 132.2, 131.1, 129.5, 126.4, 120.7, 116.9, 115.0, 114.0, 112.6, 107.2, 100.2, 71.9, 71.7, 70.8, 70.7, 70.6, 70.5, 70.3, 69.6, 69.5, 68.7, 58.9. HRMS (ESI): calculated for $C_{77}H_{111}BF_2N_2O_{26}Na$ [M+Na]$^+$, 1551.7378; found, 1551.7388.

A.2　　Optical Measurement

A.2.1　　Quantum yield calculation

The UV-Vis absorption spectra of fluorescent probes **A**, **B** and **C** for pH dependency, selectivity, photostability and solvent effect measurements were collected in the range from 300 to 800 nm with increments of 1 nm. Their corresponding fluorescence spectra were collected at the excitation wavelength of 470 nm, 490 nm, and 580 nm for fluorescent probes **A**, **B** and **C** with increments of 1 nm, respectively. The excitation and emission slit widths were set up to 3 nm. The concentration of the dye in each sample is 5 μM. Sulforhodamine 101 dye (Φ_f = 95% with excitation wavelength at 577 nm in ethanol)[145] was used as a reference standard to determine the fluorescence quantum yields of fluorescent probe **C** in ethanol and buffer solutions. Rhodamine 6G (Φ_f = 95% in ethanol)[146-147] was used as a reference standard to determine the fluorescence quantum yields of fluorescent probes **A** and **B** in ethanol and buffer solutions. Both samples and references were freshly prepared under identical conditions. The fluorescence quantum yields were calculated using the following equation:

$$\phi_X = \phi_{st}\left(\frac{Grad_X}{Grad_{st}}\right)\left(\frac{\eta_X^2}{\eta_{st}^2}\right)$$

Where the subscripts 'st' and 'X' stand for standard and test, respectively, Φ is the fluorescence quantum yield, "Grad" represents the gradient from the plot of integrated fluorescence intensity versus absorbance and η is the refractive index of the solvent.

A.2.2   Determination of pKa by fluorometric titration

The constants Ka of fluorescent probes **A**, **B** and **C** were determined in buffer solutions by fluorometric titration as a function of pH using the fluorescence spectra. The expression of the steady-state fluorescence intensity F as a function of the proton concentration has been extended for the case of a n: 1 complex between H^+ and a fluorescent probe, which expressed by the equation as below[148]:

$$F = \frac{F_{min}[H^+]^n + F_{max}K_a}{K_a + [H^+]^n}$$

F_{min} and F_{max} stand for the fluorescence intensities at maximal and minimal H^+ concentrations, respectively, and *n* is apparent stoichiometry of H^+ binding to the probe which affects the fluorescent change. Nonlinear fitting of equation expressed above to the fluorescence titration data recoded as a function of H^+ concentration with K_a and n as free adjustable parameters yields the estimated apparent constant of K_a.

A.3   MTS assay:

MTS assay was performed with HUVEC-C cells (from ATCC). The cells were plated at a density of 5,000 cells/well on a 96-well cell culture plate and incubated at 37 °C in 5% CO_2 incubator overnight. After incubation, the media was removed and the cells were washed with 1X PBS. Fresh media with 0 µM, 5 µM, 15 µM, 25 µM, or 50 µM of fluorescent probe C dissolved in DMSO (with less than <0.5% DMSO final concentration in media) were added to the wells and measured in 6 replicates for each dye concentration. Blanks used for background subtraction had everything else except the cells and were prepared at the same time. The plates were incubated at 37 °C in 5% CO_2 incubator for 48 h. After the

48-hour incubation, 20 µL of MTS solution (from CellTiter 96 Aqueous Non-Radioactive Cell proliferation Assay (MTS) kit, Promega) was added to each well. The absorbance at 490 nm was acquired after 4 h incubation at 37 °C, using an ELISA plate reader (BioTek Instruments, Inc.). Plots were normalized to control wells containing media and cells only.

Table A.1. Optical properties of fluorescent probes **A**, **B** and **C**.

|	solvent	λ_{abs} (nm)	λ_{em} (nm)	ε_{max} (10^4 $M^{-1}cm^{-1}$)	Φ_f (%)
Probe **A**	Ethanol	498	508	7.89	56
	Buffer (pH 7.4)	501	506	7.48	18
	Buffer (pH 4.0)	495	507	7.62	5.4
Probe **B**	Ethanol	515	529	10.03	8.0
	Buffer (pH 7.4)	511	523	7.86	1.3
	Buffer (pH 4.0)	502	514	9.74	0.14
Probe **C**	Ethanol	565	652	3.15	8.6
	Buffer (pH 7.4)	550	665	5.06	0.32
	Buffer (pH 4.0)	532	654	5.12	0.036
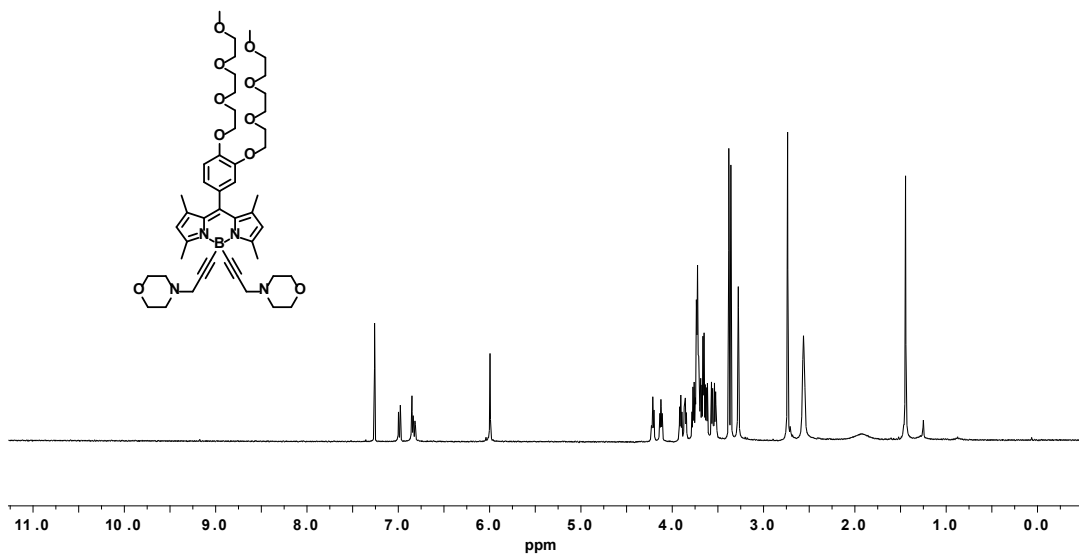
Figure A.1. ^{1}H NMR spectrum of fluorescent probe **A** in CDCl$_3$ solution.
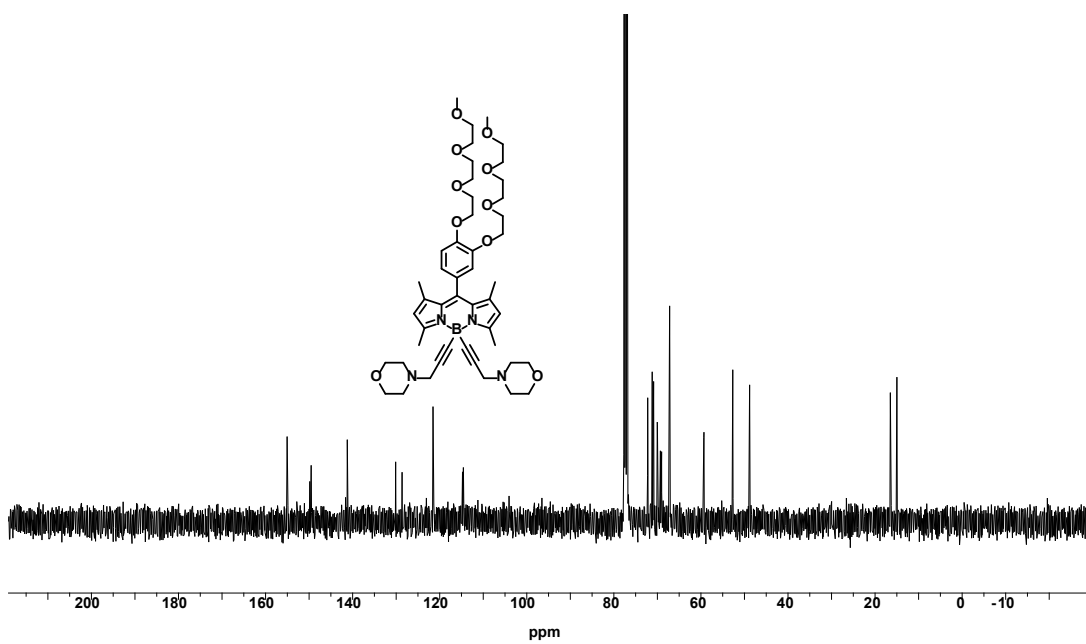
Figure A.2. ^{13}C NMR spectrum of fluorescent probe **A** in CDCl$_3$ solution.
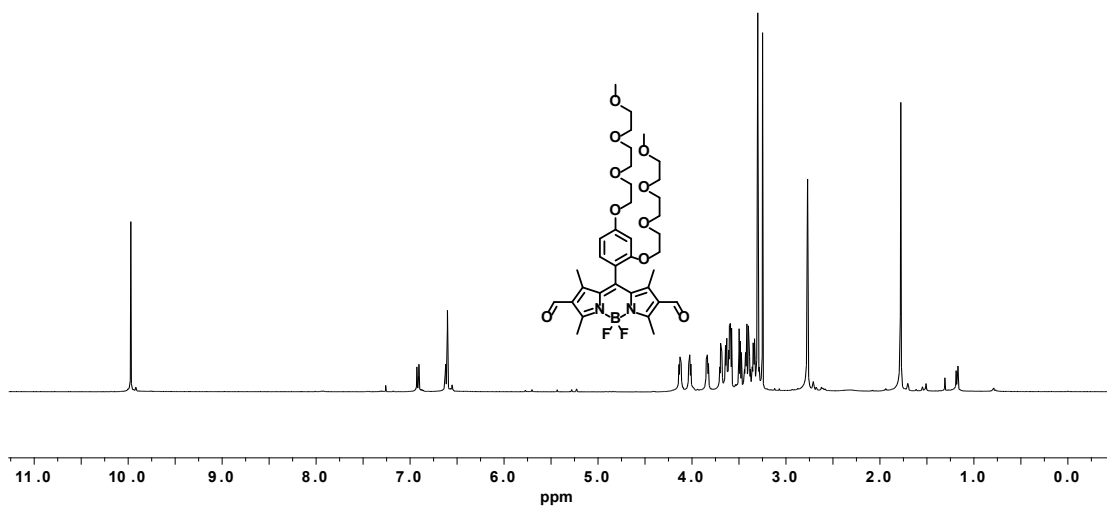
Figure A.3. ^{1}H NMR spectrum of BODIPY dye **4** in CDCl$_3$ solution.
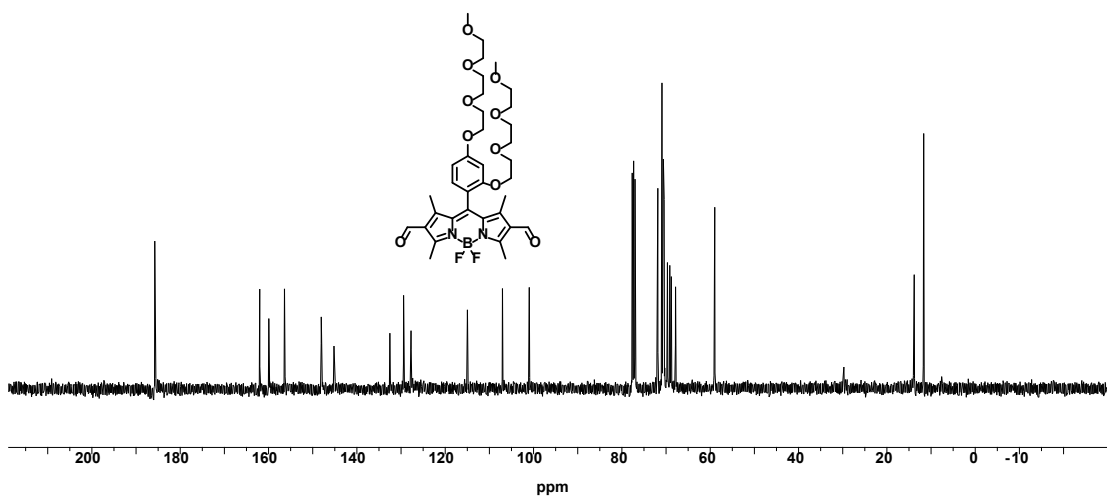
Figure A.4. ^{13}C NMR spectrum of BODIPY dye **4** in CDCl$_3$ solution.
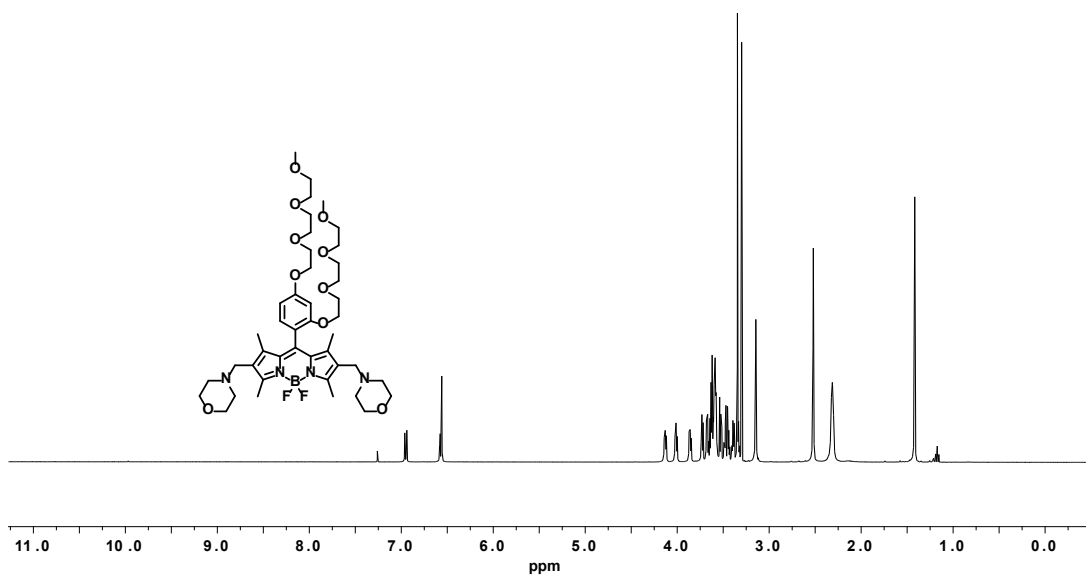
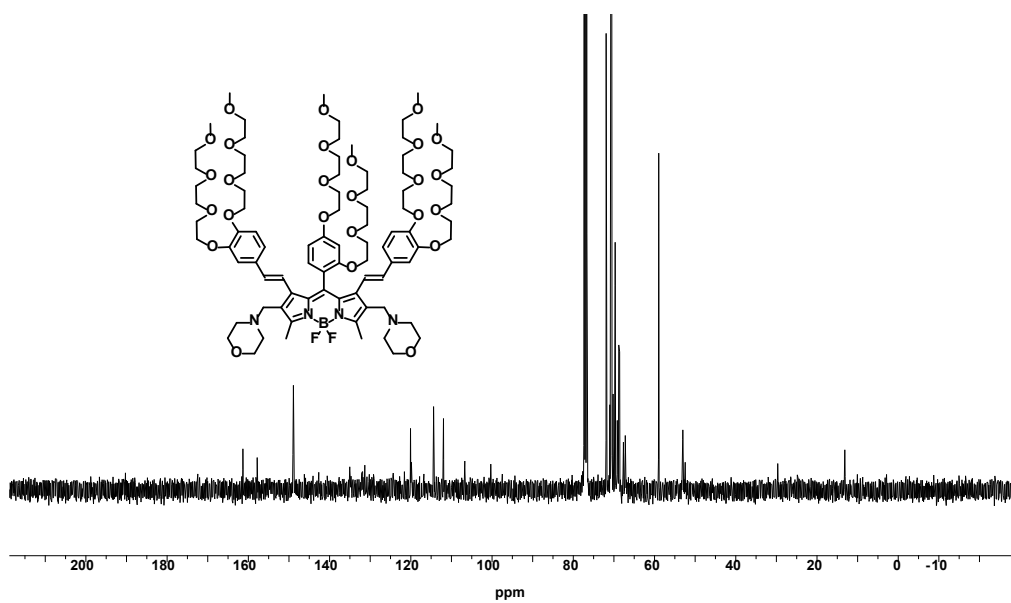**Figure A.5**. ^{1}H NMR spectrum of fluorescent probe **B** in CDCl$_3$ solution.
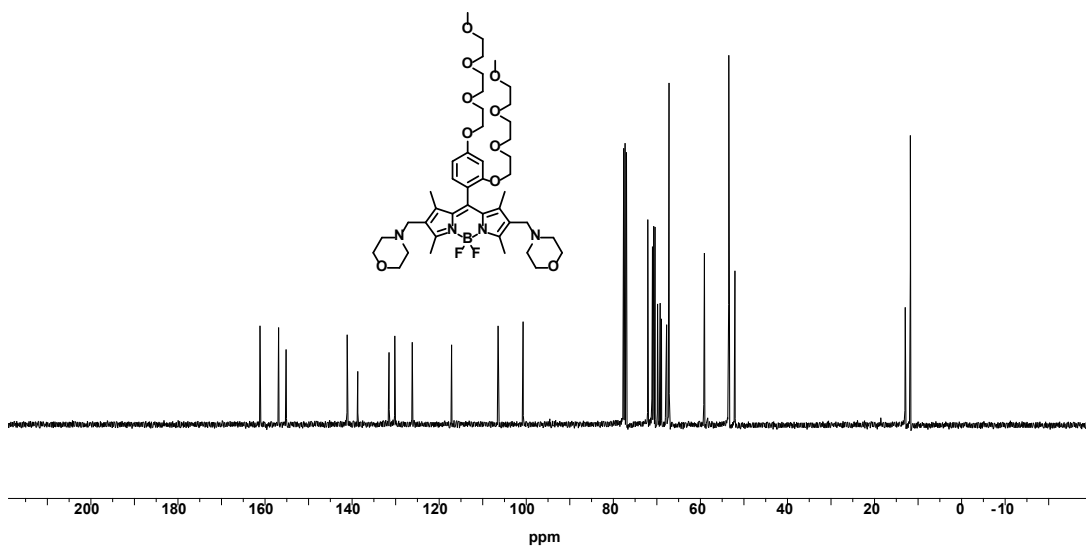
Figure A.6. ^{13}C NMR spectrum of fluorescent probe **B** in CDCl$_3$ solution.
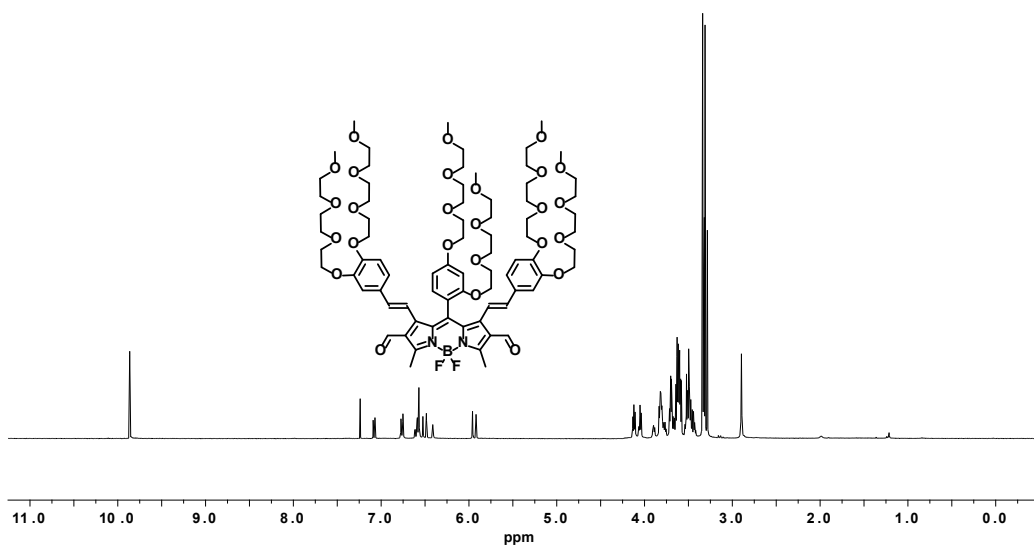
Figure A.7. ^{1}H NMR spectrum of BODIPY dye **6** in CDCl$_3$ solution.
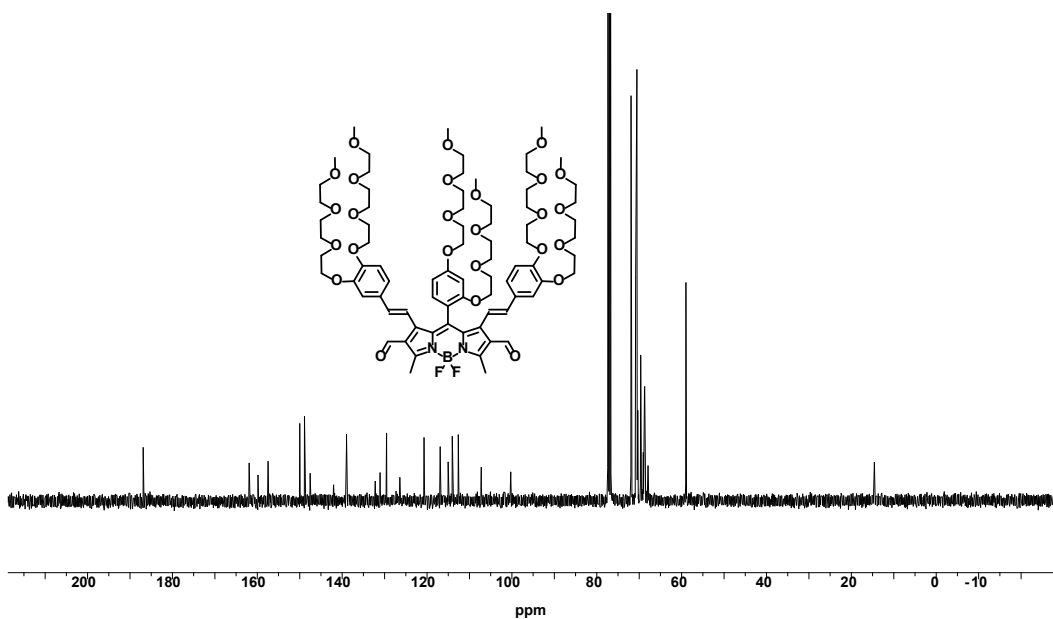
Figure A.8. ^{13}C NMR spectrum of BODIPY dye **6** in CDCl$_3$ solution.

128
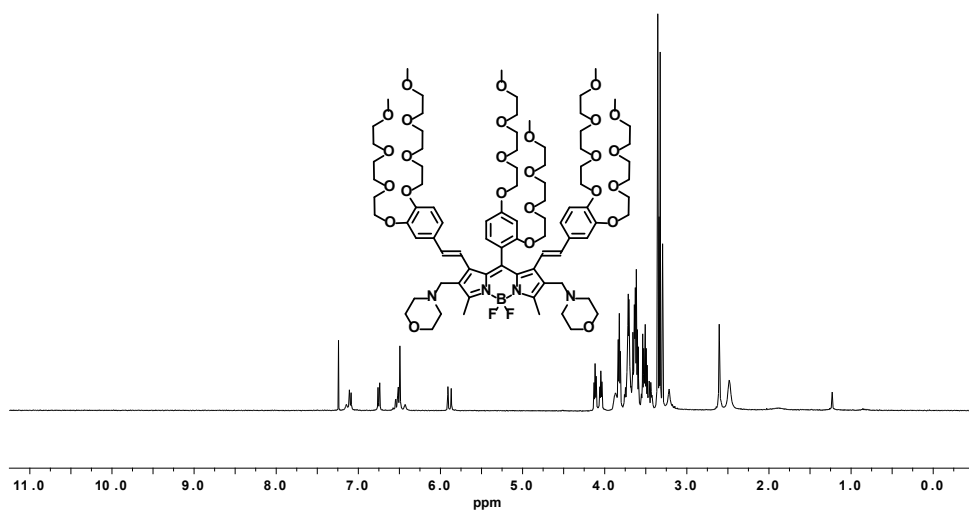
Figure A.9. ^{1}H NMR spectrum of fluorescent probe **C** in CDCl$_3$ solution.

Figure A.10. ^{13}C NMR spectrum of fluorescent probe **C** in CDCl$_3$ solution.
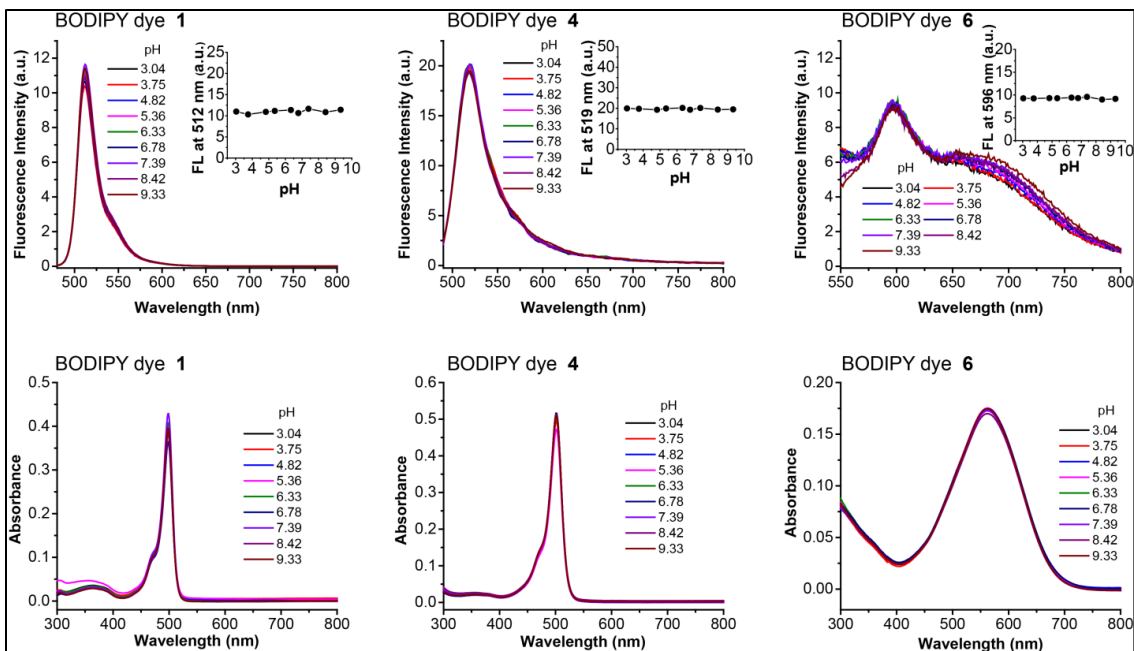
Figure A.11. Absorption and emission spectra of BODIPY dyes **1**, **4** and **6** (5 µM) in buffer solution at different pH values. The inset graphs in upper row are the corresponding changes fluorescence intensity at peak wavelengths at different pH conditions.
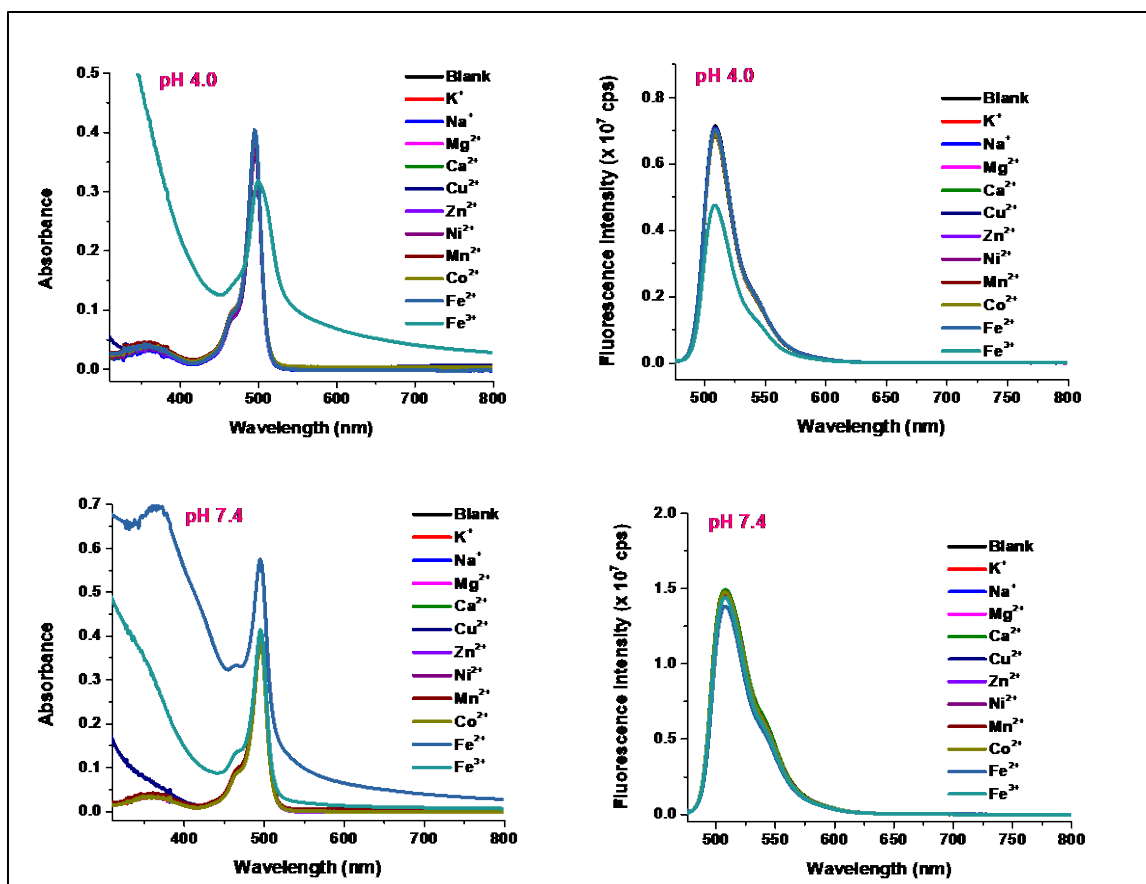
Figure A.12. Absorption and emission spectra of fluorescent probe **A** (5 μM) in the presence of various metal cations (200 μM) in buffer solution at pH 4.0 (upper row) and pH 7.4 (lower row).
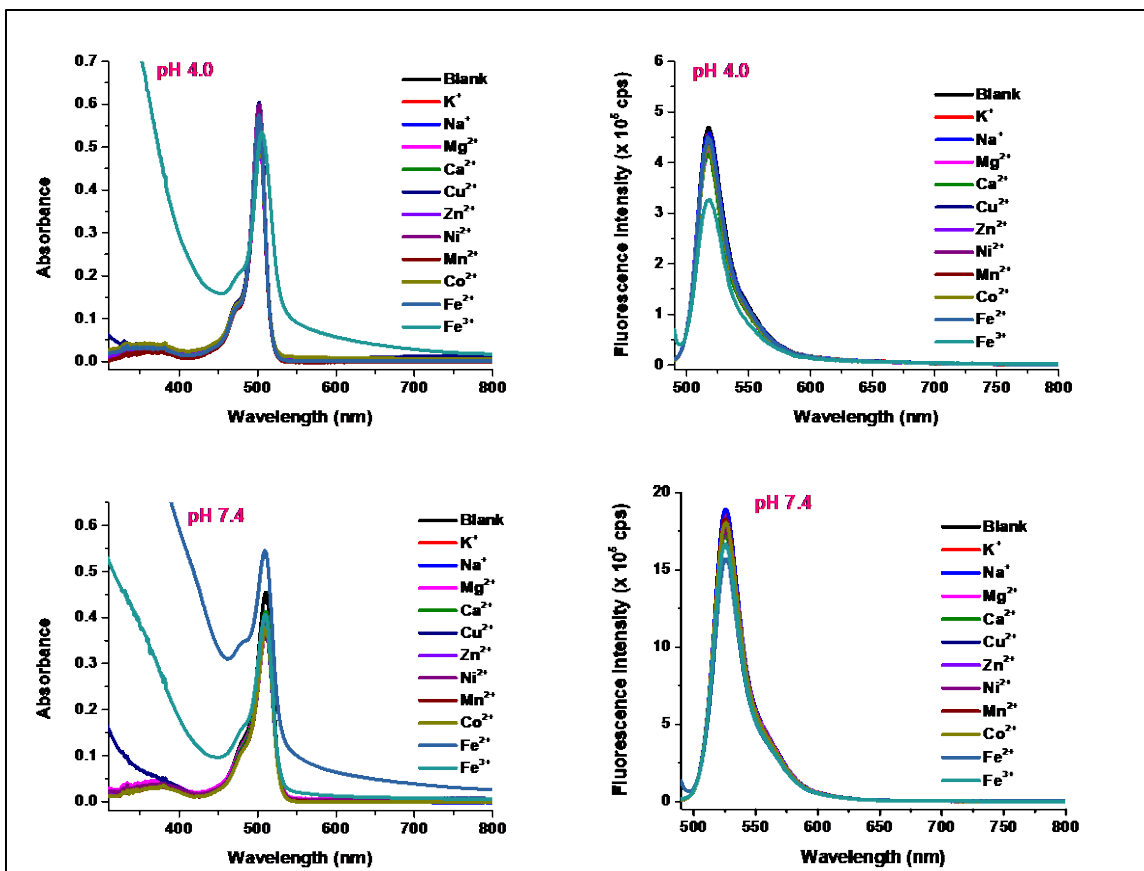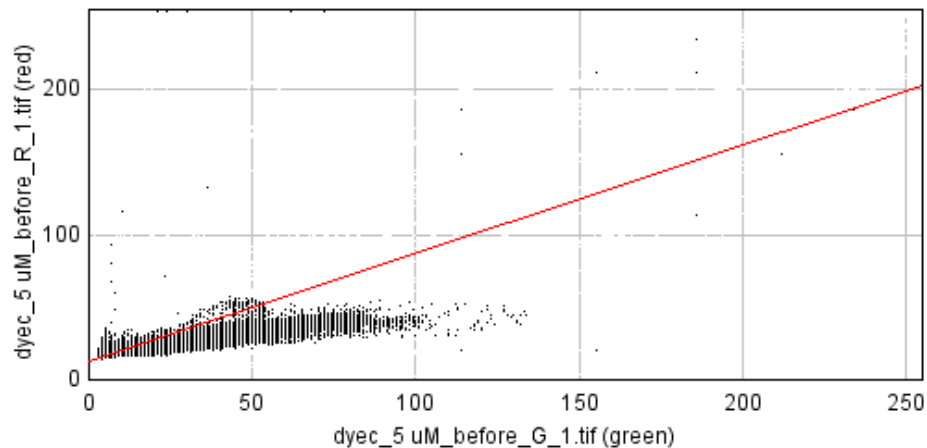
Figure A.13. Absorption and emission spectra of fluorescent probe **B** (5 μM) in the presence of various metal cations (200 μM) in buffer solution at pH 4.0 (upper row) and pH 7.4 (lower row).
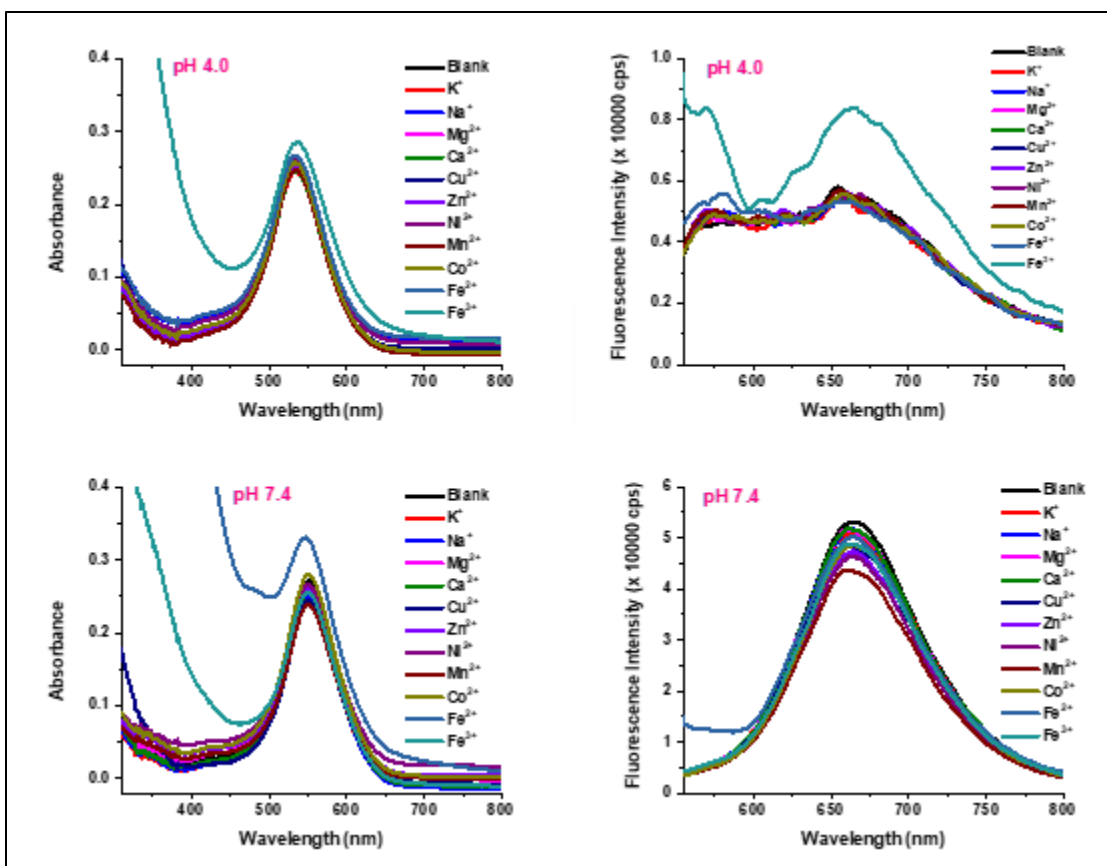
Figure A.14. Absorption and emission spectra of fluorescent probe **C** (5 μM) in the presence of various metal cations (200 μM) in buffer solution at pH 4.0 (upper row) and pH 7.4 (lower row).

Figure A.15. Red and green channel cytofluorogram of fluorescence images of cells incubated with 5 μM fluorescent probe **C** and 1 μM LysoSensor Green DND-189 for verifying their co-localization.
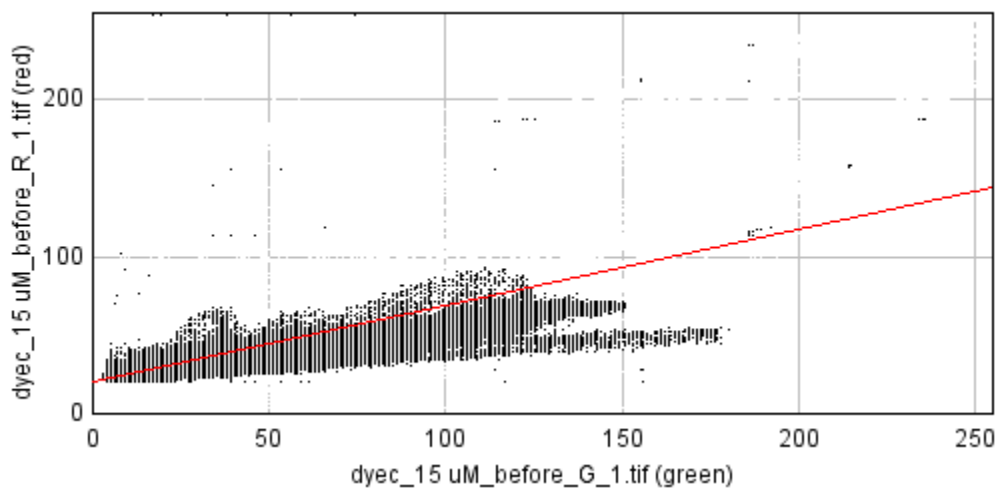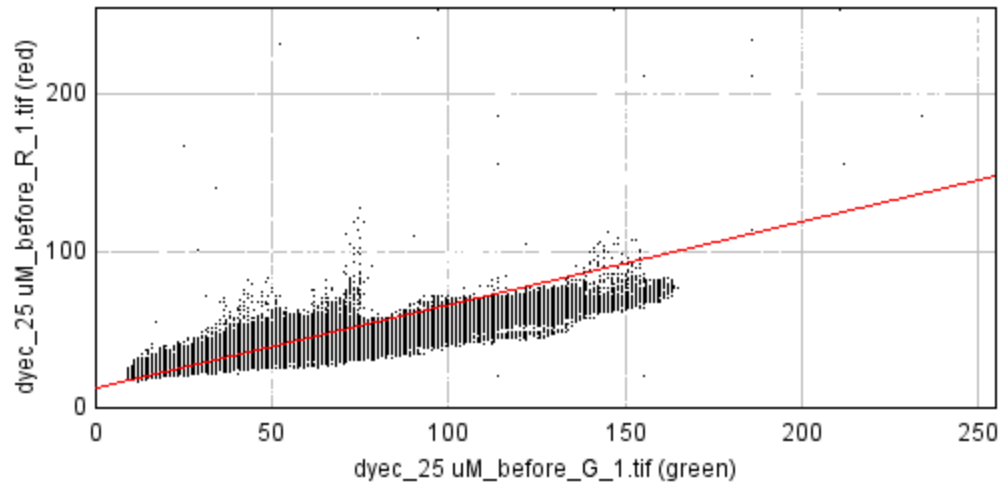

Figure A.16. Red and green channel cytofluorogram of fluorescence images of cells incubated with 15 μM fluorescent probe **C** and 1 μM LysoSensor Green DND-189 for verifying their co-localization.

Figure A.17. Red and green channel cytofluorogram of fluorescence images of cell incubated with 25 μM fluorescent probe **C** and 1 μM LysoSensor Green DND-189 for verifying their co-localization.
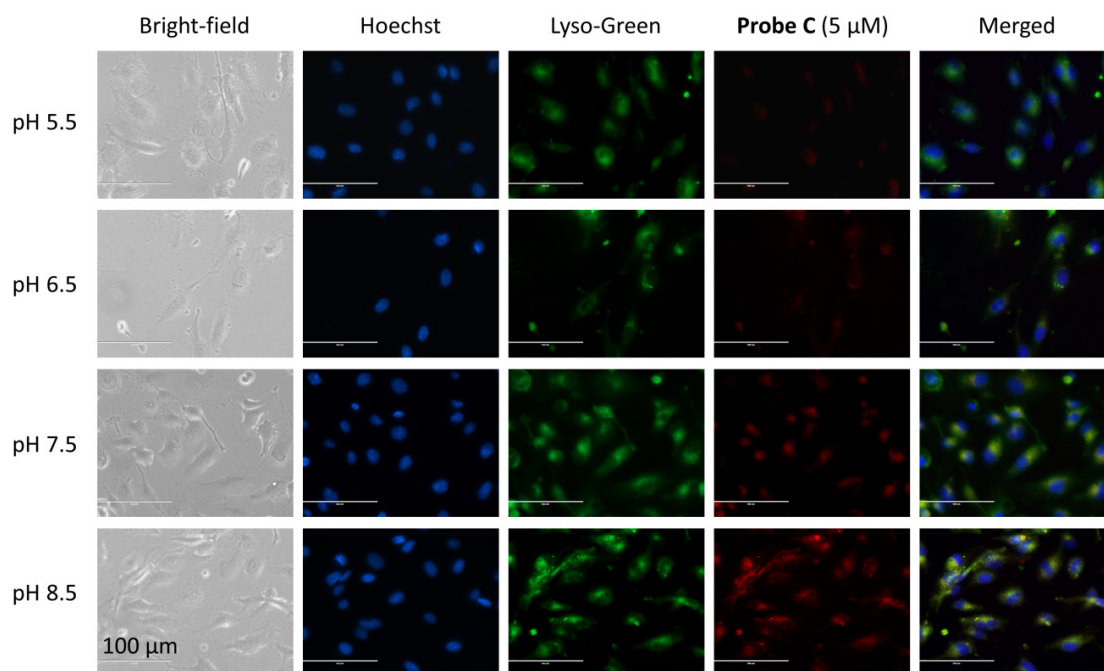
Figure A.18. Fluorescence images of HUVEC-C cells incubated with 5 μM fluorescent probe **C** at different intracellular pH values. Intracellular pH were tuned by using nigericin (5 μg·mL^{-1}) in 2 mL potassium rich PBS at different pH values (5.5, 6.5, 7.5, or 8.5). HUVEC-C cells were incubated with fluorescent probe **C** for 2 h and imaged for co-localization with 1 μM LysoSensor Green and (1 μg·mL^{-1}) Hoechst 33342 stains. Images were acquired using the inverted fluorescence microscope (AMF-4306, EVOSfl, AMG) at 40× magnification.
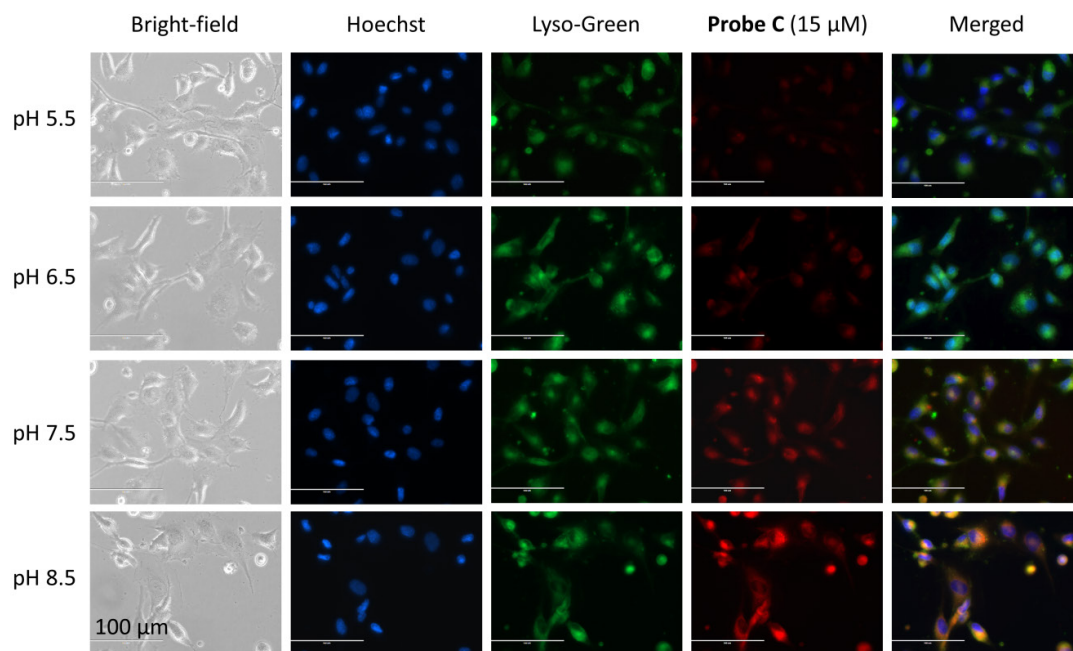
Figure A.19. Fluorescence images of HUVEC-C cells incubated with 15 µM fluorescent probe **C** at different intracellular pH values. Intracellular pH were tuned by using nigericin (5 µg·mL^{-1}) in 2 mL potassium rich PBS at different pH values (5.5, 6.5, 7.5, or 8.5). HUVEC-C cells were incubated with fluorescent probe **C** for 2 h and imaged for co-localization with 1 µM LysoSensor Green and (1 µg·mL^{-1}) Hoechst 33342 stains. Images were acquired using the inverted fluorescence microscope (AMF-4306, EVOSfl, AMG) at 40× magnification.
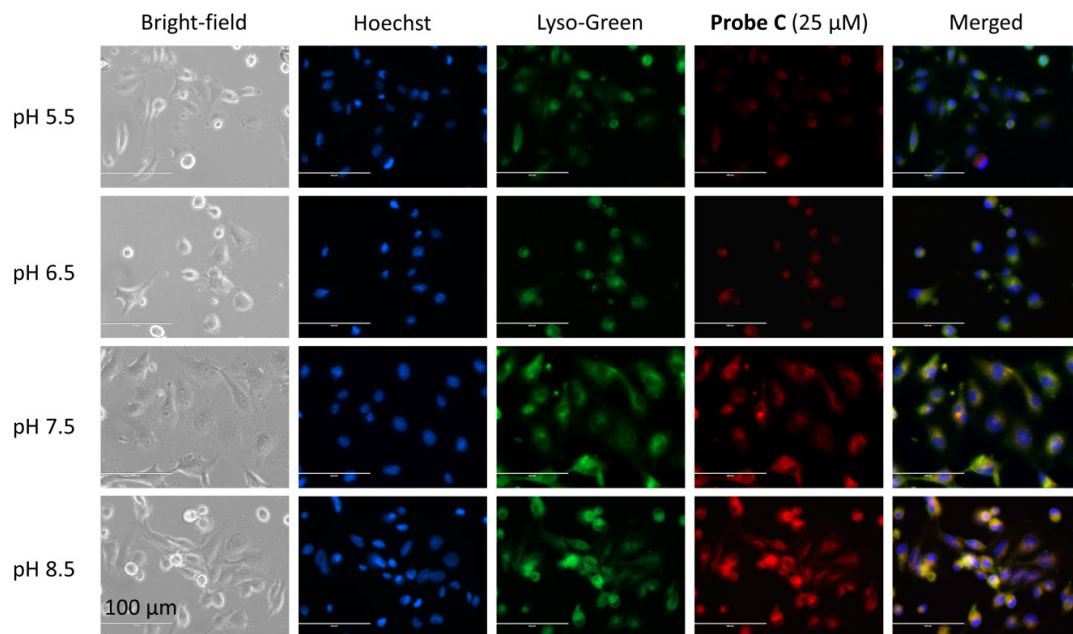
Figure A.20. Fluorescence images of HUVEC-C cells incubated with 25 μM fluorescent probe **C** at different intracellular pH values. Intracellular pH were tuned by using nigericin (5 μg·mL^{-1}) in 2 mL potassium rich PBS at different pH values (5.5, 6.5, 7.5, or 8.5). HUVEC-C cells were incubated with probe **C** for 2 h and imaged for co-localization with 1 μM LysoSensor Green and (1 μg·mL^{-1}) Hoechst 33342 stains. Images were acquired using the inverted fluorescence microscope (AMF-4306, EVOSfl, AMG) at 40× magnification.

B   Appendix B: Supporting information of chapter 3

B.1   ¹H, ¹³C NMR and HRMS spectra of probes A, B, and C
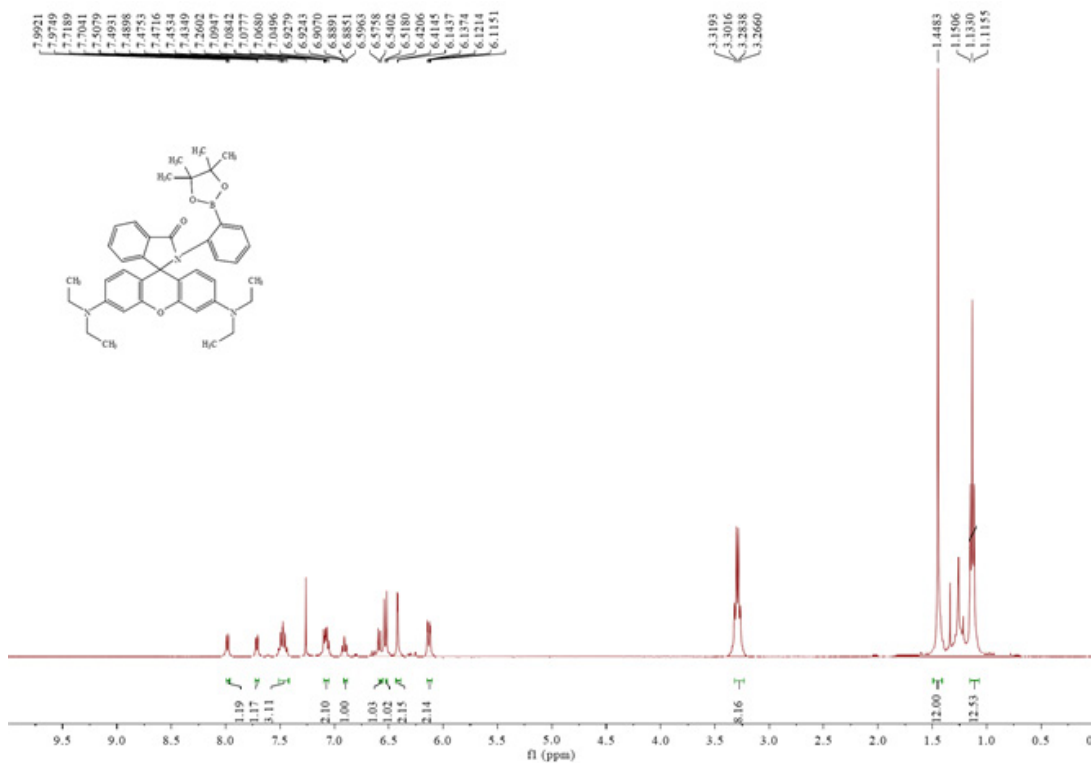

Figure B.1. ¹H NMR spectrum of probe **A** based on rhodamine dye in CD₃OD solution.
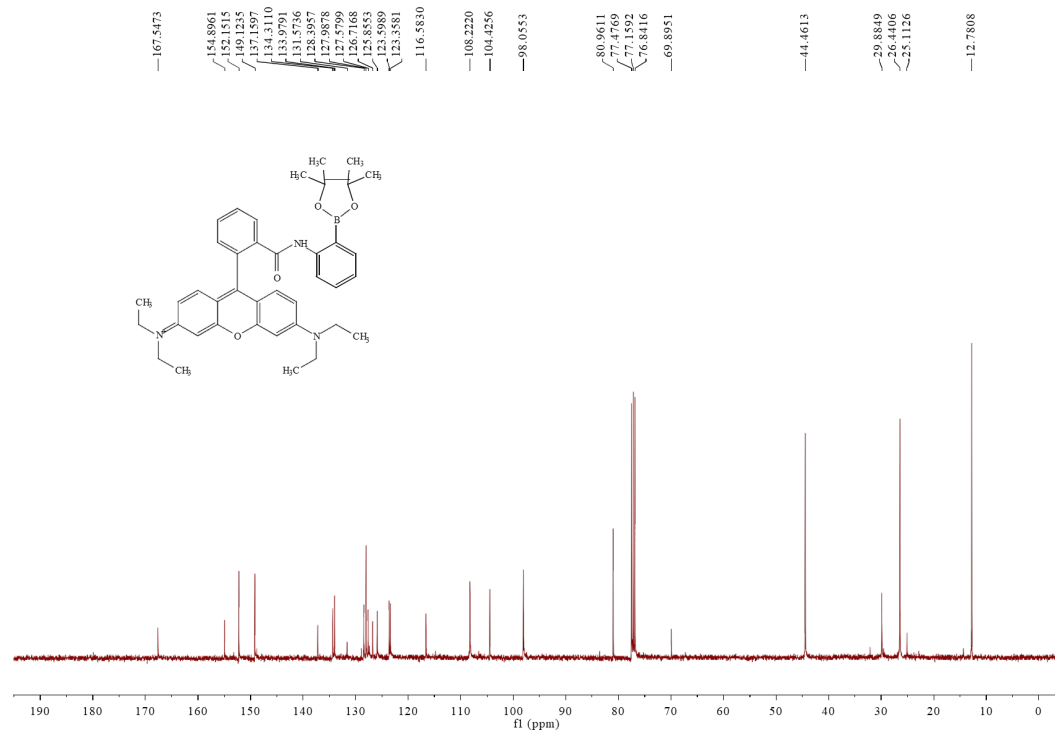
Figure B.2. ^{13}C NMR spectrum of probe **A** based on rhodamine dye in CD$_3$OD solution.
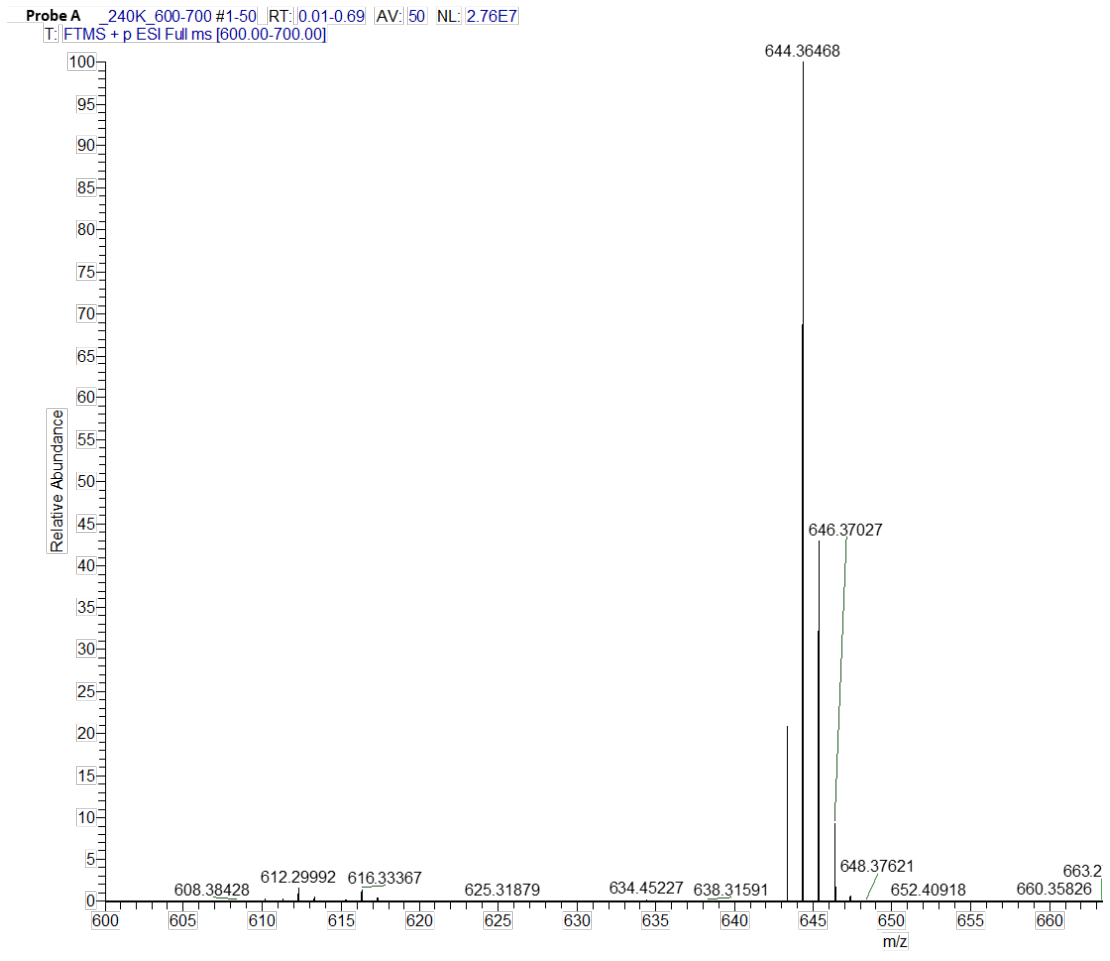
Figure B.3. High-resolution mass spectrum of probe **A**
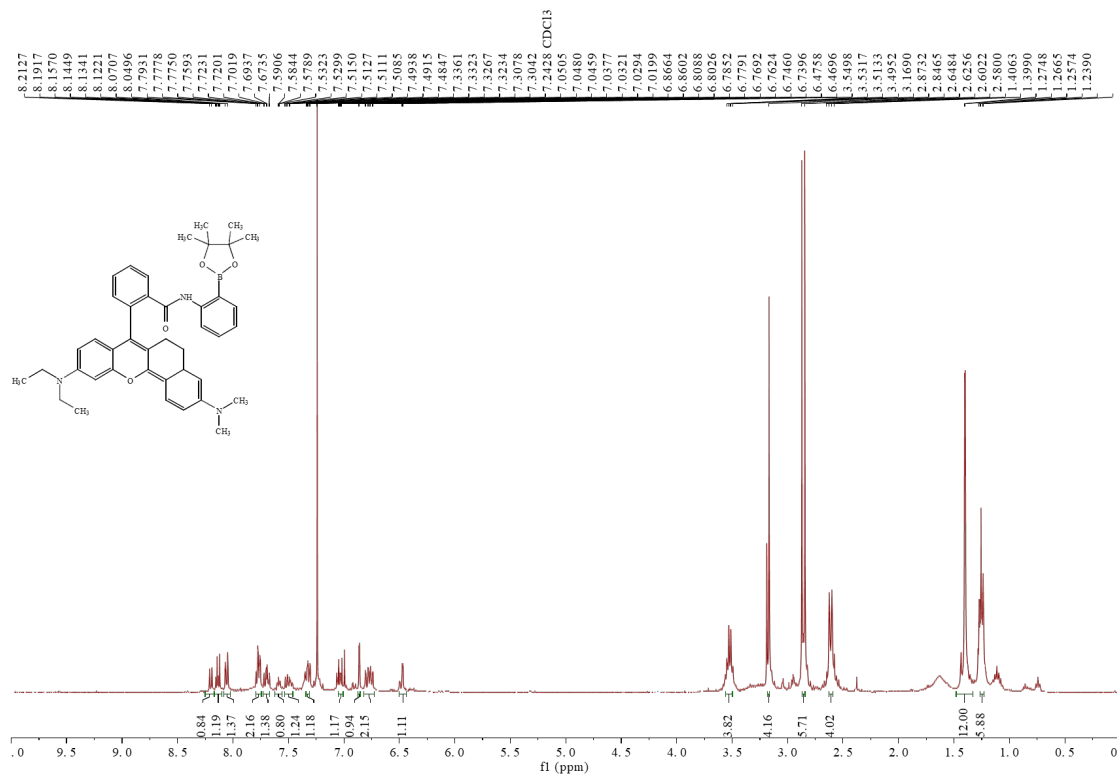
Figure B.4. ^{1}H NMR spectrum of probe **B** in acetonitrile-d_3 solution.
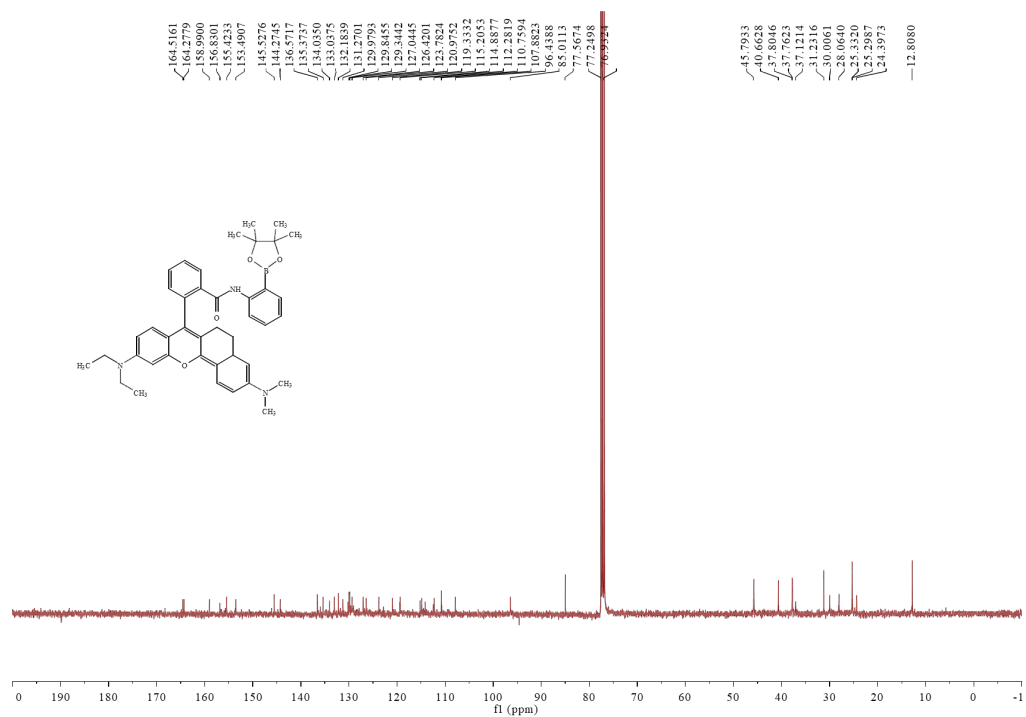
Figure B.5. ^{13}C NMR spectrum of probe **B** in acetonitrile-d_3 solution.

143

Figure B.6. High-resolution mass spectrum of probe **B**

Figure B.7. ^{1}H NMR spectrum of probe **C** based on hemicyanine dye in acetonitrile-d_3 solution.

Figure B.8. ^{13}C NMR spectrum of probe **C** based on hemicyanine dye in acetonitrile-d_3 solution.

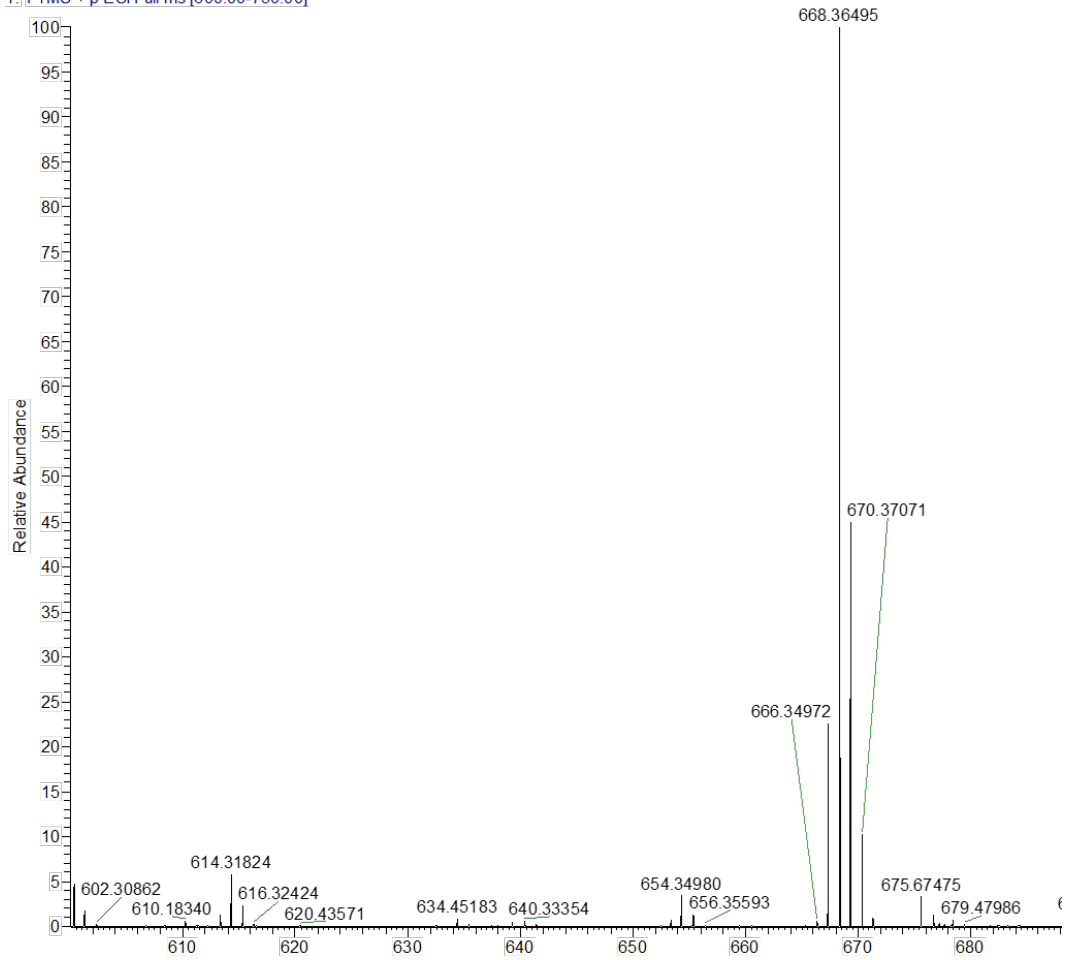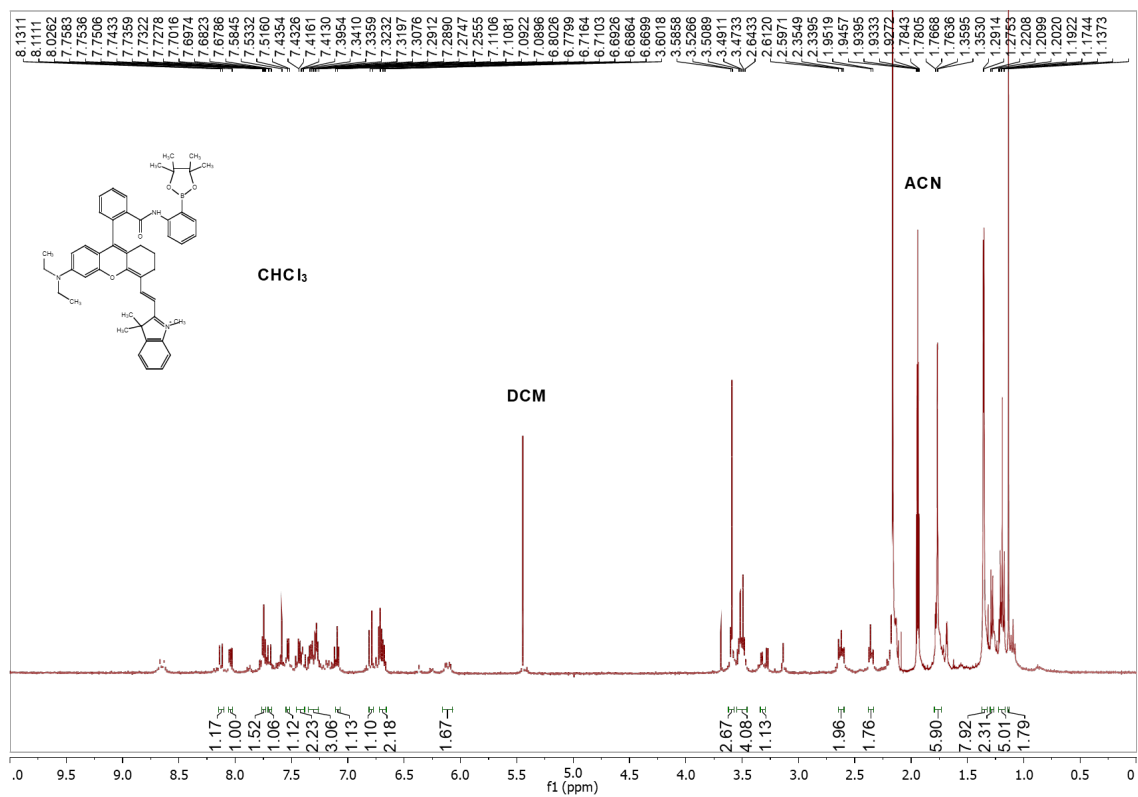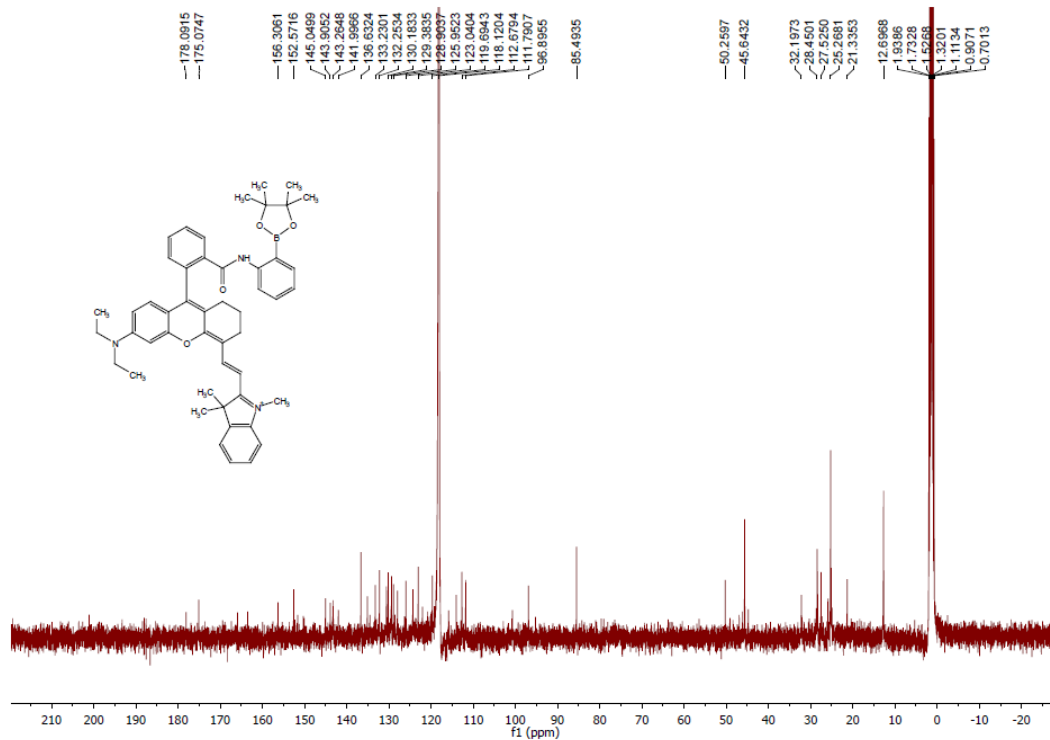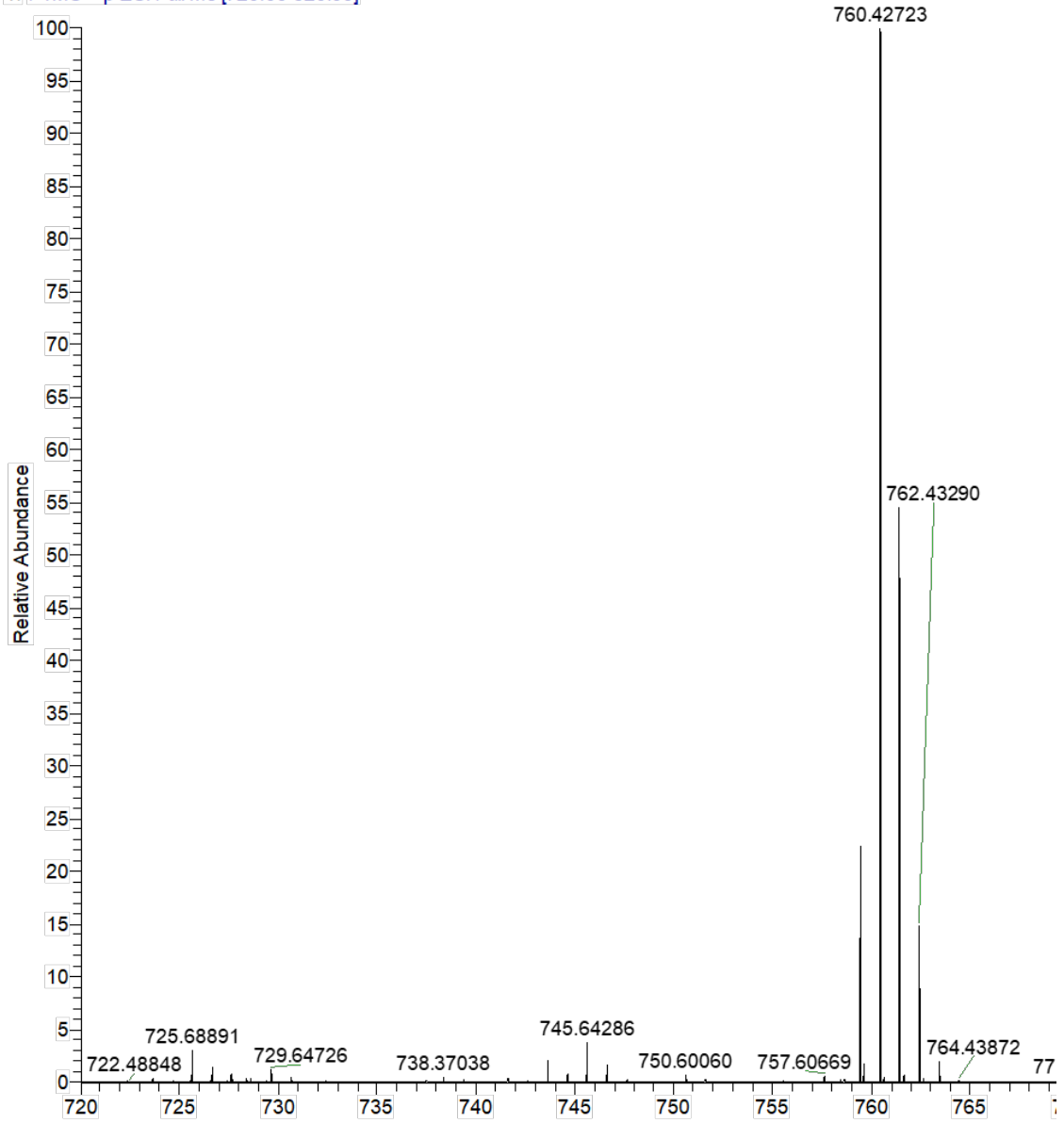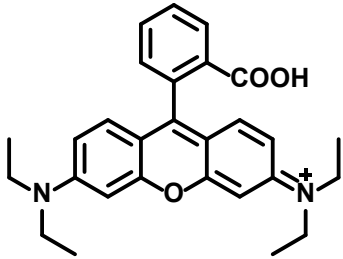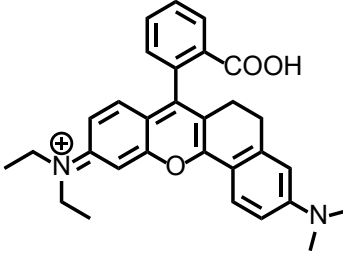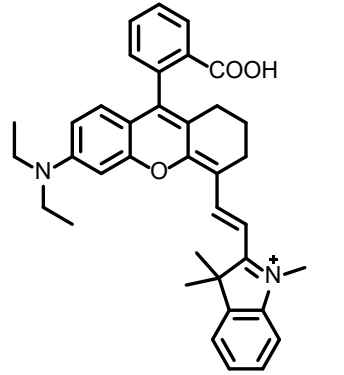**Figure B.9.** High resolution mass spectrum of probe

147

B.2   Calculation of fluorescence quantum yields of probes A, B and C

We chose rhodamine dye B, near-infrared rhodamine dye and near-infrared cyanine dye shown in **Table B1** as fluorescent standard dyes to calculate fluorescence quantum yields of probes A, B and C, respectively.

Table B.1. The standard fluorescent dyes such as rhodamine B, near-infrared rhodamine dye and near-infrared cyanine dye were used as fluorescent standard dyes to calculate the quantum yields of fluorescent probes **A-C,** respectively.

The standard reference for probe A	The standard reference for probe B	The standard reference for probe C
Rhodamine dye B (Φ = 0.31 in water) [146]	Near-infrared rhodamine dye (Φ = 0.37 pH 7.4 PBS contacting 10% EtOH)[111, 149]	Hemicyanine dye (Φ = 0.41 in EtOH)[64]

The UV-Vis absorption spectra of probes A, B and C were collected in the range from 300 to 800 nm with increments of 1 nm. The UV-Vis absorption spectra measured in freshly prepared buffer. Citrate-phosphate buffer was used for acidic pH 4.5, and PBS pH 7.4. The corresponding fluorescence spectra of probes A, B and C were collected under the excitation wavelength of 530 nm, 560 nm, and 660 nm, respectively. The excitation and emission slit widths were set to 4 nm. Rhodamine B, near-infrared rhodamine dye, and

148

near-infrared hemicyanine[111, 149] were utilized as reference standards to calculate the fluorescence quantum yields of probe A, B, and C[64] in ethanol and buffer solutions (Table B.1). The absorption and fluorescence spectra of the standard dyes listed in table B.1 were measured in pH 7.4 PBS buffer with 1% ethanol and in pH 4.5 citrate-phosphate buffer. The absorbance was kept between 0.05 and 0.1 in order to obtain optimized data. All the samples and references were freshly prepared under identical conditions. The fluorescence quantum yields were calculated according to literature4 using t equation 1 below[64]:

$$\phi_{F(X)} = \phi_{F(S)} \left(\frac{A_S F_X}{A_X F_S} \right) \left(\frac{\eta_X}{\eta_S} \right)^2 \qquad (1)$$

Where ϕ_F is the fluorescence quantum yield, A is the absorbance at the excitation wavelength, F is the area under the corrected emission curve, and n is the refractive index of the solvents used. Subscripts S and X refer to the standard and to the unknown, respectively.

Table B.2. Optical properties of fluorescent probes A, B and C

	Solvent	λ_{abs} (nm)	λ_{em} (nm)	Stock Shift (nm)	Φ_f (%)	ε ($10^5 M^{-1}$ cm^{-1})
Probe A	**Buffer (pH 7.4)**	0	0	0	0	0
	Buffer (pH 4.5)	567	585	18	26	0.4
Probe B	**Buffer (pH 7.4)**	619	650	31	9	0.846
	Buffer (pH 4.5)	623	644	21	21	1.67
Probe C	**Buffer (pH 7.4)**	724	740	16	5	1.28
	Buffer (pH 4.5)	717	744	27	10	3.01

B.3 Solvent effects on the probe fluorescence

We investigated the effect of ethanol percentage in water-ethanol mixed solution on dye fluorescence intensity (Figure B.9-B.11). Increase of the percentages of ethanol from 1.0% to 40% resulted in enhancement of fluorescence intensity of the dyes because water increase percentages can effectively prevent fluorescence quenching due to dye aggregation in aqueous solutions.
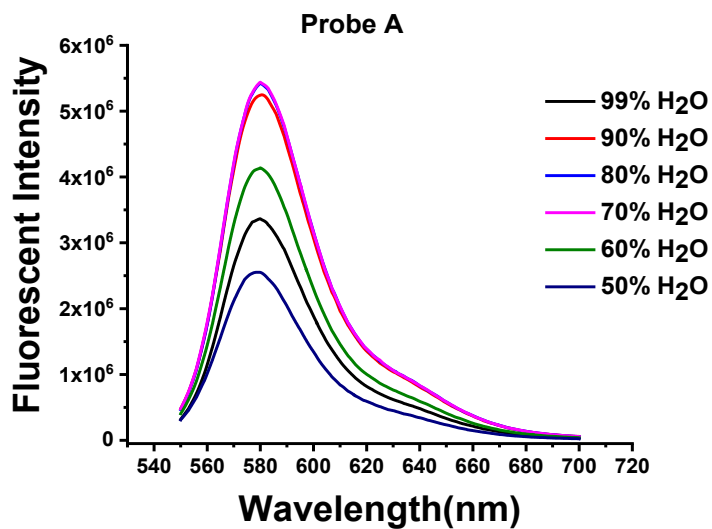
Figure B.10. Fluorescence spectra of 5 μM probe **A** based rhodamine dye B in pH

2.4 buffers with different percentages of ethanol.
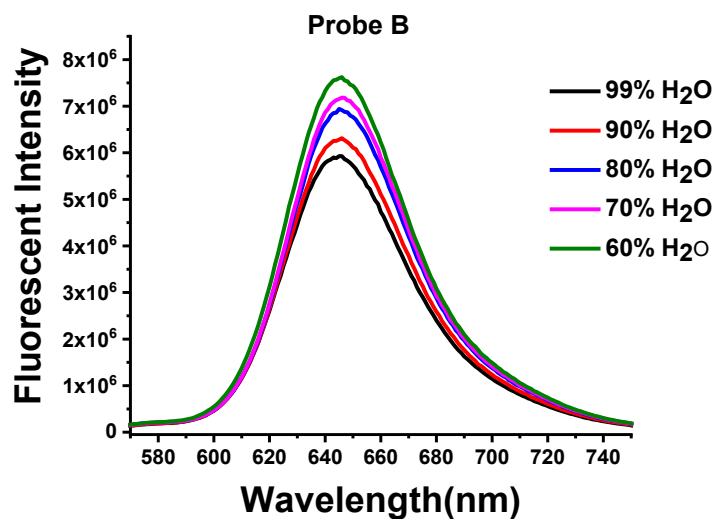
Figure B.11. Fluorescence spectra of 5 μM probe **B** based on near-infrared

rhodamine dye in pH 7.4 buffers containing different percentages of ethanol.
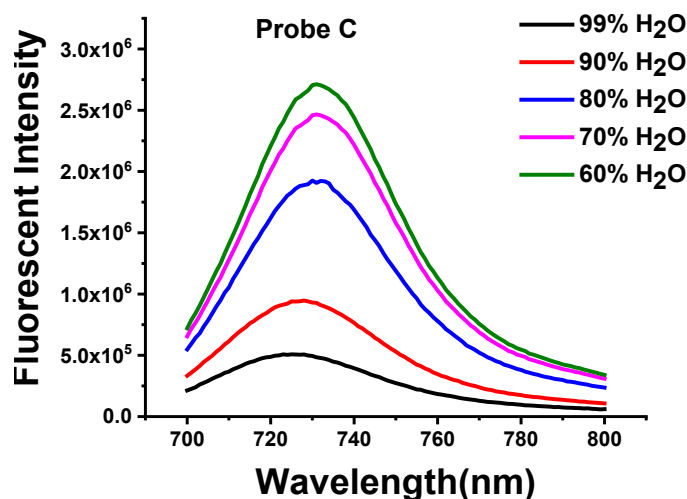
Figure B.12. Fluorescence spectra of 5 µM probe **C** based on near-infrared cyanine dye in pH 7.4 buffers containing different percentages of ethanol.

B.4 Determination of probe pKa values by fluorometric titration

The pKa values of the fluorescent probes A, B and C were calculated by applying equation 2 below[150-151] through fluorometric titration as a function of pH, which were obtained by using the fluorescence spectra. The expression of the steady-state fluorescence intensity F as a function of the proton concentration has been extended for the case of n: 1 complex between H+ and a fluorescent dye.

$$F = \frac{F_{min}[H^+]^n + F_{max}K_a}{K_a + [H^+]^n} \quad (2)$$

F_{min} and F_{max} stand for the fluorescence intensities at maximal and minimal H+ concentrations, respectively while n is apparent stoichiometry of H^+ binding to the probes

A, B and C. Nonlinear fitting of equation expressed above to the fluorescence titration data

was plotted as a function of H^+ concentration.
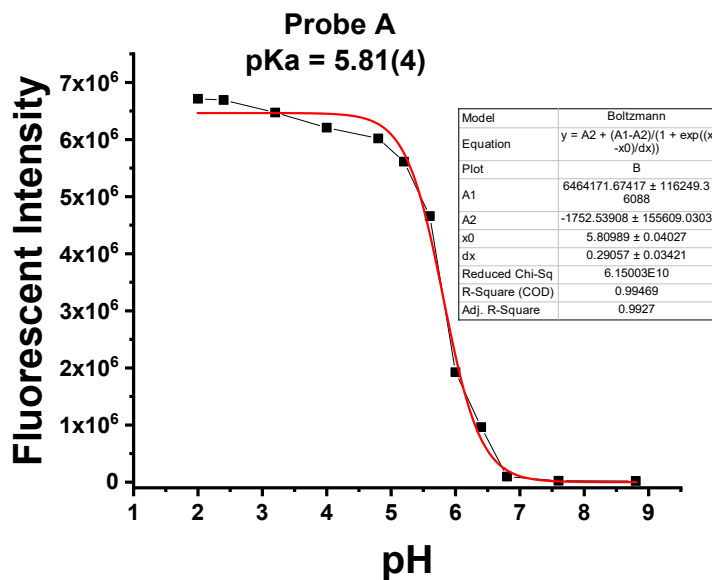
Figure B.13. Plot curve of fluorescence intensity of probe **A** versus pH.
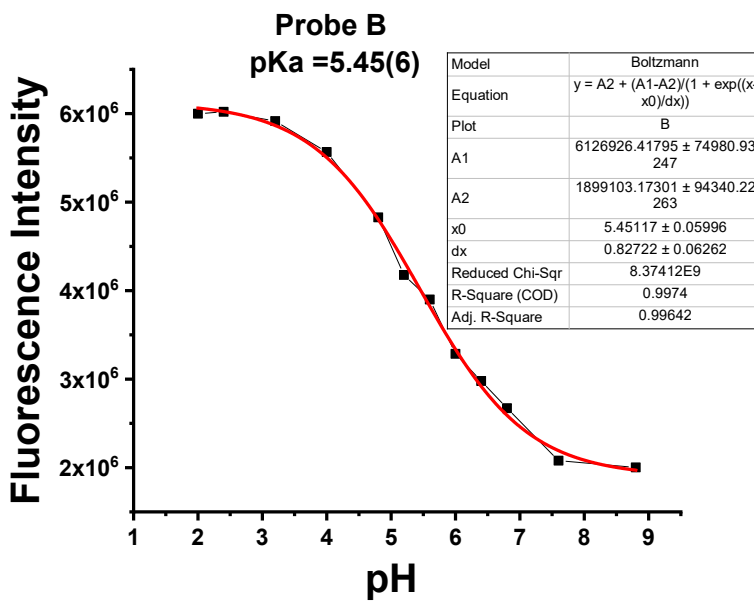
Figure B.14. Plot curve of fluorescence intensity of probe **B** versus pH.

Model	Boltzmann	
Equation	y = A2 + (A1-A2)/(1 + exp ((x-x0)/dx))	
Plot	B	
A1	525478.42152 ± 3343.18	
A2	145561.77292 ± 3310.84	
x0	6.97575 ± 0.05093	
dx	1.29804 ± 0.04943	
Reduced Chi-S	2.00025E7	
R-Square (COD	0.99937	
Adj. R-Square	0.99916	
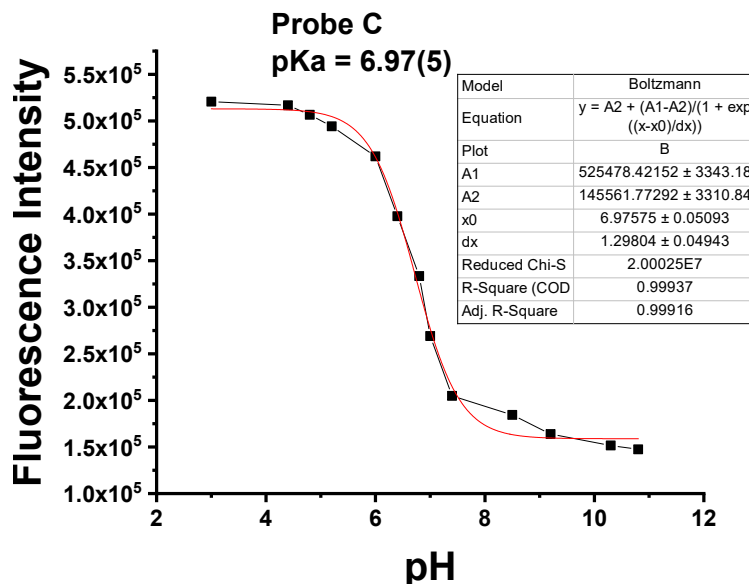
Figure B.15. Plot curve of fluorescence intensity of probe **C** versus pH.

B.5   Determination of pKa by Absorption titration

Figures B.S16-B.S19 show the results of the nonlinear regression of the λ at maximum absorption at 565 nm, 619 nm, and 714 nm of the fluorescent probes A, B and C, respectively, were calculated according to literature method affording a pKa values of 5.8(2), 5.5(1), and 6.31(6)[152-154]

$$pKa = \log\left[\left(\frac{A_{max}-A}{A-A_{min}}\right)\right] + pH \qquad (3)$$
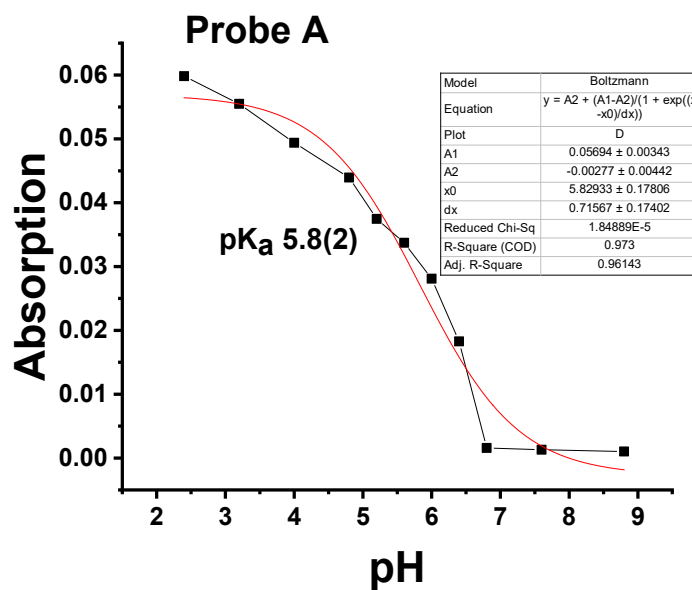
Figure B.16. Plot curve of absorption spectra of probe **A** versus pH.
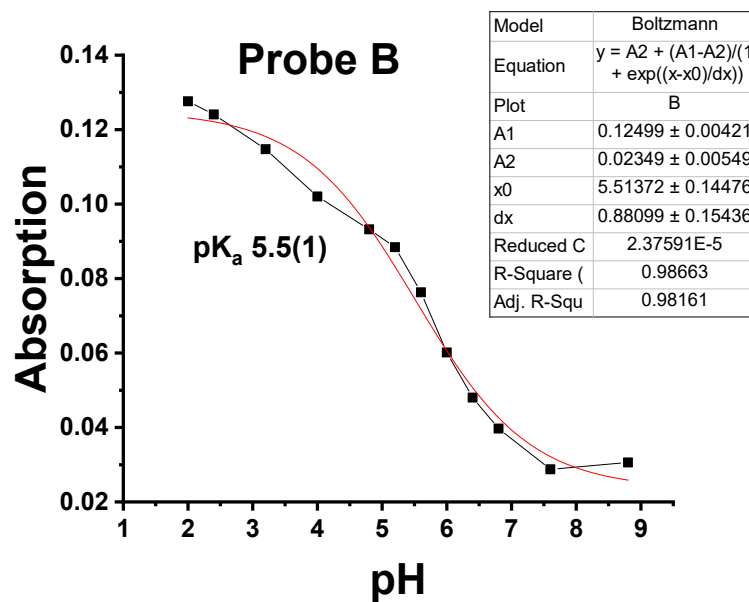
Figure B.17. Plot curve of absorption spectra of probe **B** versus pH.
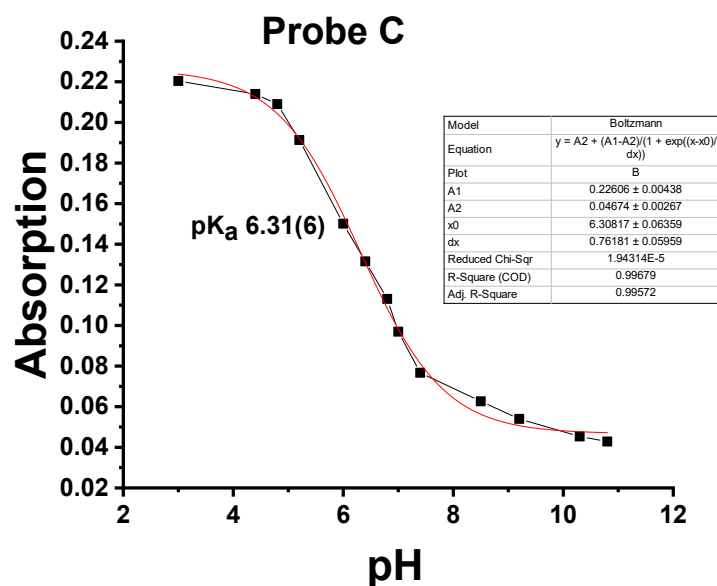
Figure B.18. Plot curve of absorption spectra of probe **C** versus pH.

B.6 Stokes Shifts of probes A, B and C.

Stokes shift is the difference between the maximum absorption λabs and maximum emission λem of a fluorophore. The Stokes shifts for the fluorescent probes A-C were calculated by taking the differences between the maximum absorption peak and the maximum emission peak (Figure S15-S17). Table 2S summarizes the Stokes shifts values of the probes A-C.
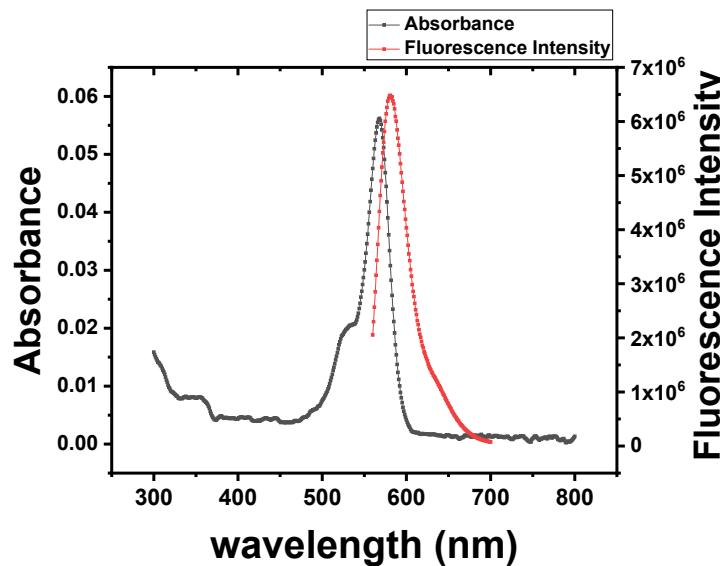
Figure B.19. Absorption and fluorescence spectra of probe **A** in pH 2.0 buffer

containing 1% ethanol. Stokes shift of probe **A** is 14 nm.
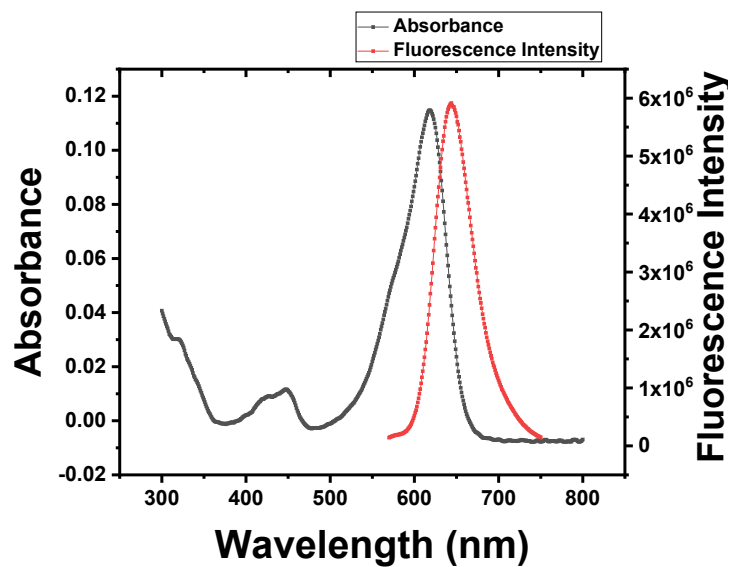
Figure B.20. Absorption and fluorescence spectra of probe **B** in 2.0 buffer containing

1% ethanol, Stokes shift of probe **B** is 23 nm.
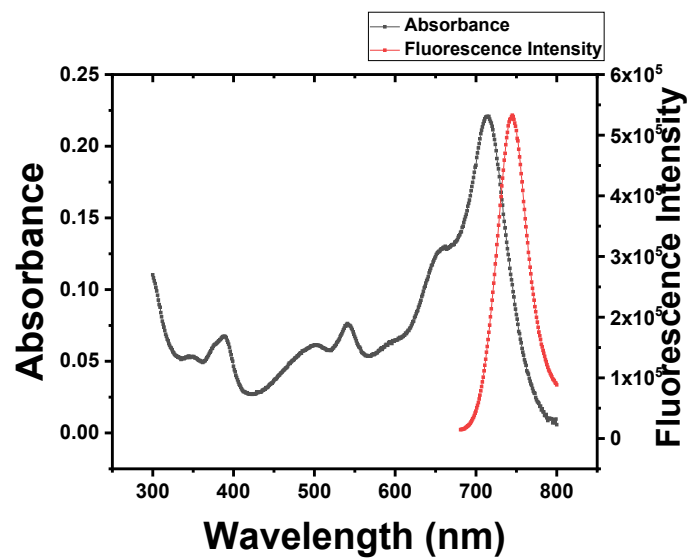
Figure B.21. Absorption and fluorescence spectra of probe **C** in 2.0 buffer containing

1% ethanol, Stokes shift of probe **C** is 31 nm

B.7   Computationally derived structures for probes A-C
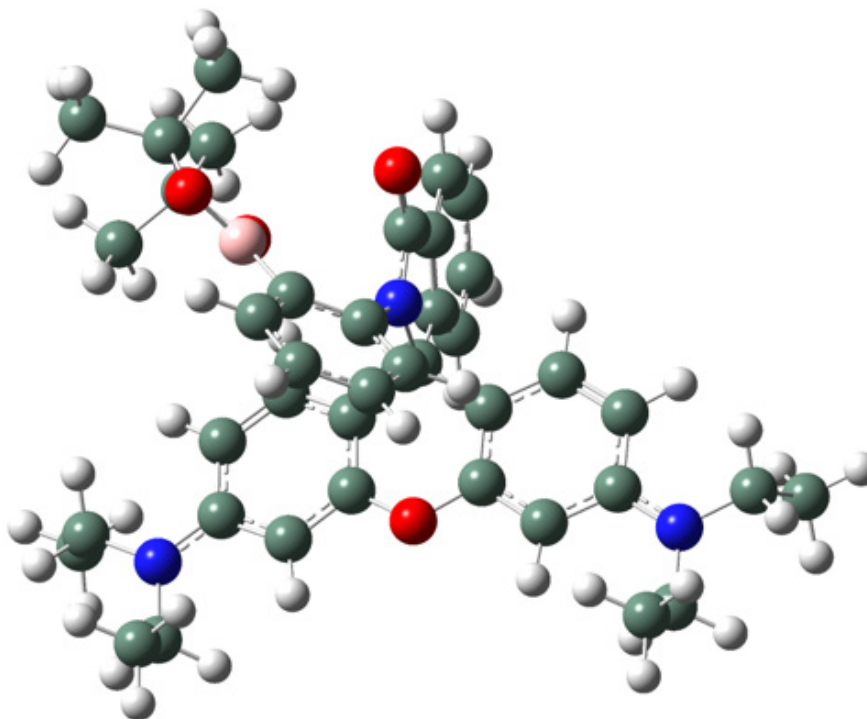
Figure B.22. Drawing of probe, **A** with atoms represented as spheres of arbitrary size (H-white, C-grey, N-blue and O-red) using the GaussView program.

Table B.3. Atomic coordinates for probe **A**.

Row	Symbol	X	Y	Z
1	C	-0.10443	-0.80064	-1.70019
2	C	-1.38118	-0.62082	-2.2518
3	C	-1.47088	-0.02141	-3.51111
4	C	1.033489	-0.40502	-2.39731
5	C	-0.34255	0.418402	-4.19093
6	C	0.913046	0.22108	-3.63055
7	B	-2.7	-1.07977	-1.5563
8	O	-3.81393	-1.4087	-2.2835
9	C	-4.74638	-2.02938	-1.35348
10	C	-4.30219	-1.41976	0.01252
11	O	-2.89055	-1.17167	-0.20885

12	C	-6.16691	-1.69728	-1.76646
13	C	-4.50775	-3.53183	-1.43514
14	C	-4.46221	-2.34458	1.205139
15	C	-4.95116	-0.07275	0.305933
16	C	-0.53332	-3.59617	3.575962
17	C	0.094652	-2.44964	4.071209
18	C	0.508634	-1.43116	3.218554
19	C	0.272532	-1.58268	1.864058
20	C	-0.34514	-2.71881	1.376758
21	C	-0.75827	-3.74346	2.21349
22	C	0.62486	-0.64063	0.739456
23	N	0.03776	-1.38747	-0.42252
24	C	-0.48936	-2.60016	-0.08731
25	O	-0.97891	-3.41475	-0.86054
26	C	2.11691	-0.50134	0.576008
27	C	2.690632	0.704991	0.192663
28	O	1.963003	1.848845	0.025859
29	C	0.668079	1.86471	0.466236
30	C	-0.00075	0.718166	0.88091
31	C	0.072488	3.116414	0.467225
32	C	-1.24925	3.280636	0.911035
33	C	-1.91883	2.123997	1.377066
34	C	-1.30259	0.893421	1.348122
35	C	2.97459	-1.5975	0.666384
36	C	4.321464	-1.51043	0.393055
37	C	4.899483	-0.27966	-0.00549
38	C	4.041301	0.827995	-0.09466
39	N	6.231921	-0.17397	-0.28446
40	N	-1.85845	4.503694	0.906092
41	C	-1.14884	5.706166	0.51688
42	C	-3.26396	4.657096	1.230134
43	C	-3.52003	4.878277	2.716262
44	C	6.845392	1.1023	-0.59564
45	C	7.10099	-1.33503	-0.31968
46	C	7.712756	-1.67084	1.03526
47	C	6.764305	1.46676	-2.07386
48	C	-1.16055	5.954173	-0.9876
49	H	-2.45123	0.112012	-3.95854
50	H	2.012387	-0.59266	-1.974
51	H	-0.44075	0.900204	-5.1583
52	H	1.805552	0.538986	-4.16

53	H	-6.39364	-2.1696	-2.7249
54	H	-6.87315	-2.08084	-1.02589
55	H	-6.31934	-0.62265	-1.86845
56	H	-5.20983	-4.07695	-0.80079
57	H	-4.65603	-3.85862	-2.46688
58	H	-3.48742	-3.78226	-1.13628
59	H	-4.12811	-1.83568	2.112132
60	H	-5.51276	-2.61559	1.336101
61	H	-3.87632	-3.25611	1.090265
62	H	-6.01406	-0.18692	0.52779
63	H	-4.46709	0.373538	1.176007
64	H	-4.84067	0.615078	-0.53549
65	H	-0.84731	-4.37338	4.264715
66	H	0.259828	-2.35332	5.139487
67	H	0.996194	-0.54209	3.604853
68	H	-1.2461	-4.62429	1.809787
69	H	0.661808	3.948006	0.104664
70	H	-2.92413	2.194628	1.769467
71	H	-1.85137	0.022445	1.683877
72	H	2.561866	-2.55873	0.958383
73	H	4.933317	-2.39571	0.502761
74	H	4.395084	1.800276	-0.41039
75	H	-1.61714	6.545796	1.037857
76	H	-0.1236	5.659258	0.893826
77	H	-3.64125	5.508051	0.656053
78	H	-3.81745	3.787357	0.866722
79	H	-4.58888	5.004882	2.909452
80	H	-3.16379	4.031516	3.307879
81	H	-3.00355	5.775383	3.06816
82	H	6.390651	1.881793	0.021594
83	H	7.891134	1.048197	-0.28077
84	H	6.549826	-2.18993	-0.71935
85	H	7.892076	-1.1289	-1.04596
86	H	8.371894	-2.53971	0.95644
87	H	8.302808	-0.83101	1.411848
88	H	6.93817	-1.89524	1.772556
89	H	7.247163	2.429784	-2.26063
90	H	7.265638	0.712242	-2.68595
91	H	5.726203	1.534875	-2.40782
92	H	-0.62174	6.873819	-1.23153
93	H	-0.68955	5.128968	-1.52702

94   H   -2.18547   6.054691   -1.35472

Table B.4. Excitation energies and oscillator strengths for probe **A**.

Excited State   1:   Singlet-A   3.3804 eV 366.77 nm f=0.0015 <S**2>=0.000
    172 -> 173   0.70413
This state for optimization and/or second-order correction.
Total Energy, E(TD-HF/TD-DFT) = -2040.96349687
Copying the excited state density for this state as the 1-particle RhoCI density.

Excited State   2:   Singlet-A   3.5452 eV 349.73 nm f=0.0023 <S**2>=0.000
    171 -> 173   0.69893

Excited State   3:   Singlet-A   3.8762 eV 319.86 nm f=0.0415 <S**2>=0.000
    172 -> 174   0.69819

Excited State   4:   Singlet-A   4.0560 eV 305.68 nm f=0.0385 <S**2>=0.000
    171 -> 174   0.65046
    172 -> 176   0.19748

Excited State   5:   Singlet-A   4.0986 eV 302.51 nm f=0.0584 <S**2>=0.000
    171 -> 174   -0.13477
    172 -> 175   0.65814
    172 -> 176   0.19754

Excited State   6:   Singlet-A   4.1314 eV 300.10 nm f=0.1238 <S**2>=0.000
    171 -> 174   -0.15760
    172 -> 175   -0.23567
    172 -> 176   0.61971

Excited State   7:   Singlet-A   4.2445 eV 292.11 nm f=0.0009 <S**2>=0.000
    170 -> 173   0.59587
    171 -> 175   0.31971
    171 -> 176   0.13410
    172 -> 178   -0.10243

Excited State   8:   Singlet-A   4.2499 eV 291.74 nm f=0.0104 <S**2>=0.000
    170 -> 173   -0.31303
    171 -> 174   -0.12475
    171 -> 175   0.28452
    171 -> 176   0.39845
    172 -> 178   -0.33311

Excited State   9:   Singlet-A   4.2767 eV 289.90 nm f=0.0134 <S**2>=0.000
    170 -> 173   -0.18888

```
171 -> 175      0.55108
171 -> 176     -0.31307
172 -> 178      0.20001


Excited State  10:      Singlet-A      4.3976 eV  281.94 nm  f=0.0342  <S**2>=0.000
171 -> 176      0.21005
171 -> 178     -0.25667
172 -> 176     -0.11965
172 -> 177      0.50930
172 -> 178      0.30066
```

The FTIR spectra of the unprotonated and protonated fluorescent probes A-B (Figures B.23, B.29, B.34, B.41, B.46, and B.51) were calculated to confirm that the geometries of the structures have been optimized to a suitable minimum.
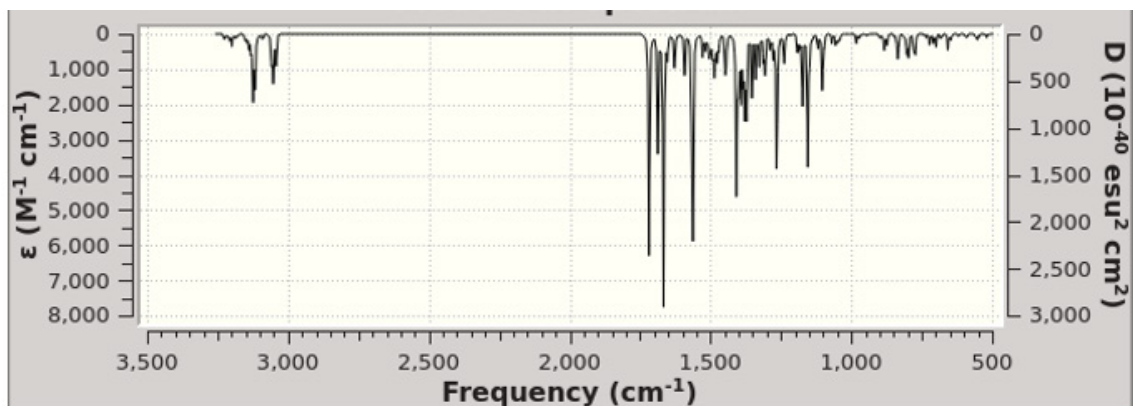
Figure B.23. Calculated (top) FTIR spectrum of probe **A**.
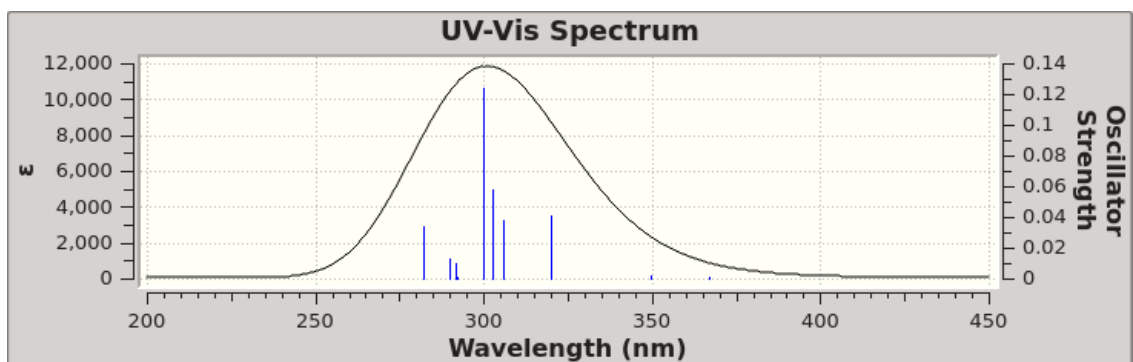
Figure B.24. Calculated UV-Vis spectrum for probe **A** in water.
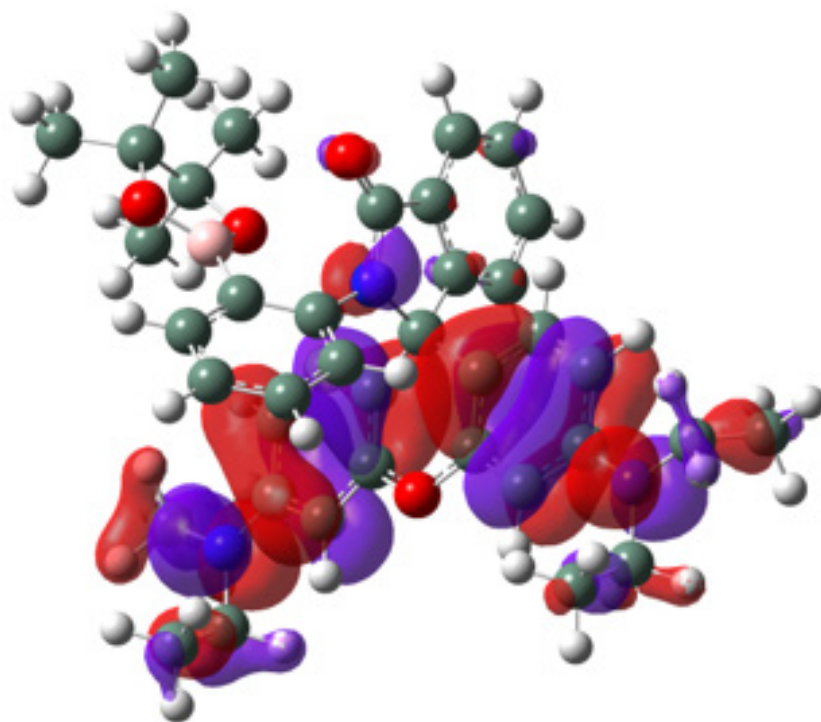
Figure B.25. MO for level 172 for probe **A** involved with the transition noted as Excited
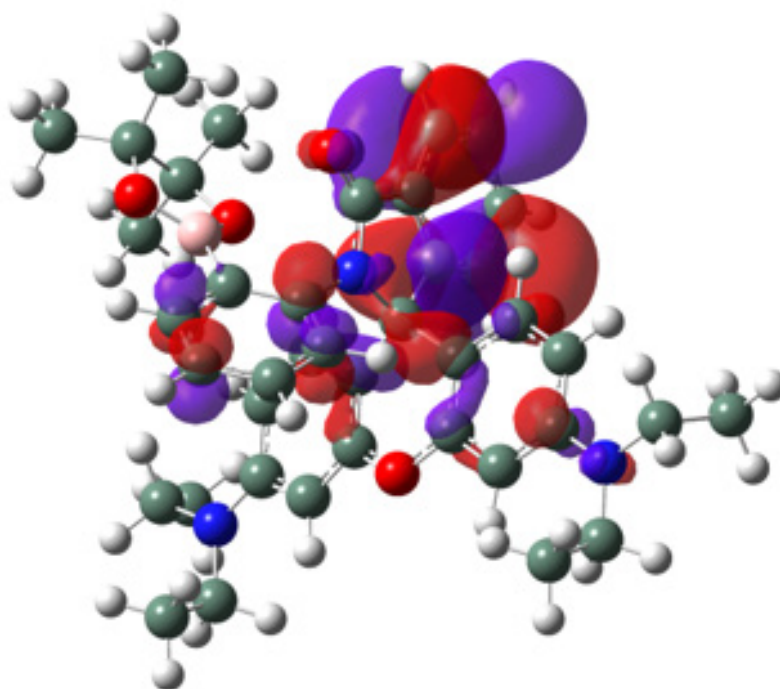
State 6 in Table B.4.

Figure B.26. MO for level 175 for probe **A** involved with the transition noted as Excited
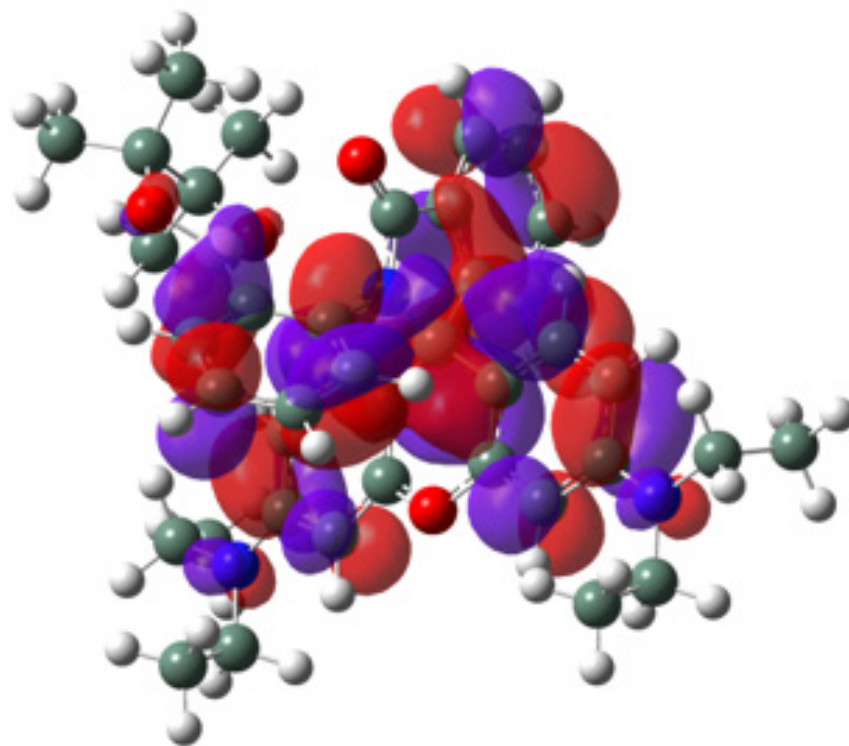
State 6 in Table B.4.

Figure B.27. MO for level 176 for probe **A** involved with the transition noted as Excited

State 6 in Table B.4.
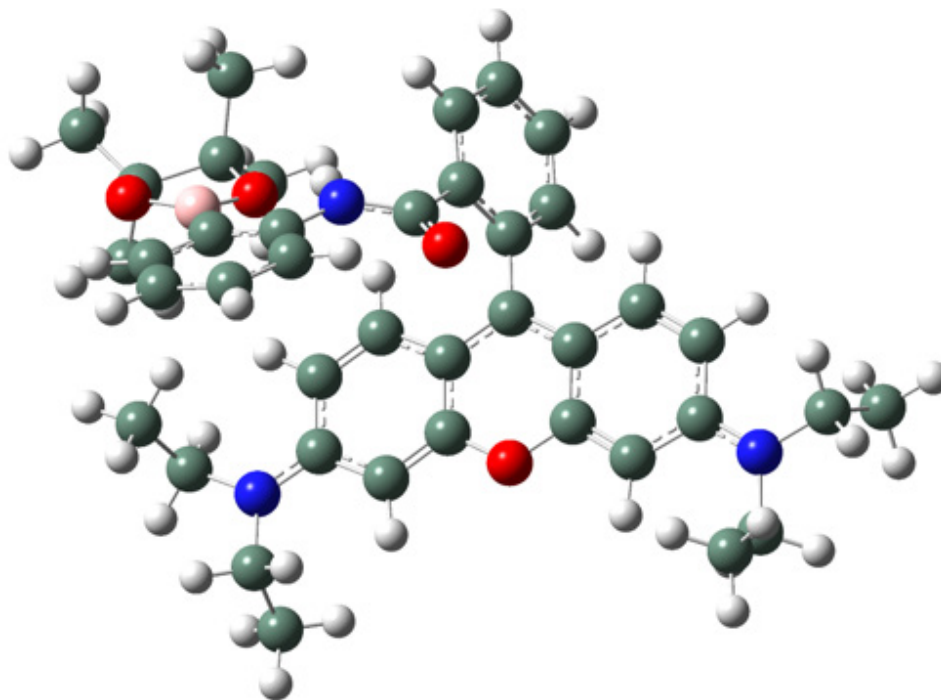
Figure B.28. Drawing of probe **AH**⁺ with atoms represented as spheres of arbitrary size (H-white, C-grey, N-blue and O-red) using the GaussView program.

Table B.5. Atomic coordinates for probe **AH**⁺

| Row	Symbol	X	Y	Z
1	C	2.041321	-0.31722	2.412743
2	C	3.337538	0.085829	2.029367
3	C	3.97193	1.076515	2.782881
4	C	1.414703	0.270263	3.512193
5	C	3.351983	1.672312	3.870862
6	C	2.071837	1.262695	4.22626
7	B	4.079251	-0.50073	0.798573
8	O	5.404141	-0.30627	0.54402
9	C	5.669255	-0.82771	-0.79176
10	C	4.500779	-1.84523	-0.99536
11	O	3.455954	-1.2678	-0.15842
12	C	5.609525	0.354886	-1.7489
13	C	7.052488	-1.44843	-0.81941
14	C	4.794701	-3.22719	-0.4295
15	C	3.987936	-1.95673	-2.4175

16	C	0.170439	-4.74969	-0.59469
17	C	-0.72017	-4.40523	-1.60237
18	C	-1.32985	-3.15675	-1.59647
19	C	-1.05578	-2.24555	-0.58182
20	C	-0.16011	-2.5966	0.435525
21	C	0.45323	-3.84365	0.419928
22	C	-1.64614	-0.89147	-0.61234
23	N	1.431925	-1.3271	1.660282
24	C	0.111113	-1.61462	1.535076
25	O	-0.79449	-1.12453	2.193866
26	C	-0.81784	0.219669	-0.81469
27	C	-1.3735	1.521117	-0.72899
28	O	-2.7022	1.695314	-0.5403
29	C	-3.52626	0.63007	-0.4029
30	C	-3.01553	-0.6937	-0.41492
31	C	-4.85461	0.912966	-0.21797
32	C	-5.78144	-0.13402	-0.02021
33	C	-5.27484	-1.47391	0.003249
34	C	-3.95267	-1.73023	-0.18202
35	C	0.572233	0.147632	-1.0775
36	C	1.3405	1.263143	-1.179
37	C	0.776266	2.57023	-1.03467
38	C	-0.61791	2.660882	-0.82704
39	N	1.54931	3.666534	-1.10069
40	N	-7.09071	0.113664	0.14826
41	C	-8.05345	-0.93728	0.457876
42	C	-7.6403	1.458645	0.034937
43	C	-7.61179	2.218289	1.354071
44	C	2.973897	3.598155	-1.40455
45	C	1.017029	5.000721	-0.85668
46	C	0.473125	5.65625	-2.11846
47	C	3.8257	3.373995	-0.164
48	C	-8.62817	-1.59317	-0.78948
49	H	4.970196	1.389577	2.493074
50	H	0.423295	-0.04992	3.797956
51	H	3.858762	2.446295	4.43702
52	H	1.573592	1.716502	5.077226
53	H	6.32782	1.110934	-1.42684
54	H	5.861352	0.051623	-2.76651
55	H	4.619095	0.812963	-1.76133
56	H	7.228617	-1.93037	-1.78402

57	H	7.808563	-0.67195	-0.68611
58	H	7.178774	-2.19037	-0.0311
59	H	3.872635	-3.81236	-0.42709
60	H	5.532161	-3.75276	-1.0387
61	H	5.166295	-3.16895	0.596042
62	H	4.784178	-2.3086	-3.07749
63	H	3.170405	-2.67975	-2.45745
64	H	3.620352	-1.00251	-2.79476
65	H	0.646348	-5.72425	-0.59601
66	H	-0.93872	-5.10604	-2.40075
67	H	-2.00813	-2.87547	-2.39497
68	H	1.143564	-4.11146	1.213281
69	H	2.025538	-1.71923	0.934529
70	H	-5.15256	1.951596	-0.19792
71	H	-5.94887	-2.30452	0.158157
72	H	-3.59851	-2.7541	-0.15913
73	H	1.037096	-0.82309	-1.19503
74	H	2.398278	1.144336	-1.35889
75	H	-1.12502	3.612676	-0.75574
76	H	-7.58862	-1.67314	1.115308
77	H	-8.8493	-0.47359	1.044675
78	H	-7.10427	2.000054	-0.74659
79	H	-8.66731	1.354124	-0.32147
80	H	-8.05037	3.210675	1.226358
81	H	-8.18477	1.690012	2.119965
82	H	-6.58989	2.339948	1.72017
83	H	3.146785	2.824497	-2.15445
84	H	3.240912	4.541041	-1.88612
85	H	0.254372	4.944584	-0.07792
86	H	1.831076	5.596941	-0.4388
87	H	0.103623	6.659227	-1.89256
88	H	1.253676	5.744841	-2.87801
89	H	-0.3488	5.076075	-2.54389
90	H	4.884412	3.339222	-0.43011
91	H	3.681986	4.182211	0.557254
92	H	3.56497	2.437335	0.332212
93	H	-9.36375	-2.35159	-0.51134
94	H	-9.12486	-0.85551	-1.42448
95	H	-7.84517	-2.07502	-1.37947

Table B.6. Excitation energies and oscillator strengths for probe **AH⁺**.

Excited State   1:   Singlet-A   2.6234 eV 472.61 nm f=0.9828 <S**2>=0.000
  172 -> 173   0.70358
This state for optimization and/or second-order correction.
Total Energy, E(TD-HF/TD-DFT) = -2041.44587968
Copying the excited state density for this state as the 1-particle RhoCI density.

Excited State   2:   Singlet-A   3.0917 eV 401.03 nm f=0.0078 <S**2>=0.000
  171 -> 173   0.69641

Excited State   3:   Singlet-A   3.1996 eV 387.49 nm f=0.0225 <S**2>=0.000
  169 -> 173   -0.18512
  170 -> 173   0.66697
  171 -> 173   0.10920

Excited State   4:   Singlet-A   3.6915 eV 335.87 nm f=0.0956 <S**2>=0.000
  166 -> 173   0.11939
  167 -> 173   -0.27224
  168 -> 173   -0.32505
  169 -> 173   0.51168
  170 -> 173   0.11849
  172 -> 174   -0.12229

Excited State   5:   Singlet-A   3.7684 eV 329.01 nm f=0.0098 <S**2>=0.000
  167 -> 173   -0.28468
  168 -> 173   -0.35045
  169 -> 173   -0.21731
  172 -> 174   0.47522

Excited State   6:   Singlet-A   3.8070 eV 325.68 nm f=0.1238 <S**2>=0.000
  167 -> 173   0.19598
  168 -> 173   0.26353
  169 -> 173   0.33080
  172 -> 174   0.50014

Excited State   7:   Singlet-A   4.0217 eV 308.29 nm f=0.0011 <S**2>=0.000
  167 -> 173   0.54611
  168 -> 173   -0.44295

Excited State   8:   Singlet-A   4.0788 eV 303.98 nm f=0.0047 <S**2>=0.000
  166 -> 173   0.65830
  172 -> 175   -0.16610

Excited State   9:   Singlet-A   4.2076 eV 294.67 nm f=0.1086 <S**2>=0.000
   165 -> 173   -0.31046
   166 -> 173   0.12989
   172 -> 175   0.41997
   172 -> 176   0.40457

Excited State 10:   Singlet-A   4.2496 eV 291.76 nm f=0.0139 <S**2>=0.000
   163 -> 173   0.14954
   165 -> 173   0.11219
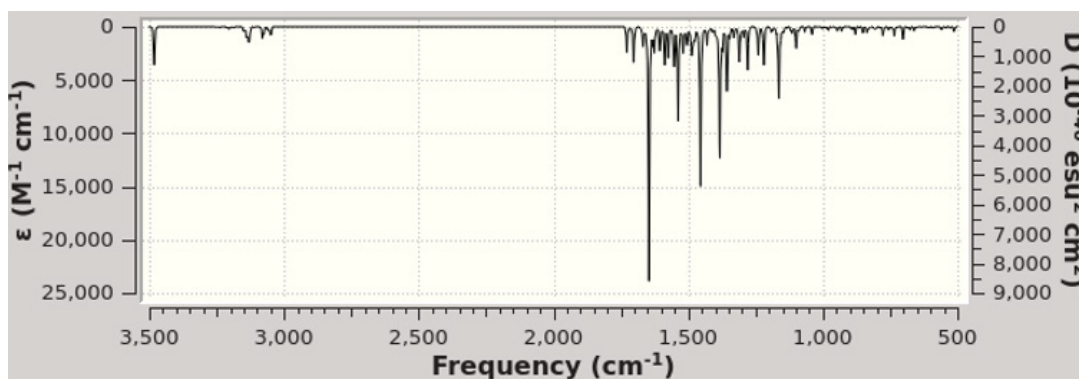   172 -> 175   0.49397
   172 -> 176   -0.43162

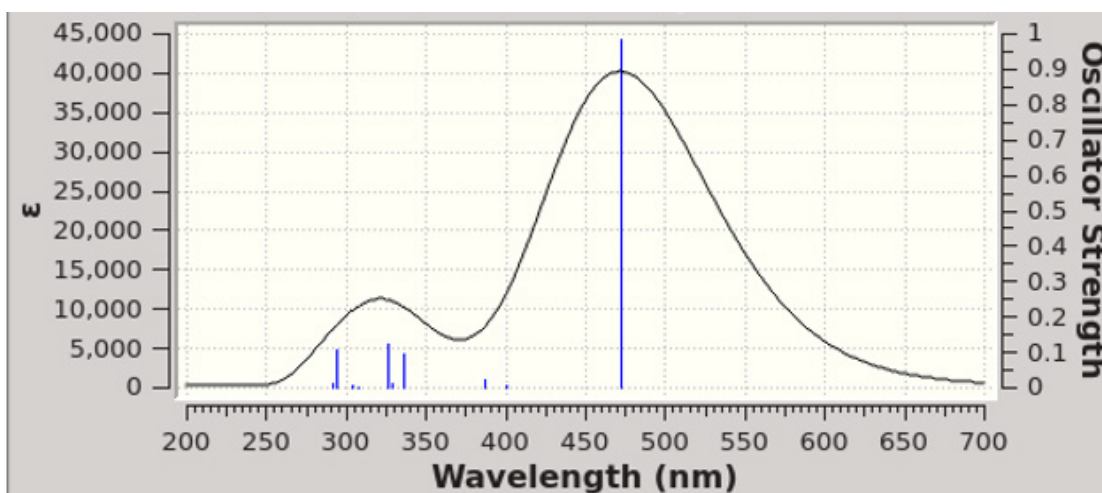**Figure B.29**. Calculated (top) FTIR spectrum of probe **AH⁺**.

Figure B.30. Calculated UV-Vis spectrum for probe **AH⁺** in water.
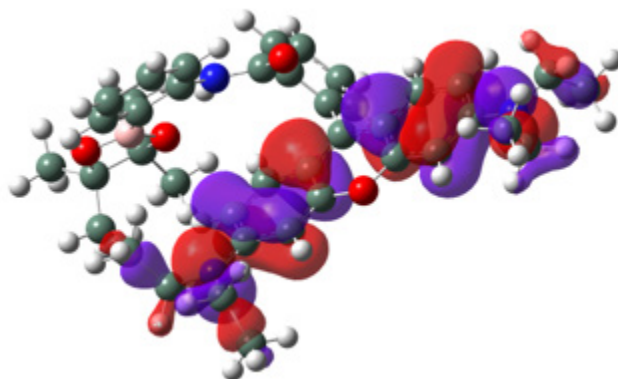
172

Figure B.31. MO for level 172 for probe **AH**⁺ involved with the transition noted as
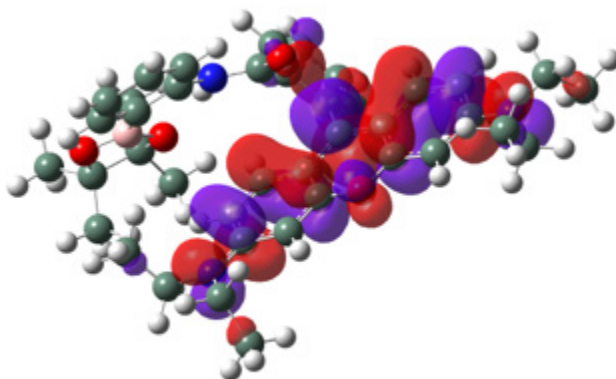
Excited State 1 in Table B.6.

Figure B.32. MO for level 173 for probe **AH**⁺ involved with the transition noted as Excited
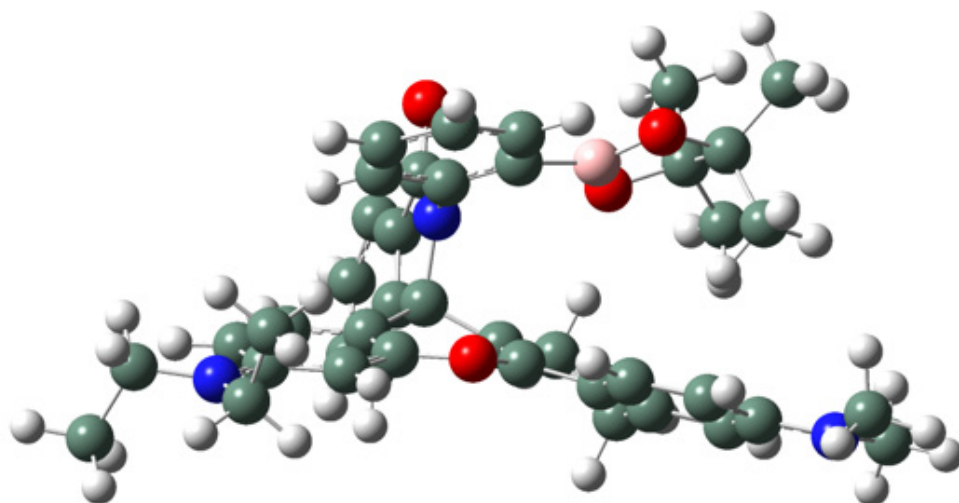
State 1 in Table B.6.

Figure B.33. Drawing of probe **B** with atoms represented as spheres of arbitrary size (H-white, C-grey, N-blue and O-red) using the GaussView program.

Table **B.7**. Atomic coordinates for probe **B**.

Row	Symbol	X	Y	Z
1	C	-1.16672	1.303049	-0.75014
2	C	-0.00035	0.546961	-1.32624
3	C	0.101849	-0.76556	-1.06142
4	O	-0.9087	-1.49804	-0.49828
5	C	-2.16269	-0.95763	-0.52392
6	C	-2.36319	0.402024	-0.74212
7	C	1.133837	1.259481	-1.99892
8	C	1.986662	0.307845	-2.83244
9	C	2.316473	-0.96	-2.09852
10	C	1.327953	-1.51832	-1.27587
11	C	-3.20459	-1.83598	-0.28682
12	C	-4.53167	-1.37574	-0.26339
13	C	-4.74461	-0.00051	-0.53047
14	C	-3.68216	0.849895	-0.75093
15	C	3.531974	-1.597	-2.25537
16	C	3.821155	-2.81239	-1.601
17	C	2.813616	-3.36434	-0.78708
18	C	1.594566	-2.72674	-0.63672

174

19	N	-5.57356	-2.2214	-0.00549
20	N	5.042618	-3.42711	-1.74943
21	C	-6.93074	-1.73416	0.15422
22	C	-5.3598	-3.63454	0.237548
23	C	-7.70762	-1.68051	-1.15569
24	C	-4.98889	-3.94686	1.683479
25	C	5.397646	-4.50264	-0.85014
26	C	6.133152	-2.68419	-2.34203
27	N	-0.82889	1.748037	0.655832
28	C	-0.79785	3.09757	0.8072
29	O	-0.57674	3.7076	1.847804
30	C	-0.85344	0.841441	1.748782
31	C	-2.10473	0.499442	2.257497
32	C	-2.22463	-0.44974	3.260636
33	C	-1.08491	-1.05922	3.769704
34	C	0.161508	-0.68337	3.291876
35	C	0.310926	0.274934	2.280066
36	B	1.77056	0.675497	1.912982
37	O	2.156139	1.559067	0.949371
38	C	3.57435	1.814549	1.142069
39	C	4.038979	0.556561	1.942538
40	O	2.822598	0.162044	2.627799
41	C	5.130245	0.825851	2.961505
42	C	4.252582	1.979087	-0.20512
43	C	-1.38725	2.638471	-1.40576
44	C	-1.12324	3.667233	-0.51988
45	C	-1.7631	2.907964	-2.70999
46	C	-1.86654	4.239587	-3.10051
47	C	-1.59355	5.276519	-2.20505
48	C	-1.21861	4.997539	-0.89673
49	C	4.428586	-0.61204	1.050444
50	C	3.670585	3.108477	1.938813
51	H	0.741154	2.044071	-2.65087
52	H	1.736785	1.762631	-1.23862
53	H	1.425329	0.035628	-3.7374
54	H	2.899643	0.8054	-3.17023
55	H	-2.95358	-2.87099	-0.09798
56	H	-5.74803	0.402005	-0.56619
57	H	-3.87735	1.90466	-0.9186
58	H	4.275576	-1.12737	-2.88741
59	H	2.98739	-4.28571	-0.24691

60	H	0.844009	-3.16459	0.012382
61	H	-7.43604	-2.39819	0.860873
62	H	-6.91231	-0.75246	0.634708
63	H	-6.28132	-4.156	-0.03446
64	H	-4.59564	-4.00918	-0.44878
65	H	-8.72686	-1.3225	-0.98625
66	H	-7.22529	-1.0115	-1.87249
67	H	-7.76752	-2.67325	-1.60974
68	H	-4.83893	-5.02115	1.820664
69	H	-4.06936	-3.43337	1.974658
70	H	-5.78274	-3.62583	2.363245
71	H	5.434223	-4.17798	0.199127
72	H	4.686966	-5.32842	-0.92791
73	H	6.377947	-4.88609	-1.12738
74	H	5.893594	-2.3833	-3.36448
75	H	6.386859	-1.78181	-1.76869
76	H	7.012994	-3.32346	-2.38593
77	H	-2.98801	0.968407	1.840744
78	H	-3.20715	-0.71649	3.636443
79	H	-1.16707	-1.81338	4.545811
80	H	1.053496	-1.13668	3.711445
81	H	6.024121	1.208231	2.462382
82	H	4.816082	1.549376	3.714079
83	H	5.399089	-0.1035	3.468547
84	H	5.330026	2.098182	-0.06585
85	H	4.079948	1.120498	-0.85367
86	H	3.877395	2.874536	-0.70575
87	H	-1.9719	2.10404	-3.40838
88	H	-2.16376	4.477751	-4.11667
89	H	-1.68044	6.305982	-2.53623
90	H	-1.01068	5.789643	-0.1852
91	H	4.562309	-1.50228	1.668915
92	H	3.655066	-0.82447	0.311841
93	H	5.366365	-0.41868	0.525508
94	H	3.156946	3.900652	1.389926
95	H	3.195693	3.009079	2.917598
96	H	4.709833	3.410144	2.083574

Table B.8. Excitation energies and oscillator strengths for probe **B**.

Excited State   1:   Singlet-A   3.3857 eV 366.20 nm f=0.0024 <S**2>=0.000
   178 -> 179   0.69791
This state for optimization and/or second-order correction.
Total Energy, E(TD-HF/TD-DFT) = -2117.13022654
Copying the excited state density for this state as the 1-particle RhoCI density.

Excited State   2:   Singlet-A   3.4776 eV 356.52 nm f=0.0117 <S**2>=0.000
   178 -> 180   0.69882

Excited State   3:   Singlet-A   3.6765 eV 337.24 nm f=0.0130 <S**2>=0.000
   176 -> 179   -0.10110
   177 -> 179   0.69249

Excited State   4:   Singlet-A   3.7853 eV 327.54 nm f=0.2651 <S**2>=0.000
   177 -> 180   -0.48571
   178 -> 181   0.49448

Excited State   5:   Singlet-A   3.8083 eV 325.57 nm f=0.1509 <S**2>=0.000
   177 -> 180   0.50625
   178 -> 181   0.47561

Excited State   6:   Singlet-A   3.9866 eV 311.00 nm f=0.0945 <S**2>=0.000
   178 -> 182   0.69277

Excited State   7:   Singlet-A   4.0599 eV 305.39 nm f=0.0397 <S**2>=0.000
   177 -> 181   0.67233
   178 -> 181   -0.10129

Excited State   8:   Singlet-A   4.0983 eV 302.53 nm f=0.0079 <S**2>=0.000
   178 -> 183   0.58475
   178 -> 184   -0.34977

Excited State   9:   Singlet-A   4.1756 eV 296.93 nm f=0.1068 <S**2>=0.000
   177 -> 183   0.11428
   177 -> 184   -0.10551
   178 -> 183   0.36540
   178 -> 184   0.54778

Excited State 10:   Singlet-A   4.3001 eV 288.33 nm f=0.0144 <S**2>=0.000
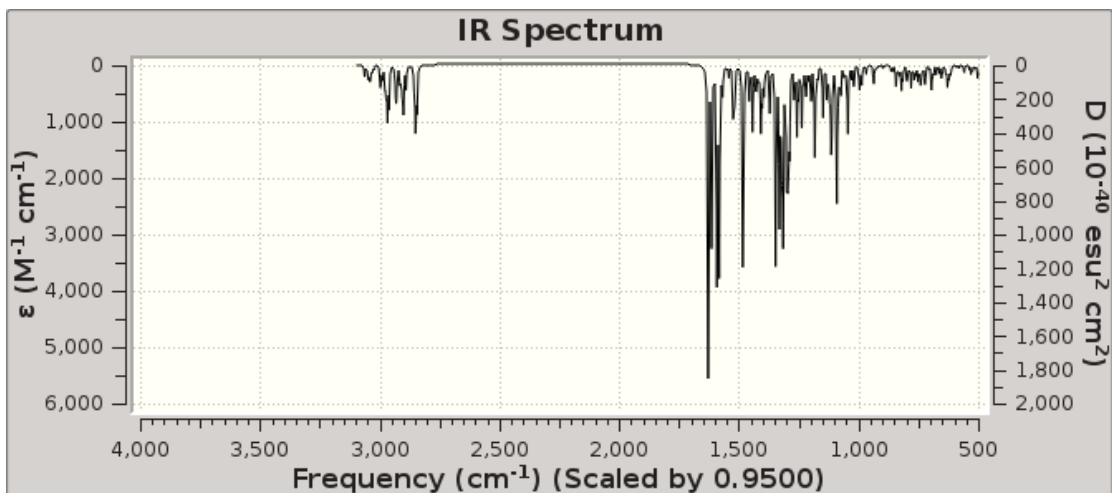   177 -> 182   0.69253

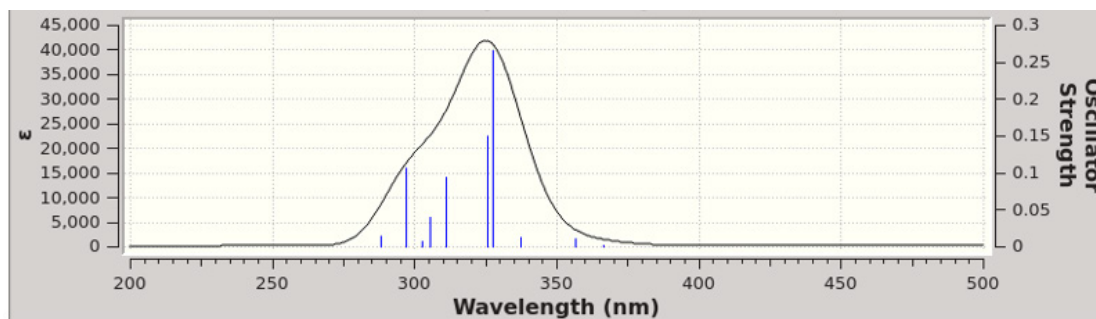**Figure B.34**. Calculated (top) FTIR spectrum of probe **B**.

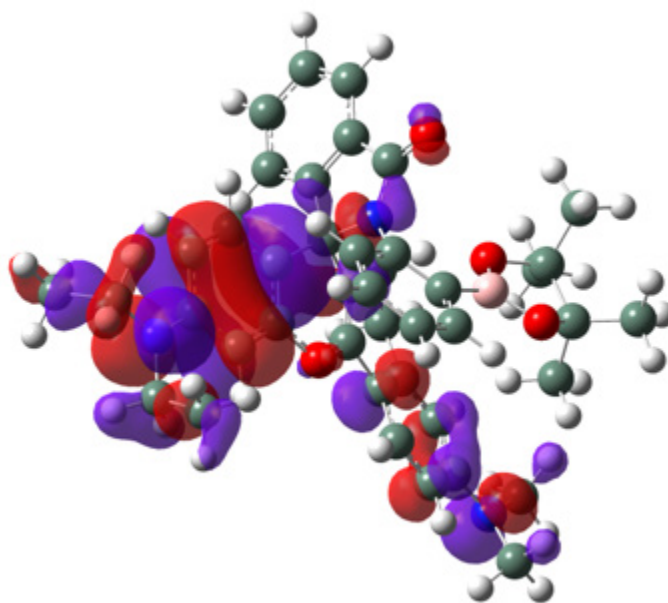**Figure B.35**. Calculated UV-Vis spectrum for probe **B** in water.

Figure B.36. MO for level 177 for probe **B** involved with the transition noted as Excited
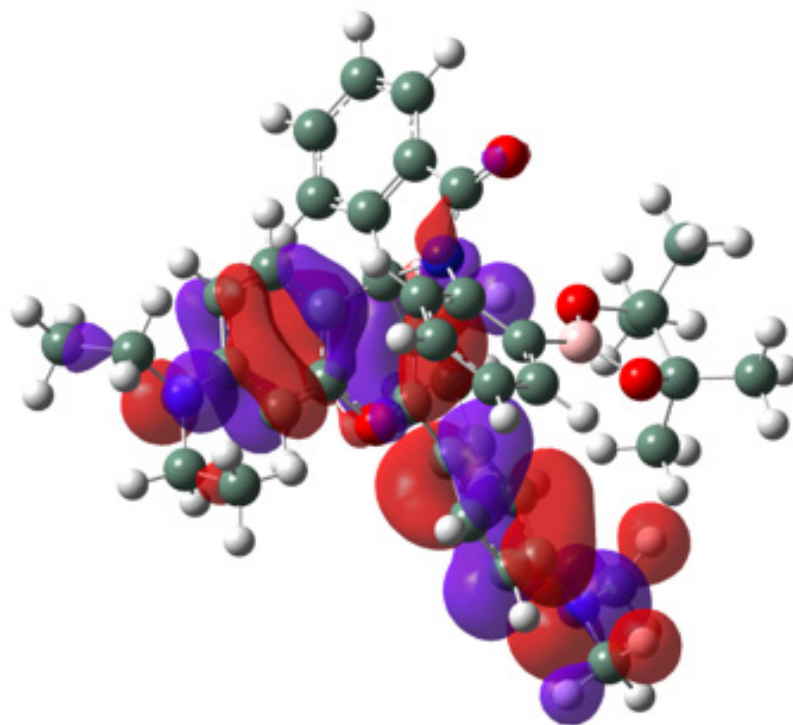
State 4 in Table B.8.

Figure B37. MO for level 178 for probe **B** involved with the transition noted as Excited
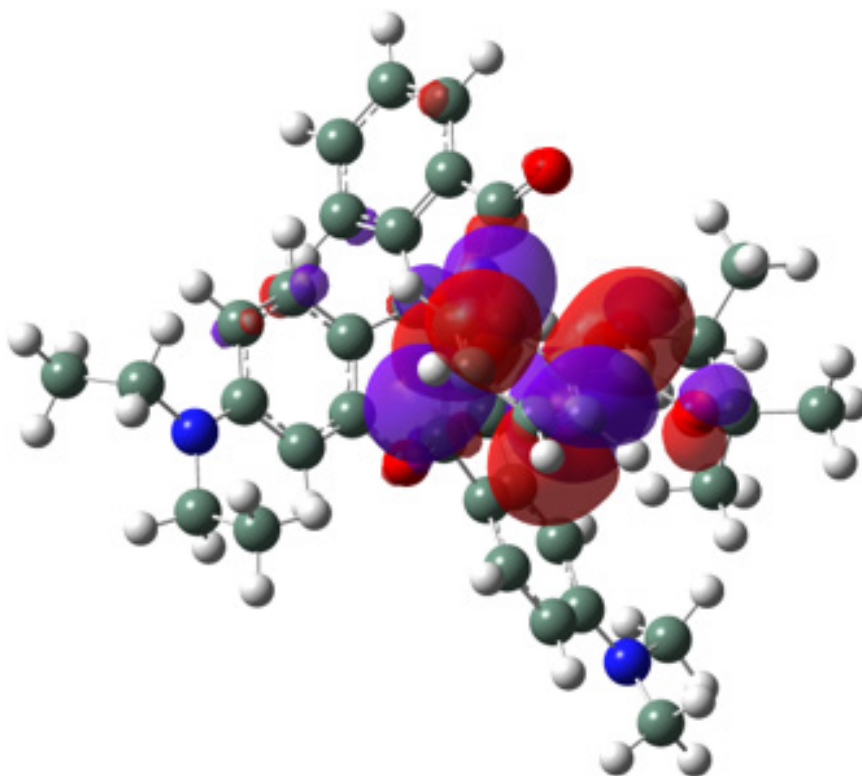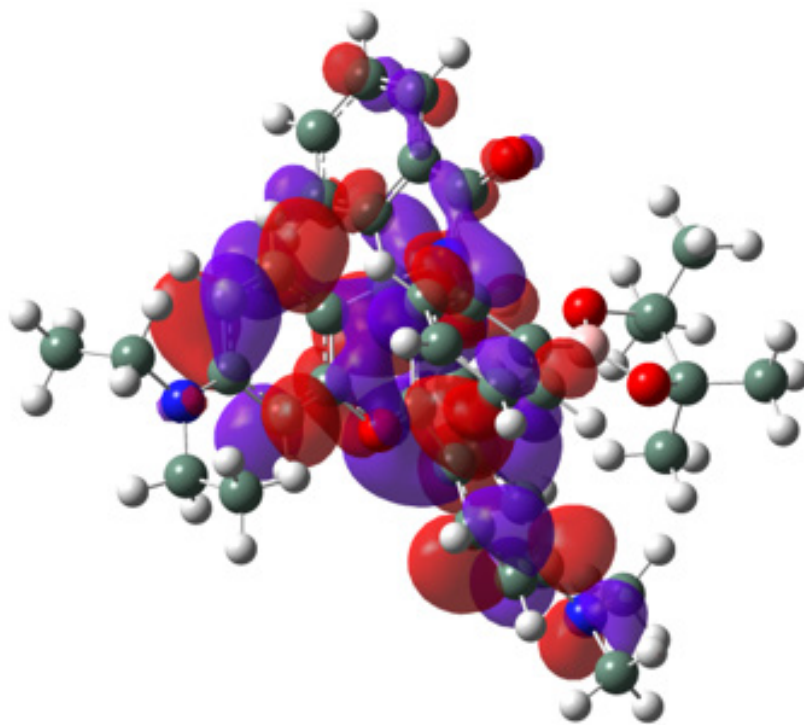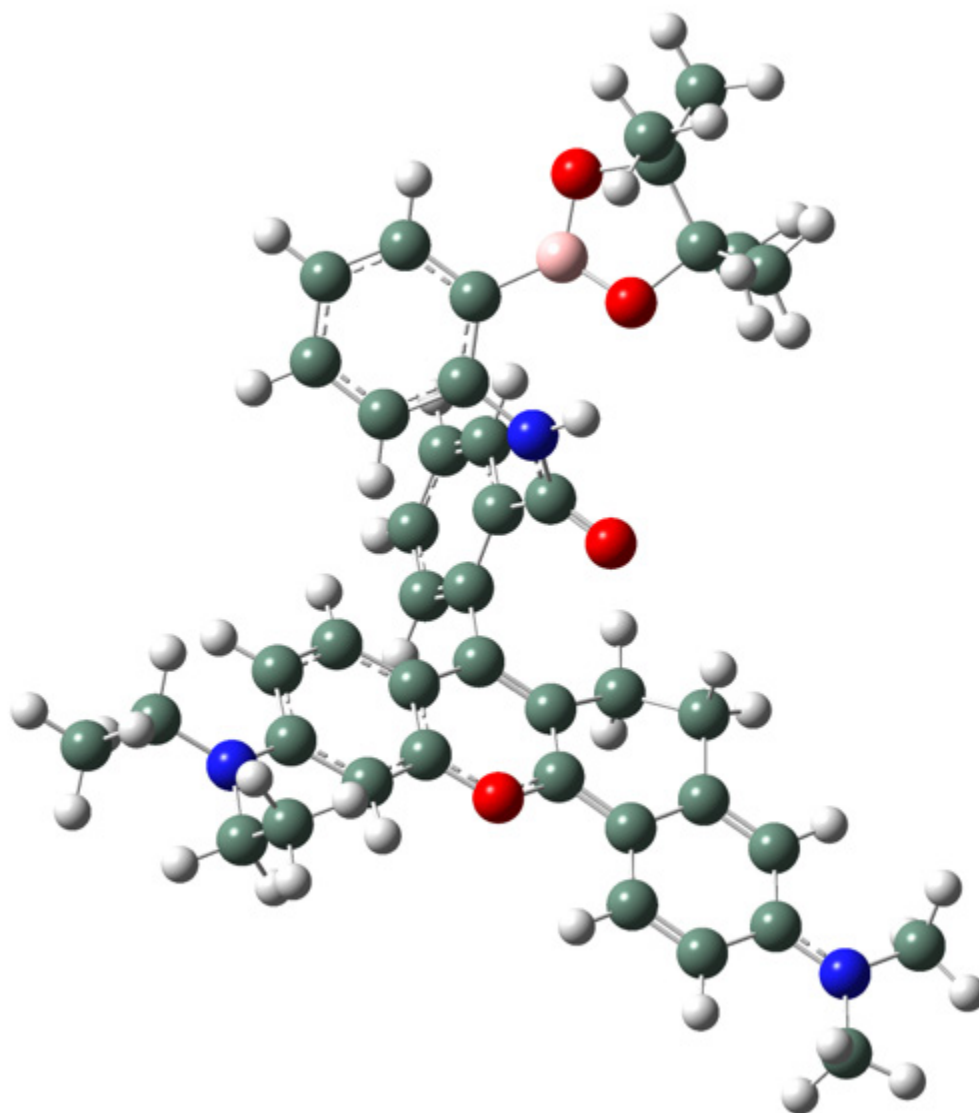
State 4 in Table B.8.

Figure B.38. MO for level 180 for probe **B** involved with the transition noted as Excited

State 4 in Table B. 8.

Figure B.39. MO for level 181 for probe **B** involved with the transition noted as Excited

State 4 in Table B.8.

Figure B. 40. Drawing of probe **BH**[+] with atoms represented as spheres of arbitrary size (H-white, C-grey, N-blue and O-red) using the GaussView program.

Table B. 9. Atomic coordinates for probe **BH**[+].

Row	Symbol	X	Y	Z
1	C	1.285801	0.51961	1.440934
2	C	2.075912	-0.60118	1.256876

3	C	3.14398	-0.52775	0.360726
4	O	3.427278	0.602448	-0.29412
5	C	2.706333	1.73414	-0.10103
6	C	1.604112	1.72036	0.776582
7	C	1.886466	-1.88862	2.002702
8	C	2.247379	-3.08718	1.136706
9	C	3.594188	-2.92142	0.494298
10	C	3.995083	-1.63006	0.078756
11	C	3.09822	2.843161	-0.81009
12	C	2.386231	4.05127	-0.66648
13	C	1.281276	4.061658	0.241793
14	C	0.913504	2.942312	0.927993
15	C	4.400392	-4.00286	0.23706
16	C	5.637208	-3.86507	-0.4426
17	C	6.015698	-2.56298	-0.86917
18	C	5.2101	-1.48567	-0.61559
19	N	2.734452	5.160623	-1.34848
20	N	6.427658	-4.93243	-0.67746
21	C	1.953958	6.389262	-1.28974
22	C	3.914137	5.19703	-2.20053
23	C	2.381786	7.307305	-0.15313
24	C	3.6321	4.722465	-3.61987
25	C	7.683408	-4.78031	-1.38621
26	C	6.030153	-6.25518	-0.23753
27	N	-2.38487	-0.13766	-0.18676
28	C	-1.3287	-0.54786	0.563149
29	O	-0.59179	-1.44213	0.164906
30	C	-3.27089	0.934125	0.030347
31	C	-2.77887	2.175375	0.424209
32	C	-3.6497	3.226625	0.663179
33	C	-5.01879	3.057757	0.483994
34	C	-5.49965	1.830838	0.05058
35	C	-4.64614	0.748066	-0.18562
36	B	-5.25017	-0.59412	-0.682
37	O	-6.58222	-0.88677	-0.61284
38	C	-6.78836	-2.1019	-1.39109
39	C	-5.37391	-2.76089	-1.35689
40	O	-4.50428	-1.59584	-1.24845
41	C	-5.00727	-3.54718	-2.59966
42	C	-7.88413	-2.92896	-0.74759
43	C	0.118498	0.483896	2.353759

44	C	-1.13673	0.04099	1.924786
45	C	0.273123	0.94086	3.659423
46	C	-0.79751	0.929751	4.543038
47	C	-2.03935	0.470503	4.122729
48	C	-2.2074	0.039226	2.816187
49	C	-5.13257	-3.60103	-0.10983
50	C	-7.20921	-1.66536	-2.78849
51	H	2.526555	-1.86933	2.894864
52	H	0.855067	-1.96537	2.34521
53	H	2.217703	-4.00769	1.723442
54	H	1.495728	-3.1868	0.344089
55	H	3.940222	2.746786	-1.48093
56	H	0.731863	4.976823	0.412976
57	H	0.092293	2.994051	1.633589
58	H	4.063245	-4.98015	0.557709
59	H	6.949416	-2.40786	-1.39243
60	H	5.522823	-0.50003	-0.94126
61	H	2.080364	6.89233	-2.25114
62	H	0.893079	6.142636	-1.22123
63	H	4.270893	6.229364	-2.21028
64	H	4.710216	4.609883	-1.7381
65	H	2.244923	6.82568	0.817911
66	H	3.435768	7.579832	-0.24884
67	H	1.791118	8.226511	-0.16574
68	H	4.53932	4.781357	-4.22597
69	H	3.280326	3.688329	-3.63026
70	H	2.867314	5.344098	-4.09199
71	H	8.36159	-4.1063	-0.85486
72	H	8.164075	-5.75178	-1.46447
73	H	7.527081	-4.39389	-2.39771
74	H	5.097539	-6.57178	-0.71448
75	H	6.807405	-6.96529	-0.50669
76	H	5.896886	-6.28964	0.847653
77	H	-2.64861	-0.7972	-0.91151
78	H	-1.71116	2.316355	0.528457
79	H	-3.25271	4.187588	0.974279
80	H	-5.70084	3.881374	0.665676
81	H	-6.56489	1.69661	-0.11006
82	H	-4.00991	-3.97685	-2.48408
83	H	-5.71359	-4.36769	-2.74663
84	H	-5.01077	-2.92064	-3.49152

85	H	-7.98219	-3.88846	-1.26114
86	H	-7.68259	-3.11755	0.306894
87	H	-8.83852	-2.40417	-0.82723
88	H	1.243777	1.303286	3.981078
89	H	-0.65962	1.280196	5.560283
90	H	-2.87801	0.452825	4.810177
91	H	-3.17767	-0.30992	2.479864
92	H	-5.70762	-4.52831	-0.14285
93	H	-4.07255	-3.85701	-0.05392
94	H	-5.40174	-3.05571	0.797688
95	H	-7.44216	-2.52729	-3.41654
96	H	-8.10507	-1.04581	-2.71233
97	H	-6.42736	-1.07908	-3.27676

Table B.10. Excitation energies and oscillator strengths for probe **BH$^+$**.

Excited State   1:   Singlet-A   2.3762 eV 521.77 nm f=0.9945 <S**2>=0.000
  178 -> 179   0.70269
This state for optimization and/or second-order correction.
Total Energy, E(TD-HF/TD-DFT) = -2117.61180338
Copying the excited state density for this state as the 1-particle RhoCI density.

Excited State   2:   Singlet-A   3.0835 eV 402.10 nm f=0.1664 <S**2>=0.000
  177 -> 179   0.68558

Excited State   3:   Singlet-A   3.2649 eV 379.75 nm f=0.0053 <S**2>=0.000
  176 -> 179   0.70314

Excited State   4:   Singlet-A   3.5843 eV 345.91 nm f=0.0343 <S**2>=0.000
  178 -> 180   0.69366

Excited State   5:   Singlet-A   3.7811 eV 327.90 nm f=0.0008 <S**2>=0.000
  174 -> 179   0.66244
  175 -> 179   0.20083

Excited State   6:   Singlet-A   3.8298 eV 323.74 nm f=0.0096 <S**2>=0.000
  173 -> 179   0.61209
  175 -> 179   -0.32762

Excited State   7:   Singlet-A   3.8823 eV 319.36 nm f=0.0242 <S**2>=0.000
  172 -> 179   0.31790
  173 -> 179   0.13643
  175 -> 179   0.28255

```
178 -> 181      0.50137
178 -> 182      0.10159
178 -> 183      0.10889

Excited State   8:     Singlet-A      3.9584 eV  313.22 nm  f=0.0770  <S**2>=0.000
    171 -> 179     -0.28634
    173 -> 179      0.26530
    174 -> 179     -0.17067
    175 -> 179      0.44187
    178 -> 181     -0.31939

Excited State   9:     Singlet-A      4.1086 eV  301.76 nm  f=0.0442  <S**2>=0.000
    171 -> 179      0.37896
    172 -> 179      0.33147
    178 -> 181     -0.29674
    178 -> 182      0.36017
    178 -> 183     -0.10480

Excited State  10:     Singlet-A      4.1762 eV  296.88 nm  f=0.0286  <S**2>=0.000
    169 -> 179      0.15181
    170 -> 179     -0.13369
    171 -> 179      0.47085
    172 -> 179     -0.27116
    173 -> 179      0.12766
    175 -> 179      0.20625
    178 -> 182     -0.25205
```
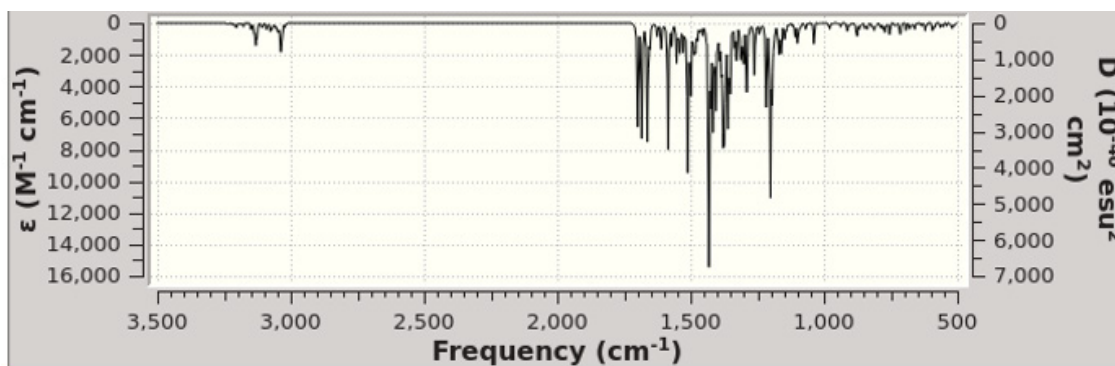
Figure B.41. Calculated (top) FTIR spectrum of probe **BH⁺**.
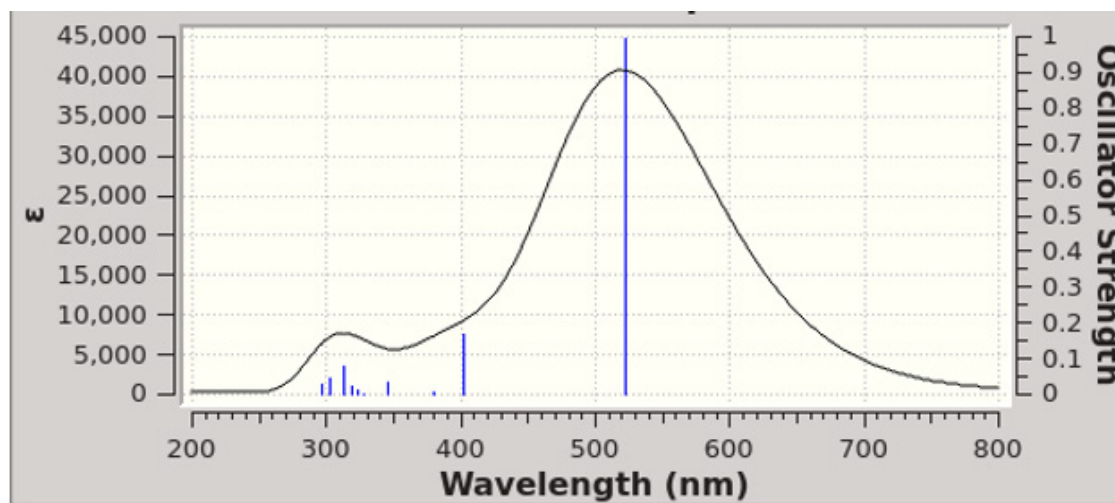
Figure B.42. Calculated UV-Vis spectrum for probe **BH⁺** in water.
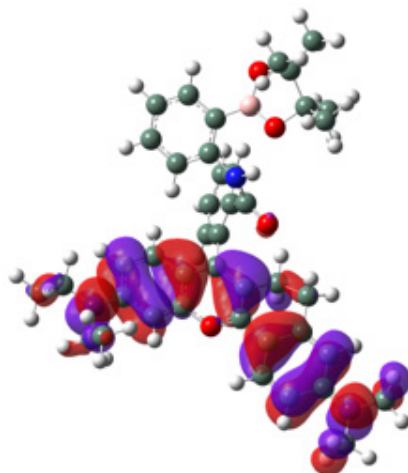
Figure B.43. MO for level 178 for probe **BH⁺** involved with the transition noted as

Excited State 1 in Table B.10.
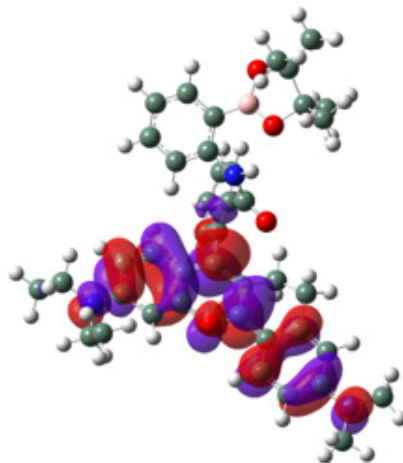
Figure B.44. MO for level 179 for probe **BH⁺** involved with the transition noted as Excited

State 1 in Table B.10.
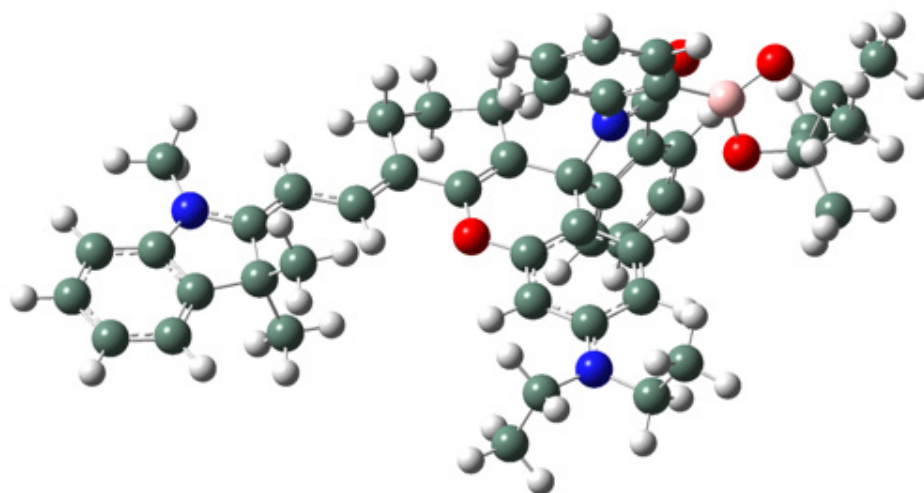
Figure B.45. Drawing of probe **C** with atoms represented as spheres of arbitrary size (H-white, C-grey, N-blue and O-red) using the GaussView program.

Table B.11. Atomic coordinates for probe **C**.

Row	Symbol	X	Y	Z
1	C	1.922208	2.624021	0.968682
2	C	0.613213	3.156939	0.866837
3	C	-0.43974	2.239997	0.725719
4	C	-0.18952	0.875789	0.678911
5	C	1.09017	0.352232	0.775377
6	C	2.133843	1.263781	0.927343
7	O	-1.29637	0.093741	0.546193
8	C	0.045806	-1.88341	0.513117
9	C	1.332279	-1.12489	0.717924
10	C	-2.40729	-1.9469	0.188711
11	C	-2.33263	-3.43543	-0.02016
12	C	-1.16648	-4.05823	0.73691
13	C	0.138435	-3.37343	0.361036
14	N	0.385201	4.504396	0.900372
15	C	-0.9352	5.057116	0.672192
16	C	1.450484	5.453896	1.157661
17	C	2.192587	5.88548	-0.10219
18	C	-1.77762	5.154332	1.939335
19	C	-1.14862	-1.26298	0.43689
20	C	-6.18334	0.475009	-0.08628

190

21	C	-7.66956	0.622831	-0.3102
22	C	-8.22568	-0.62847	-0.57214
23	N	-7.22633	-1.58966	-0.53707
24	C	-5.99818	-1.03253	-0.26184
25	C	-8.46408	1.748571	-0.28677
26	C	-9.83499	1.619401	-0.52959
27	C	-10.3787	0.366605	-0.791
28	C	-9.58409	-0.77952	-0.81738
29	C	-5.81853	0.93541	1.331196
30	C	-5.41201	1.274578	-1.14469
31	C	-7.42657	-2.99651	-0.7553
32	C	-3.56205	-1.23994	0.104928
33	N	2.335651	-1.47727	-0.33403
34	C	3.379479	-2.22853	0.138325
35	C	3.199159	-2.31726	1.597836
36	C	2.041179	-1.64922	1.946568
37	C	4.006248	-2.92742	2.545586
38	C	3.616088	-2.84231	3.875611
39	C	2.444056	-2.16713	4.230429
40	C	1.638908	-1.56748	3.267049
41	O	4.276687	-2.71931	-0.53576
42	C	2.261815	-1.01037	-1.662
43	C	3.405203	-0.47761	-2.27748
44	B	4.772239	-0.25157	-1.55912
45	O	5.967719	-0.37901	-2.21256
46	C	6.967204	0.305593	-1.4085
47	C	6.319436	0.304028	0.015373
48	O	4.900854	0.251958	-0.29427
49	C	6.594648	1.550843	0.837323
50	C	6.656949	-0.93547	0.834191
51	C	8.285533	-0.4384	-1.5036
52	C	7.111644	1.702231	-1.99973
53	C	3.29896	-0.05254	-3.6035
54	C	1.054542	-1.0779	-2.35318
55	C	2.094846	-0.10627	-4.29492
56	C	0.969684	-0.61255	-3.65873
57	C	-4.85784	-1.76947	-0.17959
58	H	2.777822	3.280204	1.059141
59	H	-1.47174	2.558599	0.662785
60	H	3.148886	0.886412	0.978472
61	H	-2.21747	-3.64756	-1.09276

62	H	-3.27123	-3.90488	0.28538
63	H	-1.10821	-5.13039	0.528081
64	H	-1.33143	-3.94723	1.814946
65	H	0.40863	-3.62574	-0.67502
66	H	0.956171	-3.75511	0.98059
67	H	-0.80413	6.050616	0.234491
68	H	-1.44875	4.463674	-0.08933
69	H	1.001815	6.32475	1.643773
70	H	2.143743	5.032139	1.889896
71	H	2.974219	6.611109	0.139214
72	H	1.506612	6.351192	-0.8149
73	H	2.660697	5.030413	-0.59582
74	H	-1.92929	4.170402	2.389547
75	H	-2.75875	5.583688	1.718571
76	H	-1.28797	5.791573	2.680615
77	H	-8.03389	2.724729	-0.08243
78	H	-10.474	2.495736	-0.5146
79	H	-11.4434	0.272157	-0.97966
80	H	-10.027	-1.74694	-1.02431
81	H	-4.75227	0.821466	1.531313
82	H	-6.07606	1.990633	1.453154
83	H	-6.3705	0.360737	2.078137
84	H	-5.66405	2.334828	-1.06082
85	H	-4.3329	1.172423	-1.0222
86	H	-5.67576	0.939438	-2.15014
87	H	-8.48125	-3.19371	-0.92809
88	H	-6.86109	-3.33877	-1.62705
89	H	-7.10468	-3.57161	0.117766
90	H	-3.48576	-0.17216	0.257373
91	H	4.911894	-3.44621	2.250723
92	H	4.223091	-3.30116	4.64885
93	H	2.158981	-2.11174	5.276128
94	H	0.725536	-1.04983	3.542019
95	H	6.105772	1.462755	1.810174
96	H	7.668117	1.663522	1.007651
97	H	6.222578	2.451187	0.348179
98	H	7.70439	-0.92521	1.142685
99	H	6.035515	-0.94375	1.731908
100	H	6.451059	-1.84968	0.277391
101	H	8.668509	-0.38306	-2.52509
102	H	9.025047	0.017277	-0.84058

103	H	8.176918	-1.48879	-1.23326
104	H	7.887106	2.273579	-1.48559
105	H	7.39205	1.614673	-3.0516
106	H	6.17288	2.258217	-1.94253
107	H	4.180948	0.349579	-4.09327
108	H	0.180397	-1.49304	-1.86864
109	H	2.035117	0.245865	-5.31955
110	H	0.020001	-0.66248	-4.18189
111	H	-4.93857	-2.83719	-0.35187

Table B.12. Excitation energies and oscillator strengths for probe **C**.

Excited State   1:   Singlet-A   2.9092 eV 426.18 nm f=0.0224 <S**2>=0.000
  203 -> 204   0.70060
This state for optimization and/or second-order correction.
Total Energy, E(TD-HF/TD-DFT) = -2388.56316867
Copying the excited state density for this state as the 1-particle RhoCI density.

Excited State   2:   Singlet-A   3.1951 eV 388.04 nm f=1.3814 <S**2>=0.000
  203 -> 205   0.69965

Excited State   3:   Singlet-A   3.3156 eV 373.95 nm f=0.0042 <S**2>=0.000
  202 -> 204   0.70100

Excited State   4:   Singlet-A   3.5969 eV 344.70 nm f=0.0076 <S**2>=0.000
  202 -> 205   0.69817

Excited State   5:   Singlet-A   3.6920 eV 335.82 nm f=0.0019 <S**2>=0.000
  203 -> 206   0.69566

Excited State   6:   Singlet-A   3.7689 eV 328.96 nm f=0.0067 <S**2>=0.000
  203 -> 207   0.52779
  203 -> 208   0.43336
  203 -> 209   0.11684

Excited State   7:   Singlet-A   3.8279 eV 323.89 nm f=0.1772 <S**2>=0.000
  203 -> 207   -0.44810
  203 -> 208   0.51909
  203 -> 209   0.11947

Excited State   8:   Singlet-A   4.0133 eV 308.93 nm f=0.0253 <S**2>=0.000
  201 -> 204   0.55573
  203 -> 208   0.10498
  203 -> 209   -0.38716

Excited State   9:   Singlet-A   4.0213 eV 308.32 nm f=0.0397 <S**2>=0.000
    201 -> 204   0.38454
    203 -> 208   -0.13261
    203 -> 209   0.55714

Excited State 10:   Singlet-A   4.0996 eV 302.43 nm f=0.0305 <S**2>=0.000
    201 -> 204   0.11135
202 -> 206   0.68589
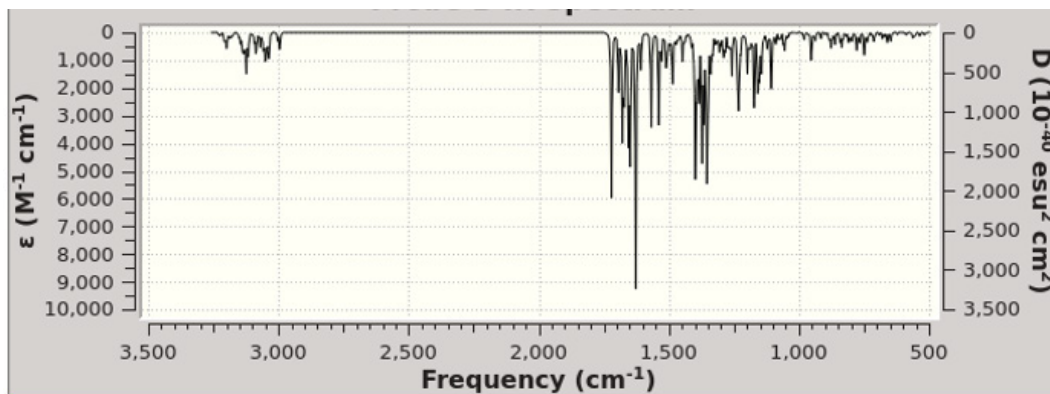
Figure B.46. Calculated (top) FTIR spectrum of probe **C**.
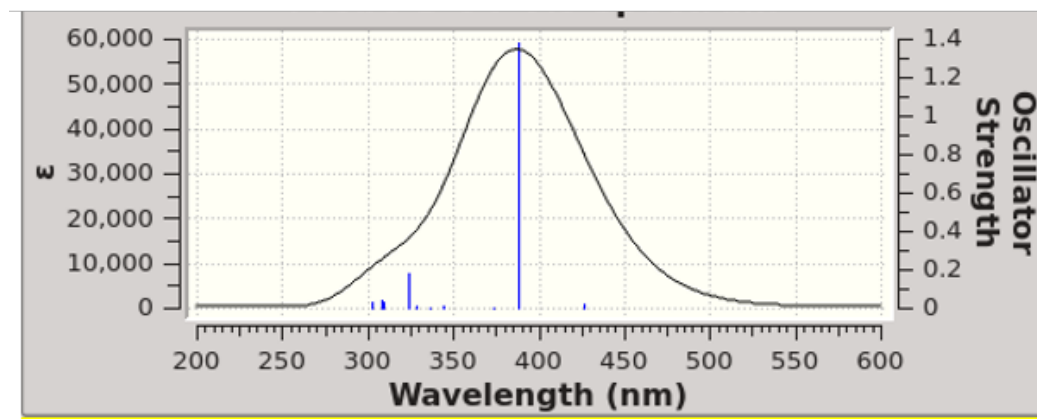
Figure B.47. Calculated UV-Vis spectrum for probe **C** in water.
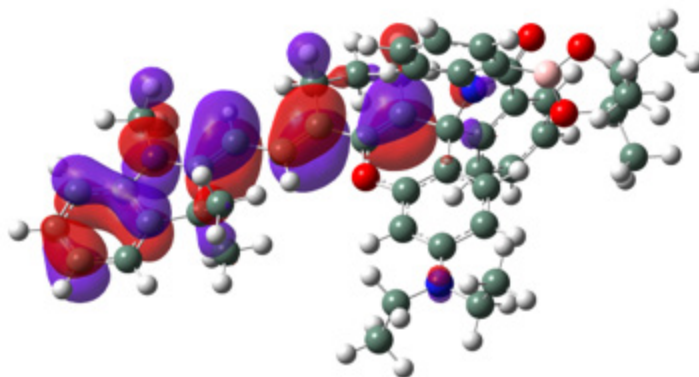
Figure B.48. MO for level 203 for probe **C** involved with the transition noted as Excited State 2 in Table B.12.
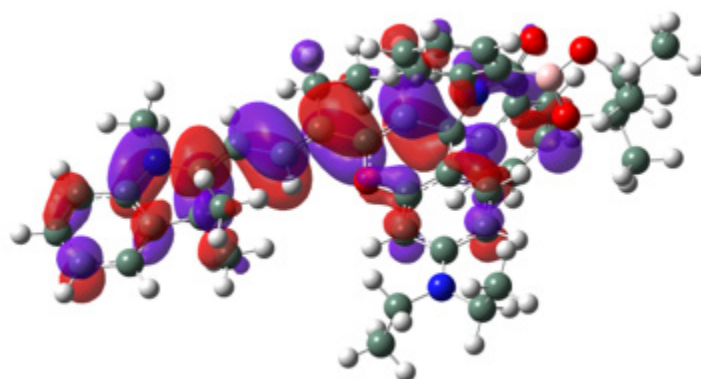
Figure B.49. MO for level 205 for probe **C** involved with the transition noted as Excited State 2 in Table B.12.
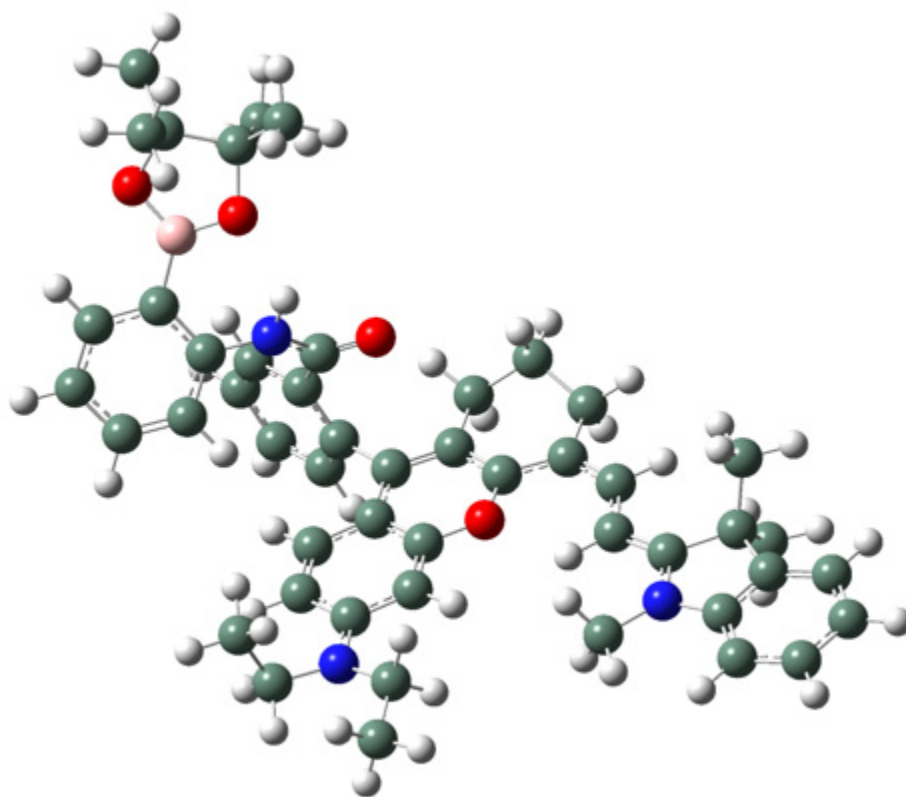
Figure B.50. Drawing of probe **CH⁺** with atoms represented as spheres of arbitrary size

(H-white, C-grey, N-blue and O-red) using the GaussView program.

Table B.13. Atomic coordinates for probe **CH⁺**.

Row	Symbol	X	Y	Z
1	C	-0.1024	3.696445	0.760643
2	C	1.148025	3.620102	0.075566
3	C	1.857871	2.407506	0.168184
4	C	1.34409	1.364287	0.9053
5	C	0.108787	1.418547	1.563825
6	C	-0.58964	2.638579	1.475767
7	O	2.093033	0.239102	0.965581
8	C	0.461722	-0.85632	2.322651
9	C	-0.33958	0.261161	2.243704
10	C	2.61433	-1.92647	1.677848
11	C	2.192351	-3.16485	2.439327
12	C	0.68156	-3.336	2.466887

13	C	0.030657	-2.09408	3.053802
14	N	1.642213	4.67531	-0.62313
15	C	0.795027	5.824252	-0.91392
16	C	2.870791	4.47744	-1.39537
17	C	3.455245	5.728882	-2.02274
18	C	-0.17582	5.576713	-2.06138
19	C	1.714833	-0.84602	1.669636
20	C	6.692225	-2.39354	-0.20698
21	C	7.879275	-1.90943	-0.99933
22	C	7.665814	-0.59344	-1.39088
23	N	6.419778	-0.17747	-0.90871
24	C	5.799148	-1.15922	-0.22255
25	C	9.04544	-2.55754	-1.34987
26	C	9.997211	-1.86696	-2.10173
27	C	9.768423	-0.54969	-2.48827
28	C	8.593961	0.113212	-2.13862
29	C	7.129232	-2.76183	1.218484
30	C	6.032517	-3.58126	-0.92246
31	C	5.866109	1.14007	-1.12542
32	C	3.859953	-1.94702	1.059816
33	N	-3.58047	-0.25194	-0.18672
34	C	-2.7218	-0.66753	0.782543
35	C	-2.82964	-0.08692	2.155804
36	C	-1.68389	0.281241	2.869622
37	C	-4.07495	-0.04026	2.778861
38	C	-4.18958	0.373221	4.097044
39	C	-3.05525	0.761092	4.798922
40	C	-1.8106	0.717397	4.184797
41	O	-1.92094	-1.56636	0.554131
42	C	-4.48948	0.821298	-0.18877
43	C	-5.764	0.642268	-0.75262
44	B	-6.22129	-0.68971	-1.40744
45	O	-7.5252	-0.97288	-1.69877
46	C	-7.52098	-2.17258	-2.5265
47	C	-6.17139	-2.84578	-2.12596
48	O	-5.3563	-1.69018	-1.77138
49	C	-5.4907	-3.61889	-3.23765
50	C	-6.27698	-3.70466	-0.87277
51	C	-8.75349	-2.99983	-2.21821
52	C	-7.54808	-1.70776	-3.97695
53	C	-6.64887	1.725558	-0.73348

54	C	-4.11482	2.058469	0.328494
55	C	-6.29469	2.947556	-0.18097
56	C	-5.01683	3.110319	0.344129
57	C	4.546104	-0.9705	0.335975
58	H	-0.68925	4.603122	0.724237
59	H	2.804129	2.257081	-0.32862
60	H	-1.52906	2.74158	2.006974
61	H	2.668504	-4.03923	1.987485
62	H	2.566792	-3.10757	3.470234
63	H	0.408547	-4.21768	3.052596
64	H	0.308628	-3.49106	1.448509
65	H	-1.0571	-2.16563	3.012287
66	H	0.30437	-1.99853	4.112799
67	H	0.263811	6.108806	-0.00502
68	H	1.442229	6.669146	-1.13992
69	H	3.620081	4.057624	-0.71839
70	H	2.692402	3.724288	-2.17531
71	H	4.398082	5.457348	-2.50264
72	H	2.810647	6.159	-2.79184
73	H	3.673332	6.496429	-1.27637
74	H	-0.78521	6.465531	-2.24297
75	H	0.362461	5.339472	-2.98258
76	H	-0.84628	4.743	-1.83811
77	H	9.223215	-3.58511	-1.04874
78	H	10.9203	-2.35944	-2.38731
79	H	10.51567	-0.02443	-3.07359
80	H	8.429088	1.138258	-2.44835
81	H	6.291323	-3.10824	1.824109
82	H	7.868817	-3.5642	1.172621
83	H	7.584385	-1.90474	1.718739
84	H	5.160995	-3.94859	-0.37979
85	H	5.717682	-3.30121	-1.92964
86	H	6.751702	-4.39922	-1.00303
87	H	5.661977	1.627	-0.16989
88	H	6.580335	1.744962	-1.67557
89	H	4.943397	1.07417	-1.7057
90	H	4.375215	-2.89411	1.180644
91	H	-3.67186	-0.91271	-0.95171
92	H	-4.95832	-0.33961	2.22536
93	H	-5.16324	0.395128	4.574355
94	H	-3.13695	1.096196	5.827442

95	H	-0.922	1.020834	4.728348
96	H	-4.56308	-4.06007	-2.86678
97	H	-6.1373	-4.4302	-3.58039
98	H	-5.2522	-2.9806	-4.08834
99	H	-6.82636	-4.62652	-1.07258
100	H	-5.27192	-3.97052	-0.53894
101	H	-6.7769	-3.16918	-0.0624
102	H	-9.64872	-2.46363	-2.54014
103	H	-8.71448	-3.94792	-2.76009
104	H	-8.8438	-3.21104	-1.1527
105	H	-7.60965	-2.55623	-4.66104
106	H	-8.42733	-1.07911	-4.13175
107	H	-6.66003	-1.12221	-4.22593
108	H	-7.63694	1.595624	-1.1641
109	H	-3.11008	2.196143	0.704567
110	H	-6.99962	3.771914	-0.17353
111	H	-4.71151	4.067715	0.754075
112	H	4.088482	-0.00565	0.193454

Table B.14. Excitation energies and oscillator strengths for probe CH^+.

Excited State   1:   Singlet-A   2.0968 eV 591.31 nm f=0.9396 <S**2>=0.000
  203 -> 204   0.70630
This state for optimization and/or second-order correction.
Total Energy, E(TD-HF/TD-DFT) = -2389.03411121
Copying the excited state density for this state as the 1-particle RhoCI density.

Excited State   2:   Singlet-A   2.8582 eV 433.78 nm f=0.2253 <S**2>=0.000
  202 -> 204   0.68916
  203 -> 206   -0.10100

Excited State   3:   Singlet-A   3.2317 eV 383.65 nm f=0.0024 <S**2>=0.000
  201 -> 204   0.70470

Excited State   4:   Singlet-A   3.3249 eV 372.89 nm f=0.0780 <S**2>=0.000
  203 -> 205   0.69494

Excited State   5:   Singlet-A   3.6229 eV 342.23 nm f=0.1536 <S**2>=0.000
  196 -> 204   -0.16190
  200 -> 204   0.36636
  203 -> 206   0.54930

Excited State   6:   Singlet-A   3.7176 eV 333.51 nm f=0.1938 <S**2>=0.000
    200 -> 204   0.57352
    203 -> 206   -0.36709

Excited State   7:   Singlet-A   3.8225 eV 324.35 nm f=0.0190 <S**2>=0.000
    196 -> 204   0.12178
    197 -> 204   0.56899
    198 -> 204   0.11791
    199 -> 204   0.34552
    203 -> 207   -0.12483

Excited State   8:   Singlet-A   3.8442 eV 322.52 nm f=0.0831 <S**2>=0.000
    199 -> 204   0.11167
    203 -> 207   0.65214
    203 -> 208   0.12953

Excited State   9:   Singlet-A   3.9056 eV 317.45 nm f=0.0976 <S**2>=0.000
    195 -> 204   -0.12709
    196 -> 204   0.21858
    197 -> 204   -0.26125
    198 -> 204   -0.28362
    199 -> 204   0.46324
    202 -> 206   -0.10576
    203 -> 206   0.11866

Excited State 10:   Singlet-A   3.9391 eV 314.75 nm f=0.0063 <S**2>=0.000
    197 -> 204   -0.24548
    198 -> 204   0.58204
    199 -> 204   0.19294
    203 -> 209   -0.18762
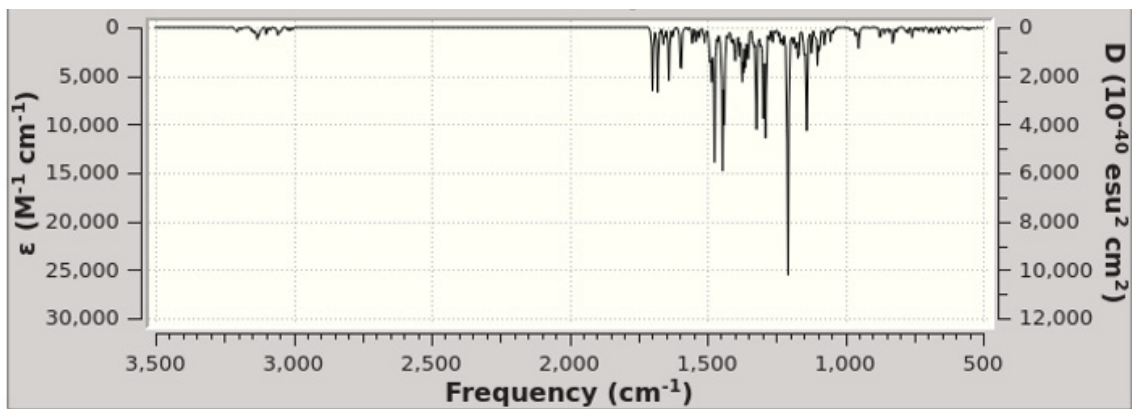
Figure B.51. Calculated (top) FTIR spectrum of probe **CH⁺**.
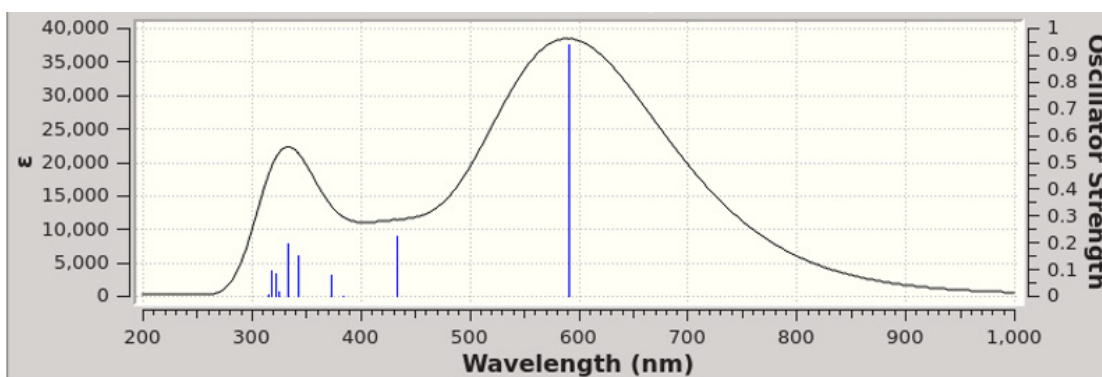
Figure B.52. Calculated UV-Vis spectrum for probe **CH⁺** in water.

202
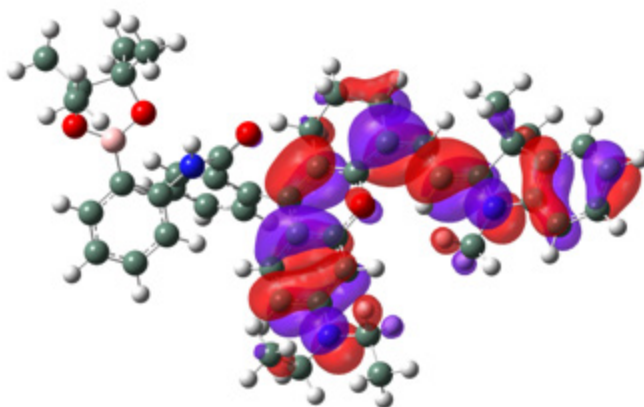
Figure B.53. MO for level 203 for probe **CH⁺** involved with the transition noted as Excited State 1 in Table B.14.
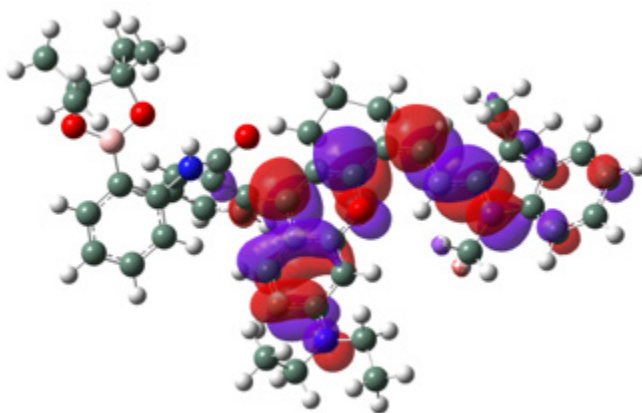
Figure B.54. MO for level 204 for probe **CH⁺** involved with the transition noted as Excited State 1 in Table B.14.

B.8 Cell culture and fluorescence imaging
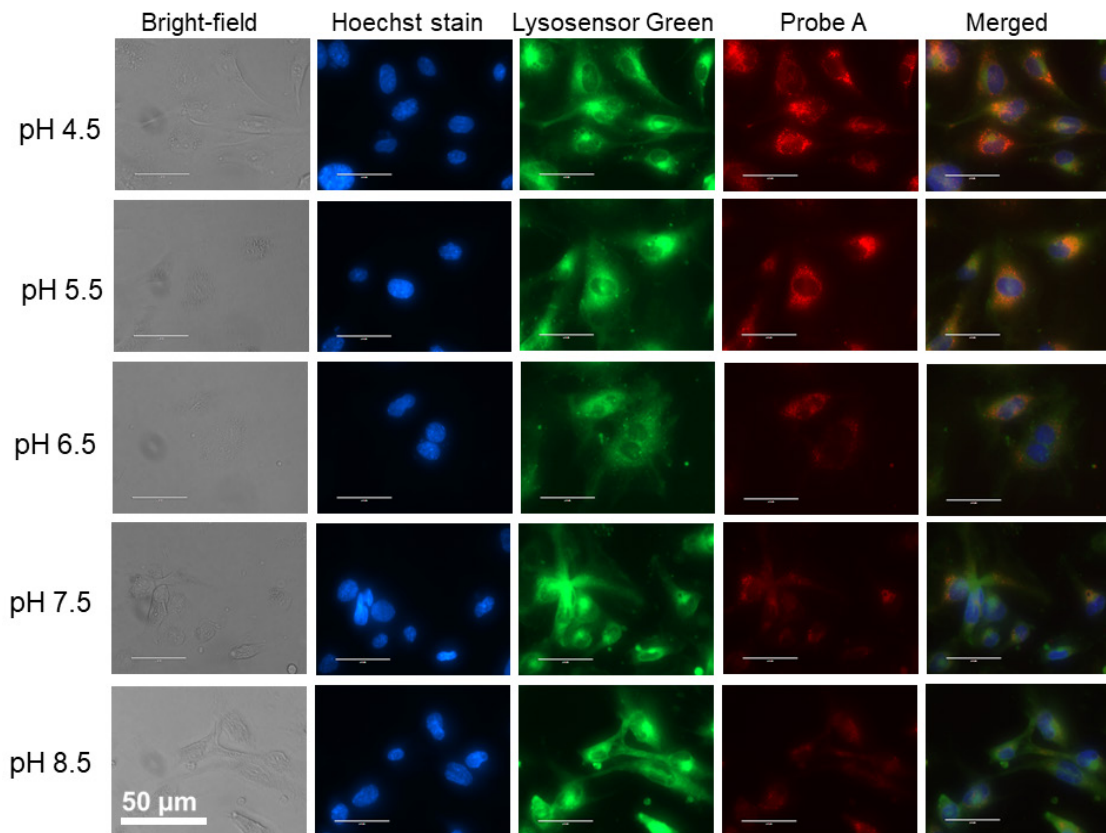
Figure B.56. Fluorescence images of Probe **A** in HUVEC-C cells. HUVEC-C cells were incubated with 10 µM probe **A** at different pH values ranging from pH 4.5 to 8.5 in presence of nigericin (1 µg/mL) for 1 h before imaging. Lysosensor Green DND-189 (1 µM) and Hoechst 33342 (1 µg/mL) was used for co-localization. The images were acquired using an inverted fluorescence microscope (AMF-4306, EVOSfl, AMG) at 60X magnification.
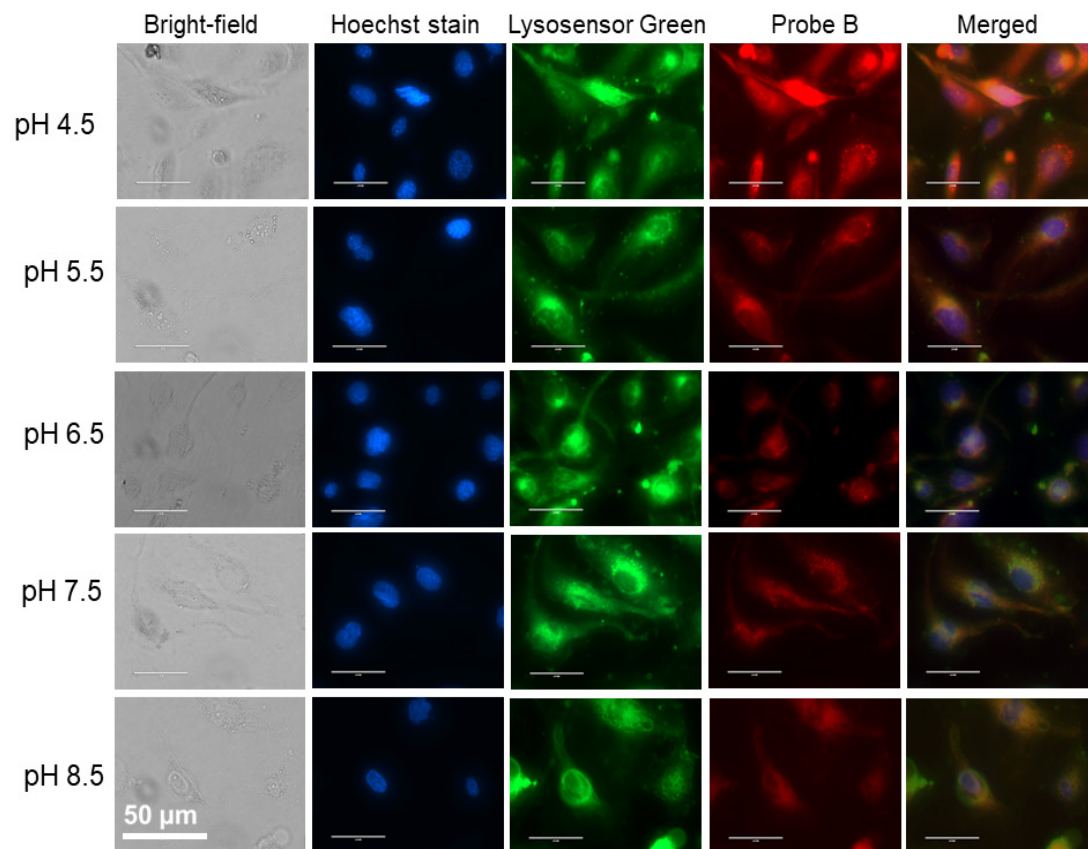
Figure B.57. Fluorescence images of Probe **B** in HUVEC-C cells. HUVEC-C cells were incubated with 5 µM probe **B** at different pH values ranging from pH 4.5 to 8.5 in presence of nigericin (1 µg/mL) for 1 h before imaging. Lysosensor Green DND-189 (1 µM) and Hoechst 33342 (1 µg/mL) was used for co-localization. The images were acquired using an inverted fluorescence microscope (AMF-4306, EVOSfl, AMG) at 60X magnification.
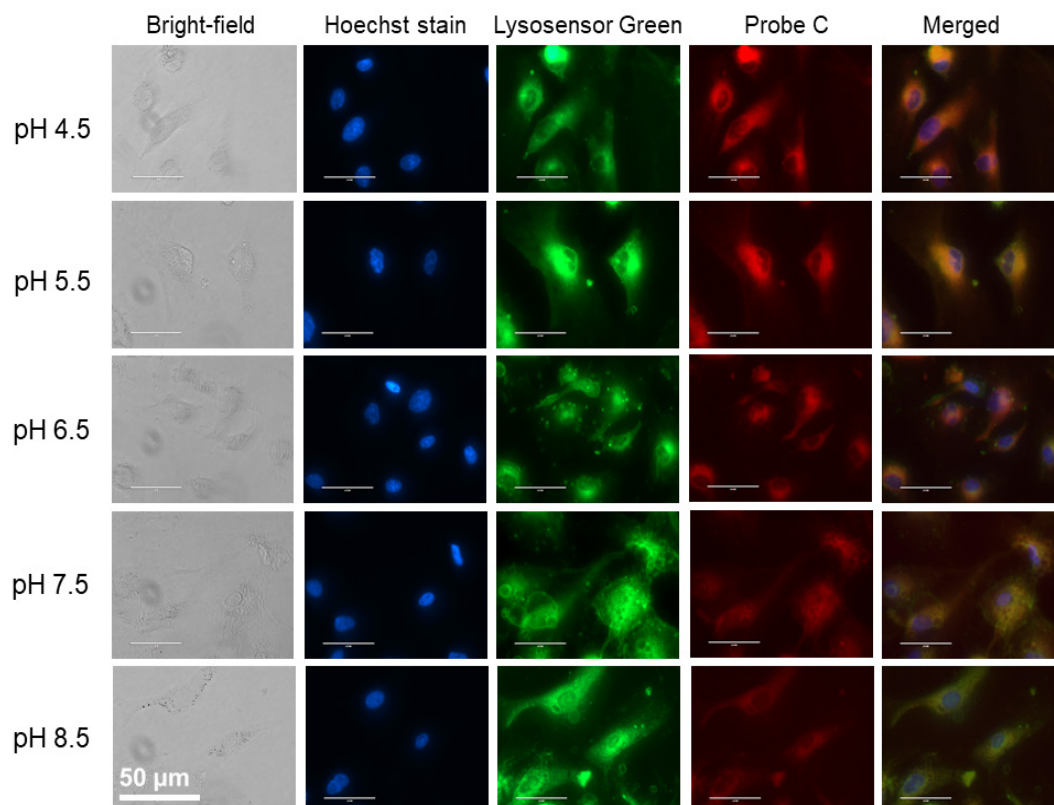
Figure B.58. Fluorescence images of Probe **C** in HUVEC-C cells. HUVEC-C cells were incubated with 5 µM probe **C** at different pH values ranging from pH 4.5 to 8.5 in presence of nigericin (1 µg/mL) for 1 h before imaging. Lysosensor Green DND-189 (1 µM) and Hoechst 33342 (1 µg/mL) were used for co-localization. The images were acquired using an inverted fluorescence microscope (AMF-4306, EVOSfl, AMG) at 60X magnification.
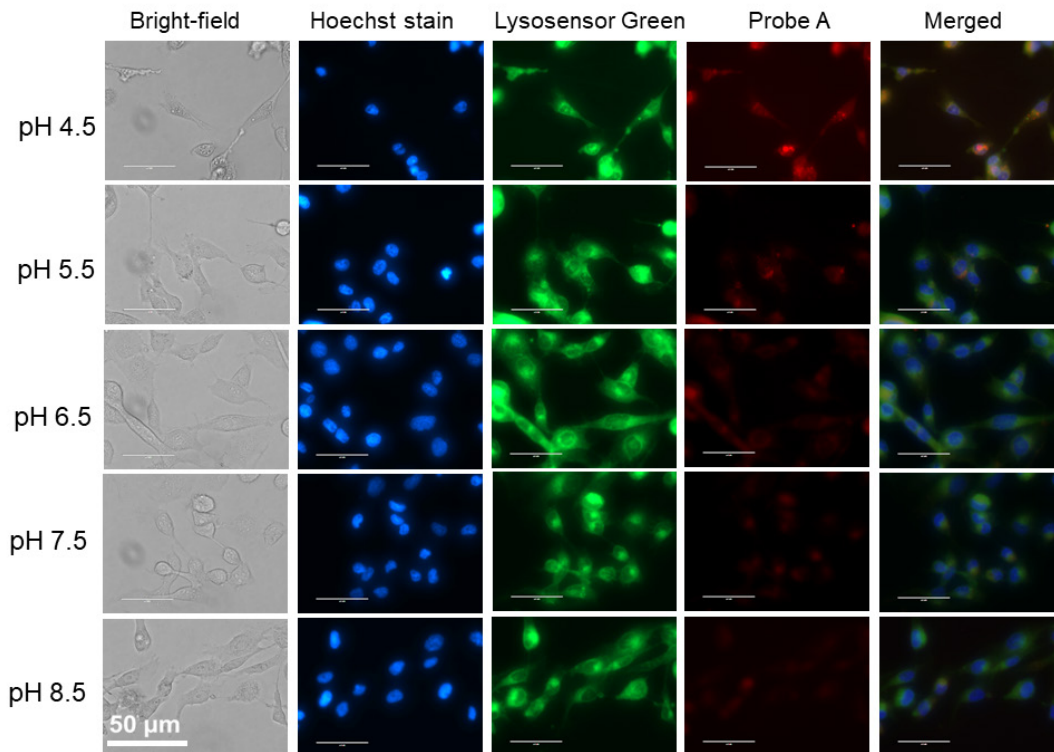
Figure B.59. Fluorescence images of Probe A in MDA-MB231 cells. MDA-MB231 cells were incubated with 5 μM probe A at different pH values ranging from pH 4.5 to 8.5 in presence of nigericin (1 μg/mL) for 1h before imaging. Lysosensor Green DND-189 (1 μM) and Hoechst 33342 (1 μg/mL) was used for co-localization. The images were acquired using an inverted fluorescence microscope (AMF-4306, EVOSfl, AMG) at 60X magnification.
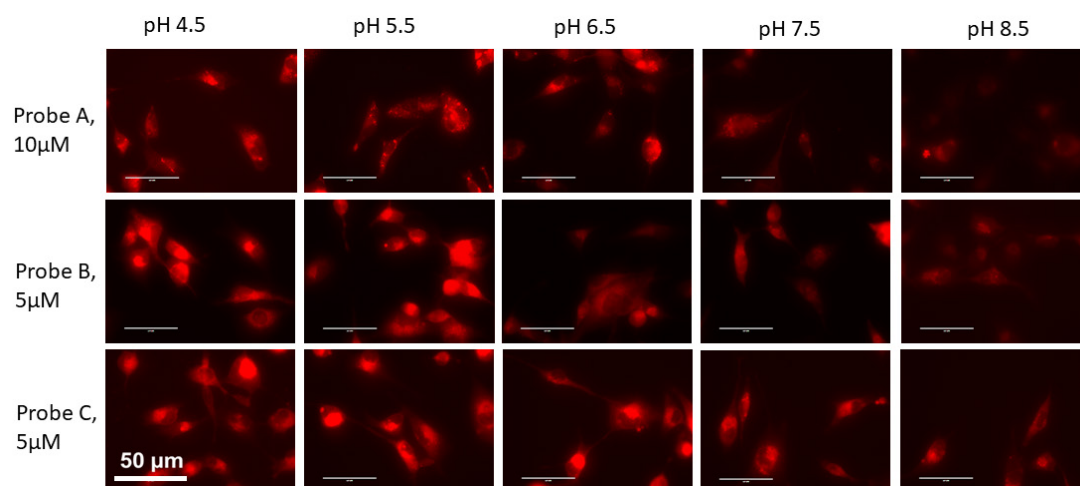
Figure B.60. Fluorescence images of Probe **A/B/C** in MDA-MB231 cells. MDA-MB231 cells were incubated with 10 µM probe **A** and 5 µM of Probe **B/C** at different pH values ranging from pH 4.5 to 8.5 in presence of nigericin (1 µg/mL) for 1 h before imaging. The images were acquired using an inverted fluorescence microscope (AMF-4306, EVOSfl, AMG) at 60X magnification. Probe **A** images were acquired using RFP light cube and CY5 light cube was used for Probe **B/C**.

| | pH 4.5 | pH 5.5 | pH 6.5 | pH 7.5 | pH 8.5 |

Probe A, 10µM

Probe B, 5µM

Probe C, 5µM

50 µm
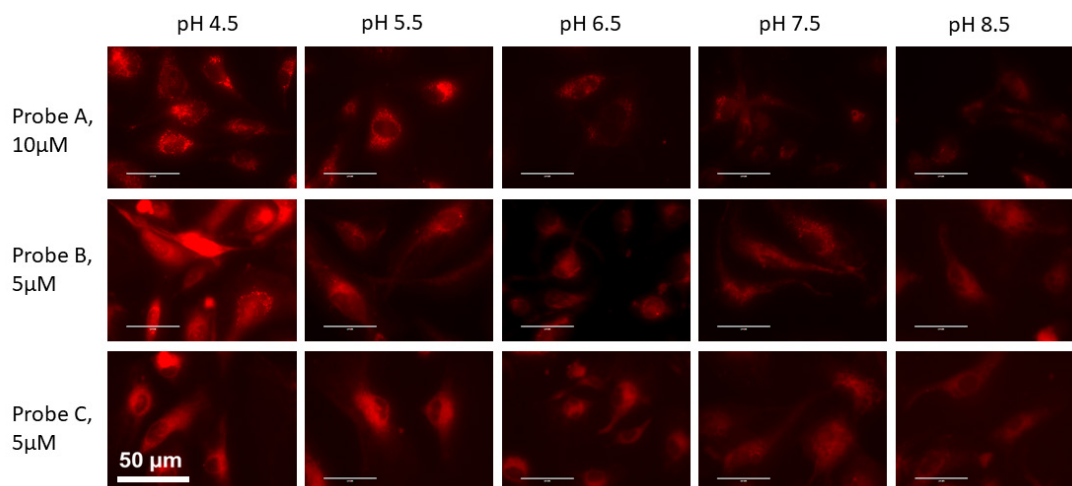
Figure B.61. Fluorescence images of Probe **A/B/C** in HUVEC-C cells. HUVEC-C cells were incubated with 10 µM probe **A** and 5 µM of Probe **B/C** at different pH values ranging from pH 4.5 to 8.5 in presence of nigericin (1 µg/mL) for 1 h before imaging. The images were acquired using an inverted fluorescence microscope (AMF-4306, EVOSfl, AMG) at 60X magnification. Probe **A** images were acquired using RFP light cube and CY5 light cube was used for Probe **B/C.**

C Appendix C: Supporting information of chapter 4

C.1 NMR and ESI-MS spectra of probe A

C.1.1 ¹H NMR Spectra for probe A
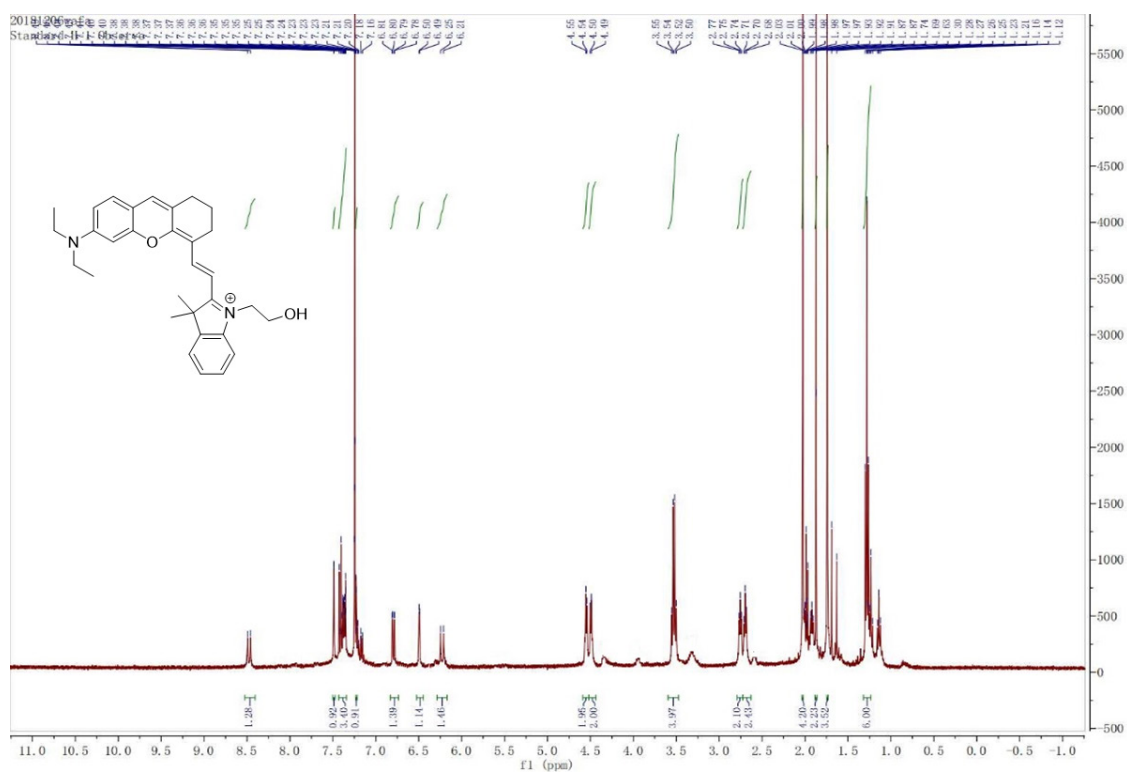
Figure C.1. ¹H NMR spectra of probe **A** in a chloroform-d solution.

C.1.2 ^{13}C NMR spectra for probe A

Figure C.2. ^{13}C NMR spectra of probe **A** in a chloroform-d solution.

C.1.3 ESI-MS spectra for probe A
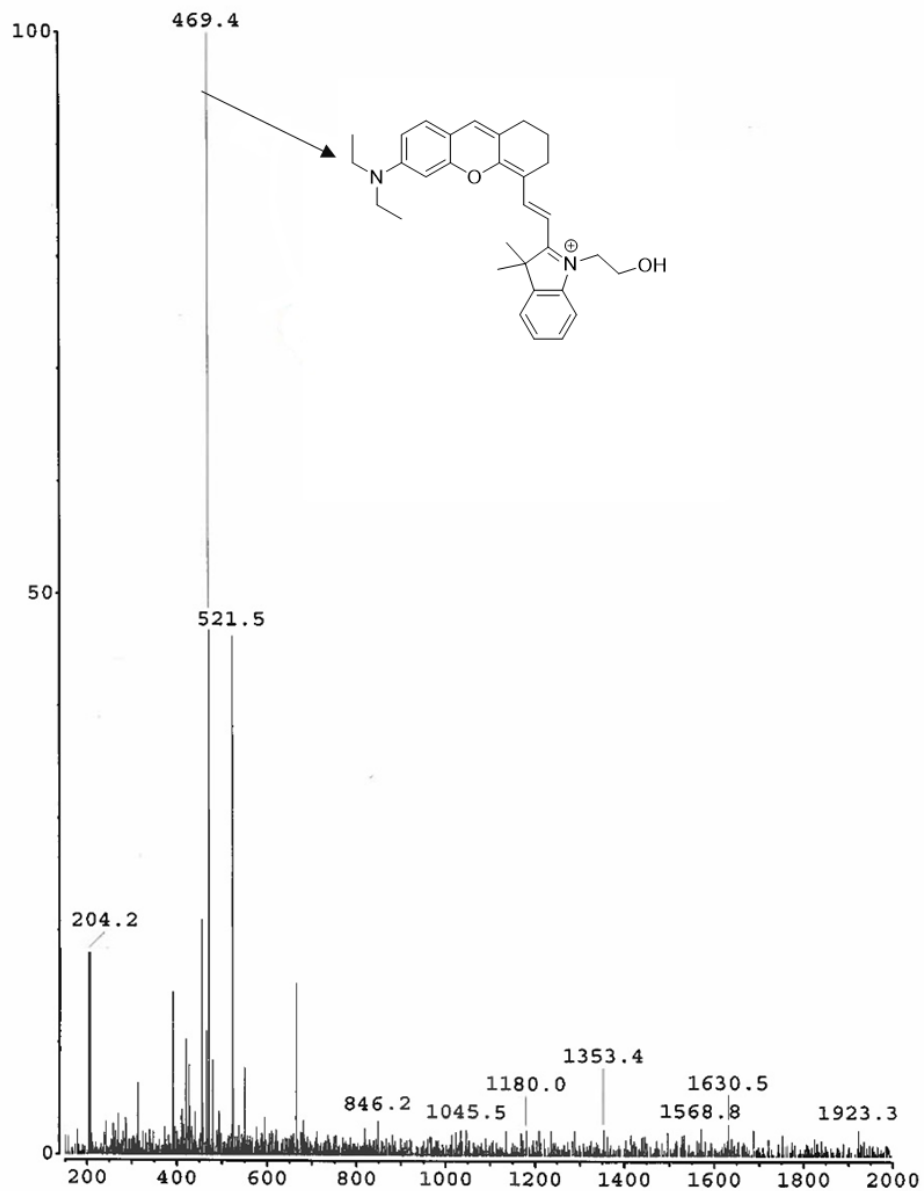
Figure C.3. Electrospray Ionization mass spectrums of probe **A.**

C.2 Calculation

C.2.1 Calculation of quantum yield

We chose the near-infrared hemicyanine dye shown in Figure S3 as fluorescent standard dye[64] to calculate fluorescence quantum yields of probes A.
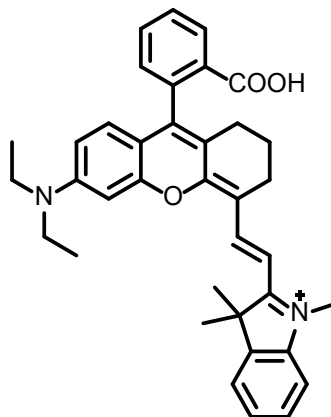
Hemicyanine dye ($\Phi = 0.41$ in EtOH)

Figure C.3: The structure of near- infrared hemicyanine[64].

The UV-Vis absorption spectrum of probe A was collected in the range from 300 to 800 nm with increments of 1 nm. The UV-Vis absorption spectra measured in freshly prepared buffer. Citrate-phosphate buffer was used for acidic pH 5.0, and phosphate buffer for pH 10.7. The fluorescence spectrum of probe A was collected under the excitation wavelength of 670 nm. The excitation and emission slit widths were set to 5 nm. NIR hemicyanine was chosen as reference standards to calculate the fluorescence quantum yields of probe A, in ethanol and buffer solutions (Figure **C.3**). The absorption and fluorescence spectrum of the standard dye was measured in pH 7.4 PBS buffer with 10% ethanol. The absorbance and fluorescence spectra of the probe A was measured in pH 5.0 citrate-phosphate buffer and in pH 10.7 phosphate buffer containing 10% EtOH. The absorbance was kept between 0.05 and 0.1 in order to obtain optimized data. The probe samples and reference were freshly

prepared under identical conditions. The fluorescence quantum yields were calculated according to literature using the equation 1 below[64] :

$$\Phi_{F(X)} = \Phi_{F(S)} (A_S F_X / A_X F_S) (n_X / n_S)^2 \qquad (1)$$

Where Φ_F is the fluorescence quantum yield, A is the absorbance at the excitation wavelength, F is the area under the corrected emission curve, and n is the refractive index of the solvents used. Subscripts s and x refer to the standard and to the unknown, respectively.

C.2.2 Calculation of pKa value by fluorometric titration

The fluorometric titration as a function of pH was obtained fluorescence spectra. The equation (2) below was used to calculate the pKa value of probe A.

$$F = \frac{F_{min}[H^+]^n + F_{max}K_a}{K_a + [H^+]^n} \qquad (2)$$

The expression of the steady-state fluorescence intensity F as a function of the proton concentration has been extended for the case of n: complex between H^+ and a fluorescent dye. Where F_{min} and F_{max} are the fluorescence intensities at maximal and minimal H^+ concentrations, respectively.

n is apparent stoichiometry of H^+ binding to the probe A. Nonlinear fitting of equation expressed above to the fluorescence titration data was plotted as a function of H^+ concentration[150-151].
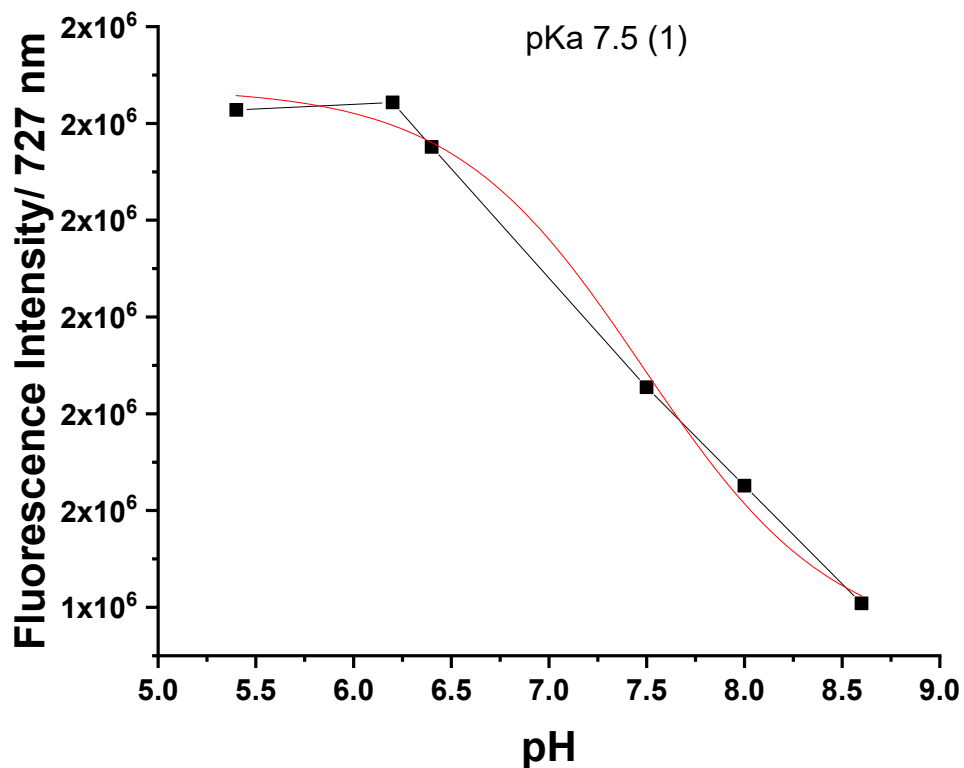
Figure C.4. Plot curve of fluorescence intensity of probe A versus pH.

C.3   Solvents Effect

The effect of ethanol percentage was investigated in water-ethanol mixed solution on dye fluorescence intensity (Figure S4). Increase of the percentages of ethanol from 10% to 90% resulted in enhancement of fluorescence intensity of the dyes because water increase percentages can effectively prevent fluorescence quenching due to dye aggregation in aqueous solutions.
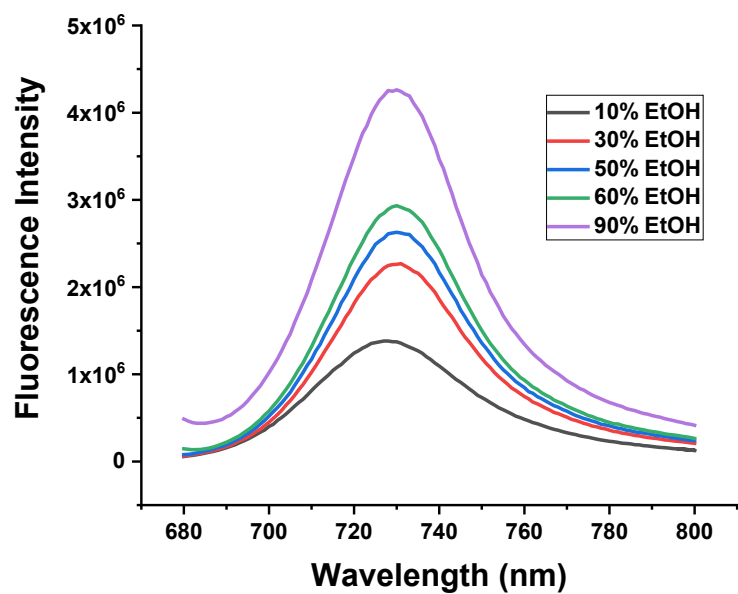
Figure C.5. Fluorescence spectra of 5 μM probe **A** in pH 5.0 buffers with different percentages of ethanol.

C.4   Computationally derived structures for probe A and AH⁺
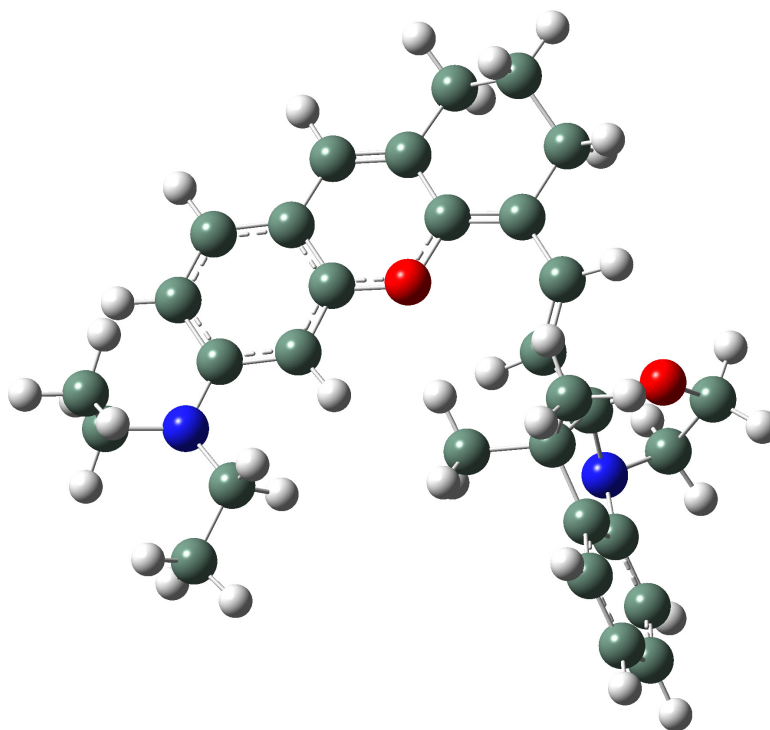
Figure C.6. Drawing of probe **A** with atoms represented as spheres of arbitrary size (H-white, C-grey, N-blue and O-red) using the GaussView program.

Table C.1. Atomic coordinates for probe **A**.

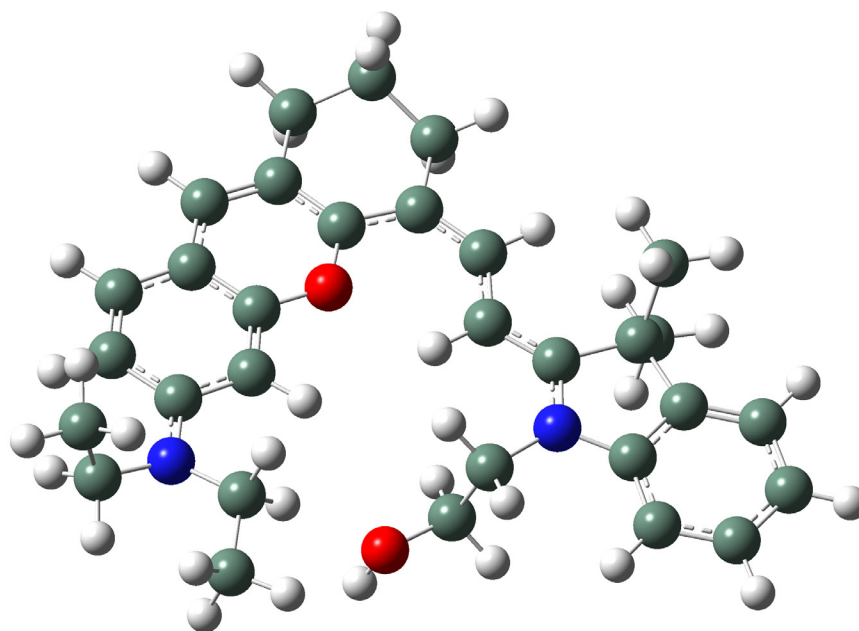| Row	Symbol	X	Y	Z
1	C	5.065562	-0.30195	0.231392
2	C	3.918238	-1.1465	0.093227
3	C	2.655842	-0.51606	0.026288
4	C	2.570472	0.857508	0.108113
5	C	3.691188	1.695034	0.248157
6	C	4.948799	1.060704	0.30816
7	O	1.328055	1.402961	0.032912
8	C	1.107847	2.734944	0.080026
9	C	2.208399	3.618407	0.21323
10	C	3.47284	3.086059	0.292677
11	C	-0.22955	3.161402	-0.01656
12	C	-0.4802	4.657831	-0.00213
13	C	0.703405	5.460642	-0.52496
14	C	1.956349	5.098755	0.261899
15	C	-1.3436	2.329105	-0.09771
16	C	-1.44635	0.936341	-0.05956
17	N	4.038025	-2.50149	0.029835
18	C	5.348935	-3.1135	-0.15602
19	C	2.849696	-3.2905	-0.31294
20	C	2.999117	-4.79088	-0.13598
21	C	5.839974	-3.04814	-1.59754
22	C	-2.64245	0.23876	-0.12328
23	C	-4.06793	0.769153	-0.23452
24	C	-4.86679	-0.51027	-0.22335
25	C	-3.99988	-1.59284	-0.11677
26	N	-2.68327	-1.11415	-0.07904
27	C	-6.23192	-0.71838	-0.28953
28	C	-6.71414	-2.02998	-0.24242
29	C	-5.83195	-3.10373	-0.12632
30	C	-4.45217	-2.9037	-0.05959
31	C	-4.45013	1.626452	0.982585
32	C	-4.29159	1.521784	-1.55506
33	C	-1.5289	-1.9787	0.048135
34	C	-1.10646	-2.12267	1.502644
35	O	0.054533	-2.92997	1.504442
36	H	6.057687	-0.73129	0.266281
37	H	1.741027	-1.07871	-0.09343
38	H	5.840598	1.672691	0.408444
39	H	4.328261	3.750475	0.389404

Row	Symbol	X	Y	Z
40	H	-1.37601	4.87539	-0.59212
41	H	-0.70675	4.979214	1.024217
42	H	0.499696	6.532647	-0.44503
43	H	0.860348	5.240429	-1.58812
44	H	2.835042	5.629837	-0.11595
45	H	1.832084	5.40953	1.308209
46	H	-2.27694	2.876612	-0.18611
47	H	-0.5422	0.357509	0.04278
48	H	6.059746	-2.64612	0.526935
49	H	5.282479	-4.14878	0.175449
50	H	2.030745	-2.96412	0.328549
51	H	2.552468	-3.06533	-1.34825
52	H	2.028251	-5.25478	-0.32872
53	H	3.714325	-5.24028	-0.82917
54	H	3.290911	-5.05344	0.884998
55	H	6.820545	-3.52354	-1.69084
56	H	5.149922	-3.56559	-2.27037
57	H	5.930477	-2.01398	-1.94166
58	H	-6.92092	0.117394	-0.37411
59	H	-7.78302	-2.21377	-0.2923
60	H	-6.22068	-4.11683	-0.08422
61	H	-3.77821	-3.74774	0.040142
62	H	-3.88934	2.561422	1.020171
63	H	-5.51325	1.874639	0.932159
64	H	-4.27199	1.083253	1.913689
65	H	-3.71512	2.446922	-1.60169
66	H	-4.0121	0.901822	-2.41011
67	H	-5.34914	1.779607	-1.65286
68	H	-1.7752	-2.95251	-0.3764
69	H	-0.71222	-1.57685	-0.55485
70	H	-0.90405	-1.13474	1.935272
71	H	-1.91692	-2.5848	2.080605
72	H	0.349497	-3.06125	2.410781

Table C.2. Excitation energies and oscillator strengths for probe A.

Excited State	Nature	E (eV)	λ (nm)	f	Orbital transitions	Normalized coefficient
1	Singlet-A	2.9705	417.39	0.5427	126 ->127	0.70254
2	Singlet-A	3.8205	324.52	0.0945	124 ->127	0.12029
					125 ->127	-0.16699
					126 ->128	0.49384
					126 ->129	-0.44206
3	Singlet-A	3.9032	317.65	0.0432	124 ->127	-0.27488
					125 ->127	0.45655
					126 ->128	0.10080
					126 ->130	-0.42340
4	Singlet-A	4.0144	308.85	0.0071	124 ->127	0.55750
					125 ->127	0.41595
5	Singlet-A	4.1347	299.86	0.0063	126 ->128	0.48025
					126 ->129	0.51226
6	Singlet-A	4.2653	290.68	0.3107	124 ->127	-0.28800
					125 ->127	0.27224
					126 ->129	-0.11983
					126 ->130	0.50848
					126 ->132	-0.10521

The FTIR spectra of the unprotonated and protonated fluorescent probe A (Figures C.7 and C.12) were calculated to confirm that the geometries of the structures have been optimized to a suitable minimum.
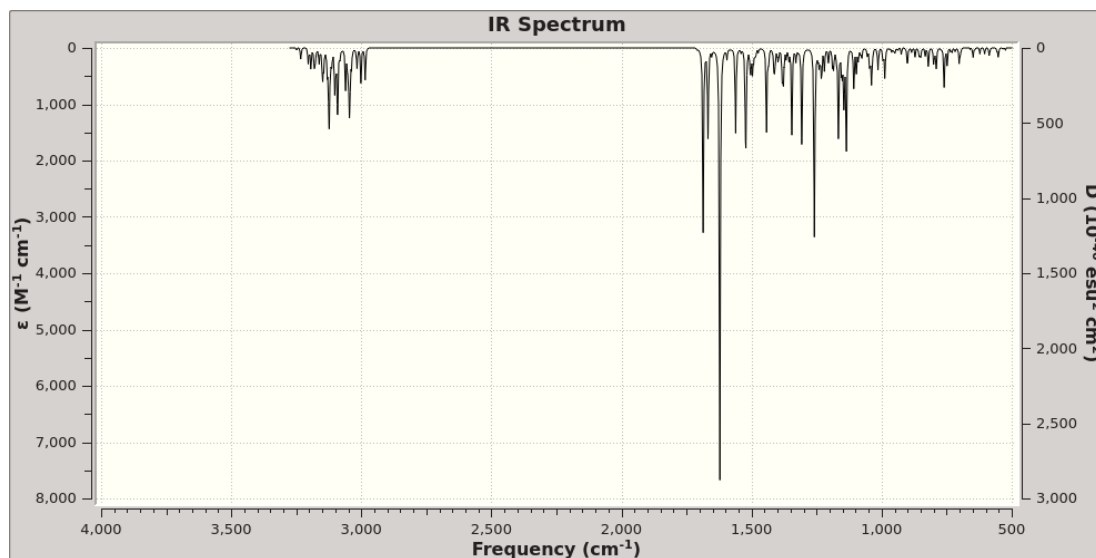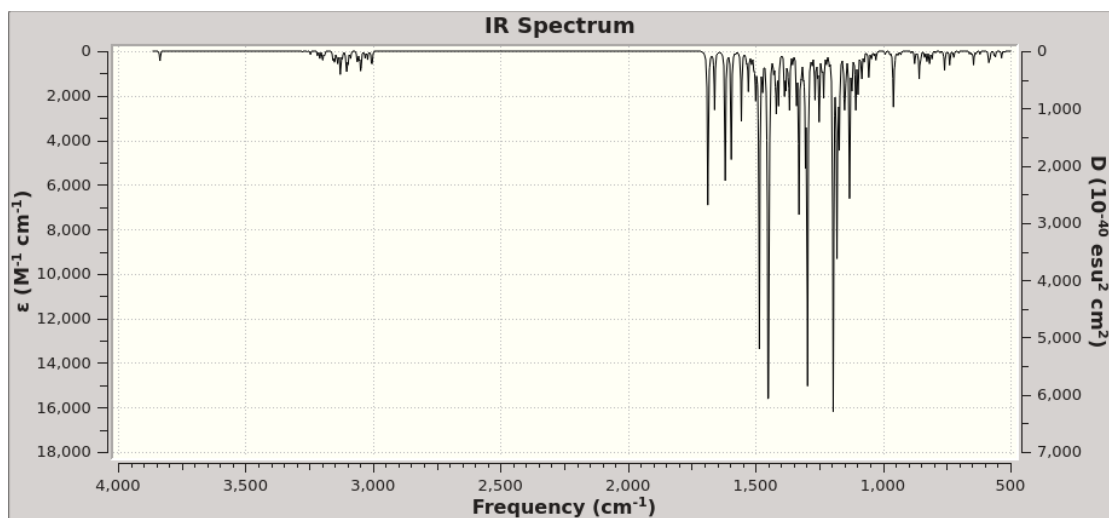

**Figure C.7**. Calculated (top) FTIR spectrum of probe **A.**
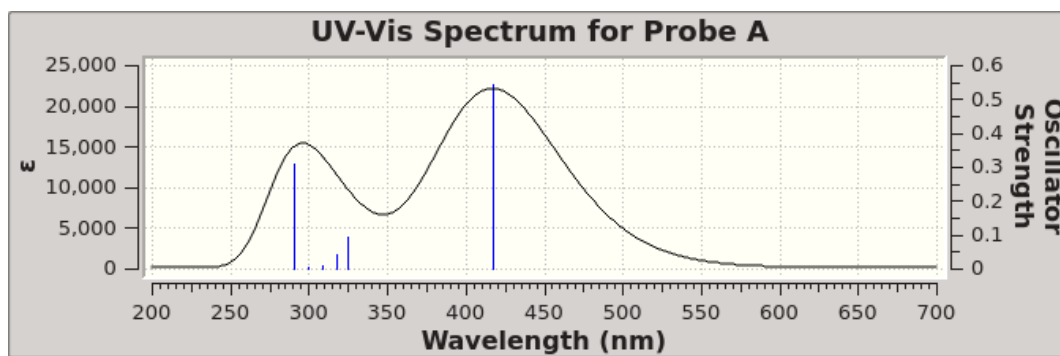
Figure C.8. Calculated UV-Vis spectrum for probe **A** in water.
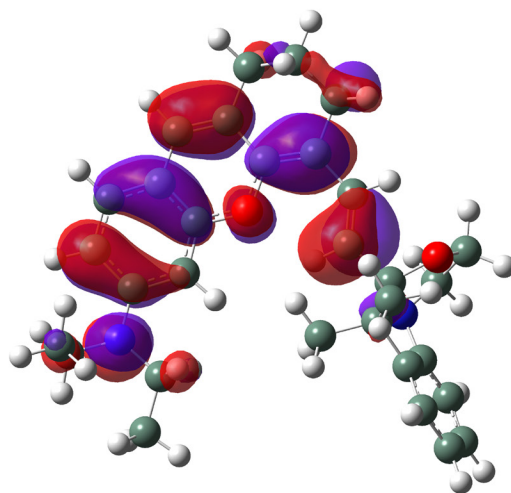
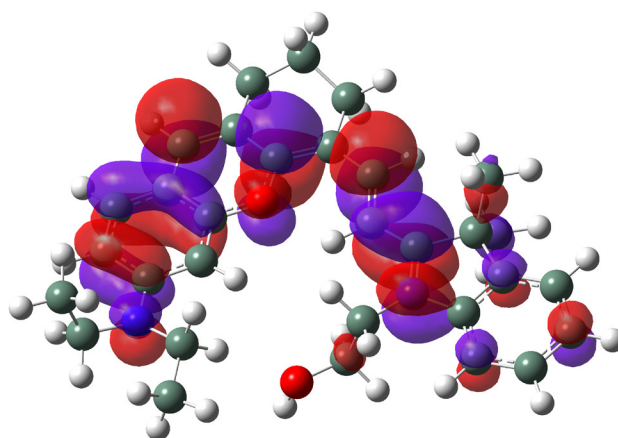**Figure C.9**. MO for level 126 for probe **A** involved with the transition noted as Excited State 1 in Table C2.
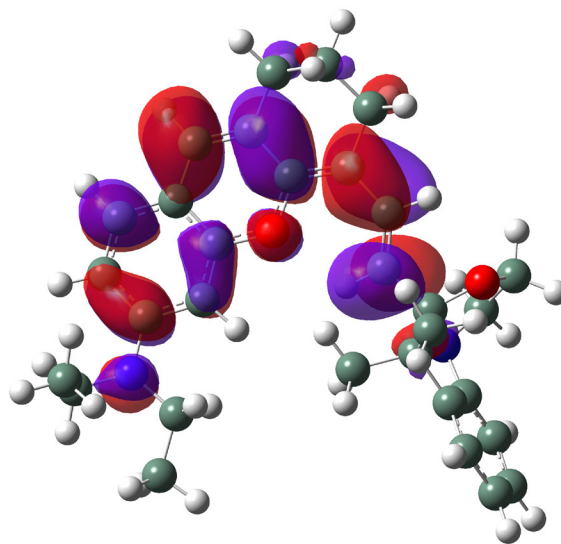
Figure C.9. MO for level 127 for probe **A** involved with the transition noted as Excited State 1 in Table C2.

Figure C.11. Drawing of probe **AH⁺** with atoms represented as spheres of arbitrary size (H-white, C-grey, N-blue and O-red) using the GaussView program.

Table C3. Atomic coordinates for probe **AH⁺**.

Row	Symbol	X	Y	Z
1	C	5.065562	-0.30195	0.231392
2	C	3.918238	-1.1465	0.093227
3	C	2.655842	-0.51606	0.026288
4	C	2.570472	0.857508	0.108113
5	C	3.691188	1.695034	0.248157
6	C	4.948799	1.060704	0.30816
7	O	1.328055	1.402961	0.032912
8	C	1.107847	2.734944	0.080026

Row	Symbol	X	Y	Z
9	C	2.208399	3.618407	0.21323
10	C	3.47284	3.086059	0.292677
11	C	-0.22955	3.161402	-0.01656
12	C	-0.4802	4.657831	-0.00213
13	C	0.703405	5.460642	-0.52496
14	C	1.956349	5.098755	0.261899
15	C	-1.3436	2.329105	-0.09771
16	C	-1.44635	0.936341	-0.05956
17	N	4.038025	-2.50149	0.029835
18	C	5.348935	-3.1135	-0.15602
19	C	2.849696	-3.2905	-0.31294
20	C	2.999117	-4.79088	-0.13598
21	C	5.839974	-3.04814	-1.59754
22	C	-2.64245	0.23876	-0.12328
23	C	-4.06793	0.769153	-0.23452
24	C	-4.86679	-0.51027	-0.22335
25	C	-3.99988	-1.59284	-0.11677
26	N	-2.68327	-1.11415	-0.07904
27	C	-6.23192	-0.71838	-0.28953
28	C	-6.71414	-2.02998	-0.24242
29	C	-5.83195	-3.10373	-0.12632
30	C	-4.45217	-2.9037	-0.05959
31	C	-4.45013	1.626452	0.982585
32	C	-4.29159	1.521784	-1.55506
33	C	-1.5289	-1.9787	0.048135
34	C	-1.10646	-2.12267	1.502644
35	O	0.054533	-2.92997	1.504442
36	H	6.057687	-0.73129	0.266281
37	H	1.741027	-1.07871	-0.09343
38	H	5.840598	1.672691	0.408444
39	H	4.328261	3.750475	0.389404
40	H	-1.37601	4.87539	-0.59212
41	H	-0.70675	4.979214	1.024217
42	H	0.499696	6.532647	-0.44503
43	H	0.860348	5.240429	-1.58812
44	H	2.835042	5.629837	-0.11595
45	H	1.832084	5.40953	1.308209
46	H	-2.27694	2.876612	-0.18611
47	H	-0.5422	0.357509	0.04278
48	H	6.059746	-2.64612	0.526935

Row	Symbol	X	Y	Z
49	H	5.282479	-4.14878	0.175449
50	H	2.030745	-2.96412	0.328549
51	H	2.552468	-3.06533	-1.34825
52	H	2.028251	-5.25478	-0.32872
53	H	3.714325	-5.24028	-0.82917
54	H	3.290911	-5.05344	0.884998
55	H	6.820545	-3.52354	-1.69084
56	H	5.149922	-3.56559	-2.27037
57	H	5.930477	-2.01398	-1.94166
58	H	-6.92092	0.117394	-0.37411
59	H	-7.78302	-2.21377	-0.2923
60	H	-6.22068	-4.11683	-0.08422
61	H	-3.77821	-3.74774	0.040142
62	H	-3.88934	2.561422	1.020171
63	H	-5.51325	1.874639	0.932159
64	H	-4.27199	1.083253	1.913689
65	H	-3.71512	2.446922	-1.60169
66	H	-4.0121	0.901822	-2.41011
67	H	-5.34914	1.779607	-1.65286
68	H	-1.7752	-2.95251	-0.3764
69	H	-0.71222	-1.57685	-0.55485
70	H	-0.90405	-1.13474	1.935272
71	H	-1.91692	-2.5848	2.080605
72	H	0.349497	-3.06125	2.410781

Table C4. Excitation energies and oscillator strengths for probe **AH$^+$**.

Excited State	Nature	E (eV)	λ (nm)	f	Orbital transitions	Normalized coefficient
1	Singlet-A	2.0899	593.26	0.7993	126 ->127	0.70631
2	Singlet-A	2.8527	434.62	0.2023	125 ->127	0.68787
					126 ->128	0.12101
3	Singlet-A	3.6147	343.00	0.1318	122 ->127	-0.24296
					124 ->127	-0.42811
					126 ->128	0.49106
4	Singlet-A	3.7149	333.75	0.3055	124 ->127	0.53865
					125 ->127	-0.10258
					126 ->128	0.41981
5	Singlet-A	3.9046	317.54	0.0383	123 ->127	0.66762
					126 ->129	-0.16028
6	Singlet-A	3.9614	312.98	0.1464	122 ->127	0.58588
					123 ->127	0.11095
					125 ->128	-0.22459
					126 ->128	0.19025
					126 ->130	-0.14800

Figure C.12. Calculated (top) FTIR spectrum of probe **AH⁺**.
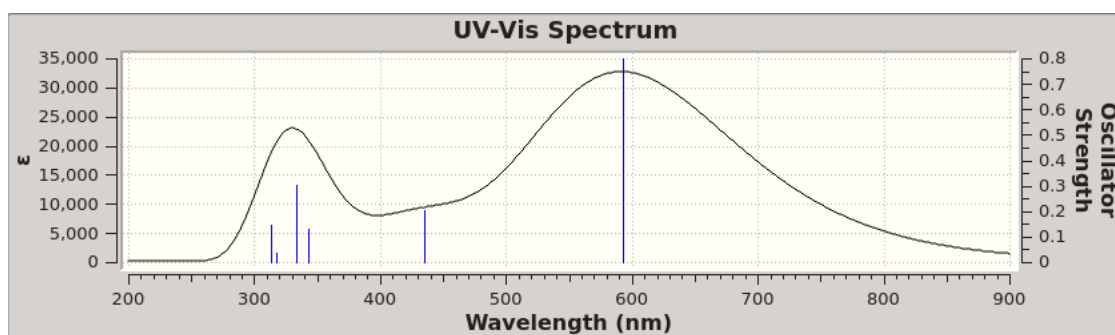
Figure C.13. Calculated UV-Vis spectrum for probe **AH⁺** in water.
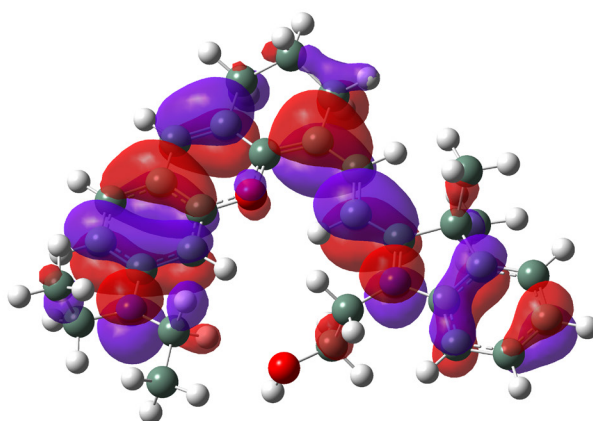
Figure C.13. MO for level 126 for probe **AH⁺** involved with the transition noted as

Excited State 1 in Table C4.

Figure C.14. MO for level 127 for probe **AH**$^+$ involved with the transition noted as

Excited State 1 in Table C4.

D   Copyright documentation

This letter is for Chapter 2.

This is a webpage prints for chapter 2

This is a webpage prints for chapter 2

Copyright Clearance Center **RightsLink®**

Home | Create Account | Help

ACS Publications
Most Trusted. Most Cited. Most Read.

Title: Unusual Fluorescent Responses of Morpholine-Functionalized Fluorescent Probes to pH via Manipulation of BODIPY's HOMO and LUMO Energy Orbitals for Intracellular pH Detection

Author: Jingtuo Zhang, Mu Yang, Wafa Mazi, et al

Publication: ACS Sensors

Publisher: American Chemical Society

Date: Feb 1, 2016

Copyright © 2016, American Chemical Society

Quick Price Estimate

Permission for this particular request is granted for print and electronic formats, and translations, at no charge. Figures and tables may be modified. Appropriate credit should be given. Please print this page for your records and provide a copy to your publisher. Requests for up to 4 figures require only this record. Five or more figures will generate a printout of additional terms and conditions. Appropriate credit should read: "Reprinted with permission from {COMPLETE REFERENCE CITATION}. Copyright {YEAR} American Chemical Society." Insert appropriate information in place of the capitalized words.

I would like to...   reuse in a Thesis/Dissertation ▼

Requestor Type   Author (original work) ▼

Portion   Full article ▼

Format   Print ▼

Will you be translating?   No ▼

Select your currency   USD - $ ▼

Quick Price   Click Quick Price

This service provides permission for reuse only. If you do not have a copy of the article you are using, you may copy and paste the content and reuse according to the terms of your agreement. Please be advised that obtaining the content you license is a separate transaction not involving Rightslink.

[QUICK PRICE]   [CONTINUE]

To request permission for a type of use not listed, please contact the publisher directly.